A Theoretical Study of Structural, Electronic and Optical Properties of ABF_3 (A, B = Alkali or Alkaline Earth and Transition Elements) Type Perovskite by Using FP-LAPW Method

Thesis submitted in fulfilment for the requirements of the Degree of Doctor of Philosophy in Physics

By

Khimananda Neupane

Registration No. and Date: MZU/Ph.D./871 of 21.04.2016

To

Department of Physics

School of Physical Sciences

Mizoram University, Aizawl

Mizoram, India

November, 2018

A Theoretical Study of Structural, Electronic and Optical Properties of ABF_3 (A, B = Alkali or Alkaline Earth and Transition Elements) Type Perovskite by Using FP-LAPW Method

Thesis submitted in fulfilment for the requirements of the Degree of Doctor of Philosophy in Physics

By

Khimananda Neupane

Registration No. and Date: MZU/Ph.D./871 of 21.04.2016

To

Department of Physics

School of Physical Sciences

Mizoram University, Aizawl

Mizoram, India

November, 2018

मिज़ोरम विश्वविद्यालय
भौतिक विज्ञान विभाग
आइजोल ७९६००४ मिज़ोरम
फोन : ०३८९-३३०५२२,९४३६१४०५२३(मो०)
फैक्स : ०३८९-२३३०५२२

प्रोफेशर राम कुमार थापा

MIZORAM UNIVERSITY
PHYSICS DEPARTMENT
AIZAWL 796 004 MIZORAM
Phones : 0389 - 2330522, 9436140523(M)
FAX : 0389 - 2330522
E-mail : r.k.thapa@gmail.com
Prof. Ram Kumar Thapa

No. MZU/PHYS/RKT/Ph.D./2018/020 Dt. 2nd Nov, 2018

Certificate

This is to certify that the thesis entitled ***'A Theoretical Study of Structural, Electronic and Optical Properties of ABF_3 (A, B = Alkali or Alkaline Earth and Transition Elements) Type Perovskite by Using FP-LAPW Method'*** *submitted by Khimamnanda Neupane, for the degree of Doctor of Philosophy under the Mizoram University, Aizawl, embodies the record of original investigations carried out by him under my supervision. He has been duly registered and the thesis presented is worthy of being considered for the award of the Ph.D degree. This work has not been submitted for any degree of any other university.*

(Prof. R. K. Thapa)
Supervisor

Declaration

==========

*I, **Khimananda Neuopane**, a Ph.D scholar in Physics Department, Mizoram University, do hereby solemnly declare that the subject matter of this thesis is the record of work done by me, that the contents of this thesis did not form bias of the award of any previous degree to me or to the best of my knowledge to anybody else, and that the thesis has not been submitted by me for any research degree in any other University/Institute.*

This thesis is being submitted to Mizoram University for the degree of Doctor of Philosophy in Physics.

(KHIMANANDA NEUPANE)

Candidate

Physics Department
Mizoram Unversity

(Prof. SUMAN RAI)

Head

(Prof. R. K. THAPA)

Supervisor

Acknowledgement

It is with deepest sense of gratitude that I wish to express my indebtedness to my most distinguished and honorable supervisor Prof. Dr. R. K. Thapa, Department of Physics, Mizoram University, Aizawl who has guided me throughout the beginning of this thesis works with the utmost sense of scientific temperament, inquisitiveness and thrust for knowledge in my mind. In fact it was him who has initiated the research topic of investigation for Ph. D. dissertation and had always been encouraging me to go ahead, sparing his precious time for my works without which I could not have completed my Ph.D. today.

I am thankful to Prof. Zaithanzauva Pachuau, Dean, School of Physical Sciences, Mizoram University, for all the necessary help and also to Prof. R.C. Tiwari (former Dean, SPS) who had been always supporting me in every respect. I thank also Prof. S. Rai, Head, Physics Department Mizoram University, extending all necessary help and facilities for the success full completion of my Ph.D. works. Thanks are also due to all the teaching and non-teaching staff members of Department of Physics, Mizoram University, for their co-operation and help whenever I approached them.

Further I am also grateful to the authority of Mizoram University for extending me financial assistance in the form of fellowship which was of immense help to me during the course of study. I am also thank full to Tribhuvan University, Nepal, Butwal Multiple Campus and Horizon Institute, Butwal for providing this opportunity.

I take this opportunity to thanks all my fellow research scholars of Physics Department, Mizoram University for being always friendly and cooperative. Thanks are especially to CMTRG group of Prof. Thapa namely Dr. Dibya Prakash Rai (PUC), Dr.

Sandeep Chhetri, Dr. Amit Shankar, Kurseong College, Dr. M.P. Ghimire, Humboldt Fellow, Leibniz Institute for Solid State and Materials Research, IFW Dresden, Germany, Dr. Rebeca Lalngaihawmi, and Dr. L.N. Devi who have always supported me and were very kind to help me in all my questionings to them sometime even very silly questions. Lalhriatpuia Hnamte and Himanshu Joshi was always present almost for my every needs whether in the laboratory or outside it.

I cannot forget at all Mrs. Kamala Thapa for her kind hospitality and motherly attitudes. She has been always creating a homely atmosphere during the period of my stay at Mizoram University.

Last but not the least, I would like to express my deep sense of gratitude to my wife Lilawati Upadhyay for her constant moral support and encouragement to complete my works. She in fact has borne the responsibilities of the family during my absence. I would like thank to my brother in law Khem, sister in law Saraswati and all Neupane's family for their good supporting and encouragement. My daughter Lenina, granddaughter Muna, son Gunjan,niece Shishta and nepheu Shekhar infact has missed me in their most prime time, I appreciate their tolerance.

Mizoram University

02 Nov, 2018 **(Khimananda Neupane)**

CONTENTS

List of Figures

List of Tables

List of Abbreviations

CBM-VBM	Conduction Band Minimum-Valence Band Maximum
DFT	Density Functional Theory
DOS	Density of States
FP-LAPW	Full-Potential Linearized Augmented Plane Wave method
GGA	Generalized Gradient Approximation
GW	Greenian Potential
KS	Kohn-Sham
LAPW	Linearized Augmented Plane Wave
LDA	Local Density Approximation
LSDA	Local Spin Density Approximation
mBJ	Modified Becke-Johnson
MT	Muffin tin
PAW	Plane Augmented Waves
PDOS	Partial Density of States
TDOS	Total Density of States
WIEN2k	Name of code used in the thesis

To my Father and mother,

I always feel your absence.....

Chapter-1

Introduction

Perovskite is a brown, yellow or grayish-black mineral with an oxide of Calcium and Titanium and sometimes containing rare Earth elements. It was first discovered in Ural mountain of Russia by Gustav Rose in 1983 and is named after Russian mineralogist L.A.Perovski. The general chemical formula for perovskite compounds is represented as ABX_3, where A and B are two cations and X is an anion that bonds to both. Perovskite material exhibit many interesting properties from both theoritical and application point of view. Colossal magnetoresistance, ferroelectricity, superconductivity, charge odering, spin dependent transport, high thermopower and transport properties are commonly observed features. These compounds are used as sensors and catalyst electrodes in certain type of fuel cells and are candidates for memory devices and spintronics application (Piskunov et al., 2004). Ferroelectric and related materials, having the chemical formula ABO_3, have been the subject of extensive investigation, both because of their technical importance and their fundamental interest to physical and materials sciences. The ideal structure is a cubic perovskite, where A and B cations are arranged on a simple cubic lattice, and O ions lie on the face centers nearest to the B cations. Barium titanate ($BaTiO_3$) is one of the most important ferroelectric oxides used in electronic applications. It has been widely used in electromechanical actuators and in sensor applications, as a major component of ceramic capacitor dielectrics, and in photogalvanic devices (Bagayoko et al.,1998, Gardana M.,1965 and Mara et al.,1954). It is also an important photo-refractive material used for applications in distortion correction and in combination with laser power.

Many kinds of perovskite crystals are abundant on Earth like the fluoroperovskites (ABF_3), oxides-perovskite (ABO_3) and nitridesperovskite (A_3BN). Attention has been focused on the electronic and optical properties of the fluoroperovskites due to their significance in the technological applications of lenses and the semiconductor industry. The cubic perovskite compound is preferable for the lens materials because it does not have birefringence that makes design of lenses difficult. The fluoroperovskites structure, ABF_3, is one of the common structures of the perovskite. The A and B elements are alkali metals (Li–Cs) and alkaline earth metals (Be–Ba), respectively.

$BaTiO_3$ is ABX_3 type perovskite which was the first advanced ceramic piezoelectric material, yet it is still often applied because of its chemical stability and high dielectric constant. Since its discovery in barium titanate ($BaTiO_3$), ferroelectricity in perovskite-structure oxides has attracted tremendous interest, ranging from fundamental studies to technological applications. It is one of the most important ferroelectric oxides used in electronic applications. Indeed, the transition-metal/oxygen bond, with its large polarizability, is particularly favourable for promoting the transition-metal off centering that can result in a ferroelectric ground state. Ferroelectricity also exist in materials which do not contain oxygen but with a particularly extensive range of fluorine in both polymers (Lovinger, 1983) and ceramics in many crystal classes (Scott *et al*., 2012). Perhaps not surprisingly given the low polarizability of bonds with fluorine, the mechanisms for ferroelectricity in fluorine-based ferroelectrics are distinct from those in oxides, ranging from molecular in ceramics (Ederer *et al*., 2006). These alternative mechanisms are of particular interest because, again unlike the oxides, they are not contra-indicated by transition metal *d* electrons, and so allow simultaneous ferroelectricity and magnetic

ordering (multiferroism). Interestingly, however, none of the known perovskite-structure fluorides is reported to be ferroelectric.

Halide perovskites have recently emerged as promising materials for low-cost, high-efficiency solar cells. The efficiency of X fluroperovskite-based solar cells has increased rapidly from 3.8% in 2009 to 19.3% in 2014, by using the all-solid-state thin-film architecture and engineering cell structures with mixed-halide perovskites. The emergence of perovskite solar cells revolutionized the field not only because of their rapidly increased efficiency, but also flexibility in material growth and architecture. The superior performance of the X fluroperovskite solar cells suggested that perovskite materials possess intrinsically unique properties.

Salehi *et al*. (2004) have studied the electronic structures and density of states (DOS) in paraelectric crystal BaTiO3 by using the full potential- linearized augmented plane wave (FP-LAPW) method. in the framework of density functional theory (DFT). In this method, exchange potentials is calculated using the generalized gradient approximation (GGA). They found the electronic energy bands and density of states for BaTiO3 to be in good agreement with both the theoretical and experimental results.

Since late 2012, organic and inorganic halides with the perovskite structure have strongly attracted the attention of the photovoltaic community when efficiencies close to 10% were first achieved in solid state cells (Lee *et al.*, 2012). The excellent properties and the innovative device possibilities in perovskite-structured organometal and metallic halides has resulted in a frenzied increase of publications reporting high efficiencies (Ball et al., 2013). Recently, 15% efficient solar cells were reported with $CH_3 NH_3PbI_3$ target efficiencies of 20% identified as a feasible

goal (Park, 2013). It is therefore pertinent to evaluate the potential and analyze the prospects of this exciting technology that have galvanized the photovoltaic research community.

Organic/inorganic metal halides as light absorbers although these class of materials have been widely studied for decades (Moller, 1958), but only recently have they been introduced in solar cells.

ABO_3 and ABF_3 have similar crystal structures and are abundantly used in many areas of scientific and technological fields. From their interesting electro-optic and electro-mechanic properties, nonlinearities, large dielectric constants, and fundamental interest in the physics of their phase transitions, they are used in scientific fields. Since they undergo phase transitions as a result of rotations of the F_6 octahedral around one of the major crystallographic axes of high temperature cubic symmetry phase, these Perovskite-type crystals having chemical formula ABF_3, of which $KCaF_3$ is an example, have been attracting serious attention. The ideal structure of perovskite fluoride $KCaF_3$ crystal compound has a simple cubic lattice, where the monovalent K atom lies in the center of the cube, the divalent Ca atom lies at the corners of the cube and the fluorine F atoms lie in the axes of the cube. Demetriou *et al.* (2005) determined the nature of high conductivity of $KCaF_3$ using single crystal neutron diffraction experiments. Daniel *et al.* (1997) presented a thorough investigation by Raman scattering of $KCaF_3$ depending on temperature, and obtained useful information on high temperature structural instabilities occurring in this compound. Flocken *et al.* (1986) made a priori theoretical study of the potential-energy surface for $KCaF_3$ and examined the relative stability of the various lower-symmetry structures generated from cubic perovskite phase by rotations of the octahedral CaF_6. Chornodolskyy *et al.* (2004) investigated the electronic calculations for ABX_3 (A = K, Rb, Cs; B = Ca; X = F) by the pseudo-potential method taking into account the gradient corrections for the

exchange-correlation energy. Watson et al. (1992) presented the results from constant pressure and constant-temperature molecular dynamics simulations on the fluoride-perovskites ($KMnF_3$, $KZnF_3$ and $KCaF_3$). His prediction was that $KCaF_3$ is super-ionic conductor. Rousseau et al. (1997) investigated the unusual mechanism of phase transition occurring in $KCaF_3$ by inelastic neutron scattering.

The energy band structures and density of states of $BaTiO_3$ have been studied by Salhei *et al*., (2004) using the FP-LAPW method. In this method, exchange potentials is calculated using the generalized gradient approximation (GGA). They found the results of calculated electronic structure, energy band structures and density of states of $BaTiO_3$ are in agreement with both the theoretical and experimental results. The structural, electronic, elastic, and dielectric properties of $KMgF_3$ in cubic perovskite structure have been studied by Pilani et al. (2013) in the framework of density functional theory. They have employed generalized gradient approximation with projector augmented wave method for calculations. The fully relaxed structural parameters are found to be in reasonable agreement with available experimental data and with previous theoretical work.

Meziani *et al.* (2012) have studied the structural, elastic and electronic properties of fluoro-perovskite $CsCaF_3$ by using the FP-LAPW to the DFT. They have found the elastic properties such as elastic constants, anisotropy factor, Shear modulus, Young's modulus, Poisson's ratio and Debye temperature in the first time. They have obtained electronic band structure and the density of states. Electronic, structural and optical properties of the cubic perovskite $CsCaF_3$ are calculated by Babu *et al.* (2012). They used FP-LAPW plus local orbitals method with generalized gradient approximation (GGA) in the framework of the density functional theory to study the above mentioned properties. The calculated lattice constant is in

agreement with the experimental result. Calculations of the optical spectra, viz., the dielectric function, optical reflectivity, absorption coefficient, real part of optical conductivity, refractive index, extinction coefficient and electron energy loss, are performed for the energy range 0–30 eV.

The existence and origin of the ferroelectric instability in the ABF_3 fluoro-perovskites have studied and found that many fluoro-perovskites have a ferroelectric instability in their high symmetric cubic structure same as in oxide perovskites (Garcia-Castro *et al*., 2013). They found no sensitive to pressure and strain in ABF_3 which are constrast to the oxide perovskites.

The structural, elastic, electronic and optical properties of cubic perovskite $CsCaCl_3$ have studied by using the FP-LAPW method in the density functional theory (Babu *et al.,* 2015). The exchange-correlation potential has evaluated using the LDA and Generalized Gradient Approximation (GGA). The calculated structural properties such as equilibrium lattice constant, the bulk modulus and pressure derivative are found in good agreement with the available data. The elastic properties such as elastic constants, anisotropic factor, Shear modulus, Young's modulus and Poisson's ratio are calculated. Again, they have calculated electric band structure, density of states and charge density which shows that this compound has an indirect energy band gap with a mixed ionic and covalent bonding. Optical spectra such as the real and imaginary parts of dielectric function, optical reflectivity, refractive index and electron energy loss are performed for the energy range of 0-30 eV.

Babu *et al.* (2015) have studied the structural, electronic and elastic properties of cubic perovskite type compound $KCaF_3$ and $RbCaF_3$ by using the FP-LAPW method. They have observed the exchange- correlation effects through the LDA and GGA exchange potentials. The calculated structural properties such as equilibrium lattice constant, the bulk modulus and its

pressure derivative are in good agreement with the available data. They have found wide band gaps of indirect type transition in these compounds, which agree with experimental values. These compounds are found as elastically anisotropic and ductile from the observations of elastic properties.

Syrotyuk et al. (2015) have studied the electronic energy band spectra of cubic $RbMF_3$ Perovskites (M= Be, Mg, Ca, Sr, Ba) within the projector augmented waves (PAW) approach by means of the ABINIT code. From this study, they have obtained good results of the electron energy bands in the LDA. Mubark *et al*. (2012) have studied the structural, electronic and optical properties for fluoroperovskite $BaXF_3$ (X = Li, Na, K, and Rb) compounds using full potential FP-LAPW method as implemented in Wien2k code. They employed the generalized gradient approximation as exchange–correlation potential. Their calculations show that these compounds have direct energy band-gap .The dielectric function, refractive index, extinction coefficient, absorption coefficient, and reflectivity are calculated. All structures in the optical response are shifted toward lower energies as moved from Li to Rb.

Murtaza et al. (2013) have studied the bonding nature as well as structural, electronic, chemical bonding and optical properties of $MCaF_3$ (M = K, Rb, Cs) using the highly accurate full potential linearized augmented plane wave method within the generalized gradient approximation (GGA). They have found that lattice constant and bulk modulus increases with the change of cation (M) from K to Cs in $MCaF_3$. From the study of band structures, they have found wide band gaps and indirect transitions for $KCaF_3$ and $RbCaF_3$, while the band gaps of $CsCaF_3$ is wide and direct transitions. From the study of optical spectra of $MCaF_3$ compound, they have found the zero frequency limits of real part of dielectric function, refractive index and reflectivity increases from K to Cs.

In this thesis we report the study of structural, electronic and optical properties of fluro perovskite ABF_3 using self-consistent full-potential linearized augmented plane wave (FP-LAPW) method on the base of density functional theory (DFT). The combinations of the alkali metals or alkaline earth metals A and the transition metals B are as A= K, Rb, Cs, Ba; B= Li, K, Rb, Ca, and Cu and Ag. The electronic property of any system strongly depends on its crystal structure, hence to study the structure of cubical perovskites crystal, we have calculated the lattice parameters corresponding to its equilibrium energy and volume deformations. The electronic properties studied in this thesis are concerned with calculation of energy band structures followed by density of states (DOS). The optical property is studied by calculations of the frequency dependent isotropic complex dielectric function, refractive index, reflectivity and energy loss spectra followed by the optical conductivity of the crystal as a function of photon energy of incident radiation. The calculated optical spectra are correlated with the calculated energy band structures. The correlational potential fuctionals are calculated for all th systems by using the GGA and mBJ methods.

The chapters in the thesis are organized as follows:

In Chapter 2, we describe the theory and methodology used in our calculation. We will present an outline of the density functional theory (DFT), FP-LAPW model using LDA, GGA as well as mBJ methods.

In Chapter 3, we discuss the structural and electronic properties of ABF_3 type perovskite with alkali metals A as K, Rb and Cs; and alkaline earth metal B as Ca.

Also in Chapter 4, we describe the structural and electronic properties of ABF_3 type perovskite with alkaline earth metal A as Ba, and alkali metals as Li, K and Rb.

In Chapter 5, we describe the structural and electronic properties of ABF_3 type perovskite with alkali metals A as Rb; and transition metal B as Cu and Ag.

In Chapter 6, results of the calculations of optical constants and other parameters are presented for ABF_3 (A = K, Rb, Cs and B = Ca), ABF_3 (A = Ba and B = Li, K, Rb) and ABF_3 (A = Rb and B= Cu, Ag) type perovskite.

Chapter 7 contains the concluding part of the thesis where we summarize the results obtained in the case of ABF_3. This is followed by references.

Chapter-2

Theoretical Formalism and Methodology

In this chapter, we will discuss the theory and the formalism used in the calculations of density of states (DOS), energy band structures and optical constants and parameters to understand the optical properties of the systems under investigations in this thesis. First the basic principle of density functional theory (DFT) is discussed which is then followed by the explanation of the essence of the Kohn-Sham equation. In the entire thesis, the calculations of DOS and energy bands followed by optical constants etc. is based on the choice of exchange correlation energy of the electrons. For this purpose, hence therefore, the methods of generalized gradient approximation (GGA) and modified Becke-Johnson (mBJ) is considered and discussed in this chapter. The discussion is also given for the formulae used for the calculation of optical constants.

2.1 Density Functional Theory

Condensed matter physics is related to the study of the physical, electronic and other basic properties of matter. We can examine and describe the nature by various experimental science, but the interaction between the experiment and theory is also necessary, in order to understand and describe the basic property of matter. The properties of matter under normal conditions are governed by the behaviour motion of electron the field of the nuclei of the constituent atoms. Thus the knowledge of the electronic band structure is essential to understand the physical properties of matter. In condensed matter physics, one studies the physical properties of the systems within the framework of already established quantum theory. Many solids, crystals are ordered and can be successfully described mathematically neglecting the defect in the crystal, which plays a major role in describing the property of matter.

In reality the matter is more complex and composed of a collection of interacting atoms, which may also be affected by some external field. Various techniques that have been developed to describe the motion of collection atoms and electrons are based on Density Functional Theory. Density functional theory (DFT) is one the most widely used technique obtainable on computational condensed matter physics, which was originally invented and developed by Kohn, Hohenberg and Sham (Hohenberg and Kohn, 1964; Kohn and Sham, 1965), provides a modern tool to study the ground state properties of atoms, molecules and solids. The Hohenberg and Kohn theorem reduces the many body problems of N electrons with 3N spatial coordinates by employing the concept of functional of the electron density. The Kohn and Sham theorem defines energy functional of the system and gives evidences to prove that the proper ground state density minimizes this energy functional. In short, these theorems assert that all information available in the wave function is also available in the ground state electron density and that this density can be found through energy minimization procedures. The computational challenge of calculating the properties of a complex material is also greatly reduced. Thus, intractable many-body problem of interacting electrons in a static external potential, within the framework of Kohn-Sham DFT (KS-DFT) is reduced to a tractable problem of non-interacting electrons moving in an effective potential. The effective potential contains the external potential and the effects of Coulomb interactions between the electrons, the exchange and correlation interactions. Modeling the latter two interactions becomes the challenge within KS-DFT.

2.2 Details of Theoretical Methodology

According to Born Oppenheimer approximation the nuclei of the many body system in an electronic structure calculation are seen as fixed generating a static external state is represented by a wave function $\Psi(\vec{r}_1,...,\vec{r}_N)$ satisfying the many-electron Schrodinger equation:

$$H\Psi = [T + V + U]\Psi = \left[\sum_i^N -\frac{h^2}{2m}\nabla_i^2 + \sum_i^N V(\vec{r}_i) + \sum_i^N U(\vec{r}_i, \vec{r}_j)\right]\Psi = E\Psi \tag{2.1}$$

where H is the electronic Hamiltonian, N is the number of electrons, T is the N-electron kinetic energy, V is the N-electron potential energy from the external field, U is the electron-electron interaction energy for the N-electron system. The operators T and U are common for similar systems, so are called Universal operators. V is system dependent, so is non-universal. Now the difference between a single particle problem and the much more complex many particle problem is the interaction term U. DFT provides a way to systematically map the many-body problem with U onto a single particle problem without U. In DFT the particle density $n(\vec{r})$ for a normalized Ψ is given by:

$$n(r) = N\int d^3 r_2 \ldots \int d^3 r_N \psi^*(r, r_2, \ldots r_N)\psi(r, r_2, \ldots r_N) \tag{2.2}$$

In reverse way, this relation states that for a given ground-sate density $n_0(\vec{r})$ it is possible to construct the corresponding ground-state wave-function $\Psi_0(\vec{r}_1 \vec{r}_2, ..., \vec{r}_N)$. In other words $\Psi_0(\vec{r}_1 \vec{r}_2, ..., \vec{r}_N)$ is a functional of $n_0(\vec{r})$ and hence the ground sate expectation values of an observable $\hat{O}$ is also a functional of $n_0(\vec{r})$.

$$O[n_0] = \langle \Psi[n_0] | T + V + U | \Psi[n_0] \rangle \tag{2.3}$$

In particular, the ground state energy is a functional of $n_0(\vec{r})$

$$E_0 = E_0[n_0] = \langle \Psi[n_0] | T + V + U | \Psi[n_0] \rangle \tag{2.4}$$

$$= \langle \Psi[n_0] | T | \Psi[n_0] \rangle + \langle \Psi[n_0] | V | \Psi[n_0] \rangle + \langle \Psi[n_0] | U | \Psi[n_0] \rangle \tag{2.5}$$

$$= T[n_0] + V[n_0] + U[n_0] \tag{2.6}$$

where the contribution of the external $\langle \Psi[n_0] | V | \Psi[n_0] \rangle$ potential can be written in terms of the ground-state density n_0

$$V[n_0] = \int V(\vec{r})\, n_0(\vec{r}) d^3r \tag{2.7}$$

More commonly, the contribution of the external potential $\langle \Psi | V | \Psi \rangle$ can be written clearly in terms of the density n as

$$V[n] = \int V(\vec{r})\, n(\vec{r}) d^3r \tag{2.8}$$

A system is defined by a definite non-universal functional V, as $T[n]$ and $U[n]$ are universal. For a given system with V as its external potential

$$E[n] = T[n] + U[n] + \int V(\vec{r})\, n(\vec{r})\, d^3r \tag{2.9}$$

In regard to $n(\vec{r})$, taking for granted one has got dependable terms for $T[n]$ and $U[n]$. A successful reduction of the energy functional will produce the ground state density $n_0(\vec{r})$ and thus all other ground state observables.

The second KS-theorem makes it possible to use the variational principle of Rayleigh-Ritz in order to find the ground-state density. Out of the infinite number of possible densities, the one which minimizes $E[n]$ is the ground-state density corresponding to the external potential $V(\vec{r})$. Of course, this can be done only if an approximation to $\langle \Psi[n] | T + V | \Psi[n] \rangle$ is known. But having found $n(\vec{r})$, all knowledge about the system is within reach. It is useful to stress the meaning of the energy functional $E[n]$ once more. When it is evaluated for the density $n(\vec{r})$ corresponding to the particular $V(\vec{r})$ for this solid, it gives the ground state energy. When it is evaluated for any other density however, the resulting number has no physical meaning (Cottenier, 2002).

Taking the energy functional without electron-electron interaction energy term

$$E_S[n]=\left\langle \Psi_S[n]\middle|\hat{T}_S+V_S\middle|\Psi_S[n]\right\rangle \tag{2.10}$$

where $\hat{T}_S$ indicates the non-interacting kinetic energy and $\hat{V}_S$ is an external effectual potential in which the particles are moving. Clearly, if $\hat{V}_S$ is $n_S(\hat{r})=n(\hat{r})$ selected be

$$\hat{V}_S=\hat{V}+\hat{U}+(\hat{T}-\hat{T}_S) \tag{2.11}$$

Consequently, we can solve the Kohn-Sham equations for this assisting non-interacting system,

$$\hat{H}_{KS}\phi_i=E_i\phi_i \tag{2.12}$$

which produces the ϕ_i orbital that reproduces the density $n(\vec{r})$ of the authentic many-body system,

$$n(\vec{r})=n_s(\vec{r})=\sum_i^N\left|\phi_i(\vec{r})\right|^2 \tag{2.13}$$

The effective single-particle potential can be written in more detail as

$$V_S(\vec{r})=V(\vec{r})+\int\frac{e^2n_S(\vec{r}')}{\left|\vec{r}-\vec{r}'\right|}d^3r'+V_{XC}\left[n_S(\vec{r})\right] \tag{2.14}$$

The second term in the above Eq. 2.14 stands for the so-called Hartree expression with the electron-electron Coulomb repulsion, while the last expression V_{XC} is called the exchange correlation potential. Now, the Hartree expression and V_{XC} depend on $n(\vec{r})$ which depends on the ϕ_i, which in turn relies on $\hat{V}_S$. Now the problem is that the Kohn-Sham equation has to be solved in a self-consistent way. One typically begins with a first guess $n(\vec{r})$ then works out the corresponding $\hat{V}_S$ and solves the Kohn-Sham equations for the ϕ_i (Kohn and Sham, 1965). The techniques in DFT are complex and different and can be understood by considering the following two approaches.

We first discuss the local density approximation (LDA) method used. The LDA is decided exclusively and based on the qualities of the electron density. The significant supposition of this

approximation is that for a molecule with many electrons in a gaseous state, the density is consistent throughout the molecule. This is not the case for molecules where the electron density is decidedly not consistent. This approximation does however work well with electronic band structure of solids and hence illustrates the scope of energies in which electrons are allowed or not allowed. Outside of these applications, however, LDA's are not very acceptable.

Secondly, the technique that unites the electron density calculations with a gradient correction factor. A gradient in mathematics is a function that measures the rate of change of some property. In this case, the gradient seems to explain the non-uniformity of the electron density and as such is known as gradient-corrected and hence is called GGA method.

2.3 Kohn-Sham Equation

Since the total energy of the system is

$$E(n) = T(n) + \int V_{ext}(r) n(r)\, dr + V_H[n] + E_{XC}[n] \tag{2.15}$$

where T is the kinetic energy of the system, V_{ext} is an external potential acting on the system, E_{XC} is the exchange-correlation energy and Hartree energy is given by

$$V_H = \frac{e^2}{2} \int \frac{n(r)\, n(r')}{|r - r'|} dr\, dr' \tag{2.16}$$

The straight forward application of this formula has two barriers: First, the exchange-correlation energy E_{XC} is not known precisely and second, the kinetic term must be created in terms of the charge density. As was first suggested by Kohn and Sham (1965), the charge density $n(r)$ can be written as the sum of the squares of a set of orthonormal wave functions $\phi_i(r)$:

$$n(r) = \sum_i^N |\phi_i(r)|^2 \tag{2.17}$$

where the single particle wave function $\phi_i(r)$ are the N lowest-energy solutions to the Kohn-Sham equation for N non-interacting electrons moving in an effectual potential $V_{eff}(r)$ given by

$$-\frac{\hbar^2}{2m}\nabla^2\phi_i(r)+V_{eff}(r)\phi_i(r)=\varepsilon_i\phi_i(r) \tag{2.18}$$

where the effectual potential is defined to be

$$V_{eff}(r)=V_{ext}(r)+e^2\int\frac{n(r')}{|r-r'|}dr'+\frac{\delta E_{XC}[n]}{\delta_n} \tag{2.19}$$

This system is then solved iteratively until self-consistency is approached. Note that the eigen values ε_i have no physical meaning but the total sum matches the energy of the entire system E through the equation:

$$E=\sum_i^N\varepsilon_i-V_H[n]+E_{XC}[n]-\int\frac{\delta E_{XC}[n]}{\delta n(r)}n(r)dr \tag{2.20}$$

There are several ways in which Kohn-Sham theory can be applied depending on what is being examined.

2.4 Generalized Gradient Approximation

The exchange-correlation energy has a gradient expansion of the type

$$E_{XC}[n(r)]=\int A_{XC}[n(r)]n(r)^{4/3}dr+\int C_{XC}[n(r)]|\nabla n(r)|^2/n(r)^{4/3}dr+..... \tag{2.21}$$

which is asymptotically valid for densities that vary slowly in space. It is well known that a straightforward evaluation of this expansion is ill-behaved, in this sense that it is not monotonically convergent and it exhibits singularities that cancel out only when an infinite number of terms are re-summed. In fact, the first order correction worsens the results and the second order correction plagued with divergences (Ma and Brueckner, 1968; Fetter and Walecka, 1971). The largest error of this approximation actually arises from the gradient contribution to the correlation term. The early work of Gross and Dreizler (1981) provided a derivation of second

order expansion of the exchange density matrix, which was later re-analyzed and extended by Perdew (1985). GGAs are typically based either on theoretical developments that reproduce a number of exact results in some known limits, for example 0 and ∞ density or the correlation potential in the He atom, or are generated by fitting a number of parameters to a molecular database. The basic idea of GGAs is to express the exchange-correlation energy in the following form:

$$E_{XC}[n(r)] = \int n(r)\varepsilon_{XC}[n(r)]dr + \int F_{XC}[n(r),\ \nabla n(r)]dr \qquad (2.22)$$

where the function F_{XC} is asked to satisfy a number of formal conditions for the exchange-correlation hole, such as sum rule, long-range decay and so on. This cannot be done by considering directly the bare gradient expansion. What is needed for the functional is a form that mimics a re-summation to infinite order and this is the main idea of the GGA, for which there is not a unique recipe. Naturally, not all the formal properties can be enforced at the same time and differentiates one functional from another. A thorough comparison of different GGAs is done by Filippi *et al.* (1994).

The generalized gradient approximation (GGA) has attracted much attention for its abstract simplicity and moderate computational workloads. At present, two GGA functional, one suggested by Becke and Perdew (BP) and the other suggested more recently by Perdew and Wang (PW), are the most popular ones in the literature (Perdew *et al.*, 1996). Many calculations assessing the accuracy of the GGA have been reported and commonly demonstrate that the GGA substantially corrects in the cohesive energies of molecules and solids. Generalized gradient approximations (GGA's) to the exchange-correlation (XC) energy in density-functional theory are at present receiving increasing attention as a straightforward substitute to improve over the local-density approximation (LDA) in *ab initio* total-energy calculations (Kresse and Furthmuller, 1996).

2.5 The Full-Potential Linearized Augmented-Plane Wave (FP-LAPW) Method

The full-potential linearized augmented-plane wave (FP-LAPW) technique is one of the most precise methods of study of the electronic structures, magnetic and optical properties of crystals and surfaces. The application of atomic forces has greatly maximized its applicability, but it is still commonly supposed that FP-LAPW computations need considerable higher computational effort in comparison with the pseudopotential plane wave (PPW) based techniques. FP-LAPW has recently showed important progress which is evident by use of researchers to work out several properties in magnetism and nuclear quantities, for example, isomer shifts, hyperfine fields, electric field gradients, and core level shifts. Nevertheless, because the computational expense and memory requirements are still fairly high, FP-LAPW implementations are suitable to fairly complicated systems. One successful implementation of the FP-LAPW technique is the program package WIEN2k, a code enhanced by Blaha, Schwarz and coworkers (Blaha *et al.*, 2012). It has been successfully implemented to a various scope of difficulties such as electric field gradients and systems such as high-temperature superconductors, minerals, surfaces of transition metals, or anti- ferromagnetic oxides and even molecules (Ernst *et al.*, 2005). So far the main disadvantage of the FP-LAPW-technique in comparison with the pseudopotential plane-wave (PPW) method has been its higher computational expense. This may be largely because of an inconsistency in optimization efforts spent on both techniques and so we have investigated the FP-LAPW technique from a computational arithmetical viewpoint. Lately, the development of the Augmented Plane Wave (APW) techniques from Slater's APW to LAPW and the new APW+lo was portrayed by Schwarz and Blaha (2003).

FP-LAPW is the one of the most precise technique for performing electronic structure calculation of a crystals and it is based on DFT. The valence states are treated relativistically incorporated with either scalar relativistic or with including spin-orbit coupling. Core states are treated fully relativistically. The FP-LAPW technique, which is like most energy-band techniques is a process for solving the Kohn-Sham equations for the ground state density, total energy and

(Kohn-Sham) eigen values (energy bands) of a many-electron system by presenting a basis set which is particularly modified to the problem. This alteration is achieved by partitioning the unit cell (Fig. 2.1) into (I) non- overlapping atomic circles (centered at the atomic sites) and (II) an interstitial region, that's to say, a region between two spaces. In the two sorts of regions, diverse basis sets are used:

i) Inside atomic sphere **t** of radius $\mathbf{R_t}$ a linear combination of radial functions times spherical harmonics $Y_{lm}(r)$ is used:

$$\phi_{kn} = \sum_{lm} \left[A_{lm} u_l \left(\vec{r}, E_l \right) + B_{lm} \dot{u}_l (\vec{r}, E_l) \right] Y_{lm}(\vec{r}) \tag{2.23}$$

where $u_l(r, E_l)$ is the (at the origin) normal way out of the radial Schrodinger equation for energy E_1 and the spherical part of the potential inside sphere, $\dot{u}_l(r, E_l)$ is the energy derived of u_l taken at the similar energy. A linear mixture of these two functions comprise the linearization of the radial function; the coefficients A_{lm} and B_{lm} are functions of k_n decided by requiring that this root function $\dot{u}_l$ goes with the equivalent basis function of the interstitial region; u_l and are achieved by numerical integration of the radial Schrodinger equation on a radial mesh inside the sphere.

(ii) In the interstitial zone a plane wave extension is applied

$$\phi_{kn} = \frac{1}{\sqrt{w}} e^{ik_n r} 、 \tag{2.24}$$

where $k_n = k + K_n$; K_n are the reciprocal lattice vectors and k is the wave vector inside the first Brillouin zone. Each plane wave is increased by an atomic-like function in every atomic sphere.

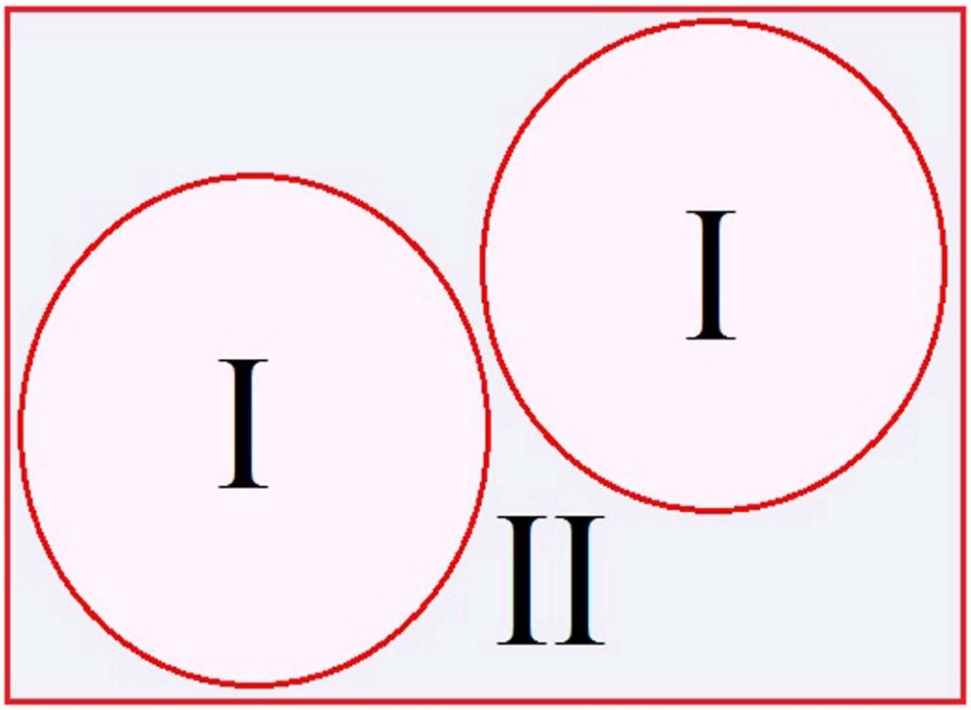

Fig. 2.1: Partitioning of the unit cell into atomic spheres (I) and an interstitial region (II)

The solutions to the Kohn-Sham equations are extended in this joint basis set of LAPW's according to the linear dissimilarity technique

$$\psi_k = \sum_n C_n \phi k_n \tag{2.25}$$

and the coefficients C_n are decided by the Rayleigh-Ritz variation rule. The union of this basis set is controlled by a disconnected parameter R_{MT} x K_{max} = 6 - 9, where R_{MT} is the smallest atomic sphere radius in the unit cell and K_{max} is the magnitude of the largest K vector. Additional (K_n independent) basis functions can be added to improve upon the linearization and to make possible a reliable treatment of semi core and valence states in one energy window additional basis functions can be added. They are called "local orbitals" and consist of a linear combination of two radial functions at two dissimilar energies and one energy derivative:

$$\phi_{lm}^{LO} = \left[A_{lm} u_l(\vec{r}, E_{1.l}) + B_{lm} \dot{u}_l(\vec{r}, E_{1.l}) + C_{lm} u_l(\vec{r}, E_{2.l})\right] Y_{l,}(\hat{r}) \tag{2.26}$$

The coefficients A_{lm}, B_{lm}, and C_{lm}, are decided by the necessities that ϕ_{lm}^{LO} should be regularized and has zero value and slope at the sphere border. The general form of potentials in the core region (I) and interstitial region (II) using FP- LAPW technique can be written as

$$V(\vec{r}) = \begin{cases} \sum_{lm} V_{lm}(\vec{r}) Y_{lm}(\hat{r}) & inside\, sphere \\ \sum_K V_K e^{ikr} & outside\, sphere \end{cases} \tag{2.27}$$

2.6 Modified Becke Johnson Potential (mBJ)

The density functionals of the local density (LDA) and generalized gradient (GGA) approximations are the standard choice for the exchange–correlation energy E_{xc}= E_x + E_c to

perform calculations on periodic solids with the Kohn–Sham method (Kohn and Sham, 1965) of density functional theory (Hohenberg and Kohn,1964), whose Eqns. are

$$\left(-\frac{1}{2}\nabla^2 + v_{eff,\sigma}^{KS}(\mathbf{r})\right)\psi_{i,\sigma}(\mathbf{r}) = \varepsilon_{i,\sigma}\psi_{i,\sigma}(\mathbf{r}) \tag{2.28}$$

where $v_{eff,\sigma}^{KS} = v_{ext} + v_{\mathrm{H}} + v_{\mathrm{xc},\sigma}$ is the Kohn–Sham multiplicative effective potential whose components are the external Hartree, and exchange–correlation($v_{\mathrm{xc},\sigma} = \delta E_{\mathrm{xc}} / \delta\rho_\sigma = v_{\mathrm{x},\sigma} + v_{\mathrm{c},\sigma}$) terms, respectively. In many cases, the LDA and GGA functionals (Perdew *et al*., 1996) are able to provide reliable results for the geometry (i.e., equilibrium structure) and electronic structure of solids. Nevertheless, some problems remain with these approximations, and the most notorious is the under estimation of the band gap, which is often too small, or even absent, compared to experimental results (Perdew, 1986). It is also well known that rigorously the Kohn–Sham eigen values should not be used for excitation energies, but it is common practice to do so. Mainly responsible for this deficiency in the band gap is the self-interaction error contained in the LDA and GGA exchange–correlation potentials (Perdew and Zunger, 1981).

There are alternative ways to have an estimate of the experimental band gap. One can use a method which lies outside the KS framework by using a non-multiplicative potential. Hybrid functionals (e.g., HSE (Heyd *et al*., 2005)), in which a fraction of exact exchange replaces a fraction of the LDA or GGA exchange, also improve the band gap. However, the hybrid methods are more expensive and also not satisfactory in all cases. Another possibility is the LDA+U (Anisimov *et al*., 1991) method, but it can only be applied to correlated and localized electrons, e.g., 3*d* or 4*f* in transition and rare-earth oxides. Very successful but also very expensive methods are the combination of LDA with dynamical mean-field theory (LDA + DMFT) (Georges *et al*,.1996) and of course GW (Bechstedt *et al*., 2009). In fact, with such non-multiplicative potentials (a part of) Δ_{xc} is contained in the CBM − VBM difference.

Nevertheless, if one wants to stay inside the KS framework and still use a computationally cheap semi-local method that leads to KS band gaps which are close to the experimental band gaps, the potential of Becke and Johnson (BJ) (Becke and Johnson, 2006) called mBJ potential can be a good starting point. The multiplicative BJ potential reads

$$v_{x,\sigma}^{BJ}(\mathbf{r}) = v_{x,\sigma}^{BJ}(\mathbf{r}) + \frac{1}{\pi}\sqrt{\frac{5}{6}}\sqrt{\frac{t_\sigma(\mathbf{r})}{\rho_\sigma(\mathbf{r})}}, \tag{2.29}$$

where $\rho_\sigma = \sum_{i=1}^{N_\sigma} |\psi_{i,\sigma}|^2$ is the electron density, the kinetic-energy density is given by

$$t_\sigma = 1/2 \sum_{i=1}^{N_\sigma} \nabla \psi_{i,\sigma}^* . \nabla \psi_{i,\sigma} \tag{2.30}$$

`

$$v_{x,\sigma}^{BJ}(\mathbf{r}) = -\frac{1}{b_\sigma(\mathbf{r})}\left(1 - e^{-x_\sigma(\mathbf{r})} - \frac{1}{2}x_\sigma(\mathbf{r})e^{-x_\sigma(\mathbf{r})}\right) \tag{2.31}$$

is the Becke-Roussel (BR) (Becke and Roussel, 1989) exchange potential, which was proposed to model the Coulomb potential created by the exchange hole. In Eq. (2.31), x_σ is determined from a nonlinear Eqn.involving $\rho_\sigma, \nabla\rho_\sigma$, $\nabla^2\rho_\sigma$, and t_σ, and then b_σ is calculated with $b_\sigma = \left[x_\sigma^3 e^{-x_\sigma}/(8\pi\rho_\sigma)\right]^{1/3}$. The asymptotic behavior of $v_{x,\sigma}^{BJ}$ is that of the exact KS exchange potential. The $\sqrt{t/\rho}$ term was introduced to reproduce the step structure of the OEP in atoms and can be considered as a kind of screening term.

The BJ exchange potential has been implemented (Tran *et al*., 2007) self- consistently into the WIEN2k code (Blaha *et al*., 2001) which is based on the full-potential (linearized) augmented plane-wave and local orbitals method to solve the KS Eqn.s for periodic systems. Tran *et al*. (2007) showed that the BJ potential improves over LDA and PBE for the description of band gaps; i.e., the obtained values for CBM − VBM were larger and hence closer to experiment. However, the improvement was moderate. Further improvement has been achieved by a modified version

(TB-mBJ) (Tran and Blaha, 2009) of the BJ exchange potential which introduces a parameter to change the relative weights of the two terms in the BJ potential:

$$V_{x,\sigma}^{MBJ}(r) = cV_{x,\sigma}^{BR}(r) + (3c-2)\frac{1}{\pi}\sqrt{\frac{5}{12}}\sqrt{\frac{2t_\sigma(r)}{\rho_\sigma(r)}} \tag{2.32}$$

Where $\rho_\sigma(r)$ is the spin dependent density of states, $t_\sigma(r)$ is the kinetic energy density and $V_{x,\sigma}^{MBJ}(r)$ is the Becke-Roussel potential (BR) (Engel, 2009). The c stands for

$$c = A + B\sqrt{\frac{1}{V_{cell}}\int d^3r \frac{|\Delta\rho(r)|}{\rho(r)}} \tag{2.33}$$

A and B are parameters adjusted to produce the best fit to the experimental values of the semiconductor band gaps. In the WIEN2k code, the kinetic-energy density t_σ is not calculated with Eqn. (2.31) but instead with the equivalent expression

$$t_\sigma = \sum_{i=1}^{N_\sigma} \varepsilon_{i,\sigma} \left|\psi_{i,\sigma}(\mathrm{r})\right|^2 - v_{eff,\sigma}^{KS}(\mathbf{r})\rho_\sigma(\mathbf{r}) + \frac{1}{4}\nabla^2\rho_\sigma(\mathbf{r}) \tag{2.34}$$

which depends on the potential $V_{eff,\sigma}^{KS}$, entering the Kohn–Sham Eqns. (Eqn. (2.28)). For the evaluation of Eqn. (2.35), the exchange–correlation part of $V_{eff,\sigma}^{KS}$ was taken from the previous iteration of the self-consistent procedure. A Newton algorithm was used to solve the non linear Eqn. for x σ in each point of space, and we ensured always obtaining a positive real value (which is unique). The calculations with the BJ exchange potential are done without correlation or in combination with LDA correlation (Perdew and Wang, 1992).

2.7 Equation of States

The behaviour of a solid under hydrostatic pressure can be described by using equation of states which is the pressure-volume or energy volume relation. All physical properties are related to the total energy of the crystal. Equilibrium lattice constant, isothermal bulk modulus, its

pressure derivative are calculated by fitting the calculated total energy to the Murnaghan's equation of state (Murnaghan, 1944), which is given by

$$E(V) = E_0 + \left[\frac{(V_0/V)^{B_0'}}{B_0' - 1} + 1 \right] - \frac{B_0 V_0}{B_0' - 1} \tag{2.35}$$

Here E_0 is the minimum energy at T = 0K, V_0 is the equilibrium volume corresponding to minimum energy of the crystal. B_0 and B_0' are the bulk modulus and pressure derive-

ative of the bulk modulus at the equilibrium volume respectively.

$$\text{Pressure } (P) = -\frac{dE}{dV} \text{ and Bulk modulus, } (B_0) = -V\frac{dP}{dV} = V\frac{d^2E}{dV^2}$$

2.8 Formalism to study Optical Properties

Interaction of radiation with matter gives various interesting phenomena such as absorption, transmission, reflection, scattering or emission. The study of these properties provides several informations with regard to the behaviour of matter in various energy ranges (Pines, 1963). The electrons of the matter absorb the energy of the incident light and jumps from occupied valence state to the unoccupied conduction state. This kind of transitions provides the understanding of the location of the initial and the final energy bands and symmetry of their associated wave functions (Callaway, 1974a). This is infact related to the response function of the system which is strongly dependent on the frequency of the incident radiation and the wave vector which is given by $\varepsilon(\omega, q)$. In the infrared and higher energy radiation (long wavelength limit) the dielectric function is dependent only on frequency compared to wave vector (Callaway, 1974b) and hence the dielectric function can be written as $\varepsilon(\omega, 0)$ which is the combination of real and imaginary parts and is given by

$$\varepsilon(\omega) \equiv \varepsilon_1(\omega) + i\varepsilon_2(\omega)\,, \tag{2.36}$$

where $\varepsilon_1(\omega)$ and $\varepsilon_2(\omega)$ are the real and imaginary parts of dielectric function. When the electromagnetic radiation falls on crystal it interacts with the electrons of the crystal. We assume that the crystal is free of imperfections, the total Hamiltonian of the electromagnetic radiation on perfect crystal is given by

$$H = \frac{1}{2m}\left(\vec{P} + e\vec{A}\right)^2 + V(\vec{r}) \tag{2.37}$$

where $\vec{P}$ is the momentum, $\vec{A}$ and $V(\vec{r})$ are the vector potential and periodic crystal potential respectively.

The first order perturbation operator describing the interaction between the radiation and the electrons is

$$H_o\left(\vec{r},t\right) = \frac{e}{m}\left(\vec{A}.\vec{p}\right) \tag{2.38}$$

The vector potential for a plane wave can be written as,

$$\vec{A} = \vec{A}_o\hat{e}\exp\left[i\left(\vec{k}.\vec{r} - \omega t\right)\right] + c.c. \tag{2.39}$$

where $\hat{e}$ the unit vector of polarization in the direction of the electric field and *c.c.* is the complex conjugate. The second term is neglected which is the emission term and only the first term is considered which gives the absorption.

The transition probability for an electron going from an occupied valence state $E_v\left(\vec{k_v}\right)$ to an empty conduction state $E_c\left(\vec{k_c}\right)$ can be written as,

$$w\left(\omega,t,\vec{k_v},\vec{k_c}\right) = \frac{e^2}{m^2\hbar^2}\left|\int_0^t dt' \int_V d\vec{r}\,\psi_c\left(\vec{k_c},\vec{r},t\right)\vec{A}.\vec{p}\psi_v\left(\vec{k_v},\vec{r},t\right)\right|^2 \tag{2.40}$$

Here, Bloch type eigen functions ψ_c and ψ_v belongs to E_v and E_c respectively and can be written as

$$\psi_v\left(\vec{k_v},\vec{r},t\right)=\exp\left[-i\hbar^{-1}E_v\left(\vec{k_v}\right)t\right]\exp\left(i\vec{k_v}.\vec{r}\right).u_v\left(\vec{k_v},\vec{r}\right) \tag{2.41}$$

Here both u_v and u_c are the periodic wave functions with periodicity of the lattice.

Combining Eqs. 2.39, 2.40, 2.41, and using

$$\vec{E}=-\frac{\delta\vec{A}}{\delta t} \tag{2.42}$$

We get

$$w\left(\omega,t,\vec{k_v},\vec{k_c}\right)=\frac{e^2E_o^2}{m^2\omega^2}\left|\int_0^t dt'\exp\left[i\hbar^{-1}\left(E_c-E_v-\hbar\omega\right)t'\right].\vec{e}.\overrightarrow{M_{cv}}\right|^2 \tag{2.43}$$

with the matrix element

$$\vec{e}.\overrightarrow{M}_{cv}=\int_v d\vec{r}\exp\left[-i\left(\vec{k_c}-\vec{k}\right).\vec{r}\right]u_c^*\vec{e}.\vec{\nabla}\exp\left(i\vec{k_v}.\vec{r}\right)u_v \tag{2.44}$$

here the matrix element will vanish unless $\vec{k_c}-\vec{k}=\vec{k}_v+\vec{k}_n$,where $\vec{k}_n$ is the reciprocal lattice vector.

Since $\vec{k}=\frac{2\pi}{\lambda}$ is very small as compared to the linear dimensions of Brillouin Zone (BZ) it can be neglected. This gives the condition that that only vertical transitions without a change of the wave vector are allowed and is called direct transitions. The integration of Eq. 2.47 over *t'* gives

$$w\left(\omega,t,\vec{k_v},\vec{k_c}\right)=\frac{e^2E_o^2}{m^2\omega^2}\left|\frac{\exp\left[i\left(E_c-E_v-\hbar\omega\right)t/\hbar\right]-1}{i\left(E_c-E_v-\hbar\omega\right)/\hbar}\vec{e}.\overrightarrow{M}_{cv}\right|^2 \tag{2.45}$$

from which we obtain the transition probability per unit time as

$$\overrightarrow{W}_{cv}=\frac{\hbar e^2E_o^2}{2\pi^2m^2\omega^2}\int d\vec{k}\left|\vec{e}.\overrightarrow{M}_{cv}\right|^2\delta\left(E_c-E_v-\hbar\omega\right) \tag{2.46}$$

The δ function contains the second selection rule and transition probability is different from zero if the initial and final state energy difference is equal to photon energy.We can now obtain the

various optical constants as follows: The frequency dependent optical conductivity (σ) given by (Reshak, 2007),

$$\sigma(\omega)=2W_{cv}\hbar\omega/\vec{E}_0^2 \tag{2.47}$$

The imaginary part of dielectric function is

$$\varepsilon_2(\omega)=\frac{4\hbar^2e^2}{\pi m^2\omega^2}\int d\vec{k}\left|\vec{e}.\overrightarrow{M}_{cv}\right|^2\delta\left(E_c-E_v-\hbar\omega\right) \tag{2.48}$$

$$\varepsilon_2(\omega)=\frac{4\hbar^2e^2}{\pi m^2\omega^2}\int_c ds\frac{\left|\vec{e}.\overrightarrow{M}_{cv}\right|^2}{\left|\vec{\nabla}_k\left(E_c-E_v\right)\right|_{E_c-E_v=\hbar\omega}} \tag{2.49}$$

The real part of the dielectric function can be calculated using the Kramers-Kronig relations from imaginary part $\varepsilon_2(\omega)$,

$$\varepsilon_1(\omega)=1+\frac{2}{\pi}\int_0^\infty\frac{\omega'}{(\omega')^2-\omega^2}\varepsilon_2(\omega')d\omega' \tag{2.50}$$

The dielectric function is not directly accessible experimentally for the optical measurements, hence they have to be calculated from the other parameters. They are reflectivity $R(\omega)$, the refractive index $n(\omega)$ and extinction coefficient $k(\omega)$. These experimentally observable quantities are related to real and imaginary parts of the dielectric function as follows:

The optical reflectivity spectra are derived from the Fresnel's formula for normal incidence assuming an orientation of the crystal surface parallel to the optical axis using the relation (Ambrosch *et al*., 1998; Yu *et al*., 1999).

$$R(\omega)=\left|\frac{\sqrt{\varepsilon(\omega)}-1}{\sqrt{\varepsilon(\omega)}+1}\right|^2 \tag{2.51}$$

While the electron loss-function $\left(-I_m\left(\frac{1}{\varepsilon}\right)\right)$ is given by (Yu et al., 1999, Fox, 2002; Dressel *et al*., 2001)

$$-I_m\left(\frac{1}{\varepsilon}\right)=L(\omega)=\frac{\varepsilon_2(\omega)}{\varepsilon_1^2(\omega)+\varepsilon_2^2(\omega)} \tag{2.52}$$

We calculate the absorption coefficient I (ω) and real part of optical conductivity $\mathrm{Re}\left|\sigma(\omega)\right|$ using the following expression (Ambrosch *et al*., 1998; Delin *et al.,* 1996)

$$I(\omega)=\alpha(\omega)=2\omega\left[\frac{\sqrt{\varepsilon_1^2(\omega)+\varepsilon_2^2(\omega)}-\varepsilon_1(\omega)}{2}\right] \tag{2.53}$$

$$\mathrm{Re}\left|\sigma(\omega)\right|=\sigma(\omega)=\frac{\omega\varepsilon_1}{4\pi} \tag{2.54}$$

Also, the optical spectra such as the refractive index, $n(\omega)$ and the extinction coefficient, $K(\omega)$, are calculated in terms of the components of the complex dielectric function as follows (Delin *et al.,*1996, Fox, 2002; Dressel *et al*., 2001).

$$n(\omega)=\left\{\frac{\varepsilon_1(\omega)}{2}+\frac{\sqrt{\varepsilon_1^2(\omega)+\varepsilon_2^2(\omega)}}{2}\right\}^2 \tag{2.55}$$

$$K(\omega)=\left\{\frac{\sqrt{\varepsilon_1^2(\omega)+\varepsilon_2^2(\omega)}}{2}-\frac{\varepsilon_1(\omega)}{2}\right\}^2 \tag{2.56}$$

2.9 The WIEN2k Code

The calculations in this work are performed using the WIEN2k computer code (Blaha *et al.*, 2012). This code contains several sub-programs, few of which are described briefly below. There are two major parts in the program, the initialization and the selfconsistent field (SCF) cycle. The flow chart of the code is given in Fig. 2.2.

• **Initialization** (Setting up the unit cell and generating the initial density):

In this sub-program, atomic densities are generated and superimposed to obtain a initial crystal density for the SCF calculation. Additionally, the atomic potentials and optionally, atomic valence densities are created. Information about *l, m* values of the lattice harmonics representation and number of Fourier coefficients of the interstitial charge density are inserted as input file in this part.

• **LAPW0** (Construction of the effective potential):

The Poisson equation is solved and the total potential is computed as the sum of the Coulomb and the exchange-correlation potential in the LAPW0 program. The electron (spin) density is used as input and the spherical (l = 0) and the non-spherical parts of the potential are generated. The exchange-correlation potential is computed numerically on a grid. Additionally, the Hellmann-Feynman force contribution to the force is also determined.

• **LAPW1 (**Solving the Kohn-Sham equations of valence electrons):

The Hamiltonian and the overlap matrix are set up in LAPW1. Their diagonalization provides the eigenvalues and eigenvectors. Both the LAPW and the APW+lo methods are supported. For maximum efficiency a mix of both are recommended, i.e. the APW+lo basis functions are used for physically meaningful *l* values, while LAPW basis functions are employed to describe higher *l*-values functions.

• **LAPW2 (**Construction of the new electron density):

The Fermi-energy is computed. The electronic charge densities are expanded according to the representation of Eq. 2.30 for each occupied state and each k-vector. Afterwards the corresponding (partial) charges inside the atomic spheres are obtained by integration.

• **LCORE (**The treatment of the core electrons):

The potential and the charge density of the core electrons are computed.

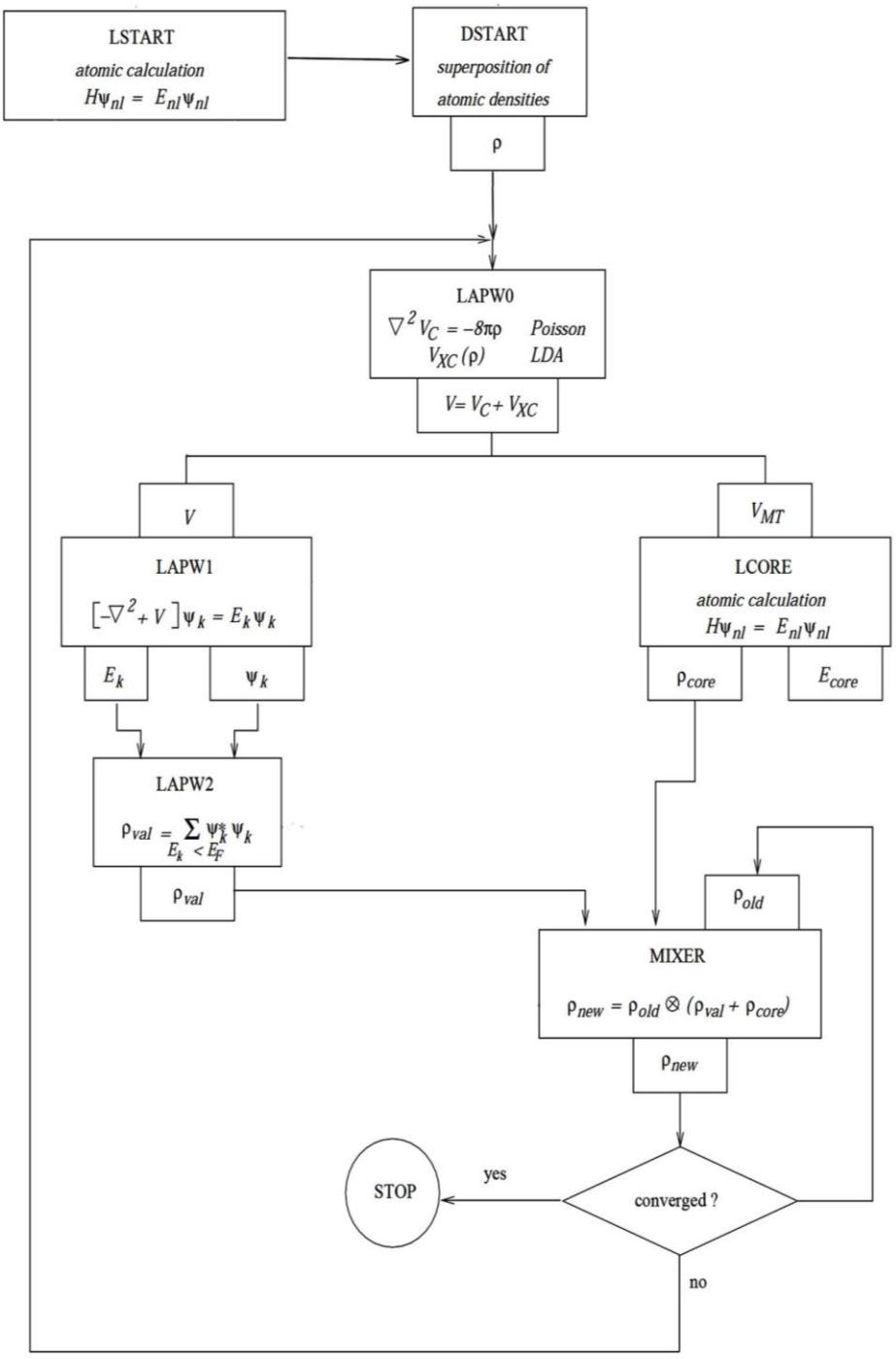

Fig. 2.2: Flow chart of WIEN2k code

• **LMIXER (**Generating the input density for the next iteration):

The electron densities of core, semi-core, and valence states are combined to yield the total new density. Taking only the new densities would, however, lead to instabilities in the iterative SCF process. To have a stable SCF cycle new and old densities need to be mixed, to obtain a new density.

$$n_{new}^{m+1} = (1-\alpha) n_{new}^{m} + \alpha n_{old}^{m} \tag{2.56}$$

here α is a mixing parameter. In the WIEN2k code this is done (mainly) using the Broyden scheme. The total energy and the atomic forces are computed in mixer, as well.

It is well known that for localized electrons LDA and GGA methods are not accurate enough for a proper description of some of the strongly correlated systems. Thus other methods like LDA+U and Orbital polarization are also implemented in this program. In WIEN2k (Blaha *et al*., 2012) the effective Coulomb- exchange interaction (U_{eff} = U −J) is used for the LDA+U calculations (Anisimov *et al.,* 1991, 1997). This particular scheme is used in WIEN2k to include double-counting corrections, however, it neglects multiple terms. It should be mentioned that the +U was used on top of GGA or LSDA parametrization of the exchange-correlation functional. A significant difference was observed using one or the other of the parameterizations.

Chapter-3

Study of Electronic Properties of Fluoride Perovskite ABF_3 with Alkali and Alkaline Earth Elements

In this chapter, we will present the results of calculations of the structural parameters like optimized lattice constants, equilibrium pressure and its derivative for the ABF_3. For our study here, we have chosen the combinations for alkali metals A and alkaline earth metals B as A = K, Rb, Cs, and B = Ca. The results of total and partial density of states and also the energy bands of these systems will be discussed here in the context of FP-LAPW model within density functional theory. The exchange correlations potentials used for the calculation is by using the GGA and mBJ potential, hence the results obtained is presented for both of these methods.

3.1 Structural Optimization

All physical and electronic properties of a solid are related to its structure, lattice constants and the total energy of the crystal. In this section, the calculations of structural optimization with cubical fluoride perovskite $ACaF_3$ (A= K, Rb, Cs) is presented. These calculations are performed with an exchange-correlation functional given by generalized gradient approximation (GGA) (Perdew *et al*., 1996) within the frame work of DFT (Hohenberg and Kohn 1964), where full-potential linearized augmented plane wave (FP-LAPW) (Singh, 1994) is adopted for the basis set. In this method the space is divided into non-overlapping muffin-tin (MT) spheres separated by an interstitial region (Fig. 2.1 of

Chapter 2), the detail of which is discussed in section 2.5 of Chapter 2. The basis functions are expanded into spherical harmonic functions inside the muffin-tin sphere and the Fourier series in the interstitial region. R_{MT} X K_{MAX} calculates the LAPW basis functions for the expansion of the charge density and the potential in the interstitial region and lattice harmonics for the expansion inside the muffin-tin spheres (where R_{MT} is the average radius of the muffin-tin spheres and K_{MAX} is the maximum value of the wave vector $\mathbf{K} = k + \mathbf{G}$). The convergence of basis set was controlled by a cutoff parameter R_{MT} X $K_{MAX} = 7$. Nonspherical contributions to the charge density and potential within the MT spheres were considered up to $l_{max} = 6$, while charge density and the potential were expanded as a Fourier series with wave vectors up to $G_{max} = 12$ $(a.u.)^{-1}$. The dependence of the total energy on the number of k points in the irreducible wedge of the first Brillouin zone has been explored within the linearized tetrahedron scheme (Bloch *et al.,* 1994). The cutoff energy which defines the separation of valence and core states was chosen as -6.0 Ry. Core states will be treated in a fully relativistic manner and the valence states are treated semi-relativistically. Self-consistency is achieved by setting the convergence of both the total energy and the eigen values to be smaller than 10^{-4} Ry.

The lattice constants that minimizes the total energy is the equilibrium lattice constant of a crystal. The structural relaxation was performed by volume optimization method based on Murnaghan's equation of states (Murnaghan, 1944). The lattice constant thus obtained from relaxed structure with minimum ground state energy is the theoretical equilibrium lattice constant which is used for the calculational purposes. We have calculated the total energy of the crystal in its equilibrium position. In order to investigate the synthesizability of the related compounds, the enthalpy (H) can be calculated by using the following relation,

$$H = E_0 + PV_0 \tag{3.1}$$

Where, P is the bulk pressure, V_O is bulk volume corresponds to minimum energy (E_o) of the system. The negative values of enthalpy indicate the stability of the compounds against decomposition into stable solid structures (Hao *et al.*, 2010). The calculated lattice constants, bulk modulus and its pressure derivative are given in Table 3.1.

In order to obtain the equilibrium lattice constant and the bulk modulus for the cubic perovskite $ACaF_3$, we performed the structural optimization by minimizing the total energy with respect to the cell parameters and the atomic positions. To study the crystal structure, we start with the total energy minimization of cubic $ACaF_3$ as a function of volume. This can be understood from the plots of the total energy as a function of volume which are shown in Figs. 3.2-3.4 for $KCaF_3$, $RbCaF_3$ and $CsCaF_3$ respectively. The energy versus volume data was fitted to a Murnaghan equation of state (Murnaghan, 1944) to obtain the equilibrium lattice constant (a), the bulk modulus (B) and its first pressure derivative (B'). We note that the result of the lattice constants obtained within our GGA calculations increases with the change of cation (A) from K to Cs which is similar to the experimental results and are shown in Table 3.1. From our calculations, we have found $KCaF_3$ has maximum value and $RbCaF_3$ has minimum value of B in compound $ACaF_3$ (A = K, Rb, Cs). From this calculation, the maximum pressure derivative (B') is found in $CsCaF_3$ compound and minimum value is found in $RbCaF_3$ compound which are given in Table 3.1

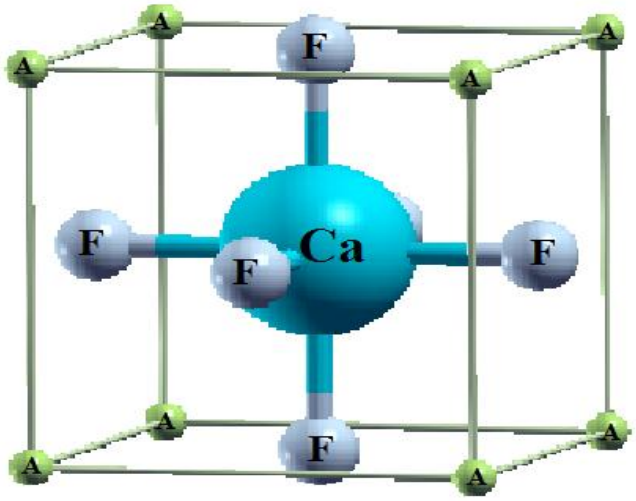

Fig. 3.1: Crystal structure for $ACaF_3$ (A = K, Rb, Cs)

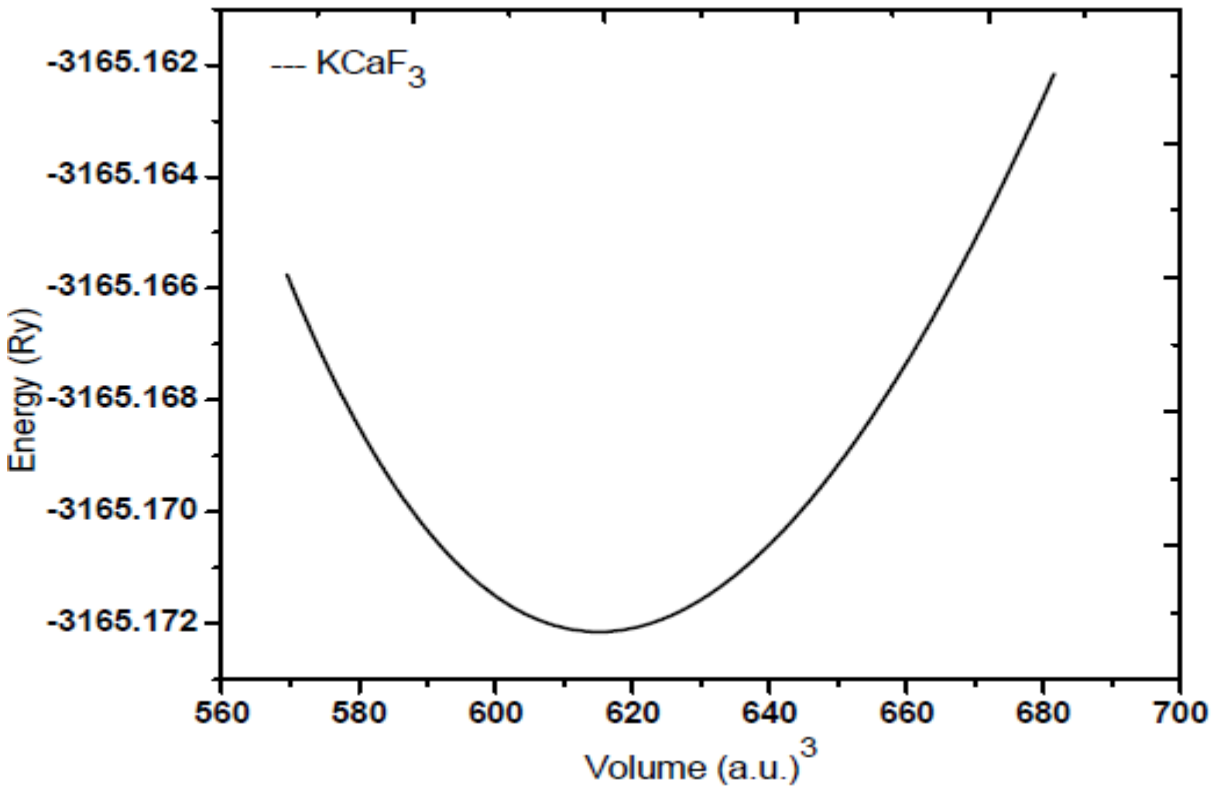

Fig. 3.2: Volume optimization curve for $KCaF_3$

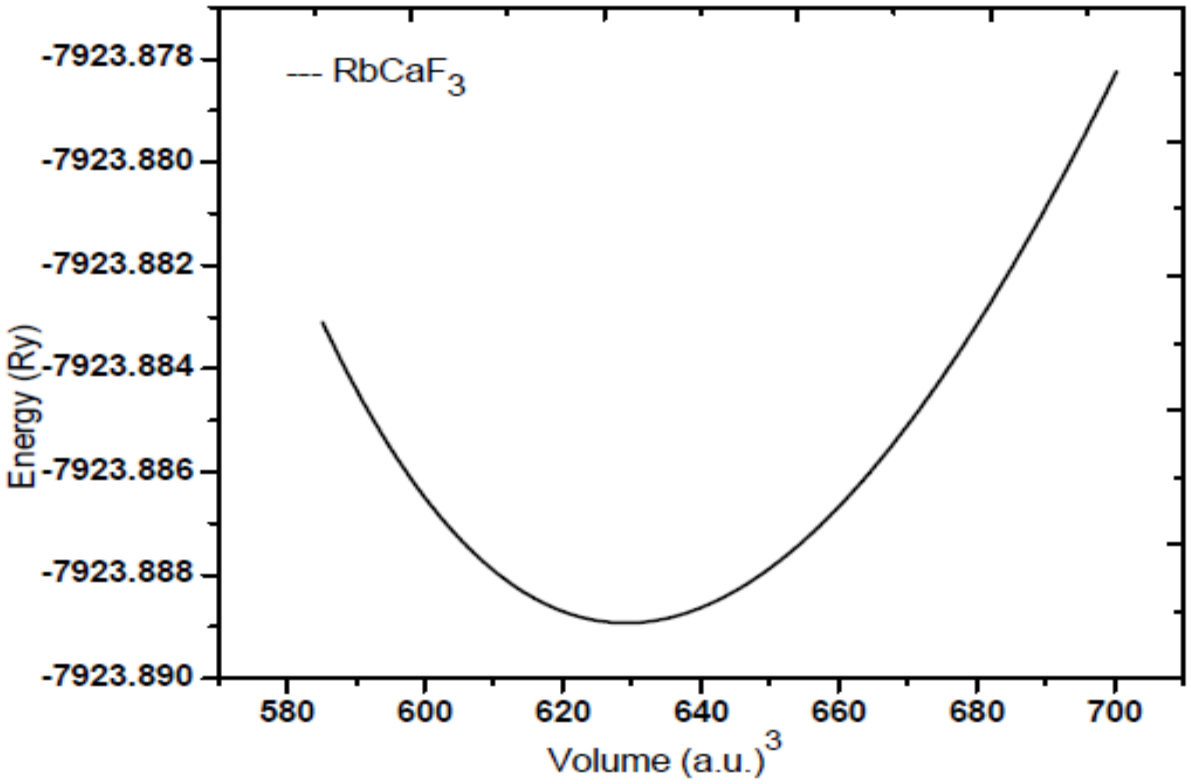

Fig. 3.3: Volume optimization curve for $RbCaF_3$

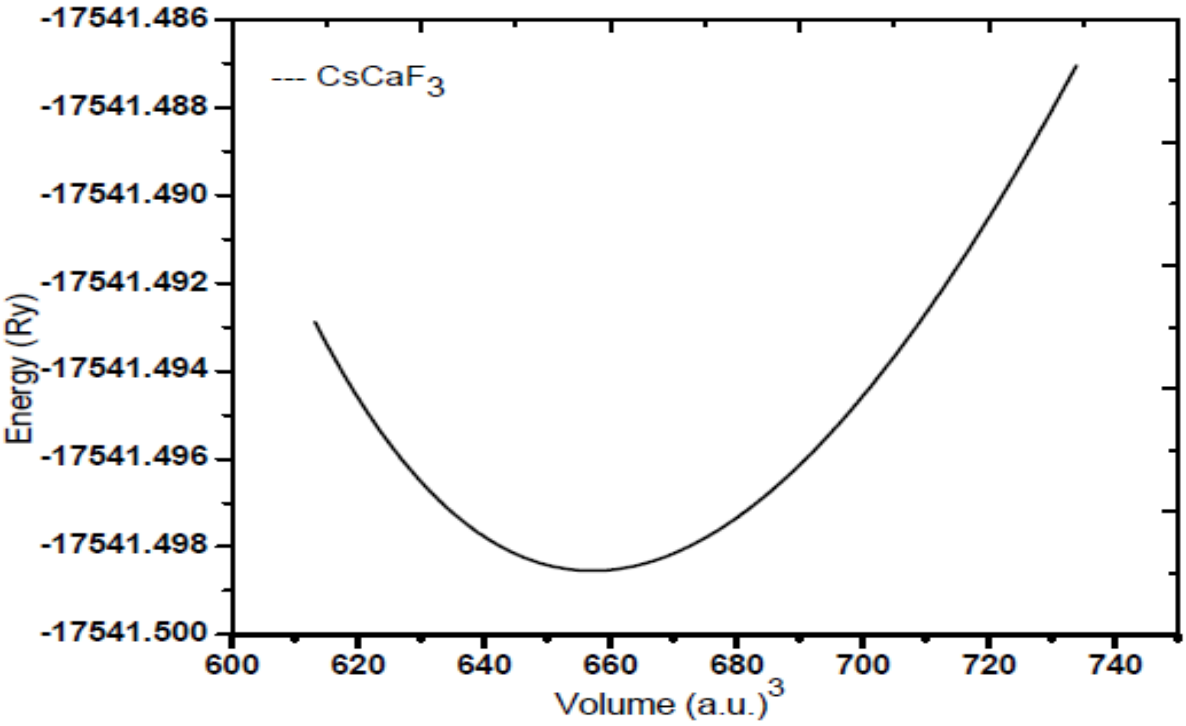

Fig. 3.4: Volume optimization curve for $CsCaF_3$

Table 3.1: Calculated lattice constant a (in Å), bulk modulus B (in GPa) and its pressure derivative B' of $ACaF_3$ are compared with other theoretical and experimental results.

Compounds	**Previous results a(in Å)**	**Calculated results a(in Å)**	**Previous results B(GPa)**	**Calculated results B(GPa)**	**Previous results B'**	**Calculated results B'**
$KCaF_3$	4.41[a] 4.529[b]	4.498 -	49.583[a] 46.0[b]	49.334 -	3.577[a] 3.95[b]	5.199 -
$RbCaF_3$	4.452[c] 4.455[d]	4.5134 -	49.77[c] -	48.067 -	5.00[c] -	4.967 -
$CsCaF_3$	4.5885[e] 4.52[f]	4.6007 -	45.77[e] -	48.1655 -	4.6278[e] -	5.8413 -

Theoretical

[a] (Babu *et al.*, 2015), [b] (Erdinc, 2011), [c] (Murtaza *et al*., 2013), [e] (Murat *et al.*, 2016), [f] (Jiang et al., 2006)

experimental

[d] (Bulou *et al.*, 1980), [f] (Jiang et al., 2006)

3.2 Study of Density of State (DOS) for Alkali and Alkaline Earth Elements

In this section, the results of calculations of density of states, will be presented for the combination of systems of choice namely $ACaF_3$ (A = K, Rb, Cs). Calculations for this purpose has been done by using the approximations for the exchange-correlation potentials such as GGA and mBJ under FP-LAPW method. The details of these methods have already been given in Chapter 2. In this method, the space is divided into non-overlapping muffin-tin (MT) spheres separated by an interstitial region. The basis functions are expanded into spherical harmonic functions inside the muffin-tin sphere ad the Fourier series in the interstitial region. The convergence of basis set was controlled by a cutoff parameter R_{MT} X K_{max} = 7 where R_{MT} is the smallest of the MT sphere radii and K_{max} is the largest reciprocal lattice vector used in the plane wave expansion. The cutoff energy which defines the separation of valence and core states was chosen as -6.0 Ry. For k point sampling, a 1000 k-point mesh in the first Brillouin zone was used. The self-consistent calculations were considered to be converged until the integrated charge difference between the last two iterations was less than 10^{-4} eV. Even though the ground state is well described by GGA, the values of the band gaps are sometimes underestimated. For this reason we have the modified Becke Johnson potential (mBJ) to calculate for improved values of the band gaps (Perdew *et al.*, 1996) for all the systems. The theoretically obtained lattice parameters calculated in Chapter 3 have been used here for DOS and energy bands calculations. We present in this section the results of total DOS and partial DOS in the case of $ACaF_3$ (A = K, Rb, Cs). The

DOS for these systems had been calculated using the same method but for the exchange correlation potential calculated by GGA and mBJ approximations.

3.2.1 Calculation of DOS by using GGA method for Alkali and Alkaline Earth Elements

(a) $KCaF_3$

In this section the calculated results of total density of states (TDOS) and partial density of states (PDOS) for $KCaF_3$ compound are given. The plot of TDOS of $KCaF_3$ and individual atoms K, Ca and F are given in Fig.3.5. In the valence region below the Fermi level, we have found the maximum peak in TDOS for $KCaF_3$ at - 0.27 eV. The occurrence of this maximum in peak in TDOS of $KCaF_3$ at -0.27 eV appears to be the contribution due to F atom. The reason being that the TDOS of F atom is also maximum at -0.27 eV. Also in valence band region, we find from the plots that the contributions to the origin of peak in TDOS of $KCaF_3$ by other atoms K and Ca is very low and hence are negligible. Similarly, in the conduction band above the Fermi level in Fig. 3.5, the maximum peak in TDOS for $KCaF_3$ is observed at 9.68 eV. The occurrence of this maximum in peak in TDOS of $KCaF_3$ at 9.68 eV is due to the main contribution by Ca atom. The reason being that the TDOS of Ca atom is also maximum at 9.68 eV. We find from the plots in Fig. 3.5, TDOS of $KCaF_3$ by other atoms K and F are very low.

In Fig. 3.6, the plots of TDOS and partial density of states (PDOS) of K atom in $KCaF_3$ compound are shown. In the valence band, we have found that there is negligible contribution to TDOS and PDOS by electrons of K atom. However in the conduction band region, we find from the plots that the maximum peak in TDOS occurs at 11.92 eV. This is

due to the main contribution by the K-d_{t2g} electrons of K atom. The reason being that the maxima of PDOS of K-d_{t2g} is also found at 11.92 eV.

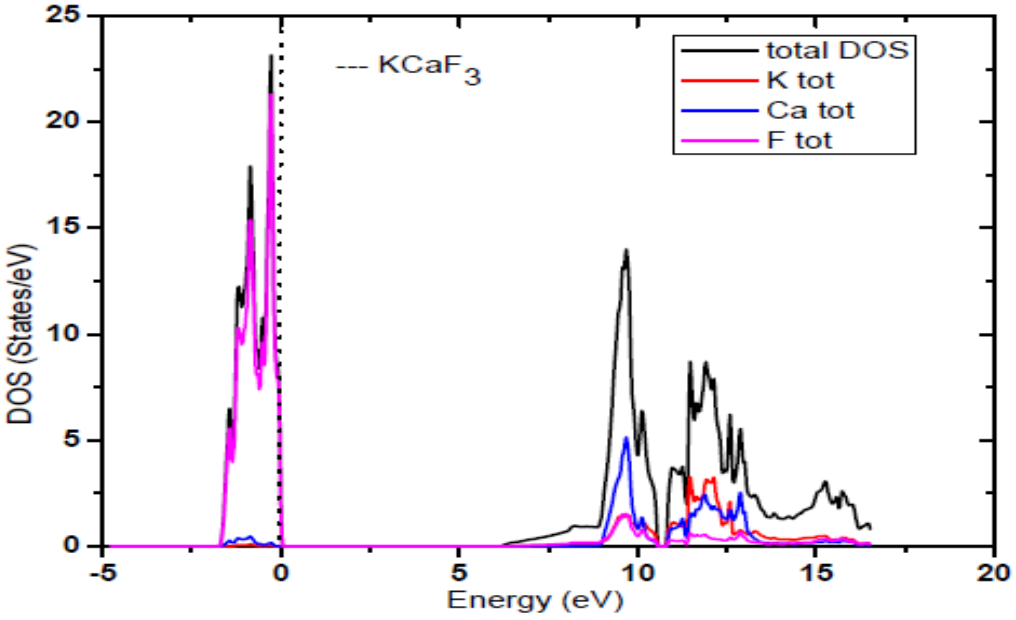

Fig. 3.5: Plots of total DOS for $KCaF_3$ and atoms K, Ca, F

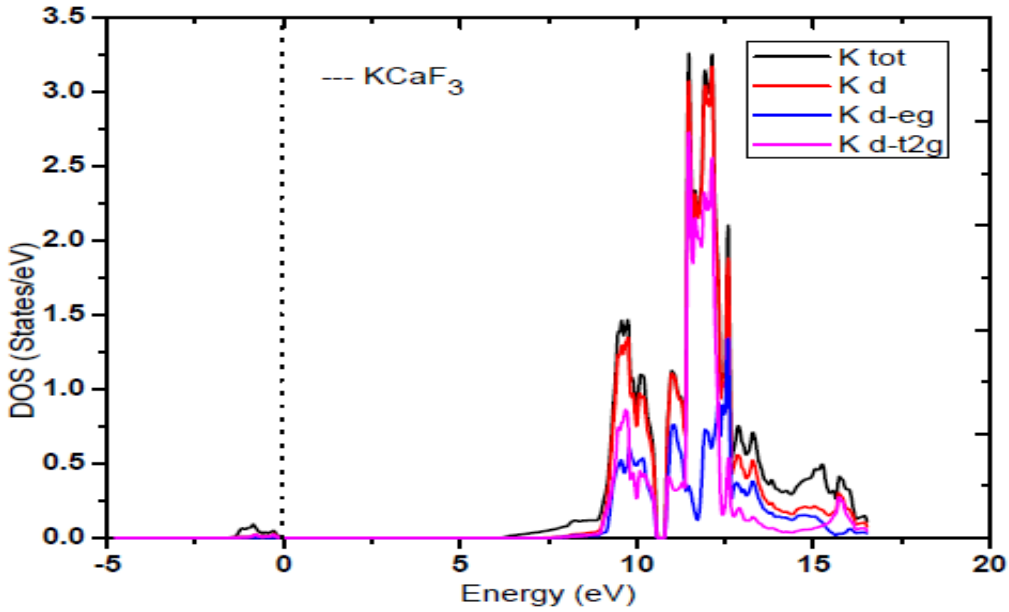

Fig. 3.6: Total and partial DOS plots of atom K

Fig.3.7 shows the plot of TDOS and PDOS of Ca atom of $KCaF_3$ compound. There is negligible contribution to TDOS and PDOS in the valence band below the Fermi level by Ca atom. However in the conduction band, a maximum peak in TDOS is observed at 9.68 eV in the conduction band. This can be attributed to Ca- d_{t2g} state electrons as shown in Fig. 3.7.

The plot of TDOS and PDOS of F atom in $KCaF_3$ compound is shown in Fig. 3.8. The maximum peak in TDOS is found at - 0.27 eV in the valence region below the Fermi level. From the plot we find that the contribution to the occurrence of this peak at -0.27 eV is due to the contribution by F_{px+py} state electrons. There is negligible contribution to TDOS and PDOS in conduction band in F atom as shown in Fig. 3.8.

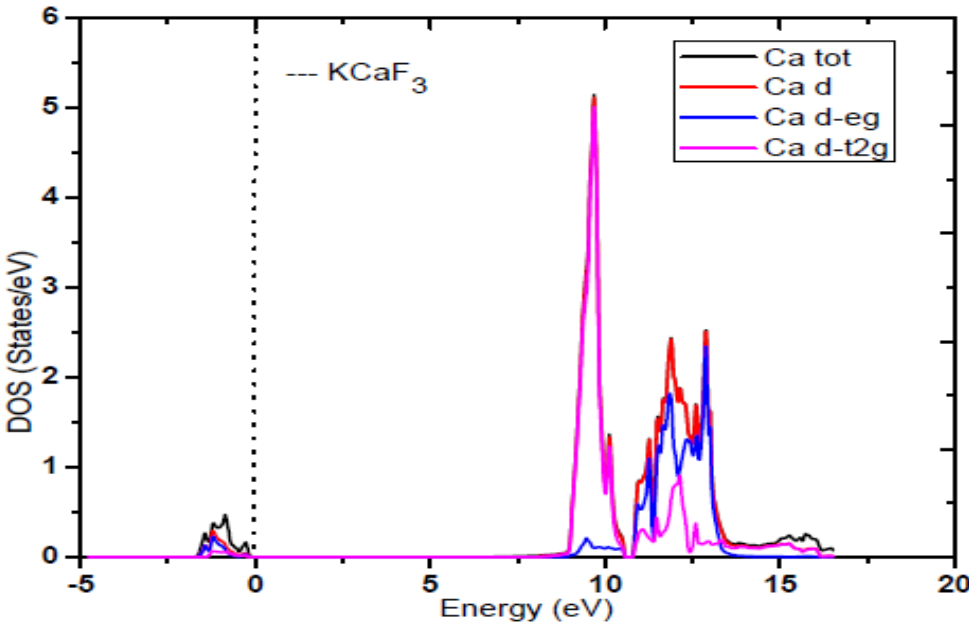

Fig. 3.7: Total and partial DOS plots of atom Ca

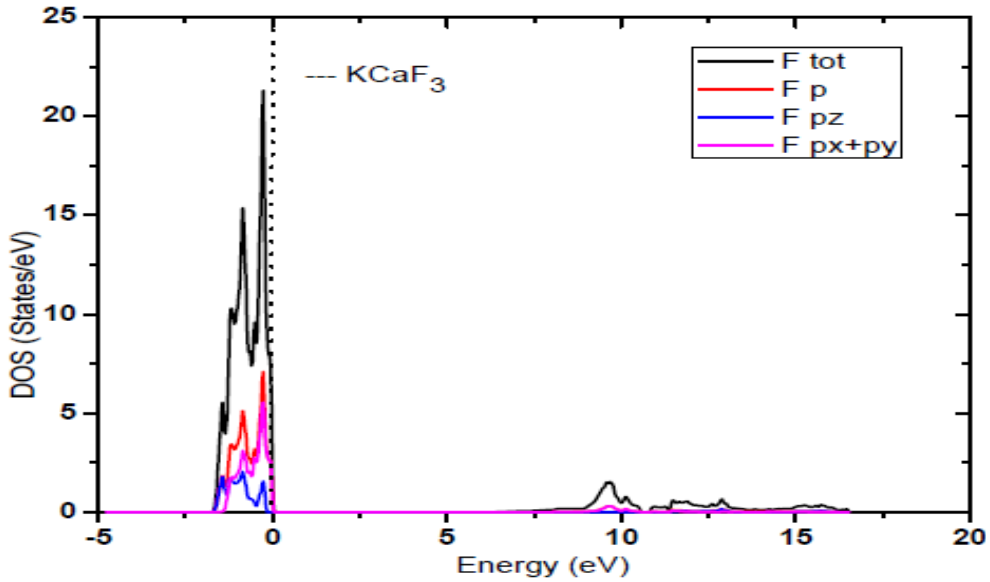

Fig. 3.8: Total and partial DOS plots of atom F

(b) $RbCaF_3$

The calculated results of total density of states (TDOS) and partial density of states (PDOS) for $RbCaF_3$ compound are given in this section. Fig.3.9 shows the plot of total density of states (TDOS) for $RbCaF_3$ and individual atoms Rb, Ca, and F. In the valence band region below the Fermi level, we have found the maximum peak in TDOS for $RbCaF_3$ at -0.25 eV. The occurrence of this maximum in peak in TDOS of $RbCaF_3$ at -0.25 eV appears to be the contribution due to F atom. The reason being that the TDOS of F atom is also maximum at -0.25 eV. Also in valence band region, we find from the plots that the contributions to the origin of peak in TDOS of $RbCaF_3$ by other atoms Rb and Ca is very low and hence are negligible. Similarly, in the conduction band above the Fermi level in Fig. 3.9, the maximum peak in TDOS for $RbCaF_3$ is observed at 9.51 eV. The occurrence of this maximum in peak in TDOS of $RbCaF_3$ at 9.51 eV is due to the main contribution by Ca atom. We find from the plots in Fig. 3.9, TDOS of $RbCaF_3$ by other atoms Rb and F are very low.

In Fig. 3.10, the plots of TDOS and partial density of states (PDOS) of Rb atom in $RbCaF_3$ compound are shown. In the valence band, we have found that there is negligible contribution to TDOS and PDOS by electrons of Rb atom. However in the conduction band region, we find from the plots that the maximum peak in TDOS occurs at 12.5 eV. This is due to the main contribution by the Rb-d_{t2g} electrons of Rb atom. The reason being that the maxima of PDOS of Rb-d_{t2g} is also found at 12.5 eV which is seen in Fig. 3.10.

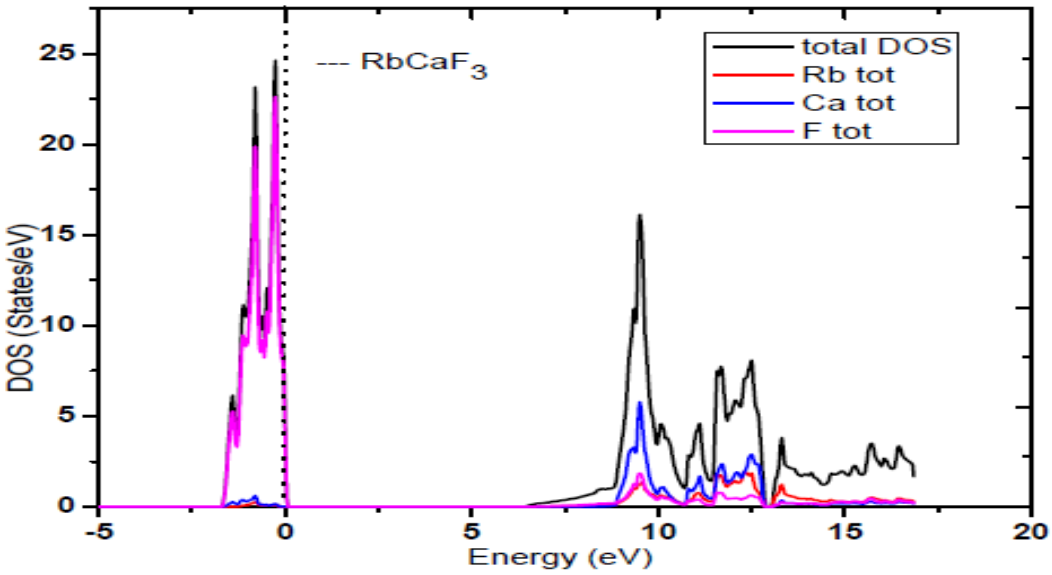

Fig. 3.9: Total DOS plots for $RbCaF_3$ and atoms Rb, Ca, F

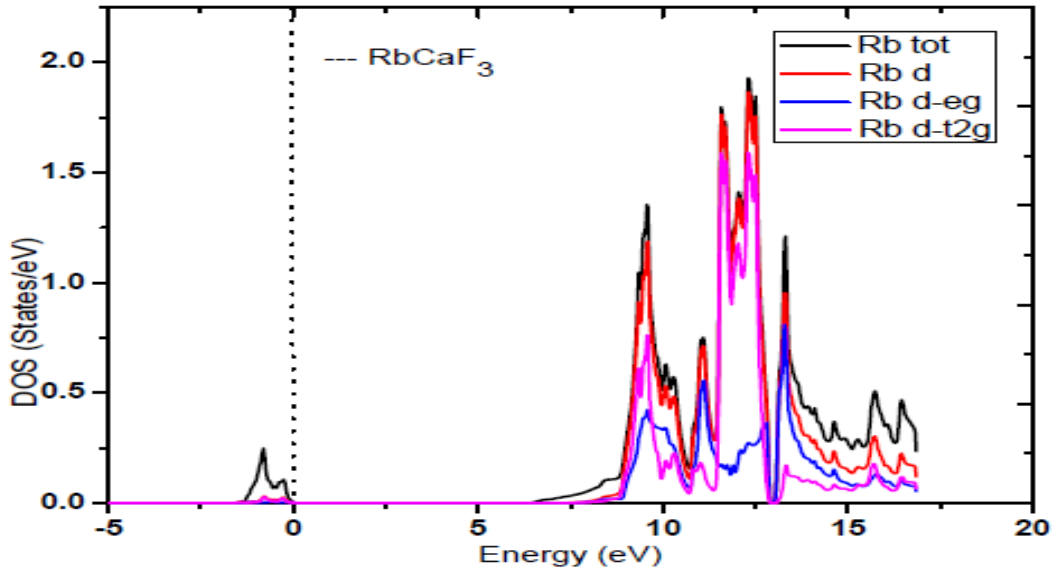

Fig. 3.10: Total and partial DOS plots for Rb atom

Fig.3.11 shows the plot of TDOS and PDOS of Ca atom of $RbCaF_3$ compound. There is negligible contribution to TDOS and PDOS by Ca atom in the valence band below the Fermi level. However in the conduction band, a maximum peak in TDOS is observed at 9.51 eV in the conduction band. This can be attributed to Ca-d_{t2g} state electrons as shown in Fig. 3.11.

The plot of TDOS and PDOS of F atom in $RbCaF_3$ compound is shown in Fig. 3.12. The maximum peak in TDOS is found at - 0.25 eV in the valence region below the Fermi level. From the plot we find that the contribution to the occurrence of this peak at -0.25 eV is due to the contribution by F_{px+py} state electrons. There is negligible contribution to TDOS and PDOS in conduction band in F atom as shown in Fig. 3.12.

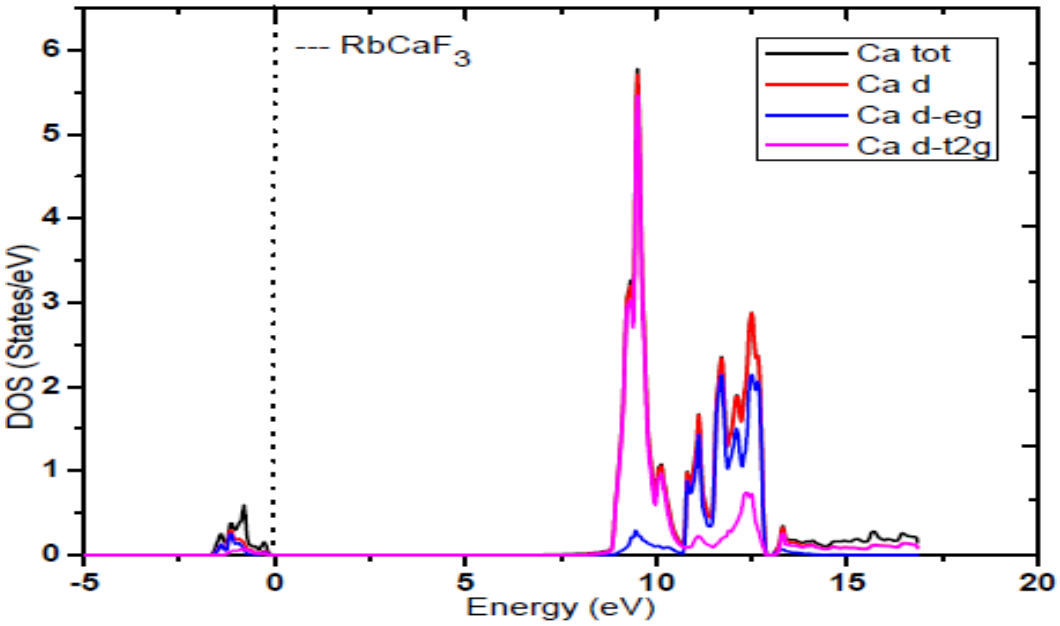

Fig. 3.11: Total and partial DOS plots for Ca atom

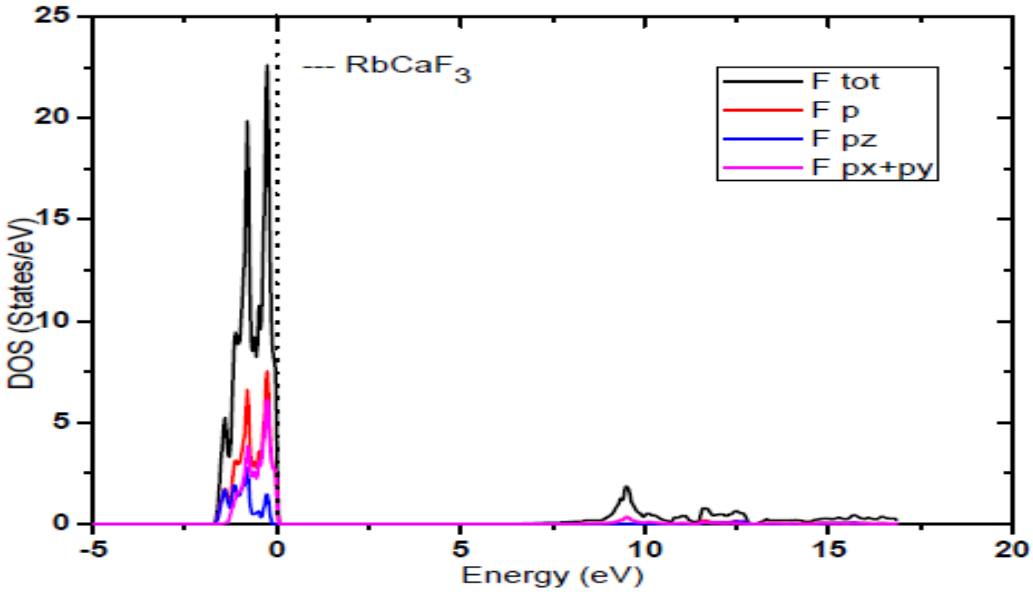

Fig. 3.12: Total and partial DOS plots for F atom

(c) $CsCaF_3$

The calculated results of total density of states (TDOS) and partial density of states (PDOS) for $CsCaF_3$ compound are given in this section. Fig.3.13 shows the plot of total density of states (TDOS) for $CsCaF_3$ and individual atoms Cs, Ca, and F. In the valence region below the Fermi level, we have found the maximum peak in TDOS for $CsCaF_3$ at -0.51 eV. The occurrence of this maximum in peak in TDOS of $CsCaF_3$ at -0.51 eV appears to be the contribution due to F atom. The reason being that the TDOS of F atom is also maximum at -0.51 eV. Also in valence band region, we find another peak in TDOS of $CsCaF_3$ at - 4.51 eV. The occurrence of this maximum in peak in TDOS of $CsCaF_3$ at -4.51 eV appears to be the contribution due to Cs atom. The reason being that the TDOS of Cs atom is also maximum at -4.51 eV. We have found from the plots that the contributions to the origin of peak in TDOS of $CsCaF_3$ by other atom Ca is very low and hence is negligible. Similarly, in the conduction band above the Fermi level in Fig. 3.13, the maximum peak in TDOS for $CsCaF_3$ is observed at 8.79 eV. The occurrence of this maximum in peak in TDOS of $RbCaF_3$ at 8.79 eV is due to the main contribution by Ca atom. We find from the plots in Fig. 3.13, TDOS of $CsCaF_3$ by other atoms Cs and F are very low.

In Fig. 3.14, the plots of TDOS and partial density of states (PDOS) of Cs atom in $CsCaF_3$ compound are shown. In the valence band, we have found that the maximum peak in TDOS occurs at – 4.51 eV. This is due to the main contribution by the Cs-*p* electrons of Cs atom. However in the conduction band region, we find from the plots that a small peak in TDOS occurs at 8.79 eV. This is due to the main contribution by the Cs-d_{t2g} states of electrons of Cs atom. The reason is that the peak of PDOS of Cs-d_{t2g} is also found at 8.79 eV which is seen in Fig. 3.14.

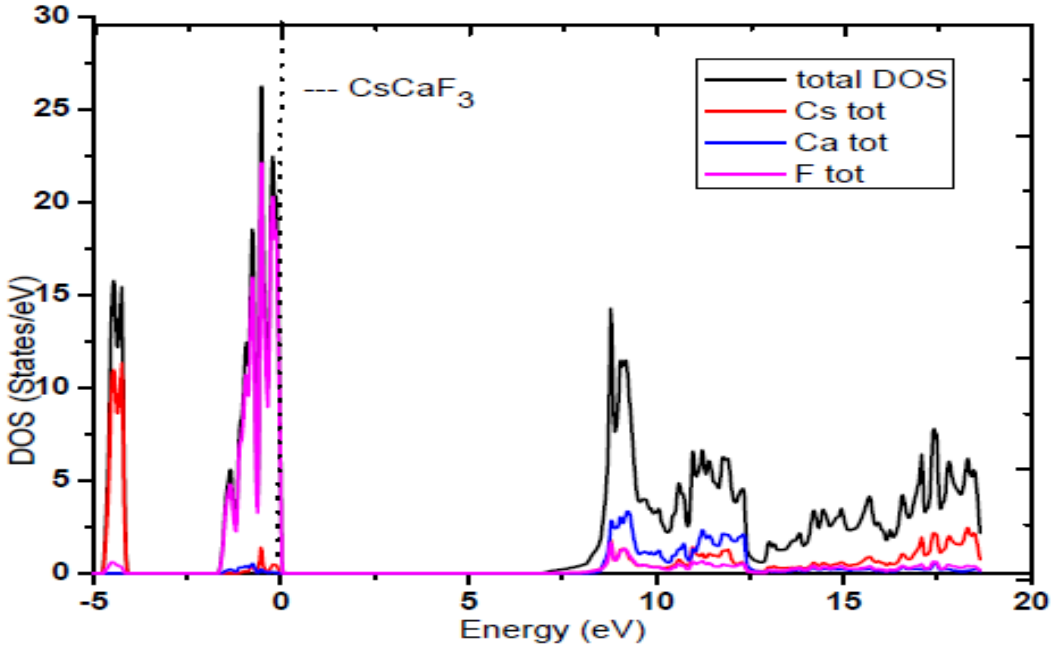

Fig. 3.13: Total DOS plots for $CsCaF_3$ and atoms Cs, Ca, F

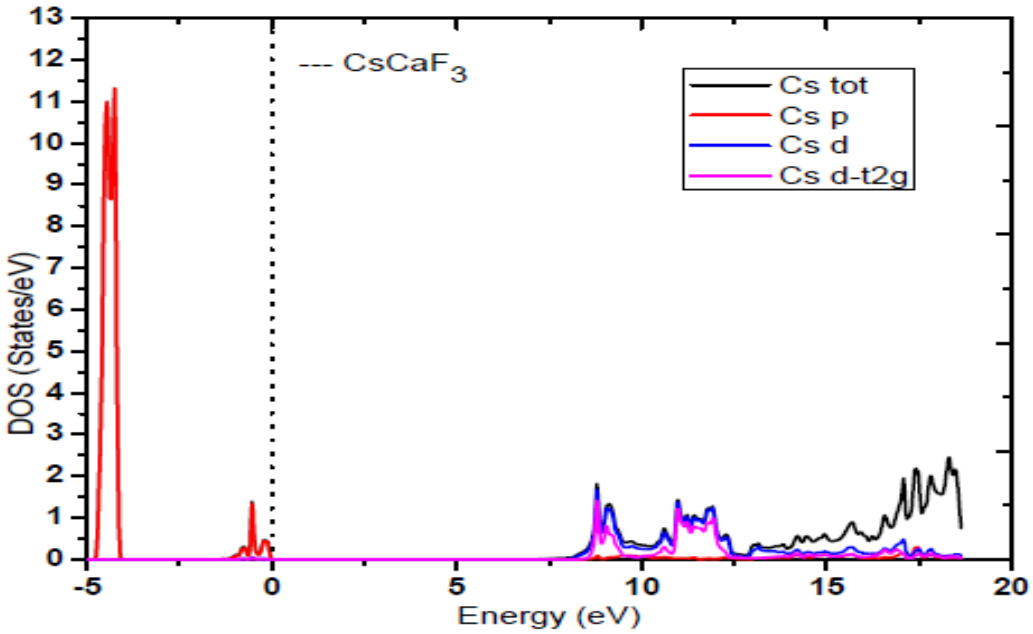

Fig. 3.14: Total and partial DOS for atom Cs

Fig.3.15 shows the plot of TDOS and PDOS of Ca atom of $CsCaF_3$ compound. There is negligible contribution to TDOS and PDOS by Ca atom in the valence band below the Fermi level. However in the conduction band, a maximum peak in TDOS is observed at 9.25 eV. This can be attributed to Ca-d_{t2g} state electrons of atom Ca as shown in Fig. 3.15.

The plot of TDOS and PDOS of F atom in $CsCaF_3$ compound is shown in Fig. 3.16. The maximum peak in TDOS is found at - 0.21 eV in the valence region below the Fermi level. From the plot we find that the contribution to the occurrence of this peak at -0.21 eV is due to the contribution by F_{px+py} state electrons. There is negligible contribution to TDOS and PDOS in conduction band region in F atom as shown in Fig. 3.16.

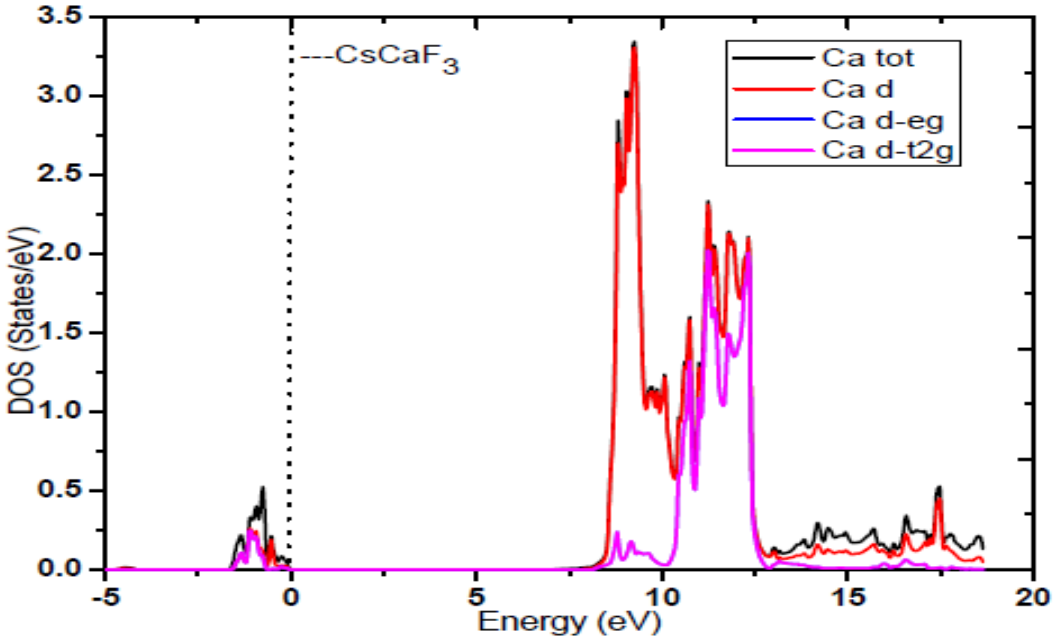

Fig. 3.15: Total and partial DOS for atom Ca

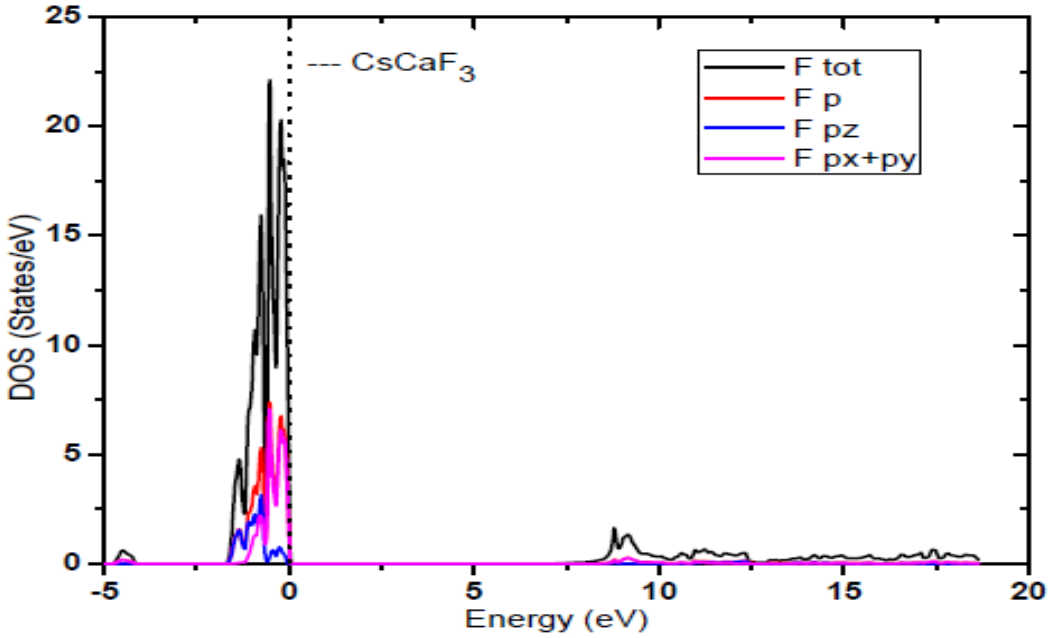

Fig. 3.16: Total and partial DOS for atom F

3.2.2 Calculation of DOS by using mBJ method for Alkali and Alkaline Earth Elements

(a) $KCaF_3$

The calculated results of total density of states (TDOS) and partial density of states (PDOS) for $KCaF_3$ compound are given in this section. Fig.3.17 shows the plot of total density of states (TDOS) for $KCaF_3$ and individual atoms K, Ca, and F. In the valence region below the Fermi level, we have found the maximum peak in TDOS for $KCaF_3$ at -0.21 eV. The occurrence of this maximum in peak in TDOS of $KCaF_3$ at -0.21 eV appears to be the contribution due to F atom. The reason being that the TDOS of F atom is also maximum at -0.21 eV. We have found from the plots that the contributions to the origin of peak in TDOS of $KCaF_3$ by other atoms K and Ca are very low and hence is negligible. Similarly, in the conduction band above the Fermi level in Fig. 3.17, the maximum peak in TDOS for $KCaF_3$ is observed at 11.12 eV. The occurrence of this maximum in peak in TDOS of $KCaF_3$ at 11.12 eV is due to the main contribution by Ca atom. We find another peak in TDOS of $KCaF_3$ at 13.27 eV from the plots in Fig. 3.17 due to the main contribution of K atom. TDOS of $KCaF_3$ by other atom F is very low.

In Fig. 3.18, the plots of TDOS and partial density of states (PDOS) of K atom in $KCaF_3$ compound are shown. In the valence band, we have found that there is negligible contribution to TDOS and PDOS by electrons of K atom. However in the conduction band region, we find from the plots that the maximum peak in TDOS occurs at 13.27 eV. This is due to the main contribution by the K-d_{t2g} electrons of K atom. The reason being that the maxima of PDOS of K-d_{t2g} is also found at 13.27 eV.

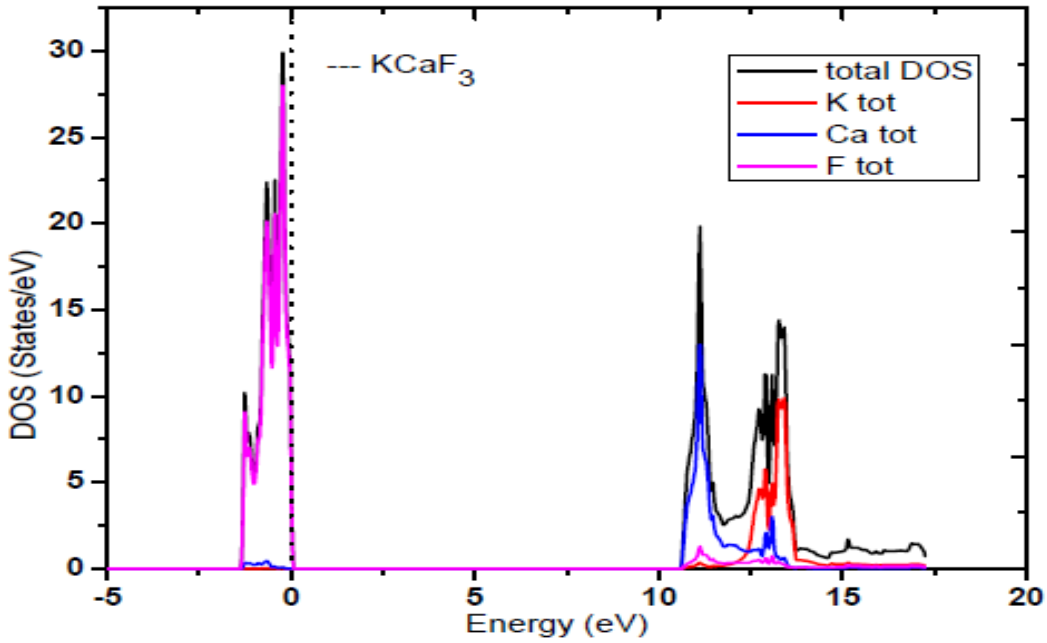

Fig. 3.17: Total DOS plots for $KCaF_3$ and atoms K, Ca, F

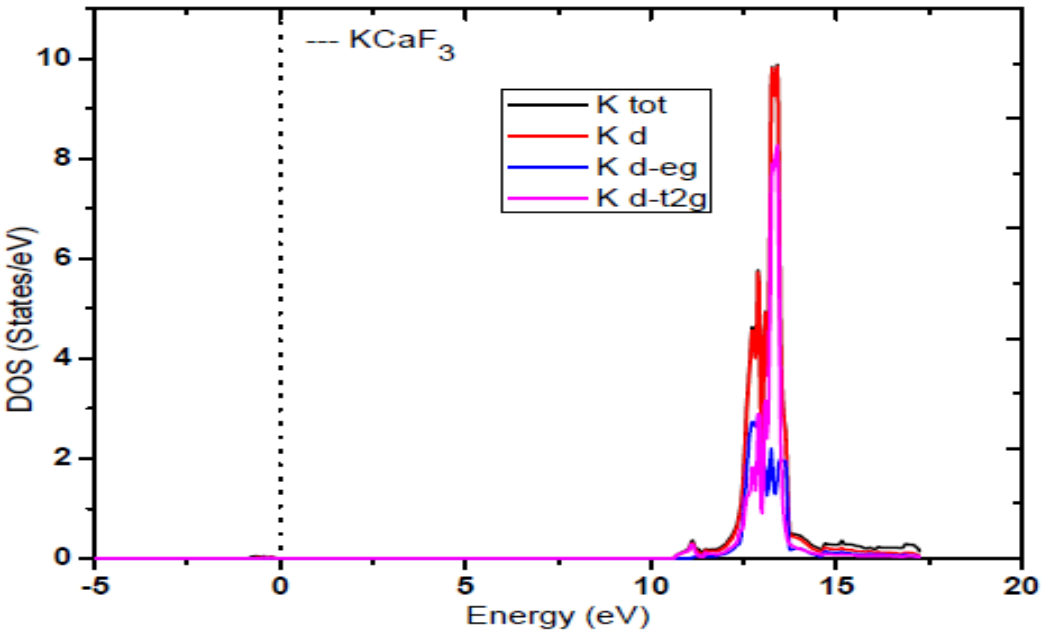

Fig. 3.18: Total and partial DOS plots for atom K

Fig.3.19 shows the plot of TDOS and PDOS of Ca atom of $KCaF_3$ compound. There is negligible contribution to TDOS and PDOS in the valence band below the Fermi level by Ca atom. However in the conduction band, a maximum peak in TDOS is observed at 11.12 eV in the conduction band. This can be attributed to Ca-d_{t2g} state electrons which is shown in Fig. 3.19.

The plot of TDOS and PDOS of F atom in $KCaF_3$ compound is shown in Fig. 3.20. From this plot, we have observed a narrow peak in TDOS at – 0.21 eV in the valence region below the Fermi level. From the plot we find that the contribution to the occurrence of this peak at -0.21 eV is due to the contribution by F_{px+py} state electrons of atom F. There is negligible contribution to TDOS and PDOS in conduction band in F atom as shown in Fig. 3.20.

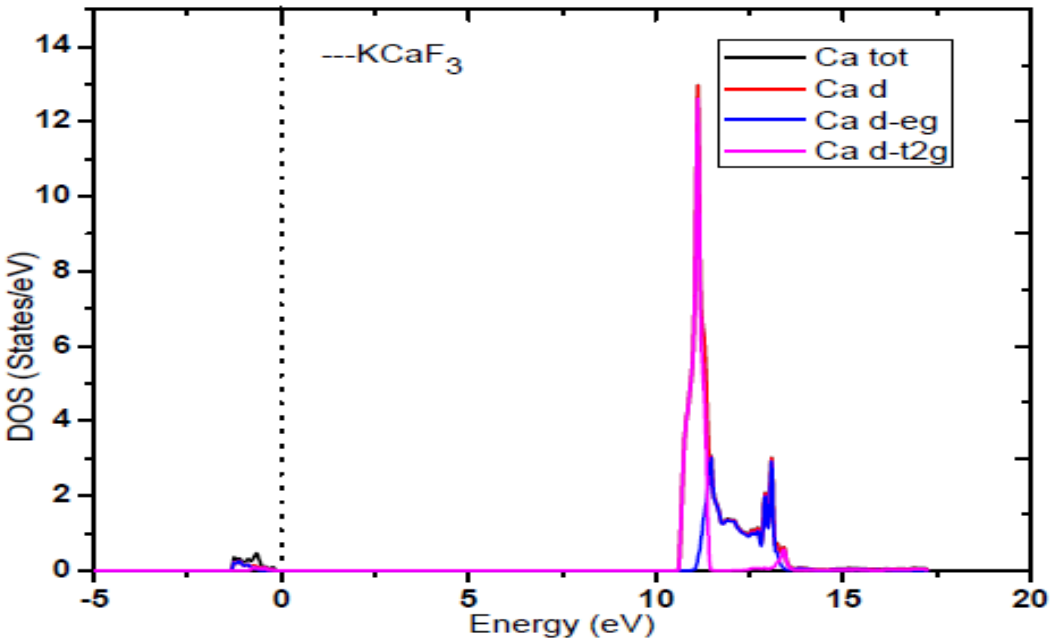

Fig. 3.19: Total and partial DOS plots for atom Ca

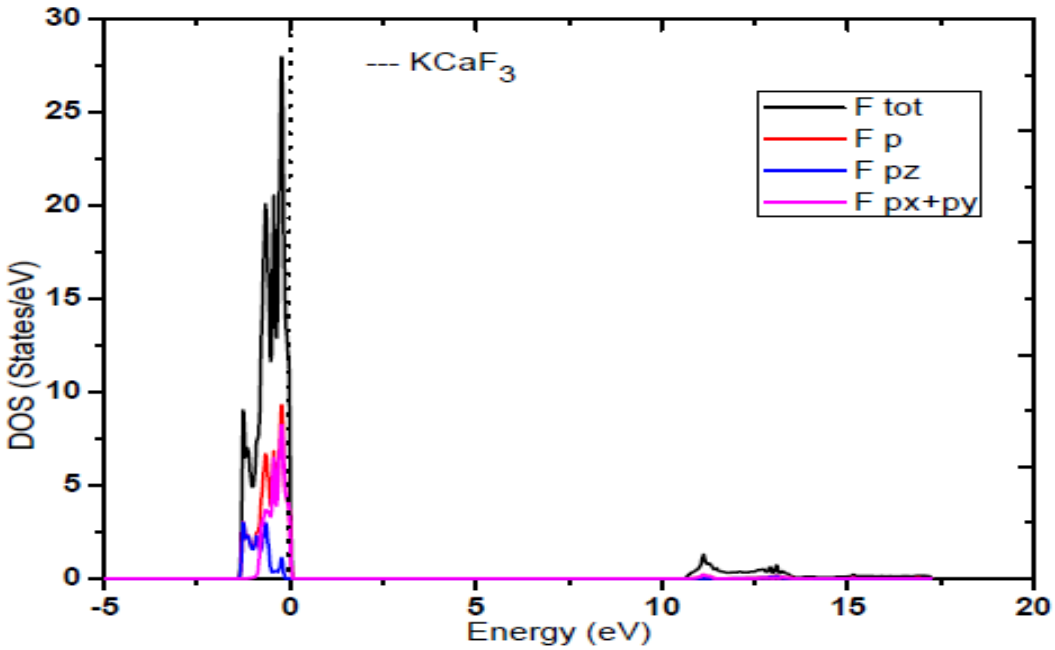

Fig. 3.20: Total and partial DOS plots for atom F

(b) $RbCaF_3$

The calculated results of total density of states (TDOS) and partial density of states (PDOS) for $RbCaF_3$ compound are given in this section. Fig.3.21 shows the plot of total density of states (TDOS) for $RbCaF_3$ and individual atoms Rb, Ca, and F. In the valence region below the Fermi level, we have found the maximum peak in TDOS for $RbCaF_3$ at -0.21 eV. The occurrence of this maximum in peak in TDOS of $RbCaF_3$ at -0.21 eV appears to be the contribution due to F atom. The reason being that the TDOS of F atom is also maximum at -0.21 eV. Also in valence band region, we find from the plots that the contributions to the origin of peak in TDOS of $RbCaF_3$ by other atoms Rb and Ca is very low and hence are negligible. Similarly, in the conduction band above the Fermi level in Fig. 3.21, the maximum peak in TDOS for $RbCaF_3$ is observed at 10.99 eV. The occurrence of this maximum in peak in TDOS of $RbCaF_3$ at 10.99 eV is due to the main contribution by Ca atom. We find another peak in TDOS of $RbCaF_3$ by the contribution of other atom Rb at 13.33 eV in the conduction band in Fig. 3.21. We find very low contribution in TDOS of $RbCaF_3$ by other atom F.

In Fig. 3.22, the plots of TDOS and partial density of states (PDOS) of Rb atom in $RbCaF_3$ compound are shown. In the valence band, we have found that there is negligible contribution to TDOS and PDOS by electrons of Rb atom. However in the conduction band region, we find from the plots that the maximum peak in TDOS occurs at 13.33 eV. This is due to the main contribution by the Rb-d_{t2g} electrons of Rb atom. The reason being that the maximum of PDOS of Rb-d_{t2g} is also found at 13.33 eV which is seen in Fig. 3.22.

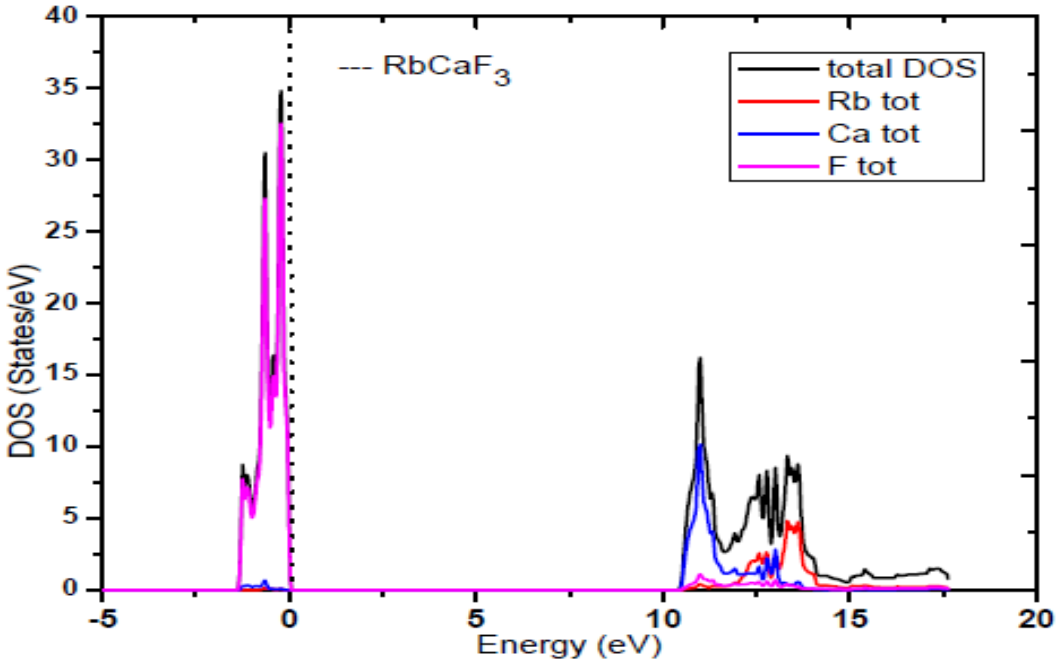

Fig. 3.21: Total DOS plots for $RbCaF_3$ and atoms Rb, Ca, F

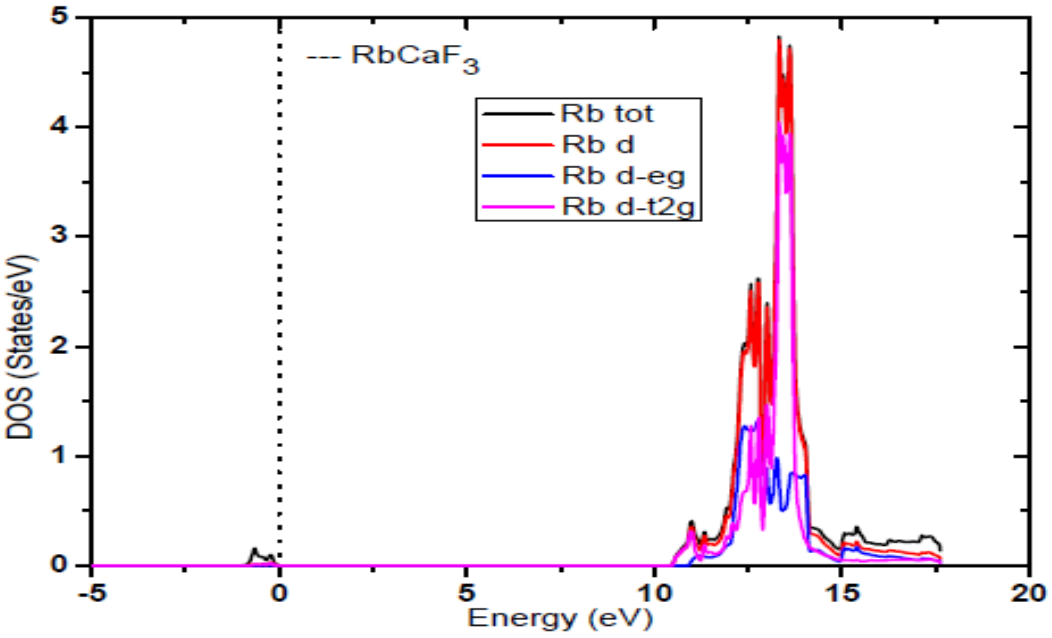

Fig.3.22: Total and partial DOS plots for atom Rb

Fig.3.23 shows the plot of TDOS and PDOS of Ca atom of $RbCaF_3$ compound. There is negligible contribution to TDOS and PDOS by Ca atom in the valence band below the Fermi level. However in the conduction band, a maximum peak in TDOS is found at 10.99 eV. This can be attributed to Ca-d_{t2g} state electrons of atom Ca as shown in Fig. 3.23.

The plot of TDOS and PDOS of F atom in $RbCaF_3$ compound is shown in Fig. 3.24. The maximum peak in TDOS is found at - 0.21 eV in the valence region below the Fermi level. From the plot we find that the contribution to the occurrence of this peak at -0.21 eV is due to the contribution by F_{px+py} state electrons. There is negligible contribution to TDOS and PDOS in conduction band in F atom as shown in Fig. 3.24.

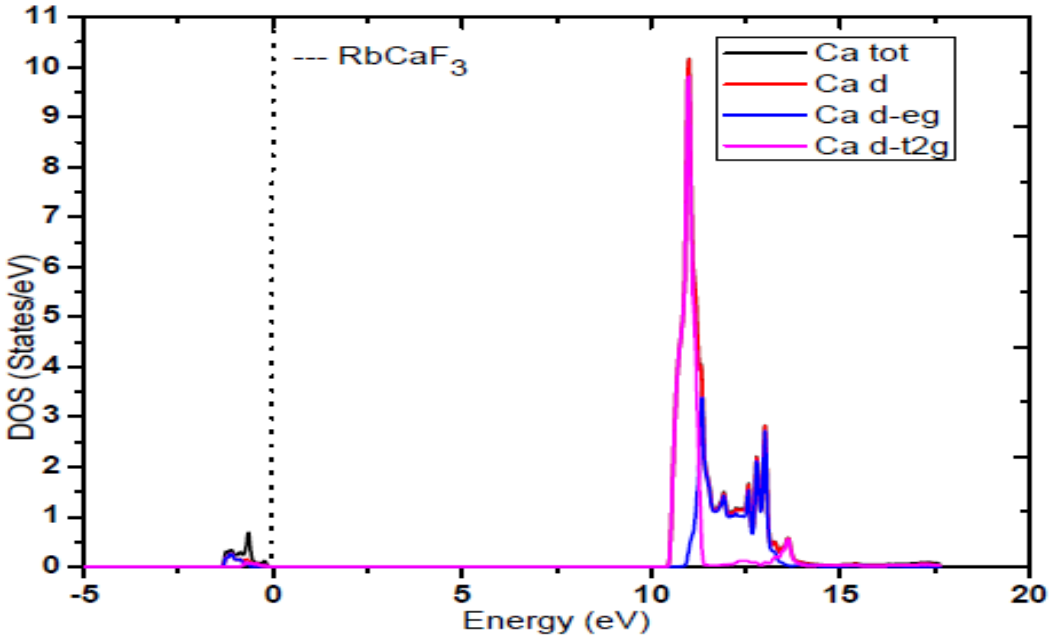

Fig. 3.23: Total and partial DOS plots for atom Ca

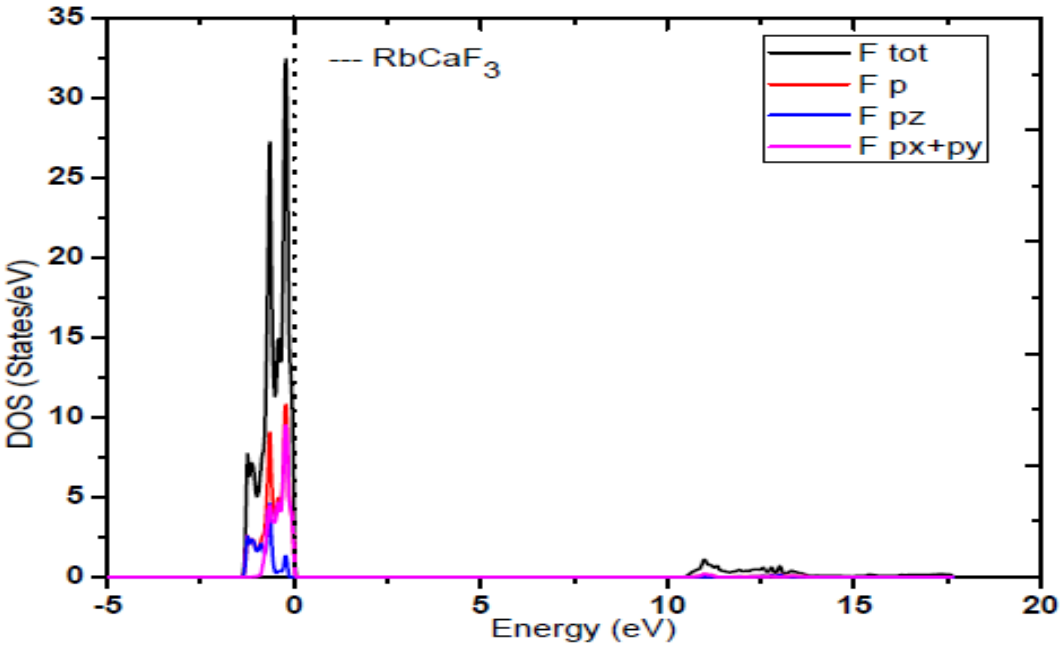

Fig. 3.24: Total and partial DOS plots of atom F

(c) $CsCaF_3$

The calculated results of total density of states (TDOS) and partial density of states (PDOS) for $CsCaF_3$ compound are given in this section. Fig.3.25 shows the plot of total density of states (TDOS) for $CsCaF_3$ and individual atoms Cs, Ca, and F. In the valence region below the Fermi level, we have found the maximum peak in TDOS for $CsCaF_3$ at -0.38 eV. The occurrence of this maximum in peak in TDOS of $CsCaF_3$ at -0.38 eV appears to be the contribution due to F atom. The reason being that the TDOS of F atom is also maximum at -0.38 eV. Also in valence band region, we find another peak in TDOS of $CsCaF_3$ at - 4.51 eV. The occurrence of this maximum in peak in TDOS of $CsCaF_3$ at -4.51 eV appears to be the contribution due to Cs atom. The reason being that the TDOS of Cs atom is also maximum at -4.51 eV. We have found from the plots that the contributions to the origin of peak in TDOS of $CsCaF_3$ by other atom Ca is very low and hence is negligible. Similarly, in the conduction band above the Fermi level in Fig. 3.25, the maximum peak in TDOS for $CsCaF_3$ is observed at 10.52 eV. The occurrence of this maximum in peak in TDOS of $RbCaF_3$ at 8.79 eV is due to the main contribution by Ca atom. We find from the plots in Fig. 3.25, TDOS of $CsCaF_3$ by other atoms Cs and F are very low.

In Fig. 3.26, the plots of TDOS and partial density of states (PDOS) of Cs atom in $CsCaF_3$ compound are shown. In the valence band, we have found that the maximum peak in TDOS occurs at – 4.51 eV. This is due to the main contribution by the Cs-*p* electrons of Cs atom. However in the conduction band region, we find from the plots that a small peak in TDOS occurs at 12.51 eV. This is due to the main contribution by the Cs-d_{t2g} states of electrons of Cs atom. The reason is that the peak of PDOS of Cs-d_{t2g} is also found at 12.51 eV which is seen in Fig.3.26.

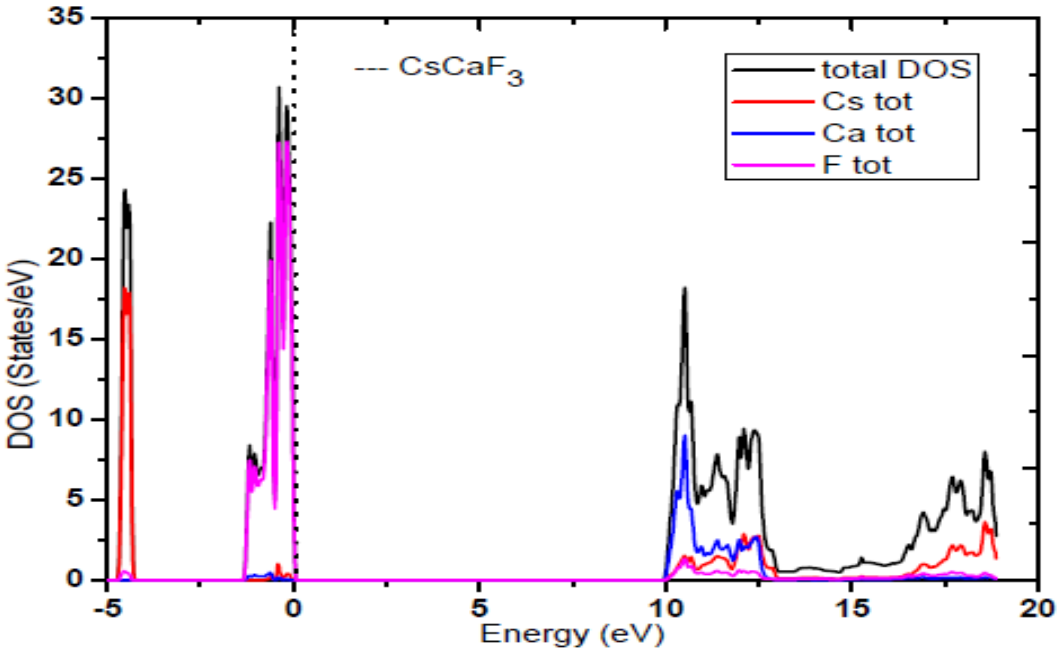

Fig. 3.25: Total DOS plots for $CsCaF_3$ and atoms Cs, Ca, F

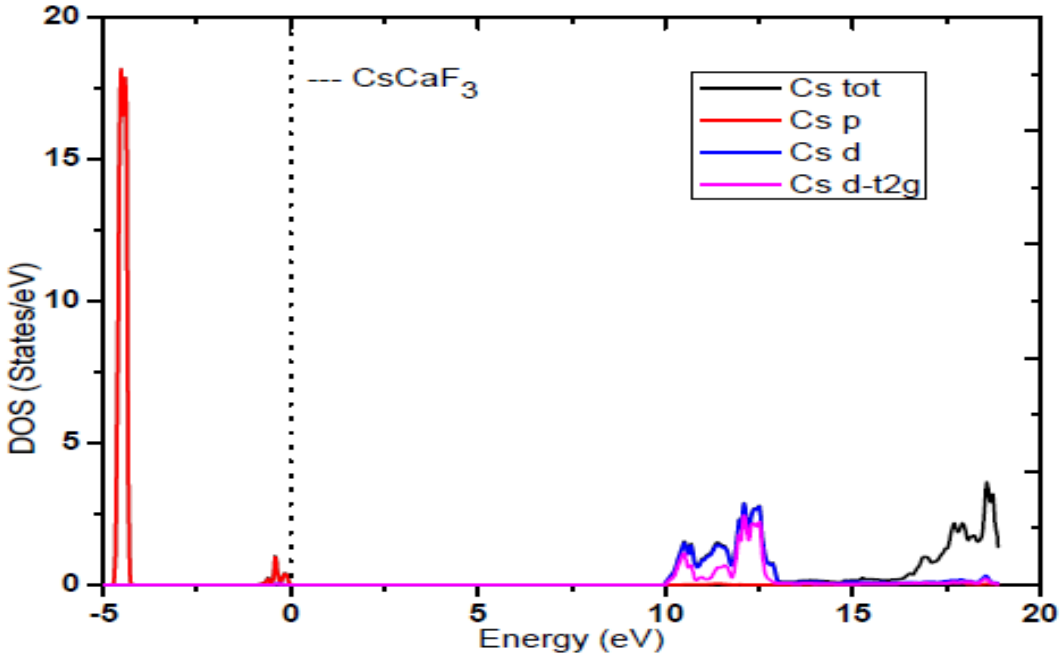

Fig. 3.26: Total and partial DOS plots for atom Cs

Fig.3.27 shows the plot of TDOS and PDOS of Ca atom of $CsCaF_3$ compound. There is negligible contribution to TDOS and PDOS by Ca atom in the valence band below the Fermi level. However in the conduction band, a maximum peak in TDOS is observed at 10.52 eV. This can be attributed to Ca-d_{t2g} state electrons of atom Ca as shown in Fig. 3.27.

The plot of TDOS and PDOS of F atom in $CsCaF_3$ compound is shown in Fig. 3.28. The maximum peak in TDOS is found at - 0.38 eV in the valence region below the Fermi level. From the plot we find that the contribution to the occurrence of this peak at -0.38 eV is due to the contribution by F_{px+py} state electrons. There is negligible contribution to TDOS and PDOS in conduction band region in F atom as shown in Fig. 3.28.

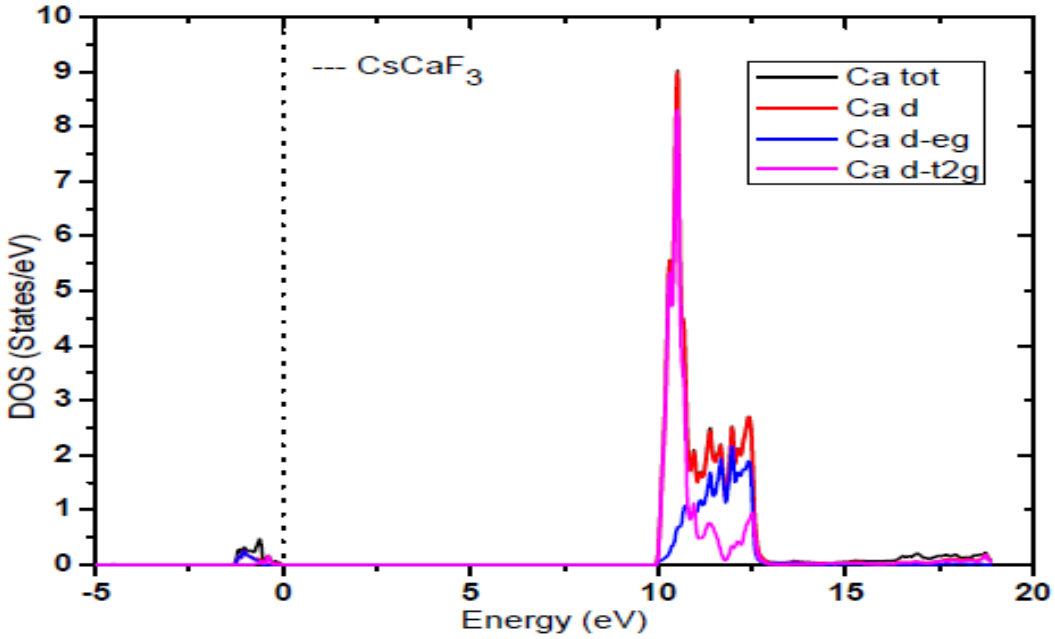

Fig. 3.27: Total and partial DOS plots for atom Ca

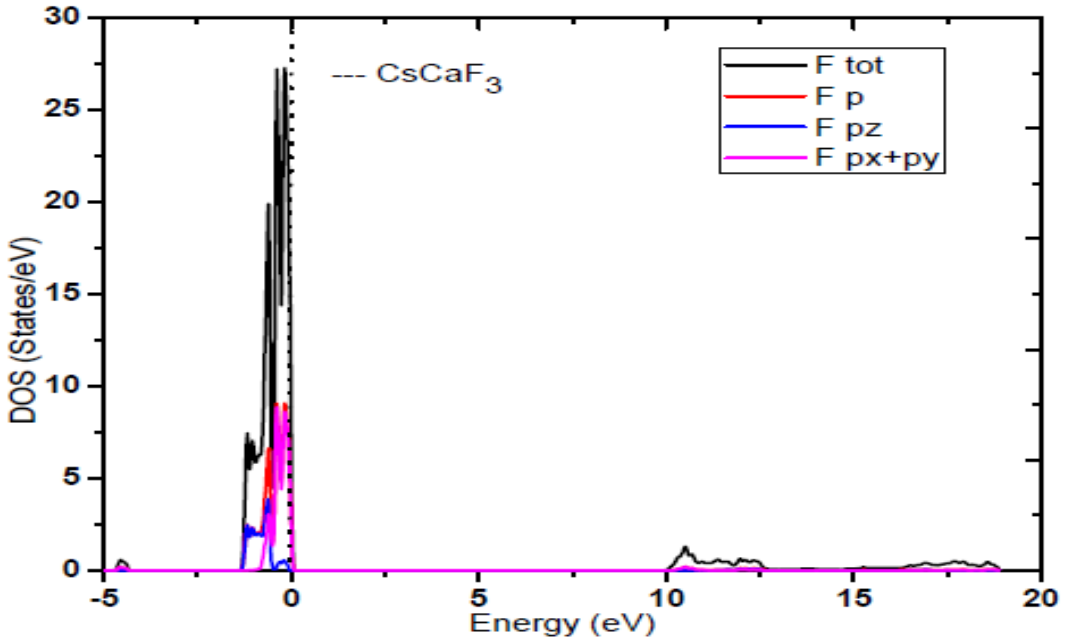

Fig. 3.28: Total and partial DOS plots of atom F

3.3 Electronic Band Structures for Alkali and Alkaline Earth Elements

We present here the result for each compound calculated by using GGA method which is followed by results of calculation done by suing mBJ potential. In this section, the results of calculation of band structures in the case of a combination of $ACaF_3$ (A= K, Rb, Cs) is presented. Calculations have been done by using FP-LAPW method as discussed in Chapter 2. For this purpose, the approximations for exchange-correlation potential used is Generalised Gradient approximation (GGA).The calculated band gaps obtained by using the GGA approximations is underestimated i.e. usually smaller than experimentally obtained values in most of the insulating materials. Hence in order to reproduce a comparable value of band gaps, modified Becke-Johnson (mBJ) potential approach will also be used to calculate the energy gaps in the system. The mBJ potential is used in conjunction with the WIEN2k code to calculate band gaps (E_{BG}) as in the case of GGA approaches.

3.3.1 Study of Energy Bands for Alkali and Alkaline Earth Elements

a) Energy Bands of $ACaF_3$ (A = K, Rb, Cs) using GGA method

The electronic properties of $ACaF_3$ (A = K, Rb, Cs) are calculated with first principles FP-LAPW method using GGA and mBJ exchange potential. To calculate DOS and band structure of $ACaF_3$, the optimized lattice parameters are used. The calculated electronic band structures for fluoroperovskites $ACaF_3$ (A = K, Rb, Cs) along the high-symmetry directions of the Brillouin zone are shown in Figs. 3.29-3.31. We have found that the maximum of the valence band are found to be at a symmetry point R whereas the minimum conduction bands are located at the Γ point of the Brillouin zone in $ACaF_3$ compounds, resulting into indirect band gaps in all the compounds. The calculated indirect band gaps (R - Γ) are found as 6.1 eV, 6.3 eV and 6.9 eV for $KCaF_3$, $RbCaF_3$ and $CsCaF_3$ respectively by using the GGA approach.

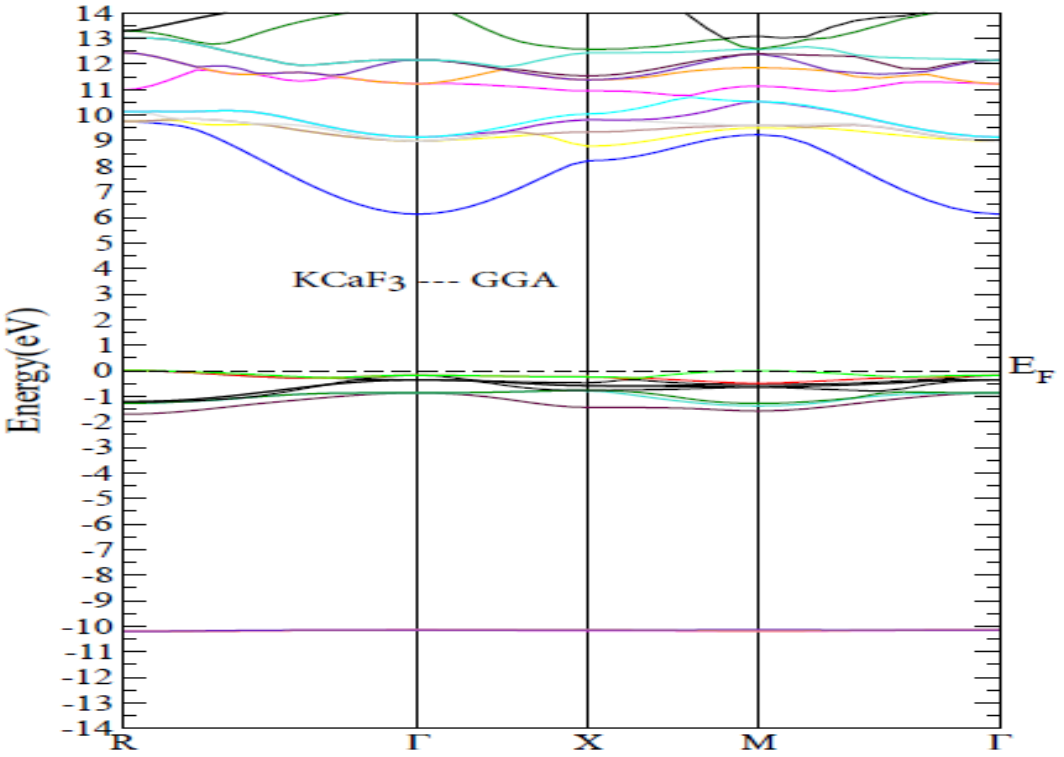

Fig. 3.29: Band structures for $KCaF_3$ in GGA

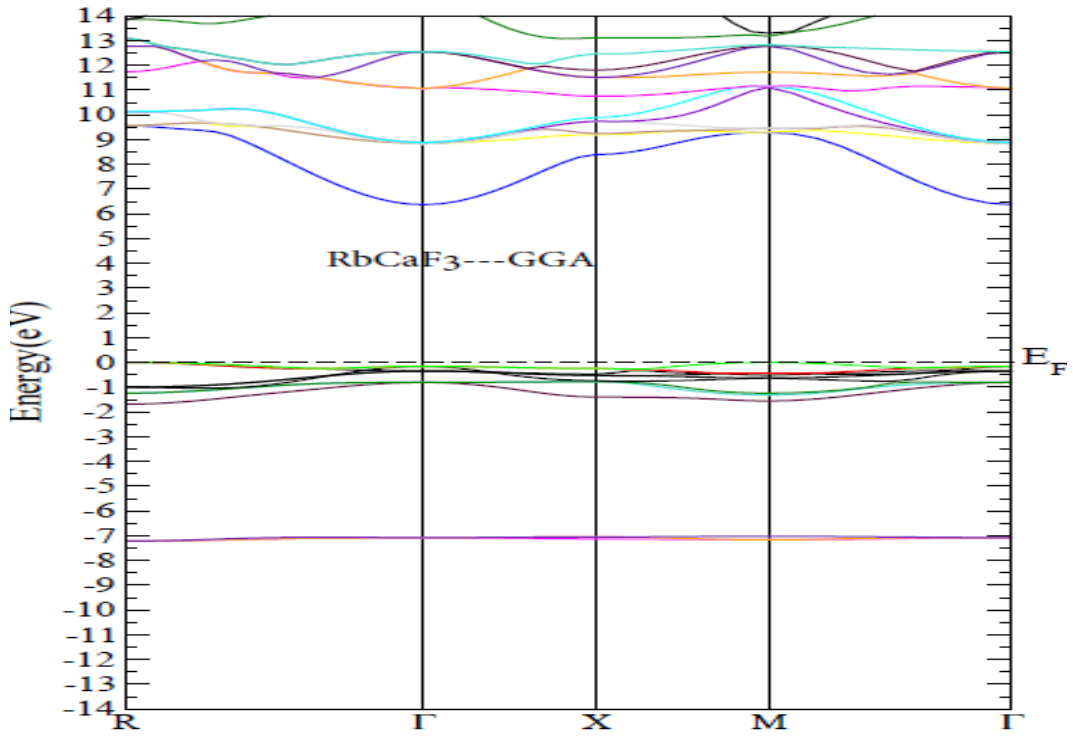

Fig. 3.30: Band structures for $RbCaF_3$ in GGA

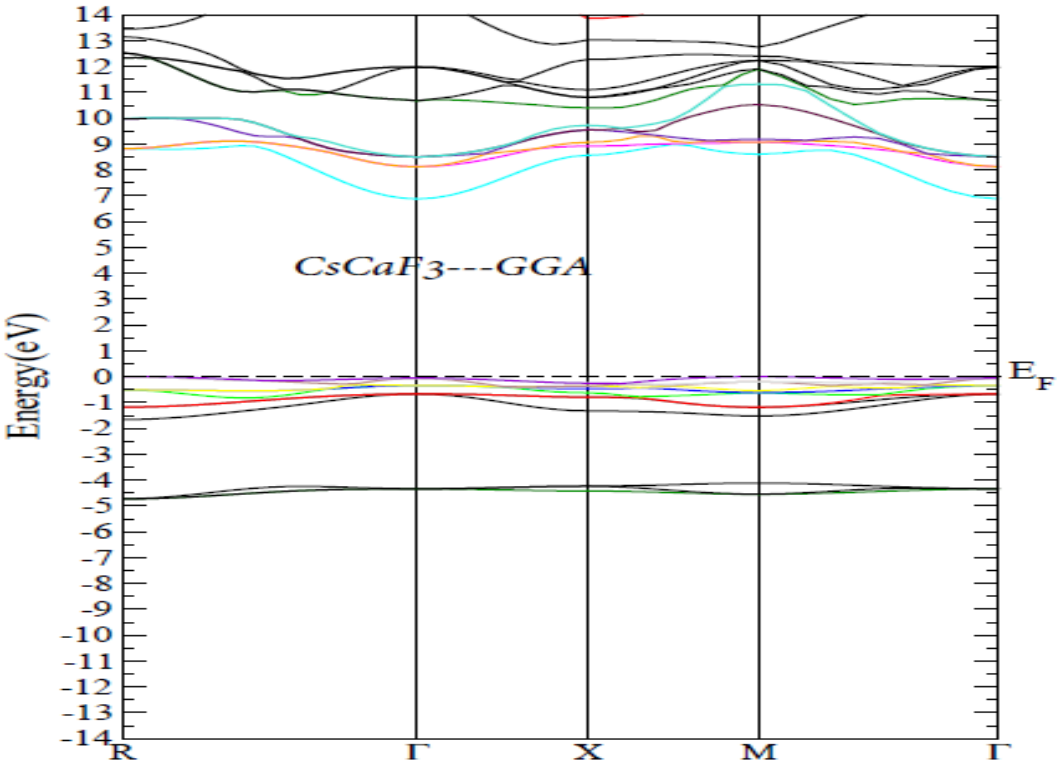

Fig. 3.31: Band structures for $CsCaF_3$ in GGA

(b) Energy Bands of $ACaF_3$ (A = K, Rb, Cs) using mBJ method

In this section, the calculated results of energy bands by using mBJ method is presented. Gaps arise due to indirect type of transition of electrons in the symmetry direction R - Γ as shown in Figs.3.33-3.35. The calculated values of energy band gaps for the systems are 10.6 eV, 10.4 eV and 9.8 eV for $KCaF_3$, $RbCaF_3$ and $CsCaF_3$ respectively. The origin of such band gaps are found to be due to the contribution by F*px+py* state electrons of the systems in the valence band below the Fermi level. In the conduction bands, Ca d-t2g state electrons are mostly contributing to the origin of gaps. This is also evidenced by the study of DOS and PDOS as shown in section 3.2.2. From our study, we have found the energy band gaps are increased through 73.7%, 65% and 42% for KCaF, $RbCaF_3$ and $CsCaF_3$ respectively in mBJ approach than in GGA.

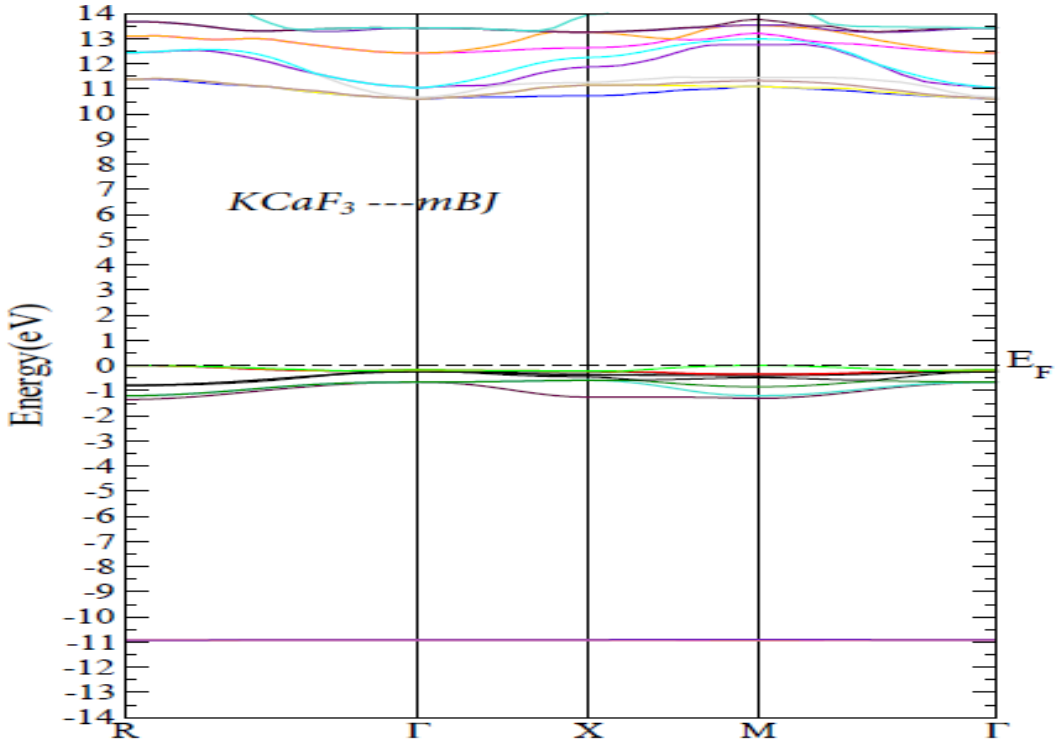

Fig. 3.32: Band structures for $KCaF_3$ in mBJ

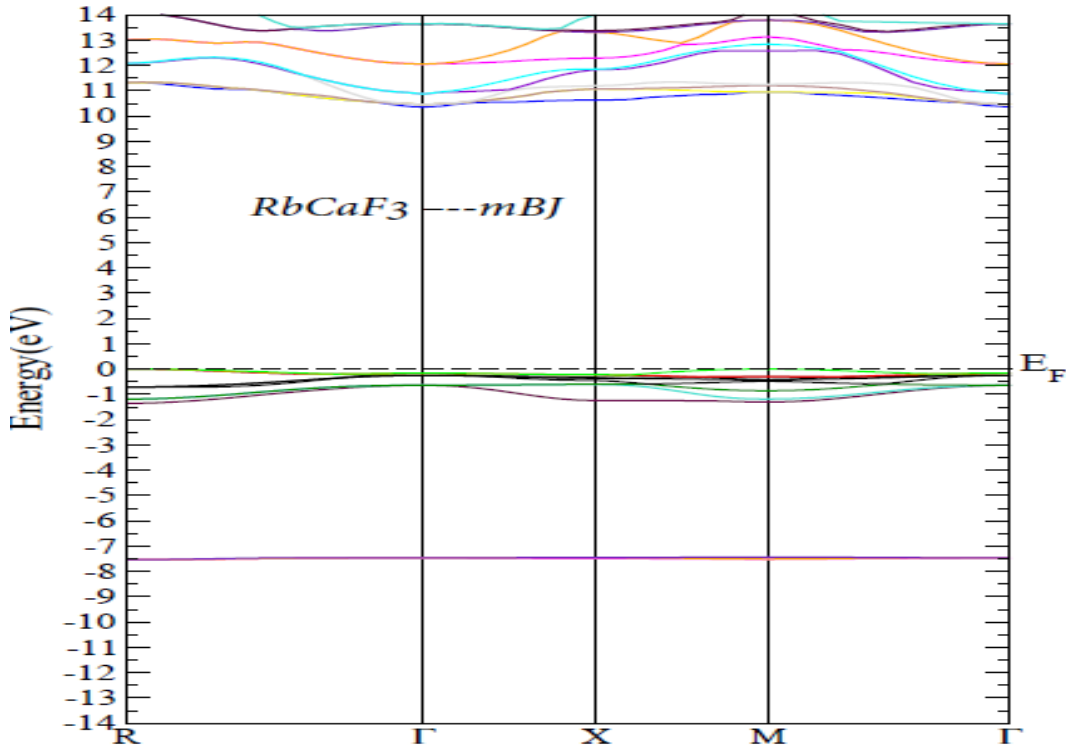

Fig. 3.33: Band structures for $RbCaF_3$ in mBJ

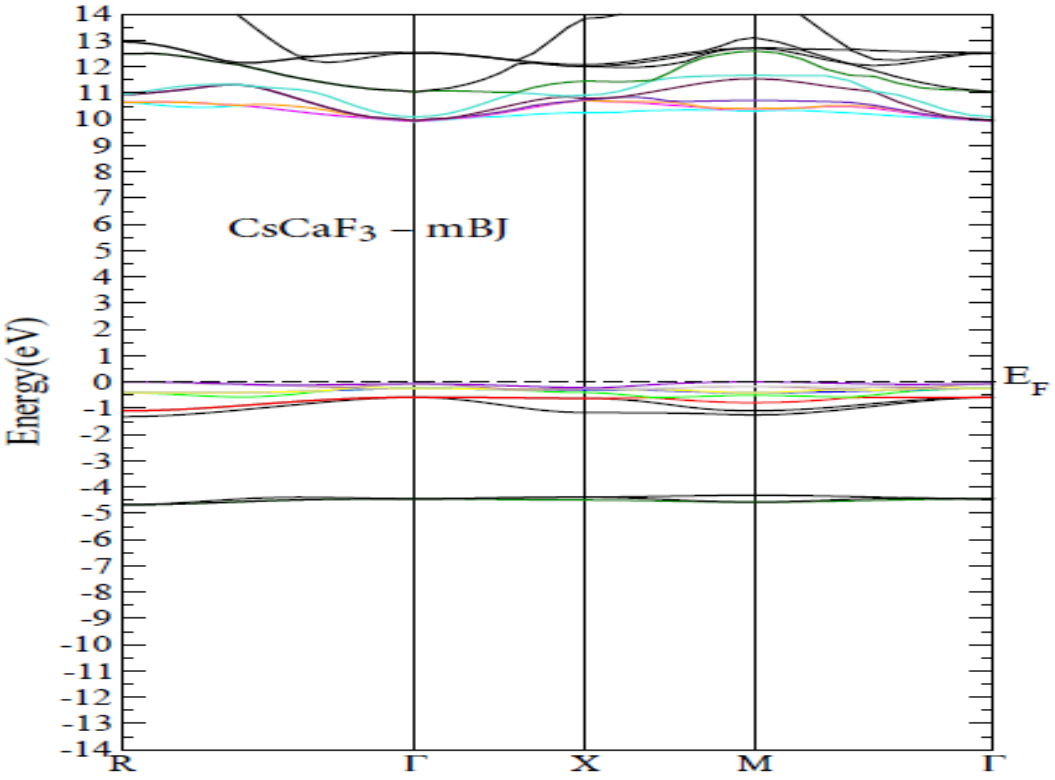

Fig. 3.34: Band structures for $CsCaF_3$ in mBJ

Chapter-4

Study of Electronic Properties of Fluoride Perovskite with Alkaline Earth and Alkali Elements

In this chapter, we will present the results of calculations of the structural parameters like optimized lattice constants, equilibrium pressure and its derivative for the ABF_3 type perovskite. We have chosen alkaline earth metal A as Ba, and alkali metals B as Li, K and Rb respectively. The results of total and partial density of states and also the energy bands of these systems will be discussed here in the context of FP-LAPW model within density functional theory. The exchange correlations potentials used for the calculation is by using the GGA and mBJ potential, hence the results obtained is presented for both of these methods.

4.1 Structural Optimization

All physical and electronic properties of a solid are related to its structure, lattice constants and the total energy of the crystal. In this section, the calculations of structural optimization with cubical fluoride perovskite $BaBF_3$ (B = Li, K, Rb) is presented. These calculations are performed with an exchange-correlation functional given by generalized gradient approximation (GGA) (Perdew *et al*., 1996) within the frame work of DFT (Hohenberg and Kohn 1964), where full-potential linearized augmented plane wave (FP-LAPW) (Singh, 1994) is adopted for the basis set. In this method the space is divided into non-overlapping muffin-tin (MT) spheres separated by an interstitial region (Fig. 2.1 of Chapter-2), the detail of which is discussed in section 2.7 of Chapter-2. The basis functions

are expanded like as in section 3.1 of chapter-3. The calculated lattice constants, bulk modulus and its pressure derivative are given in Table 4.1.

In order to obtain the equilibrium lattice constant and the bulk modulus for the cubic perovskite $BaBF_3$, we performed the structural optimization by minimizing the total energy with respect to the cell parameters and the atomic positions. To study the crystal structure, we start with the total energy minimization of cubic $BaBF_3$ as a function of volume. This can be understood from the plots of the total energy as a function of volume which are shown in Figs. 4.2-4.4 for $BaLiF_3$, $BaKF_3$ and $BaRbF_3$ respectively. The energy versus volume data was fitted to a Murnaghan equation of state (Murnaghan, 1944) to obtain the equilibrium lattice constant (a), the bulk modulus (B) and its first pressure derivative (B'). We note that the result of the lattice constants obtained within our GGA calculations increases with the change of cation (B) from Li to Rb which is similar to the previous results and are shown in Table 4.1. From our calculations, we have found $BaLiF_3$ has maximum value and $BaRbF_3$ has minimum value of B in compound $BaBF_3$ (B = Li, K, Rb). From this calculation, the maximum pressure derivative (B') is found in $BaLiF_3$ compound and minimum value is found in $BaRbF_3$ compound which are given in Table 4.1.

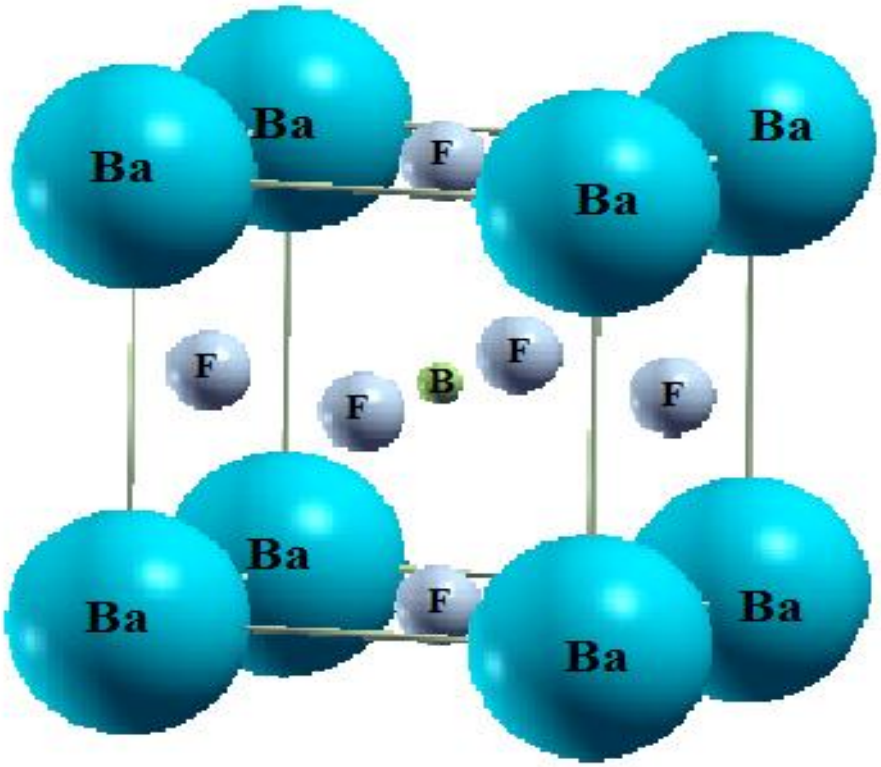

Fig. 4.1: Crystal structure for $BaBF_3$ (B = Li, K and Rb)

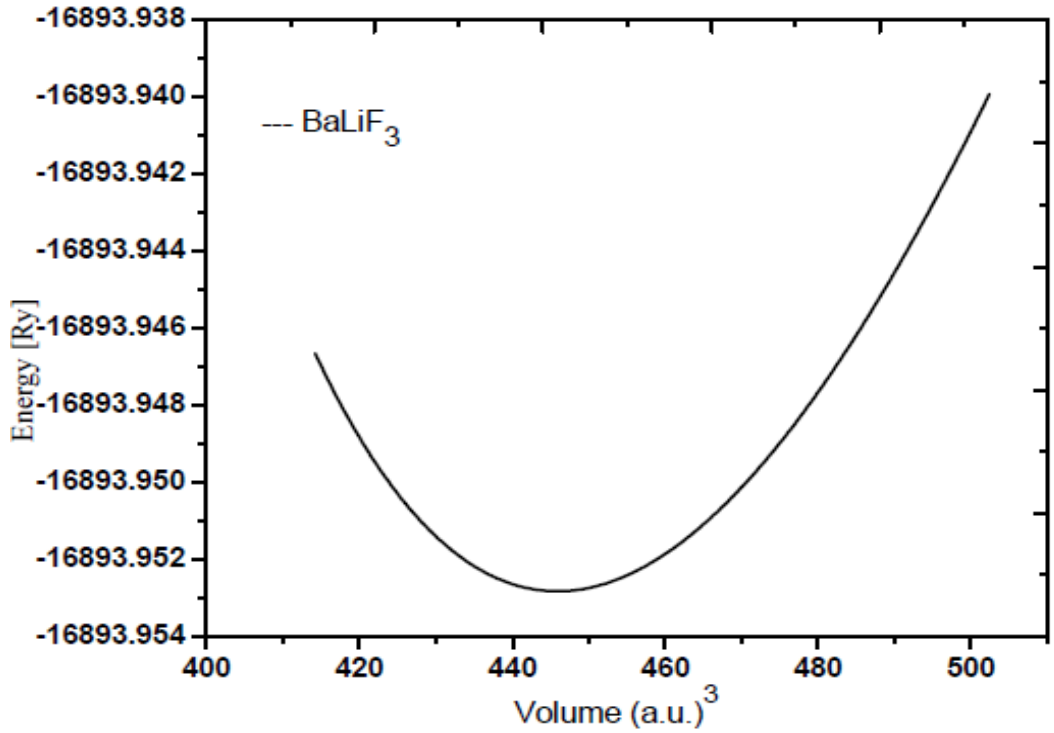

Fig. 4.2: Volume optimization curve for $BaLiF_3$

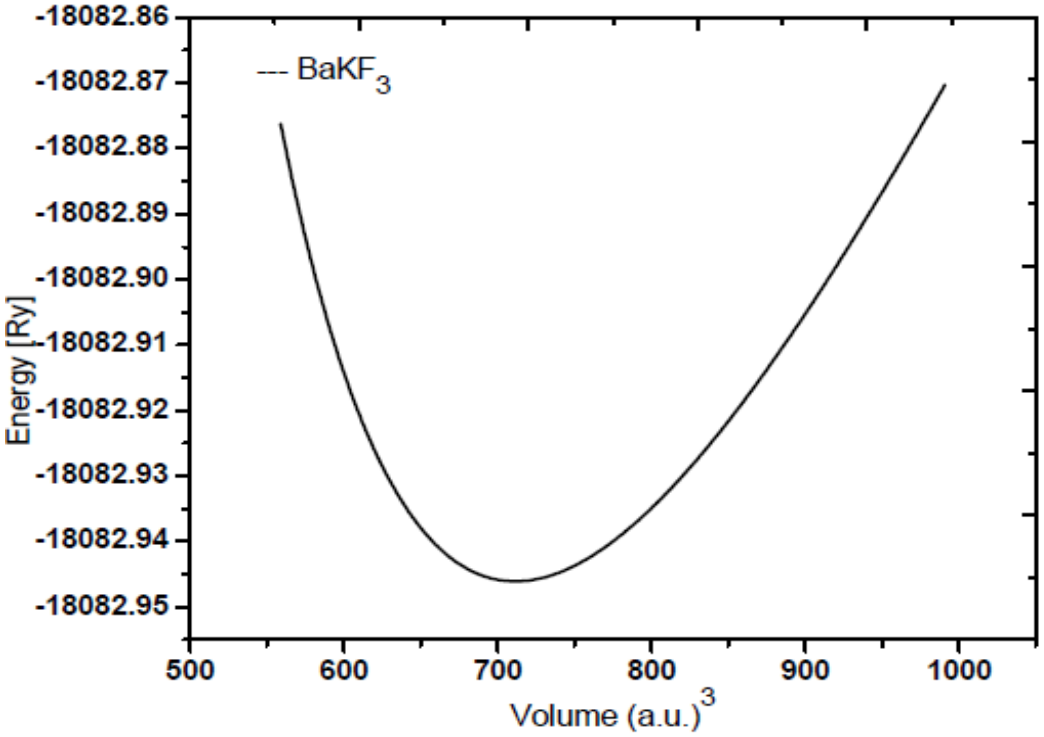

Fig. 4.3: Volume optimization curve for $BaKF_3$

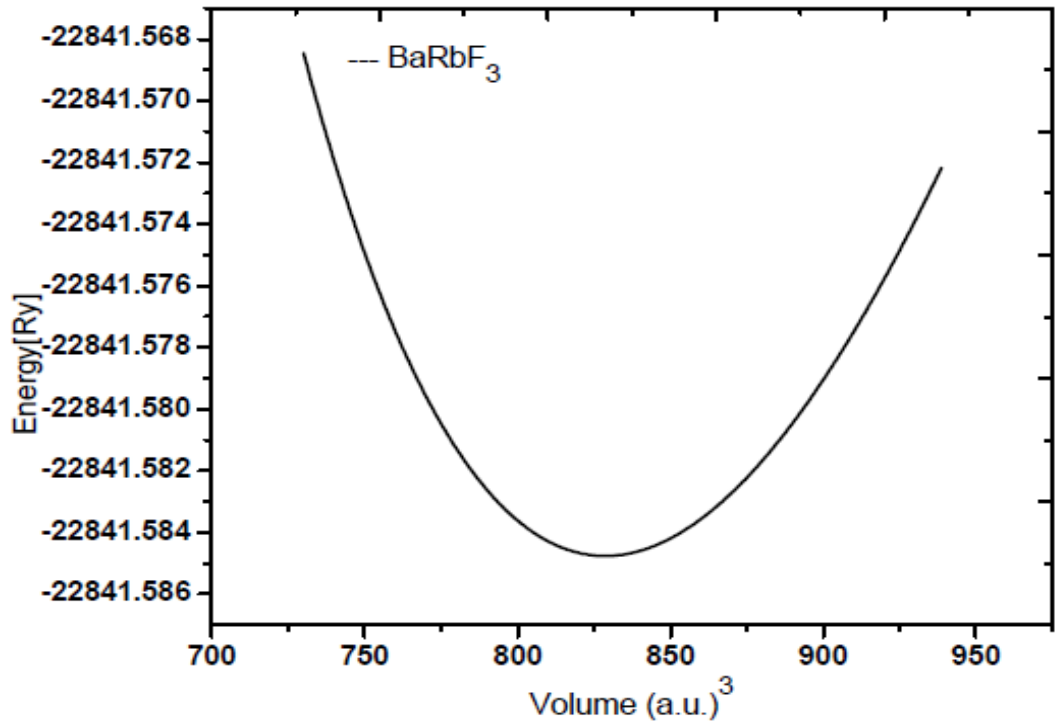

Fig. 4.4: Volume optimization curve for $BaRbF_3$

Table 4.1: Calculated lattice constant a (in Å), bulk modulus B (in GPa) and its pressure derivative B' of $BaBF_3$ compound are compared with other available results.

Compounds	**Previous results a(in Å)**	**Calculated results a(in Å)**	**Previous results B(GPa)**	**Calculated results B(GPa)**	**Previous results B'**	**Calculated results B'**
$BaLiF_3$	4.04[a] 4.05[b]	4.0427 -	66.46[a] 64.45[b]	68.354 -	5.17[a] 4.6[b]	5.628 -
$BaKF_3$	4.72[a]	4.724	37.48[a]	37.556	4.51[a]	5.024
$BaRbF_3$	4.96[a]	4.970	31.72[a]	37.550	4.66[a]	4.6871

[a] (Mubark *et al.*, 2012), [b] (Soleimanpour, 2015),

4.2 Calculations of Density of State (DOS) for Alkaline Earth and Alkali Elements

In this section, the results of calculations of density of states, will be presented for the combination of systems of choice namely $BaBF_3$ (B = Li, K, Rb). The calculations for this purpose have been done by using the approximations for the exchange-correlation potentials such as GGA and mBJ under FP-LAPW method. The details of these methods have already been given in Chapter-2. In this method, the space is divided into non-overlapping muffin-tin (MT) spheres separated by an interstitial region. The basis functions are expanded into spherical harmonic functions inside the muffin-tin sphere ad the Fourier series in the interstitial region. The convergence of basis set was controlled by a cutoff parameter R_{MT} X K_{max} = 7 where R_{MT} is the smallest of the MT sphere radii and K_{max} is the largest reciprocal lattice vector used in the plane wave expansion. The cutoff energy which defines the separation of valence and core states was chosen as -6.0 Ry. For k point sampling, a 1000 k-point mesh in the first Brillouin zone was used. The self-consistent calculations were considered to be converged until the integrated charge difference between the last two iterations was less than 10^{-4} eV. Even though the ground state is well described by GGA, the values of the band gaps are sometimes underestimated. For this reason we have the modified Becke Johnson potential (mBJ) to calculate for improved values of the band gaps (Perdew *et al*., 1996) for all the systems. The theoretically obtained lattice parameters calculated in Chapter 3 have been used here for DOS and energy bands calculations. We present in this section the results of total DOS and partial DOS in the case of $BaBF_3$ (B= Li, K, Rb). The DOS for these systems had been calculated using the same method but for the exchange correlation potential calculated by GGA and mBJ approximations.

4.2.1 Calculation of DOS by using GGA method for Alkaline Earth and Alkali Elements

(a) $BaLiF_3$

In this section the calculated results of total density of states (TDOS) and partial density of states (PDOS) for $BaLiF_3$ compound are given. The plot of TDOS of $BaLiF_3$ and individual atoms Ba, Li and F are given in Fig.4.5. In the valence region below the Fermi level, we have found the maximum peak in TDOS for $BaLiF_3$ at – 1.11 eV. The occurrence of this maximum in peak in TDOS of $BaLiF_3$ at -1.11 eV appears to be the contribution due to F atom. The reason is that the TDOS of F atom is also maximum at -1.11 eV. Also in valence band region, we find from the plots that the contributions to the origin of peak in TDOS of $BaLiF_3$ by other atoms Ba and Li is very low and hence are negligible. Similarly, in the conduction band above the Fermi level in Fig. 4.5, the maximum peak in TDOS for $BaLiF_3$ is observed at 13.36 eV. The occurrence of this maximum in peak in TDOS of $BaLiF_3$ at 13.36 eV is due to the main contribution by Ba atom. The reason is that the TDOS of Ba atom is also maximum at 13.36 eV. We find from the plots in Fig. 4.5, TDOS of $BaLiF_3$ by other atoms Li and F are very low.

In Fig. 4.6, the plots of TDOS and partial density of states (PDOS) of Ba atom in $BaLiF_3$ compound are shown. In the valence band, we have found that there is negligible contribution to TDOS and PDOS by electrons of Ba atom. However in the conduction band region, we find from the plots that the maximum peak in TDOS occurs at 13.36 eV. This is due to the main contribution by the Ba-*f* electrons of Ba atom. The reason being that the maxima of partial DOS of Ba-*f* is also found at 13.36 eV.

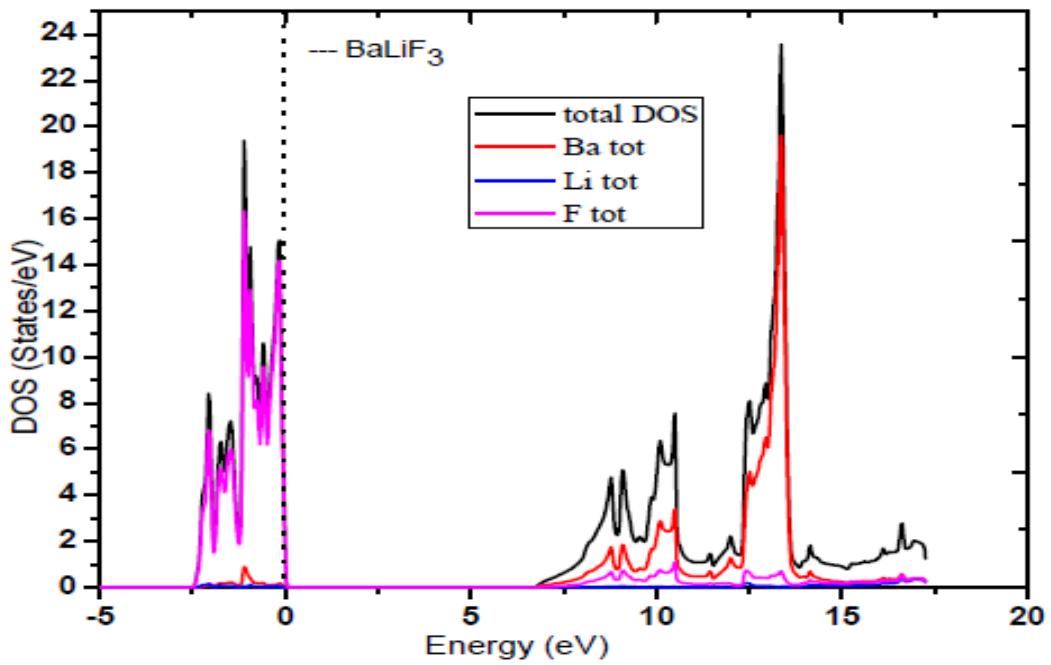

Fig. 4.5: Plots of total DOS for $BaLiF_3$ and atoms Ba, Li, F

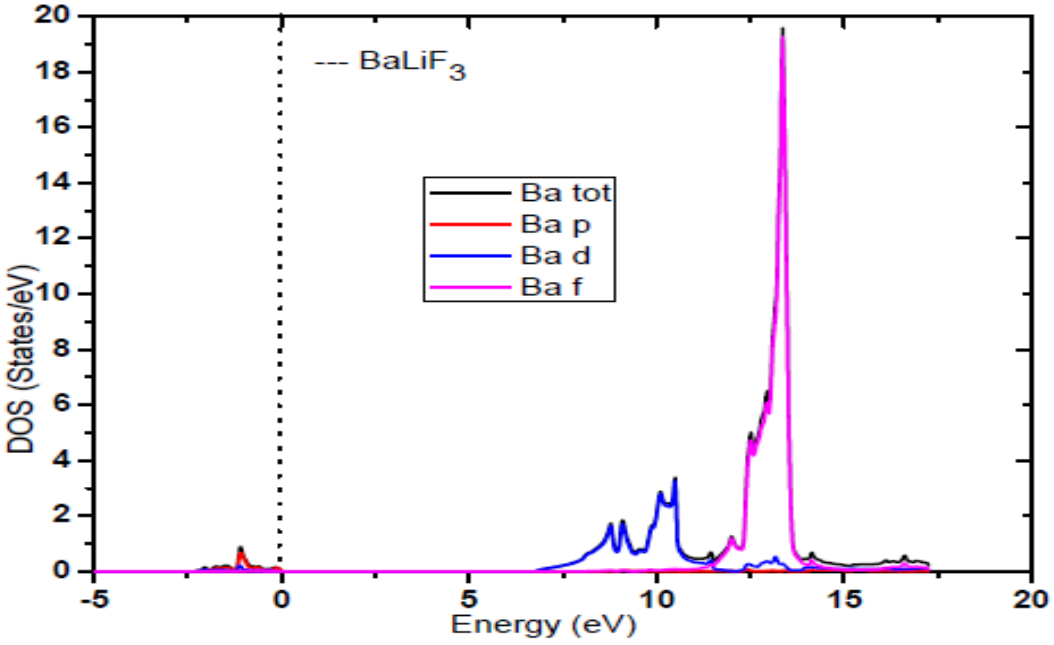

Fig. 4.6: Total and partial DOS plots for atom Ba

Fig.4.7 shows the plot of TDOS and PDOS of Li atom of $BaLiF_3$ compound. We have observed very small peaks in TDOS of atom Li at the range of 2.5 eV to 0 eV in the valence band. These small peaks in TDOS of Li atom at the range of 2.5 eV to 0 eV are due to the contribution of Li-*s*, Li-*p* and *Li-d* state electrons of atom Li. However, in the conduction band, we have observed a sharp narrow peak in TDOS is observed at 17.06 eV due to the hybridization of Li- *s* and Li- *d* state electrons that is seen in Fig.4.7.

The plot of TDOS and PDOS of F atom in $BaLiF_3$ compound is shown in Fig. 4.8. The maximum peak in TDOS is found at – 1.11 eV in the valence region below the Fermi level. From the plot we find that the contribution to the occurrence of this peak at -1.11 eV is due to the contribution by F-*p* state electrons. There is negligible contribution to TDOS and PDOS in conduction band in F atom as shown in Fig. 4.8.

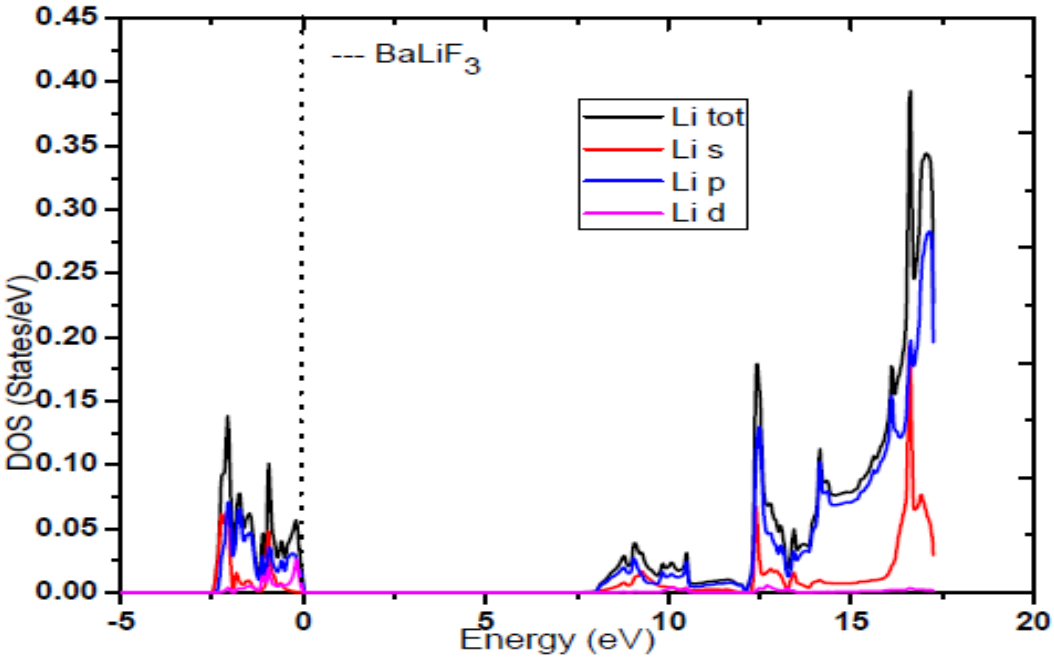

Fig. 4.7: Total and partial DOS plots for atom Li

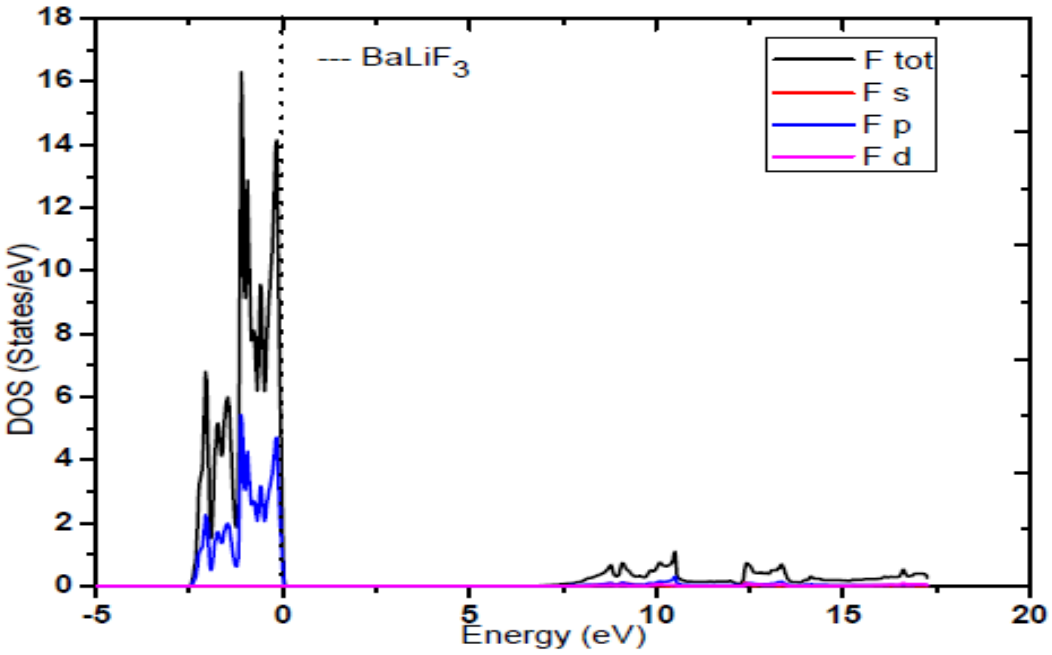

Fig. 4.8: Total and partial DOS plots for atom F

(b) $BaKF_3$

The calculated results of total density of states (TDOS) and partial density of states (PDOS) for $BaKF_3$ compound are given in this section. Fig.4.9 shows the plot of total density of states (TDOS) for $BaKF_3$ and individual atoms Ba, K, and F. In the valence band region below the Fermi level, we have found the maximum peak in TDOS for $BaKF_3$ at - 0.89 eV. The occurrence of this maximum in peak in TDOS of $BaKF_3$ at -0.89 eV appears to be the contribution due to F atom. The reason being that the TDOS of F atom is also maximum at -0.89 eV. Also in valence band region, we find from the plots that the contributions to the origin of peak in TDOS of $BaKF_3$ by other atoms Ba and K is very low and hence are negligible. Similarly, in the conduction band above the Fermi level in Fig. 4.9, the maximum peak in TDOS for $BaKF_3$ is observed at 10.04 eV. The occurrence of this maximum in peak in TDOS of $BaKF_3$ at 10.04 eV is due to the main contribution by Ba atom. We find from the plots in Fig. 4.9, TDOS of $BaKF_3$ by other atoms K and F are very low.

In Fig. 4.10, the plots of TDOS and partial density of states (PDOS) of Ba atom in $BaKF_3$ compound are shown. In the valence band, we have found that there is negligible contribution to TDOS and PDOS by electrons of Ba atom. However in the conduction band region, we find from the plots that the maximum peak in TDOS occurs at 10.18 eV. This is due to the main contribution by the Ba-*f* electrons. The reason is that the maximum of PDOS of Ba-*f* is also found at 10.18 eV which is seen in Fig. 4.10.

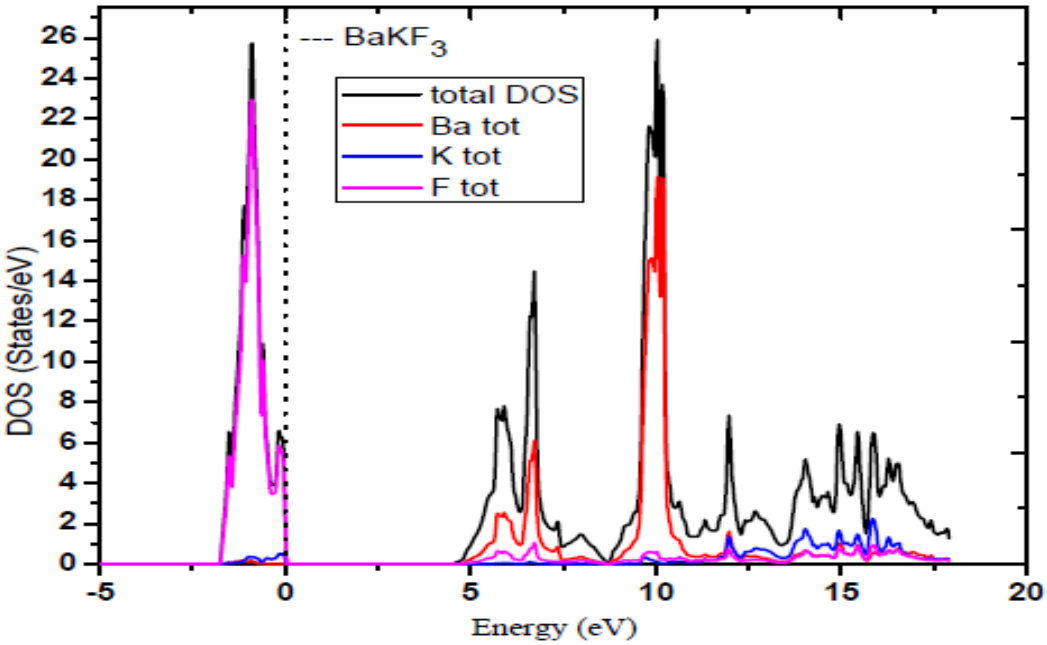

Fig. 4.9: Plots of total DOS for $BaKF_3$ and atoms Ba, K, F

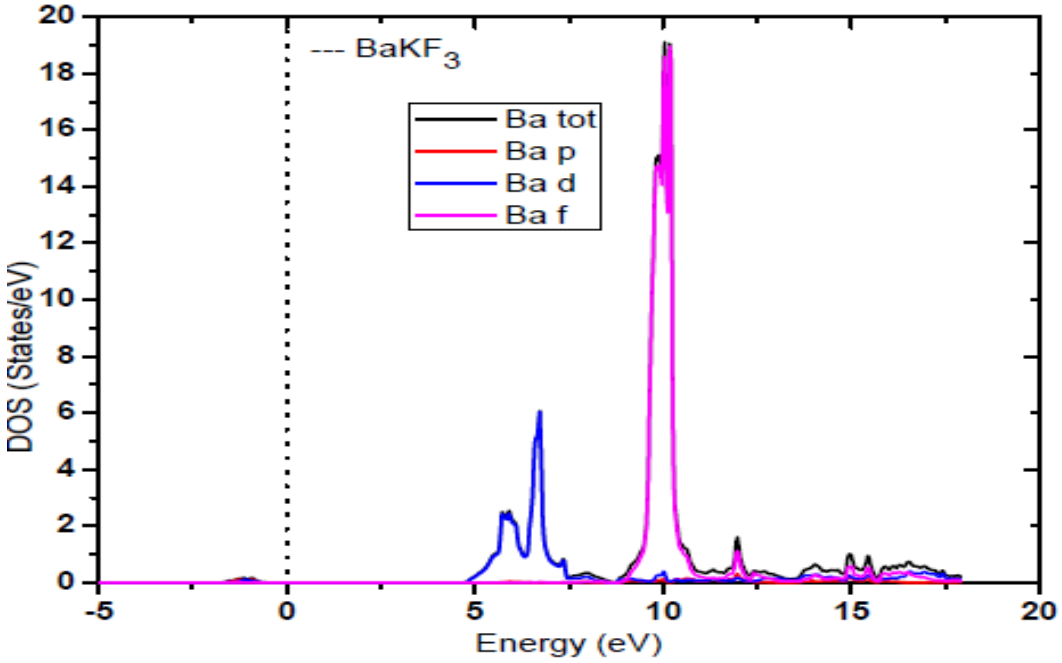

Fig. 4.10: Total and partial DOS plots for atom Ba

Fig.4.11 shows the plot of TDOS and PDOS of K atom of $BaKF_3$ compound. We have observed very small peaks in TDOS at the range of -2.5 eV to 0 eV in the valence band below the Fermi level. These small peaks are contributed by the K-s, K-p and K-d state electrons. There is negligible contribution to TDOS and PDOS by Ca atom in the valence band below the Fermi level. However in the conduction band, a narrow sharp peak in TDOS is observed at 15.84 eV. The occurrence of this maximum peak in TDOS of atom K is due to the contribution of K-d state electrons. We have observed other small peaks from 9.2 - 17.0 eV due to the contribution of *s*, *p* and *d* state electrons of K atom. Which is seen in Fig.4.11.

The plot of TDOS and PDOS of F atom in $BaKF_3$ compound is shown in Fig. 4.12. The maximum peak in TDOS is found at - 0.89 eV in the valence region below the Fermi level. From the plot we find that the contribution to the occurrence of this peak at -0.89 eV is due to the contribution by F-*p* state electrons. There is negligible contribution to TDOS and PDOS in conduction band in F atom as shown in Fig. 4.12.

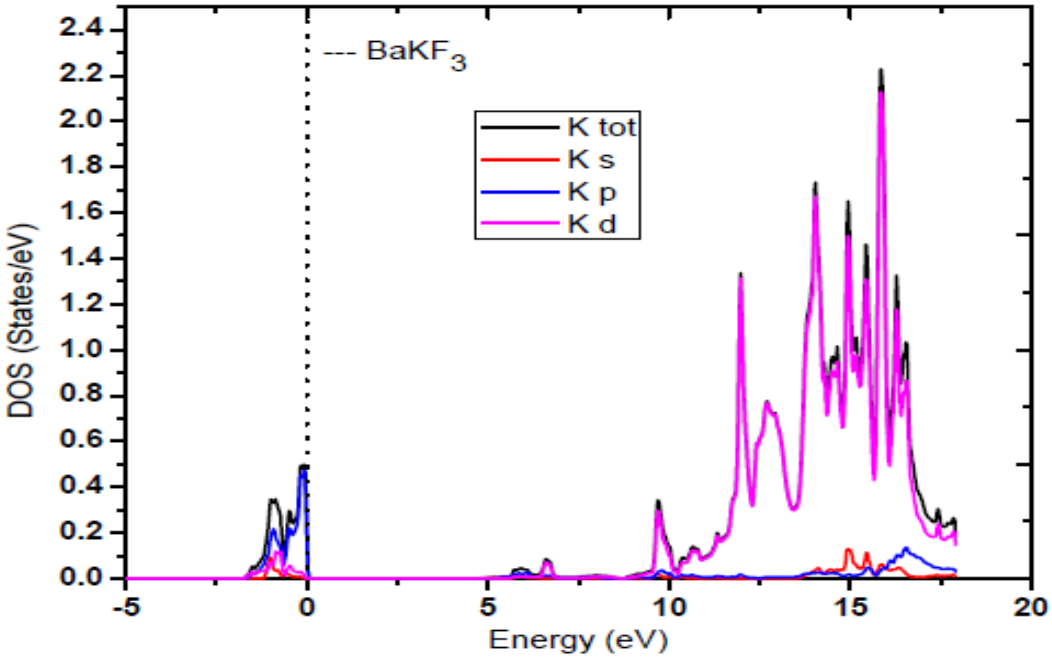

Fig. 4.11: Total and partial DOS plots for atom K

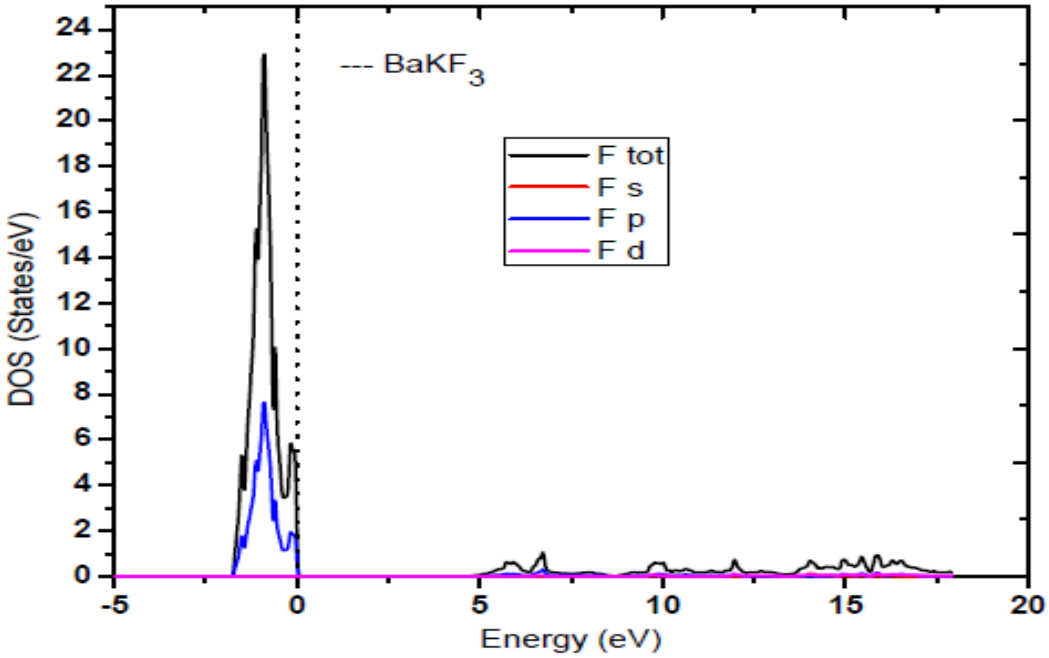

Fig. 4.12: Total and partial DOS plots for atom F

(c) $BaRbF_3$

The calculated results of total density of states (TDOS) and partial density of states (PDOS) for $BaRbF_3$ compound are given in this section. Fig.4.13 shows the plot of total density of states (TDOS) for $BaRbF_3$ and individual atoms Ba, Rb, and F. In the valence region below the Fermi level, we have found the maximum peak in TDOS for $BaRbF_3$ at – 1.93 eV. The occurrence of this maximum in peak in TDOS of $BaRbF_3$ at -1.93 eV appears to be the contribution due to F atom. The reason is that the TDOS of F atom is also maximum at -1.93 eV. Also in valence band region, we find from the plots that the contributions to the origin of peak in TDOS of $BaRbF_3$ by other atoms Ba and Rb is very low and hence are negligible. Similarly, in the conduction band above the Fermi level in Fig. 4.13, the maximum peak in TDOS for $BaRbF_3$ is observed at 8.6 eV. The occurrence of this maximum in peak in TDOS of $BaRbF_3$ at 8.6 eV is due to the main contribution by Ba atom. We find from the plots in Fig. 4.13, TDOS of $BaRbF_3$ by other atoms Rb and F are very low.

In Fig. 4.14, the plots of TDOS and partial density of states (PDOS) of Ba atom in $BaRbF_3$ compound are shown. In the valence band, we have found that the contribution in TDOS and PDOS by atom Ba is negligible. However in the conduction band region, we find from the plots that a maximum peak in TDOS occurs at 8.6 eV. This is due to the main contribution by the Ba-f states of electrons of Ba atom. The reason isthat the peak of PDOS of Ba-f is also found at 8.6 eV which is seen in Fig. 4.14.

.

.

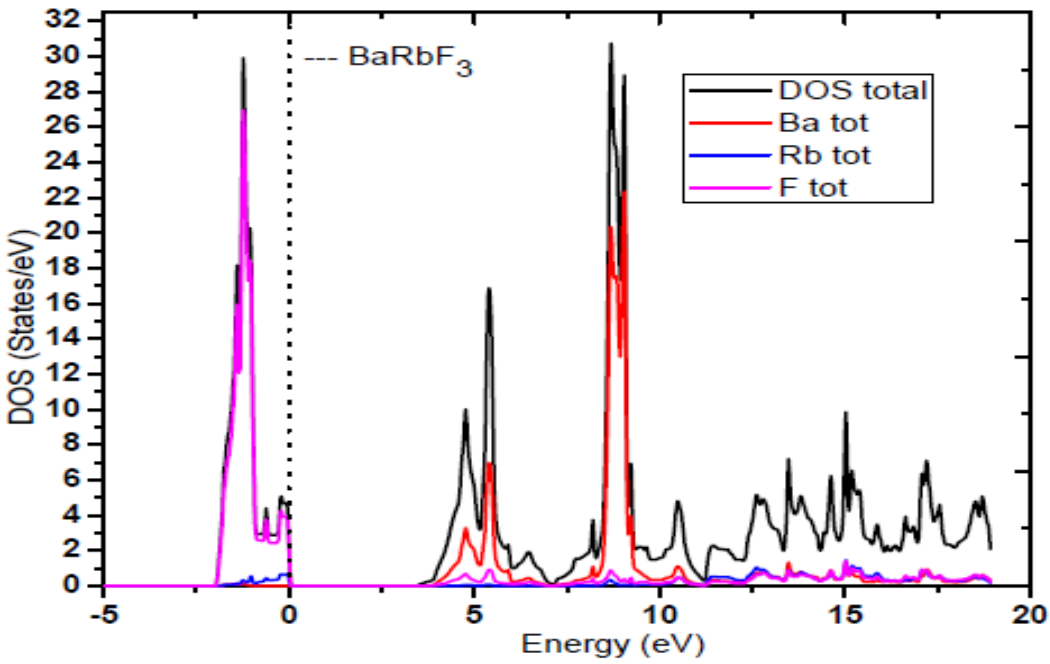

Fig. 4.13: Plots of total DOS for $BaRbF_3$ and atoms Ba, Rb, F

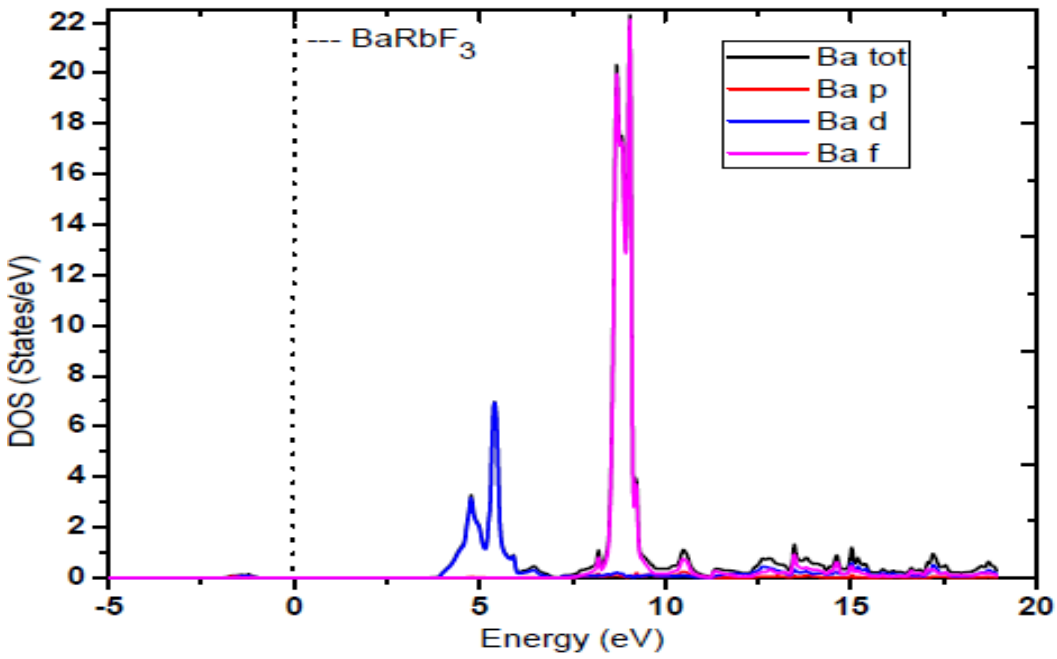

Fig. 4.14: Total and partial DOS plots for atom Ba

The plot of TDOS and PDOS of Rb atom of $BaRbF_3$ compound is shown in Fig.4.15. We have observed very small peaks in TDOS and PDOS at the range of -2.0 eV to 0 eV in the valence band region. This is found due to the contribution by Rb-*p* state electrons. However, in the conduction band, we have observed narrow peaks in TDOS and PDOS having small magnitude of height in the range of 8.0 eV to 18.0 eV. This is found due to the main contribution of Rb-*d* state electrons which is seen in Fig.4.15.

The plot of TDOS and PDOS of F atom in $BaRbF_3$ compound is shown in Fig. 4.16. The maximum peak in TDOS is found at – 1.93 eV in the valence region below the Fermi level. From the plot we find that the contribution to the occurrence of this peak at -1.93 eV is due to the contribution by F-*P* state electrons. There is negligible contribution to TDOS and PDOS in conduction band region in F atom as shown in Fig. 4.16.

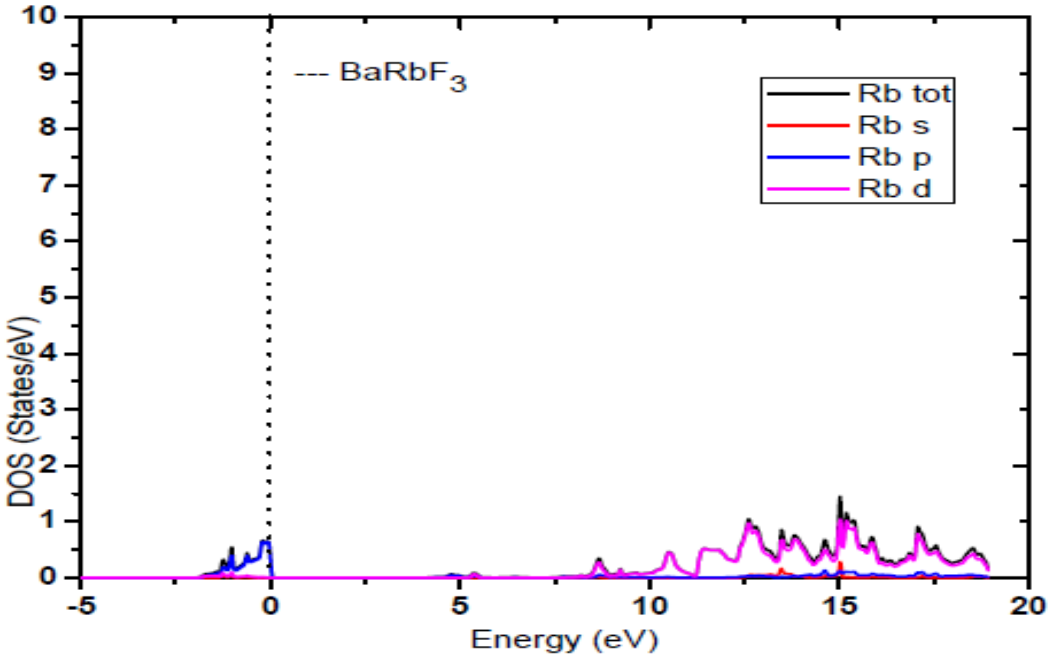

Fig. 4.15: Total and partial DOS plots for atom Rb

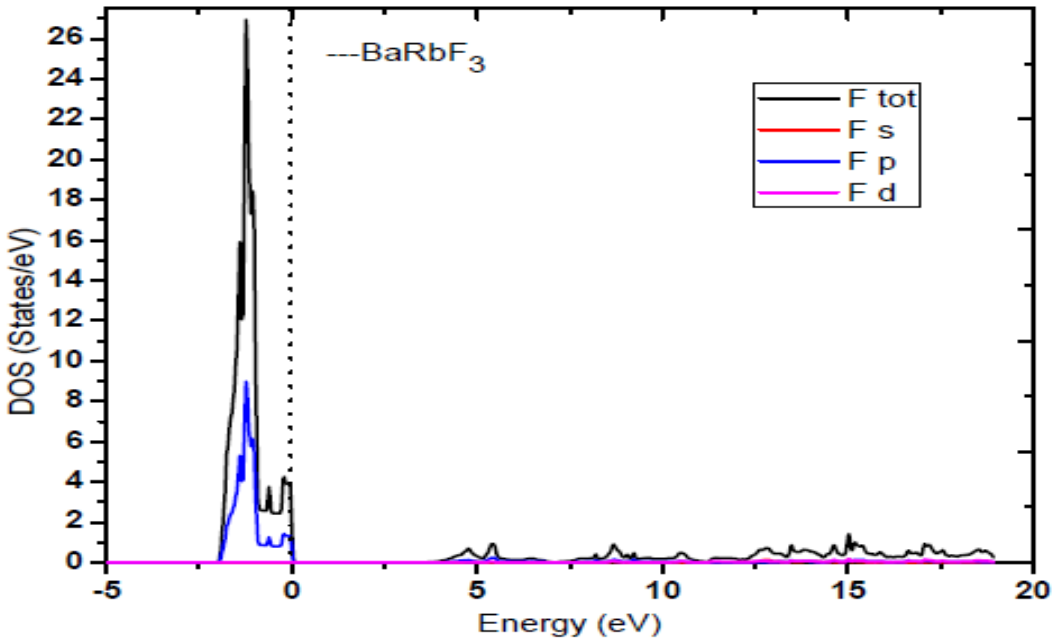

Fig. 4.16: Total and partial DOS plots for atom F

4.2.2 Calculation of DOS by using mBJ potential for Alkaline Earth and Alkali Elements

(a) $BaLiF_3$

The calculated results of total density of states (TDOS) and partial density of states (PDOS) for $BaLiF_3$ compound are given in this section. Fig.4.17 shows the plot of total density of states (TDOS) for $BaLiF_3$ and individual atoms Ba, Li, and F. In the valence region below the Fermi level, we have found the maximum peak in TDOS for $BaLiF_3$ at -0.87 eV. The occurrence of this maximum in peak in TDOS of $BaLiF_3$ at -0.87 eV appears to be the contribution due to F atom. The reason being that the TDOS of F atom is also maximum at -0.87 eV. We have found from the plots that the contributions to the origin of peak in TDOS of $BaLiF_3$ by other atoms Ba and Li are very low and hence are negligible. Similarly, in the conduction band above the Fermi level in Fig. 4.17, the maximum peak in TDOS for $BaLiF_3$ is observed at 13.43 eV. The occurrence of this maximum in peak in TDOS of $BaLIF_3$ at 13.43 eV is due to the main contribution by atom Ba.

In Fig. 4.18, the plots of TDOS and partial density of states (PDOS) of Ba atom in $BaLiF_3$ compound are shown. In the valence band, we have found that there is negligible contribution to TDOS and PDOS by electrons of atom Ba. However in the conduction band region, we find from the plots that the maximum peak in TDOS occurs at 13.43 eV. This is due to the main contribution by the Ba-*f* State electrons of Ba atom which is seen in Fig.4.18.

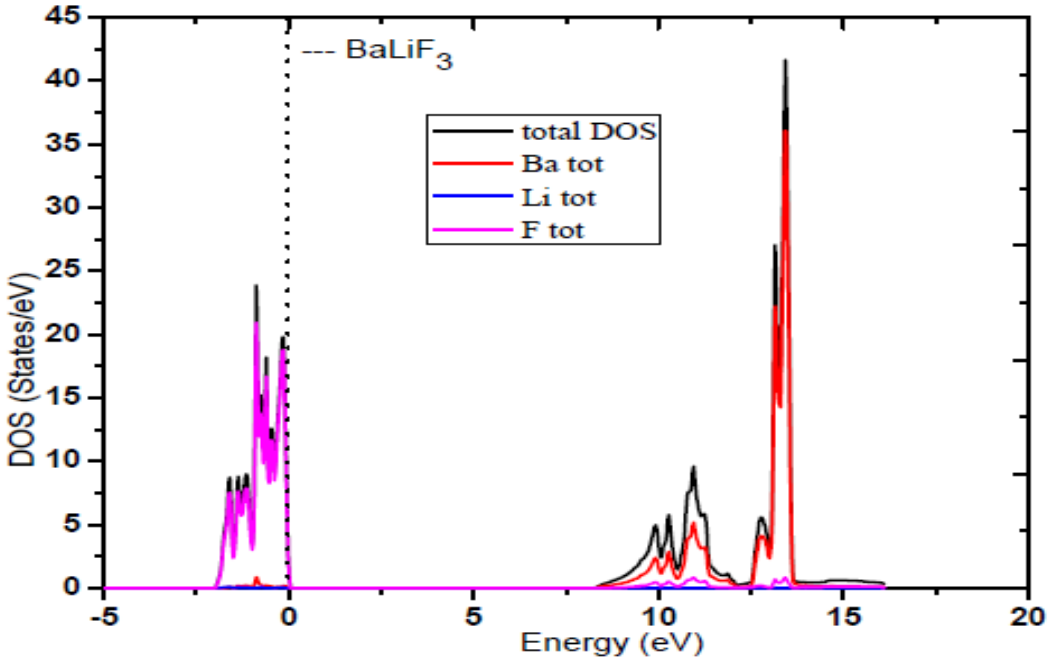

Fig. 4.17: Plots of total DOS for $BaLiF_3$ and atoms Ba, Li, F

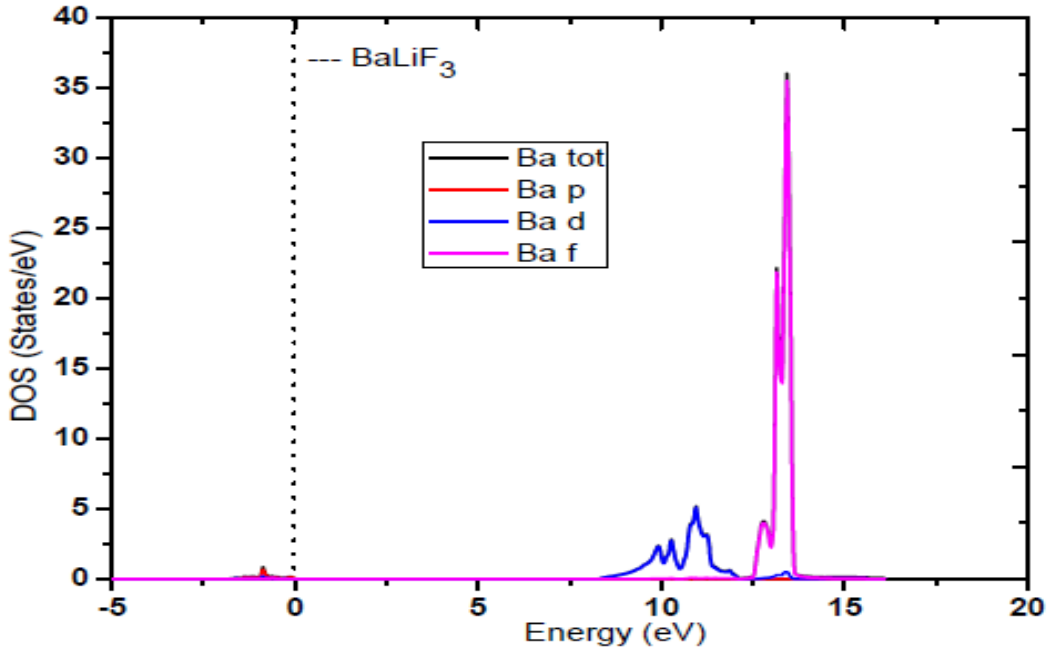

Fig. 4.18: Total and partial DOS plots for atom Ba

The plot of TDOS and PDOS of Li atom of $BaLiF_3$ compound is shown in Fig.4.19. There is negligible contribution to TDOS and PDOS in the valence band below the Fermi level by Li atom. However in the conduction band, a maximum peak in TDOS is observed at 13.32 eV. This can be attributed to Li-*s* state electrons which is shown in Fig. 4.19.

The plot of TDOS and PDOS of F atom in $BaLiF_3$ compound is shown in Fig. 4.20. From this plot, we have observed a narrow peak in TDOS at – 0.87 eV in the valence region below the Fermi level. From the plot we find that the contribution to the occurrence of this peak at -0.87 eV is due to the contribution by F-*p* state electrons of atom F. There is negligible contribution to TDOS and PDOS in conduction band in F atom as shown in Fig. 4.20.

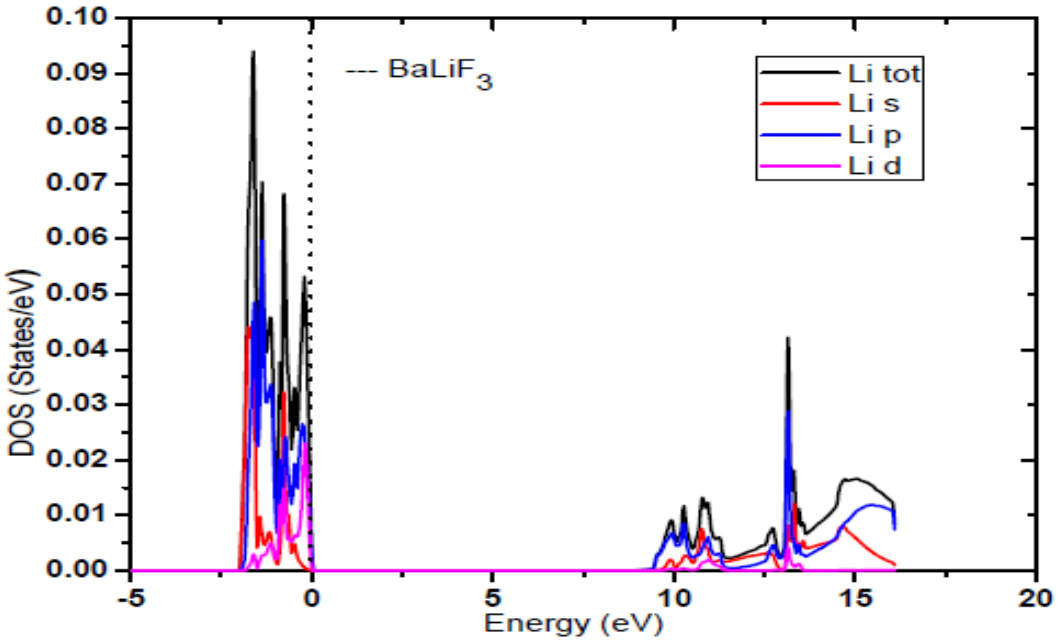

Fig. 4.19: Total and partial DOS plots for atom Li

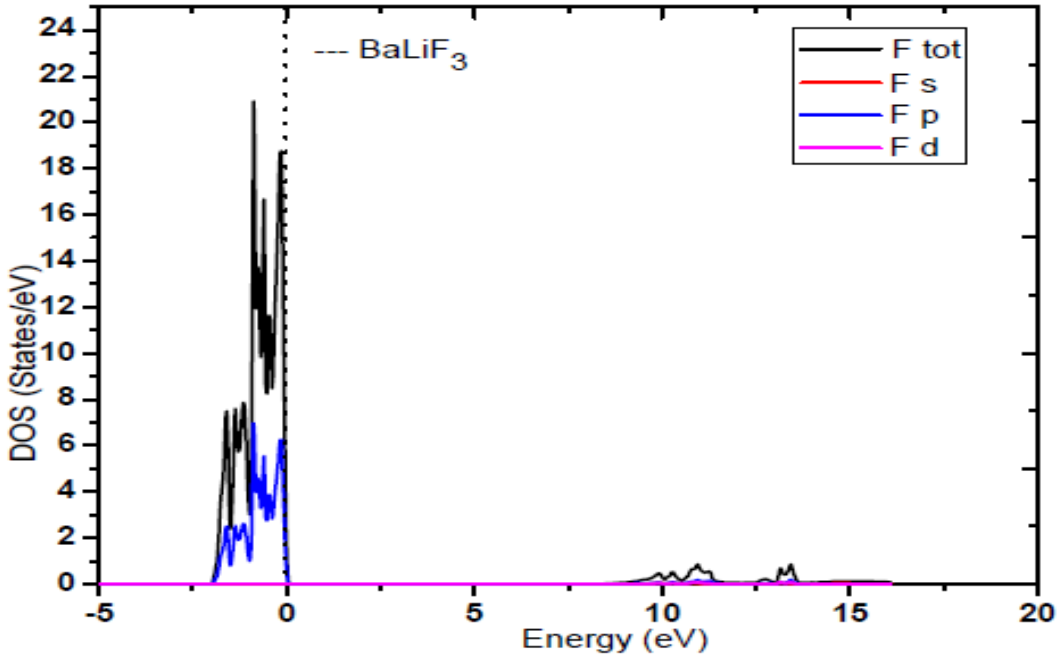

Fig. 4.20: Total and partial DOS plots for atom F

(b) $BaKF_3$

The calculated results of total density of states (TDOS) and partial density of states (PDOS) for $BaKF_3$ compound are given in this section. Fig.4.21 shows the plot of total density of states (TDOS) for $BaKF_3$ and individual atoms Ba, K, and F. In the valence region below the Fermi level, we have found the maximum peak in TDOS for $BaKF_3$ at - 0.63 eV. The occurrence of this maximum in peak in TDOS of $BaKF_3$ at -0.63 eV appears to be the contribution due to F atom. The reason being that the TDOS of F atom is also maximum at -0.63 eV. Also in valence band region, we find from the plots that the contributions to the origin of peak in TDOS of $BakF_3$ by other atoms Ba and K is very low and hence are negligible. Similarly, in the conduction band above the Fermi level in Fig. 4.21, the maximum peak in TDOS for $BaKF_3$ is observed at 9.92 eV. The occurrence of this maximum in peak in TDOS of $BaKF_3$ at 9.92 eV is due to the main contribution by atom Ba. The reason is that the TDOS of Ba atom is also maximum at 9.92 eV. We find negligible contribution in TDOS of $BaKF_3$ by atoms K and F which is seen in Fig.4.21.

In Fig. 4.22, the plots of TDOS and partial density of states (PDOS) of Ba atom in $BaKF_3$ compound are shown. In the valence band, we have found that there is negligible contribution to TDOS and PDOS by electrons of atom Ba. However in the conduction band region, we find from the plots that the maximum peak in TDOS occurs at 9.92 eV. This is due to the main contribution by the Ba-*f* state electrons. The reason is that the maximum of PDOS of Ba-*f* is also found at 9.92 eV which is seen in Fig.4.22.

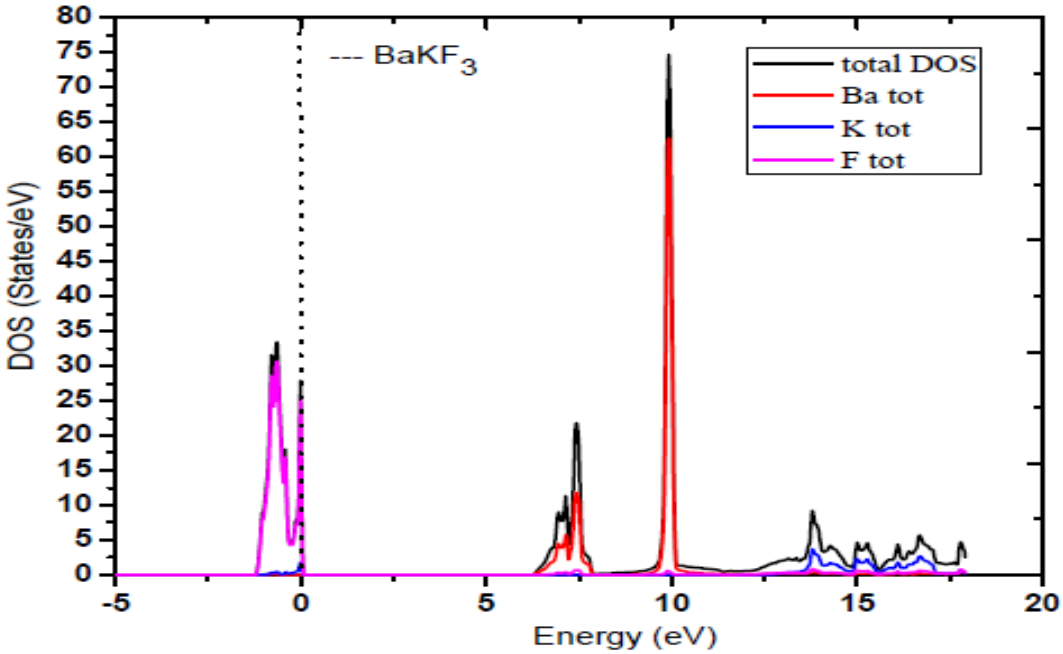

Fig. 4.21: Plots of total DOS for $BaKF_3$ and atoms Ba, K, F

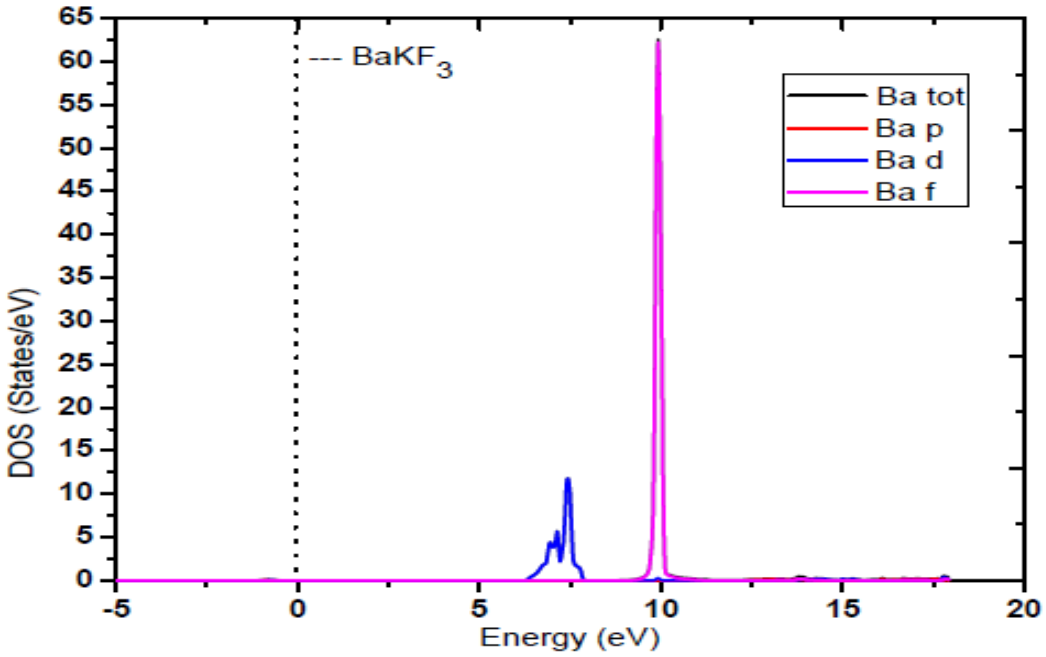

Fig.4.22: Total and partial DOS plots for atom Ba

The plot of TDOS and PDOS of K atom of $BaKF_3$ compound is shown in Fig. 4.23. We have found in the valence band below the Fermi level, the contribution of K-*p* state is found in TDOS in atom K. However in the conduction band, a maximum peak in TDOS is found at 13.81 eV. This can be attributed to K-*d* state electrons of atom K as shown in Fig. 4.23.

The plot of TDOS and PDOS of F atom in $BaKF_3$ compound is shown in Fig. 4.24. The maximum peak in TDOS is found at - 0.63 eV in the valence region below the Fermi level. From the plot we find that the contribution to the occurrence of this peak at -0.63 eV is due to the contribution by F-*p* state electrons. There is negligible contribution to TDOS and PDOS in conduction band in F atom as shown in Fig. 4.24.

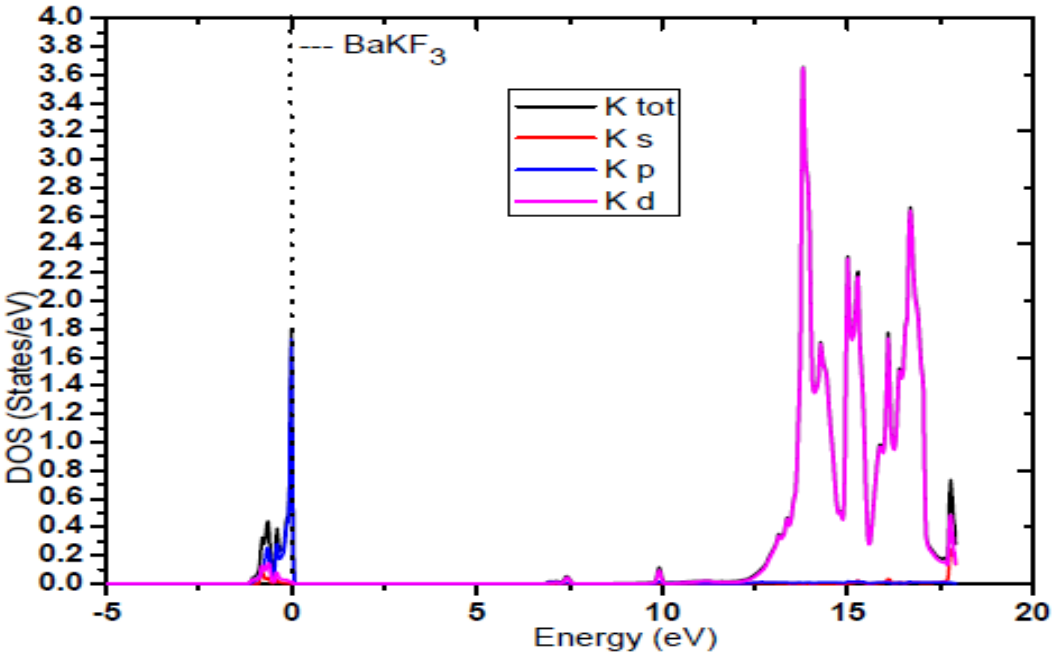

Fig. 4.23: Total and partial DOS plots for atom K

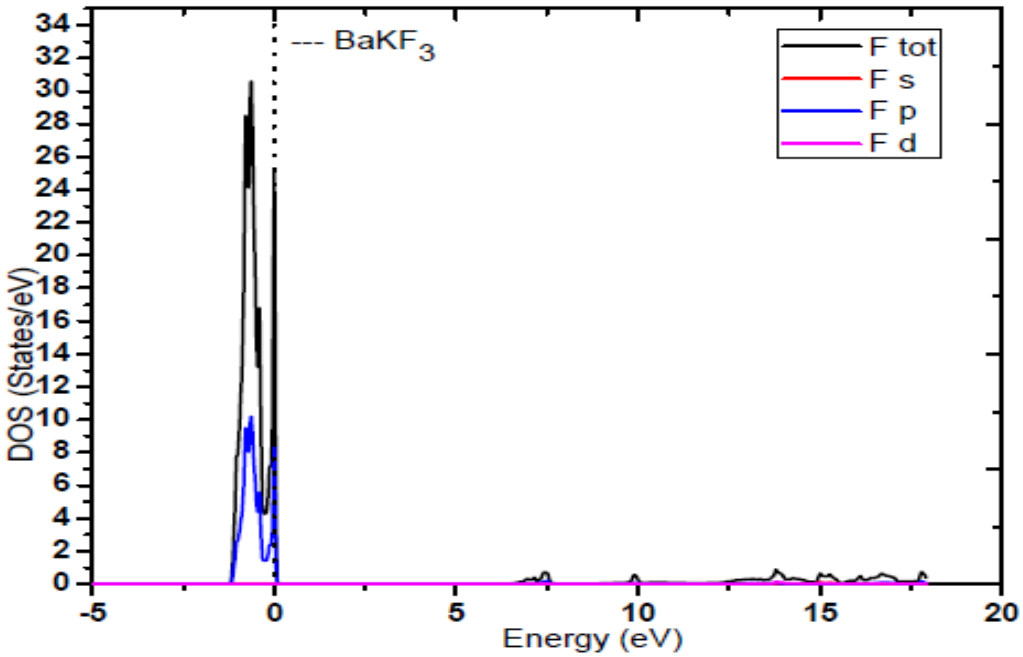

Fig. 4.24: Total and partial DOS plots for atom F

(c) $BaRbF_3$

Fig. 4.25 shows the total density of states (TDOS) of $BaRbF_3$ and individual atoms Ba, Rb and F. In the valence region below the Fermi level, a maximum peak in TDOS is found at – 0.91 eV. The occurrence of this maximum in peak in TDOS of $BaRbF_3$ at -0.91 eV appears to be the contribution due to F atom. The reason being that the TDOS of F atom is also maximum at -0.91 eV. Also in valence band region, we find from the plots that the contributions to the origin of peak in TDOS of $BaRbF_3$ by other atoms Ba and Rb is very low and hence are negligible. However in the conduction band above the Fermi level in Fig. 4.25, a maximum peak in TDOS is found at 8.71 eV. The occurrence of this maximum in peak in TDOS of $BaRbF_3$ at 8.71 eV appears to be the contribution due to Ba atom. The reason is that the TDOS of F atom is also maximum at 8.71 eV. We find negligible contribution in TDOS of $BaRbF_3$ by atoms Rb and F which is seen in Fig.4.25.

In Fig. 4.26, the plots of TDOS and partial density of states (PDOS) of Ba atom in $BaRbF_3$ compound are shown. In the valence band, we have found that there is negligible contribution to TDOS and PDOS by electrons of atom Ba. However in the conduction band region, we find from the plots that the maximum peak in TDOS occurs at 8.71 eV. This is due to the main contribution by the Ba-*f* state electrons. The reason is that the maximum of PDOS of Ba-*f* is also found at 8.71 eV which is seen in Fig.4.26.

.

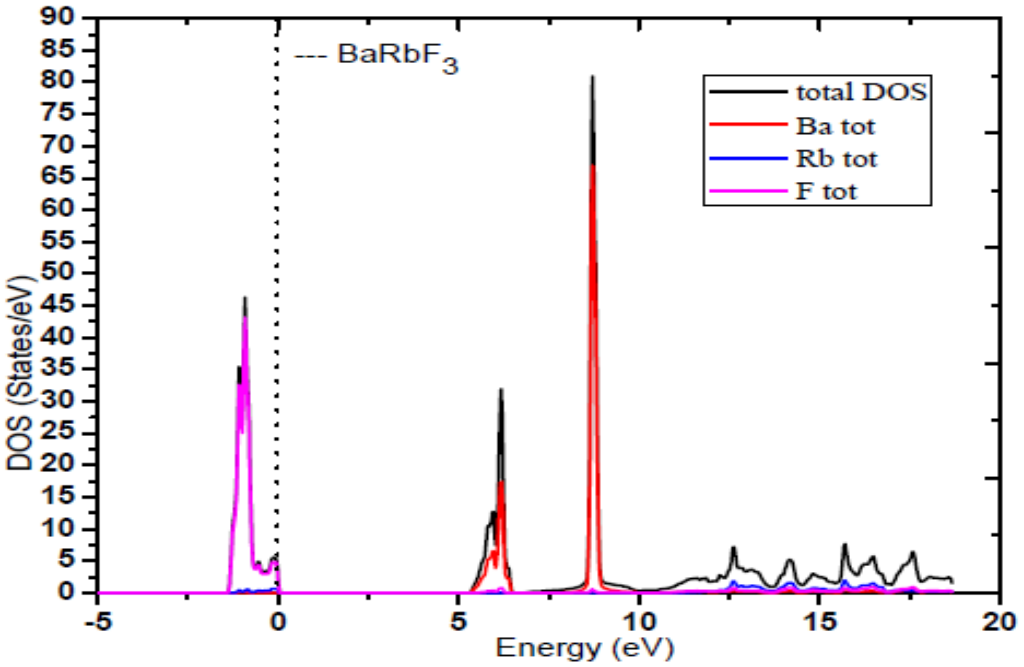

Fig. 4.25: Plots of total DOS for $BaRbF_3$ and atoms Ba, Rb, F

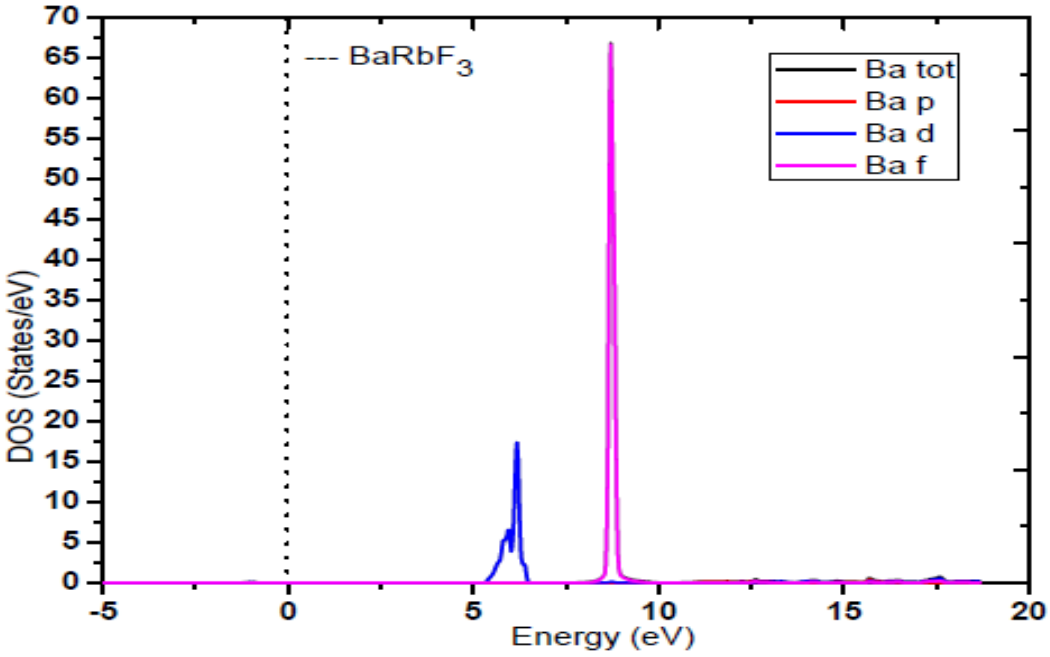

Fig. 4.26: Total and partial DOS plots for atom Ba

The plot of TDOS and PDOS of Rb atom of $BaRbF_3$ compound is shown in Fig. 4.27. We have found in the valence band below the Fermi level, the contribution of Rb-*p* state is found in TDOS in atom Rb. However in the conduction band, a maximum peak in TDOS is found at 15.71 eV. This is due to the main contribution by the Rb-*d* state electrons. This can be attributed to Rb-*d* state electrons of atom Rb as shown in Fig. 4.27.

The plot of TDOS and PDOS of F atom in $BaRbF_3$ compound is shown in Fig. 4.28. The maximum peak in TDOS is found at - 0.91 eV in the valence region below the Fermi level. From the plot we find that the contribution to the occurrence of this peak at -0.91 eV is due to the contribution by F-*p* state electrons. There is negligible contribution to TDOS and PDOS in conduction band in F atom as shown in Fig. 4.28.

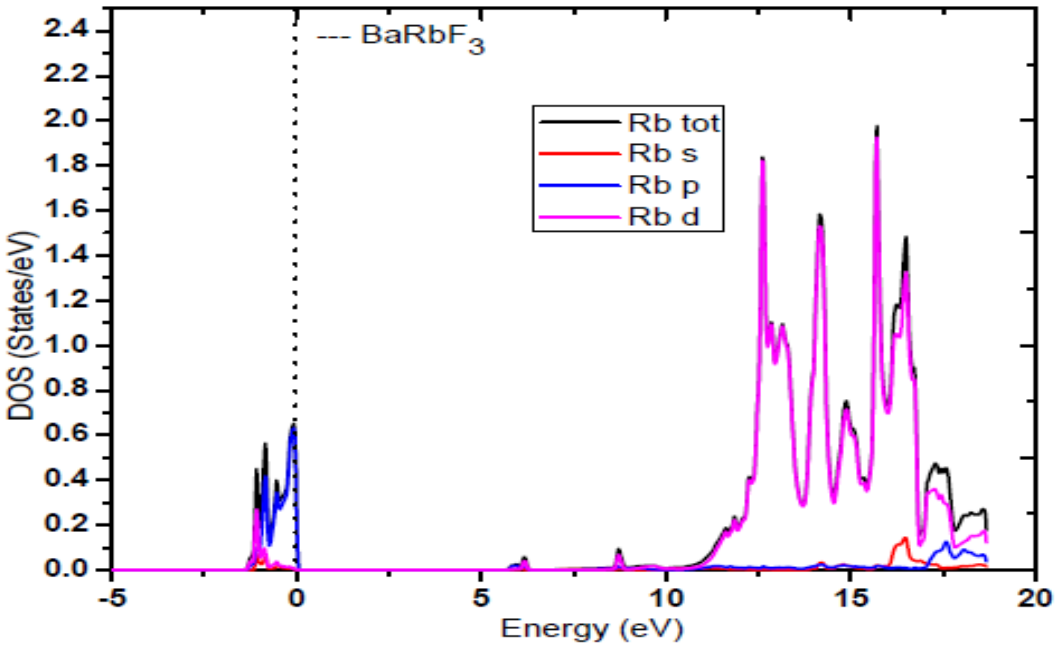

Fig. 4.27: Total and partial DOS plots for atom Rb

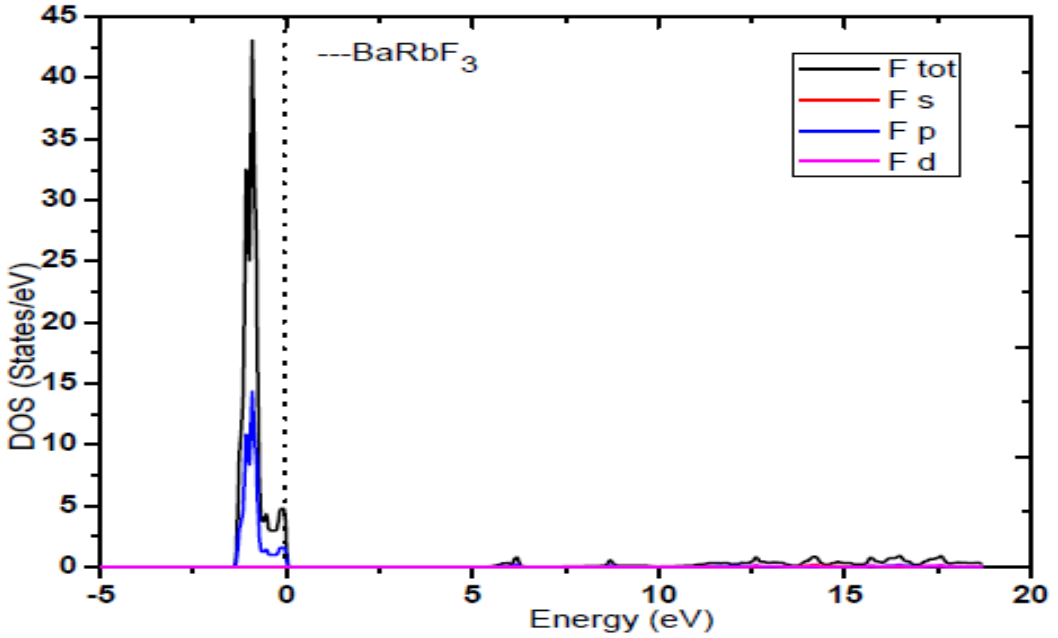

Fig. 3.28: Total and partial DOS plots for atom F

4.3 Electronic Band Structures for Alkaline Earth and Alkali Elements

We present here the result for each compound calculated by using GGA method which is followed by results of calculation done by suing mBJ potential. In this section, the results of calculation of band structures in the case of a combination of $BaBF_3$ (B = Li, K, Rb) is presented. Calculations have been done by using FP-LAPW method as discussed in Chapter 2. For this purpose, the approximations for exchange-correlation potential used is Generalised Gradient approximation (GGA).The calculated band gaps obtained by using the GGA approximations is underestimated i.e. usually smaller than experimentally obtained values in most of the insulating materials. Hence in order to reproduce a comparable value of band gaps, modified Becke-Johnson (mBJ) potential approach will also be used to calculate the energy gaps in the system. The mBJ potential is used in conjunction with the WIEN2k code to calculate band gaps (E_{BG}) as in the case of GGA approaches.

4.3.1 Study of Energy Bands for Alkaline Earth and Alkali Elements

(a) Energy Bands of $BaBF_3$ (B = Li, K, Rb) using GGA method

The electronic properties of $BaBF_3$ (B = Li, K, Rb) are calculated with first principles FP-LAPW method using GGA and mBJ exchange potential. To calculate DOS and band structure of $BaBF_3$, the optimized lattice parameters are used. The calculated electronic band structures for fluoroperovskites $BaBF_3$ (B = Li, K, Rb) along the high-symmetry directions of the Brillouin zone are shown in Figs. 4.29-4.31. We have found that the maximum of the valence band are found to be at a symmetry point Γ and the minimum conduction bands are located at the Γ point of the Brillouin zone in $BaBF_3$ compounds, resulting into direct band gaps in all the compounds. The calculated direct band gaps $(\Gamma - \Gamma)$ are found as 6.9 eV, 4.8 eV and 3.9 eV for $BaLiF_3$, $BaKF_3$ and $BaRbF_3$ respectively on the GGA approach.

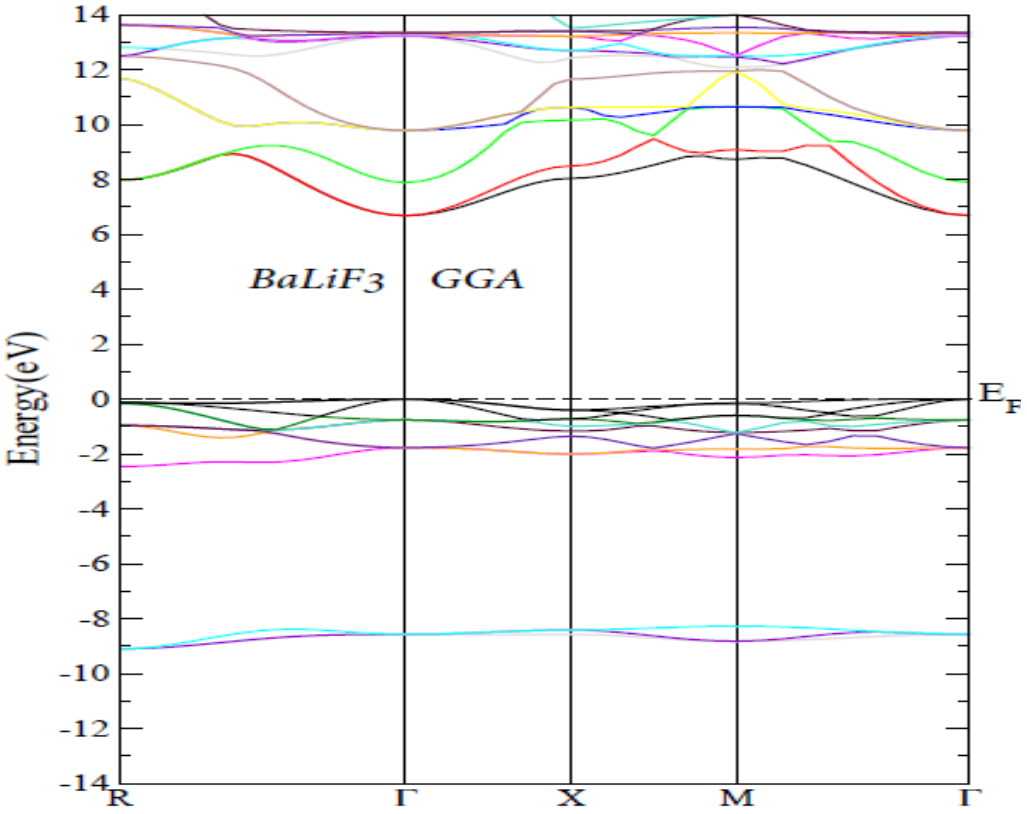

Fig. 4.29: Band structures for $BaLiF_3$ in GGA

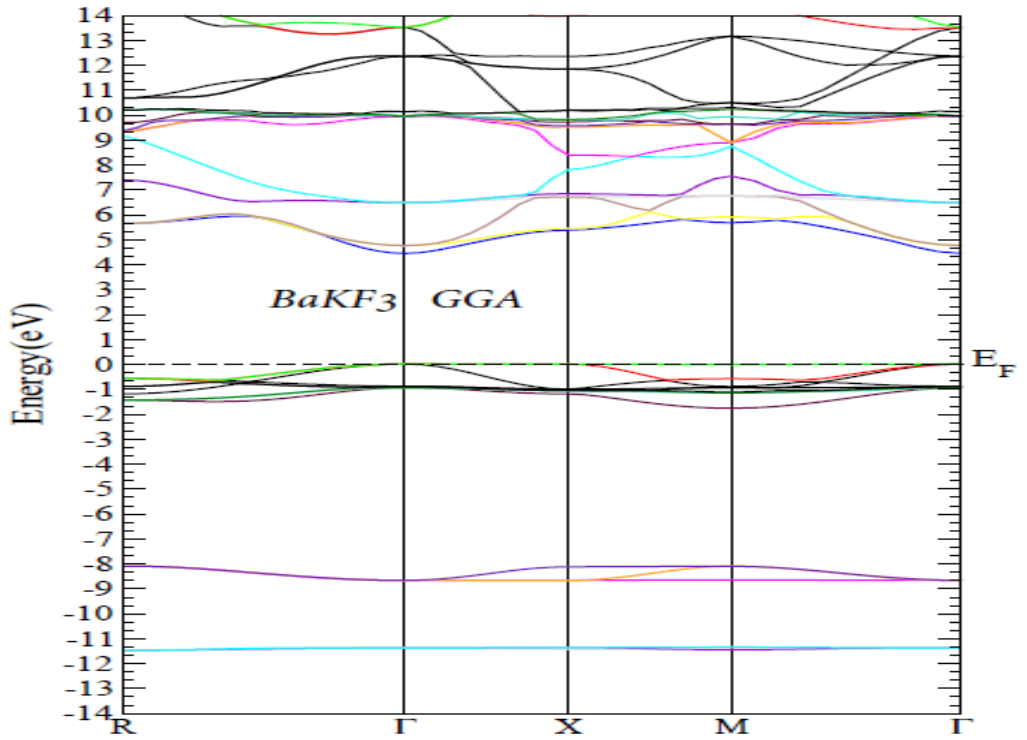

Fig. 4.30: Band structures for $BaKF_3$ in GGA

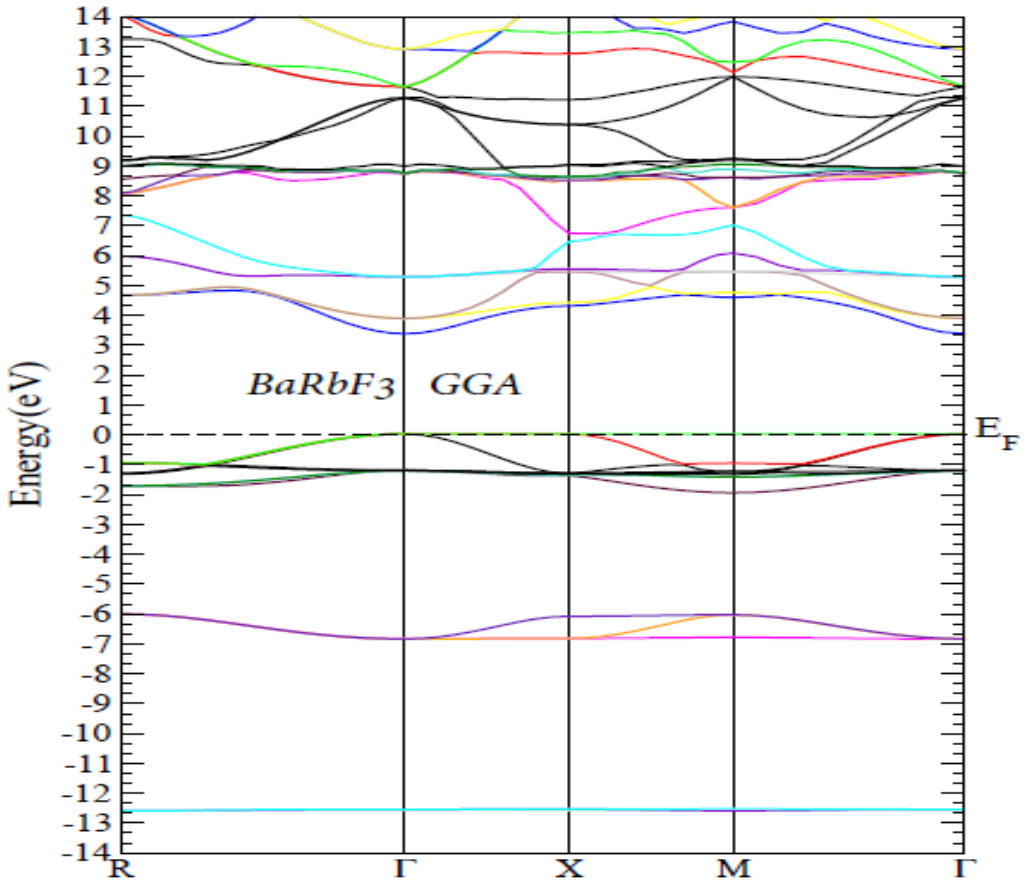

Fig. 4.31: Band structures for $BaRbF_3$ in GGA

(b) Energy Bands of $BaBF_3$ (B = Li, K, Rb) using mBJ potential

The electronic properties of $BaBF_3$ (B = Li, K, Rb) are calculated with first principles FP-LAPW method using GGA and mBJ exchange potential. To calculate DOS and band structure of $BaBF_3$, the optimized lattice parameters are used. The calculated electronic band structures for fluoroperovskites $BaBF_3$ (B = Li, K, Rb) along the high-symmetry directions of the Brillouin zone are shown in Fig. 4.32-4.34. We have found that the maximum of the valence band are found to be at a symmetry point Γ and the minimum conduction bands are located at the Γ point of the Brillouin zone in $BaBF_3$ compounds, resulting into direct band gaps in all the compounds. The calculated direct band gaps $(\Gamma-\Gamma)$ are found as 8.3 eV, 6.3 eV and 5.3 eV for $BaLiF_3$, $BaKF_3$ and $BaRbF_3$ respectively on the mBJ approach. From the study of DOS, the band gaps are found due to the contribution of F-*2p* state electrons in the valence band below the Fermi level and most of Ba-*d* state electrons in conduction band above the Fermi level in mBJ approach.

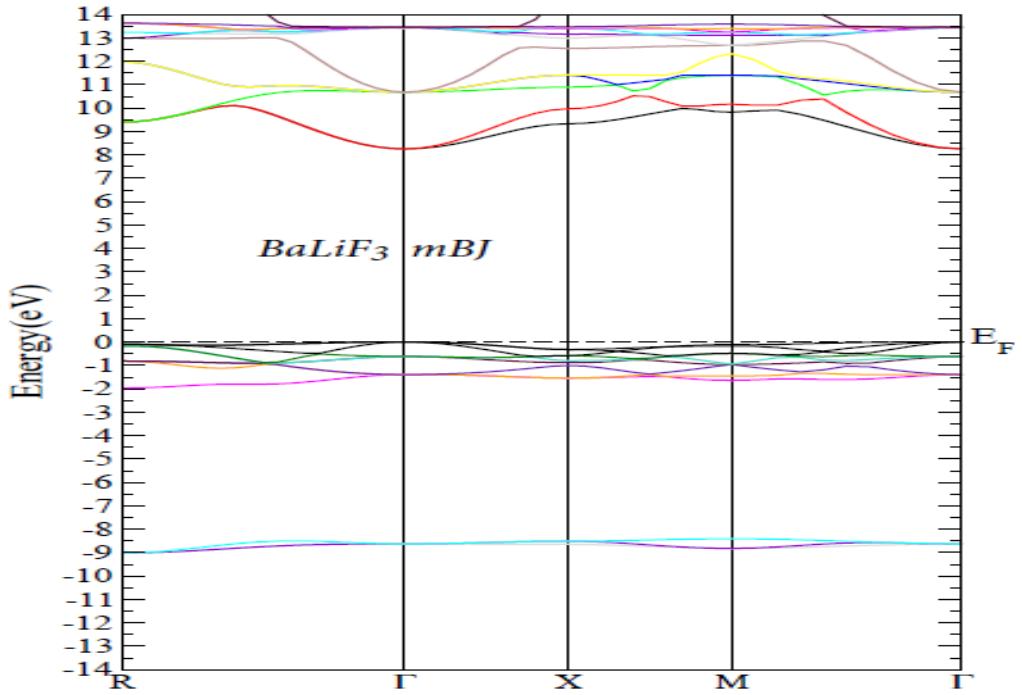

Fig. 4.32: Band structures for $BaLiF_3$ in mBJ

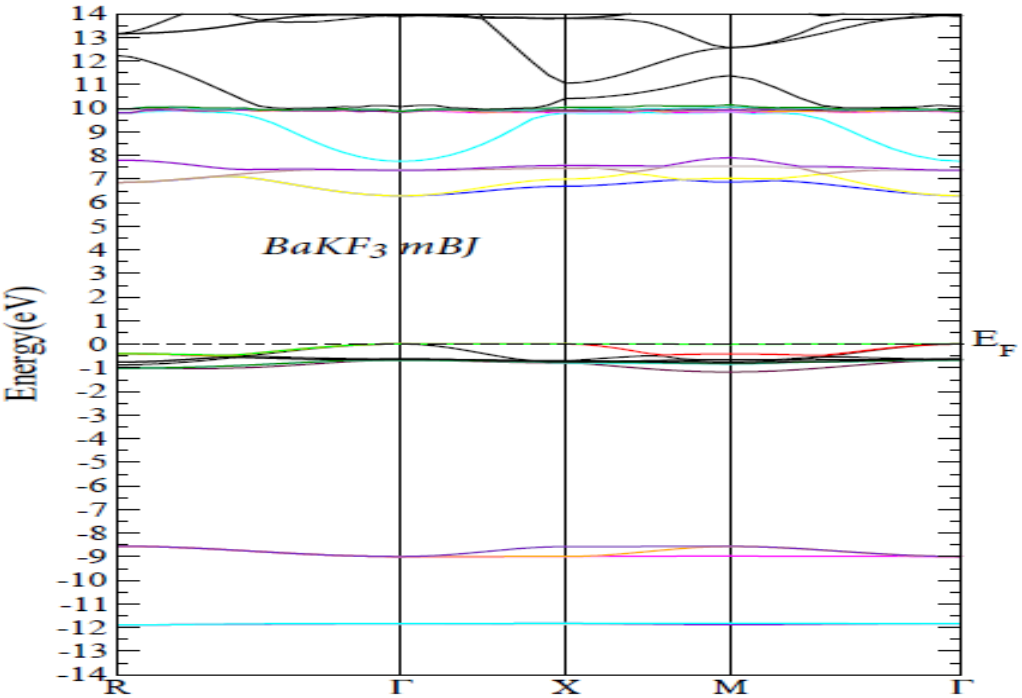

Fig. 4.33: Band structures for $BaKF_3$ in mBJ

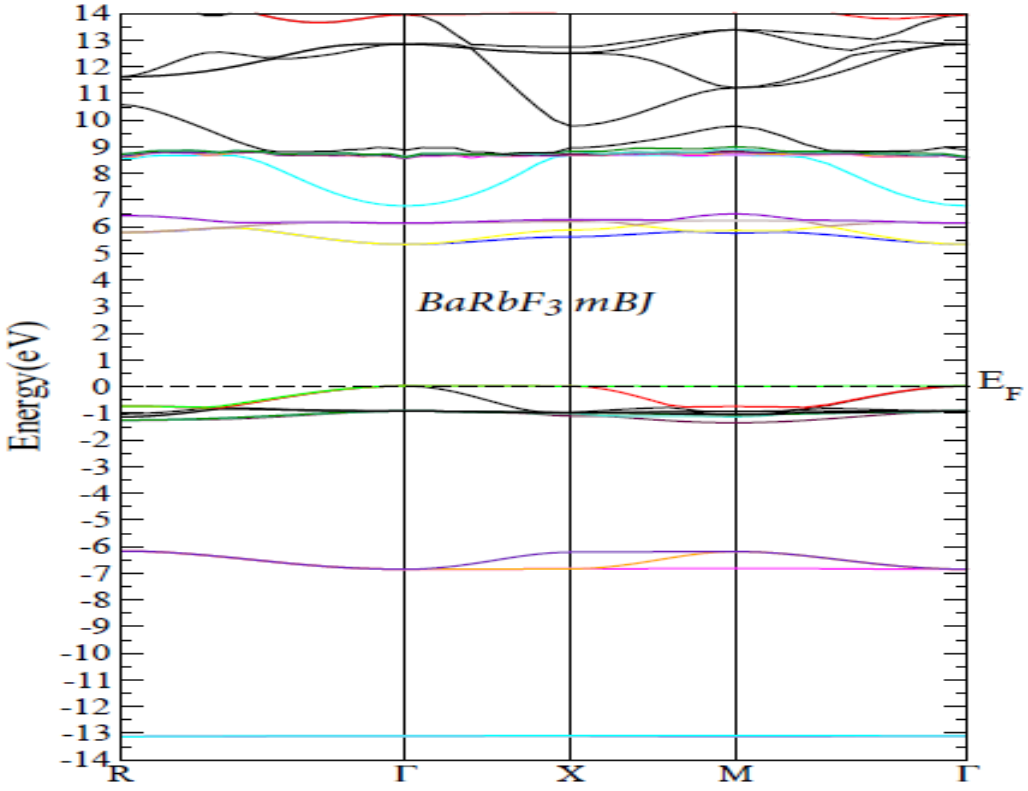

Fig. 4.34: Band structures for $BaRbF_3$ in mBJ potential

Chapter-5

Study of Electronic Properties of Fluoride Perovskite with Alkali and Transition Elements

In this chapter, we will present the results of calculations of the structural parameters like optimized lattice constants, equilibrium pressure and its derivative for the ABF_3 type perovskite. We have chosen the combinations of alkali metal as A = Rb, and transition metals B = Cu, Ag. The results of total and partial density of states and also the energy bands of these systems will be discussed here in the context of FP-LAPW model within density functional theory. The exchange correlations potentials used for the calculation is by using the GGA and mBJ potential, hence the results obtained is presented for both of these methods.

5.1 Structural Optimization

All physical and electronic properties of a solid are related to its structure, lattice constants and the total energy of the crystal. In this section, the calculations of structural optimization with cubical fluoride perovskite $RbBF_3$ (B = Cu, Ag) is presented. These calculations are performed with an exchange-correlation functional given by generalized gradient approximation (GGA) (Perdew *et al*., 1996) within the frame work of DFT (Hohenberg and Kohn 1964), where full-potential linearized augmented plane wave (FP-LAPW) (Singh, 1994) is adopted for the basis set. In this method the space is divided into non-overlapping muffin-tin (MT) spheres separated by an interstitial region (Fig. 2.1 of Chapter-2), the detail of which is discussed in section 2.5 of Chapter-2. The basis functions

are expanded like as in section 3.1 of chapter-3. The calculated lattice constants, bulk modulus and its pressure derivative of the compound $RbBF_3$ are given in Table 5.1.

In order to obtain the equilibrium lattice constant and the bulk modulus for the cubic perovskite $RbBF_3$, we performed the structural optimization by minimizing the total energy with respect to the cell parameters and the atomic positions. To study the crystal structure, we start with the total energy minimization of cubic $RbBF_3$ as a function of volume. This can be understood from the plots of the total energy as a function of volume which are shown in Figs. 5.3-5.4 for $RbCuF_3$ and $RbAgF_3$ respectively. The energy versus volume data was fitted to a Murnaghan equation of state (Murnaghan, 1944) to obtain the equilibrium lattice constants (a = b, c), the bulk modulus (B) and its first pressure derivative (B'). We note that the result of the lattice constants obtained within our GGA calculations increases with the change of cation (B) from Cu to Ag which is similar to the experimental results and are shown in Table 5.1. From our calculations, we have found $RbCuF_3$ has more value of B than in $RbAgF_3$. From this calculation, we have found more pressure derivative (B') in $RbAgF_3$ than in $RbCuF_3$compound.

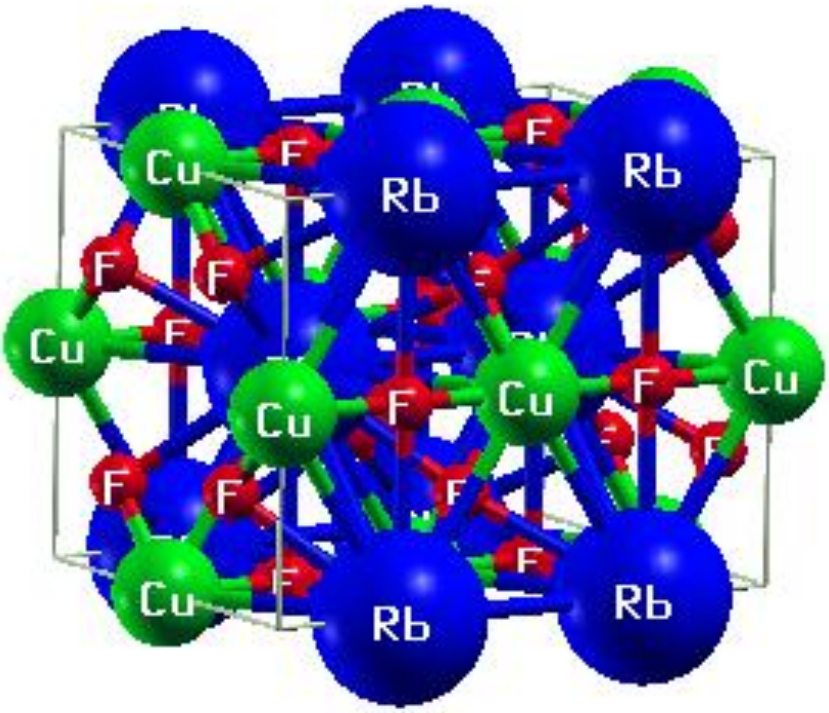

Fig. 5.1: Crystal structure for $RbCuF_3$

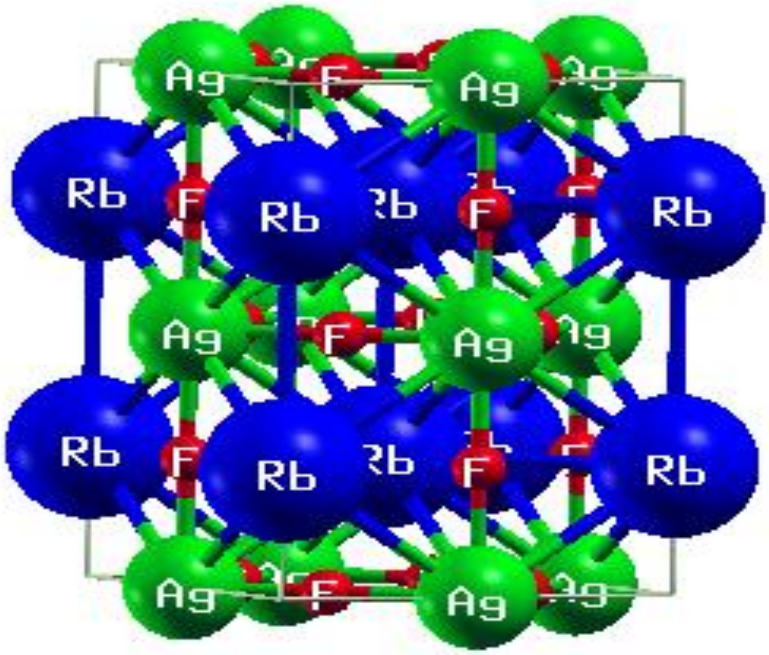

Fig. 5.2: Crystal structure for $RbAgF_3$

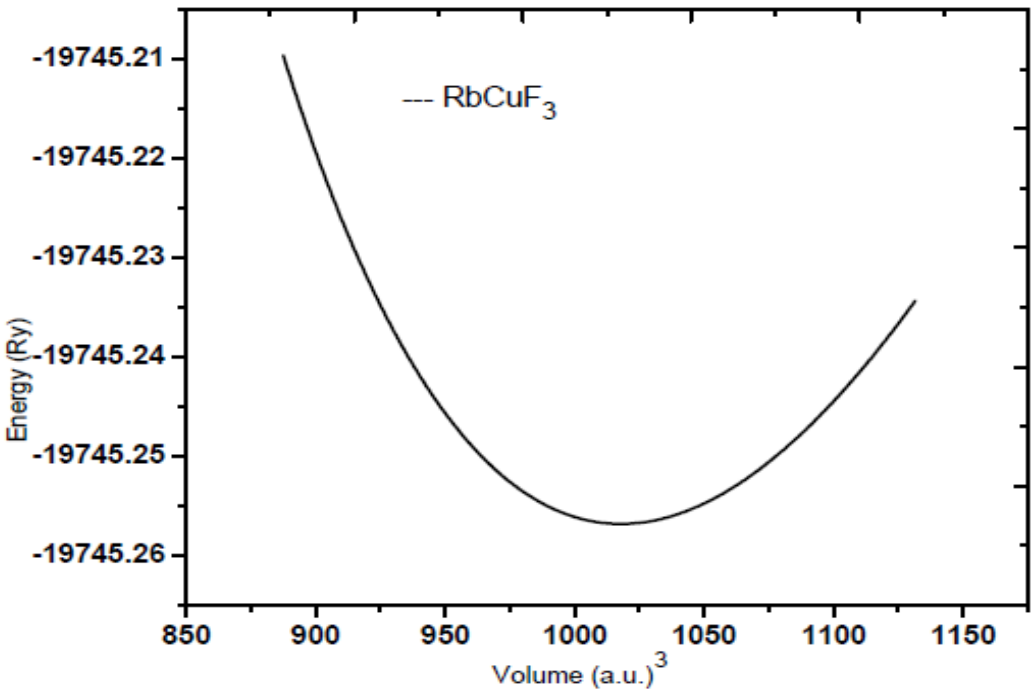

Fig. 5.3: Volume optimization curve for $RbCuF_3$

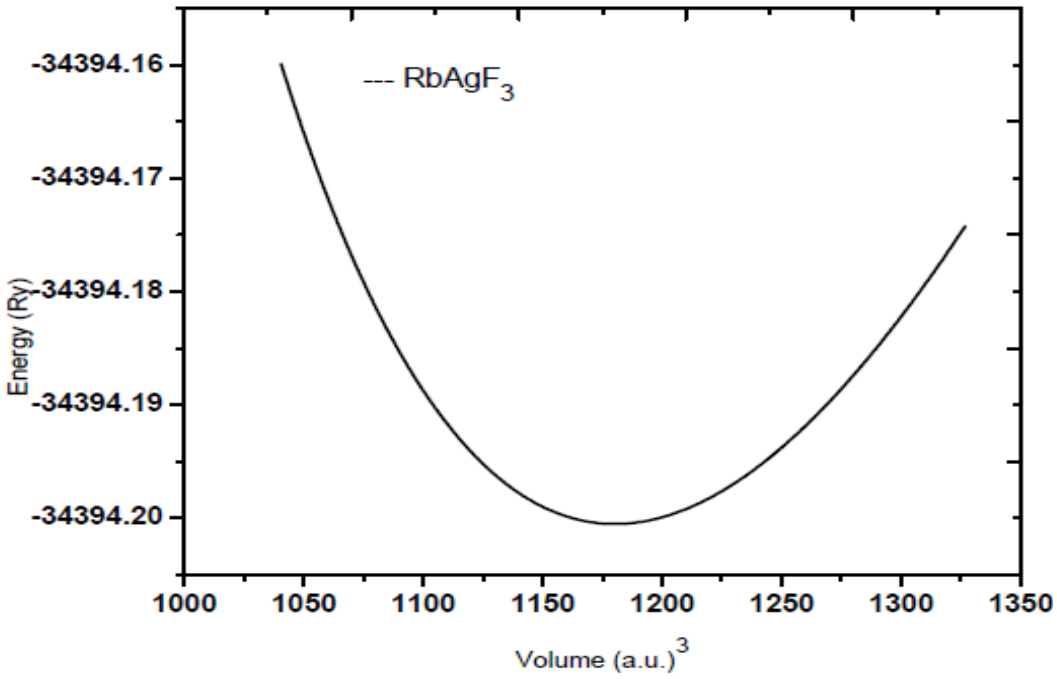

Fig. 5.4: Volume optimization curve for $RbAgF_3$

Table 5.1: Calculated lattice constants (a = b, c) in Å, bulk modulus B in GPa and its pressure derivative B' of $RbBF_3$ (B = Cu, Ag) are given in the following table.

Compounds	**Previous lattice constants (a = b, c) in Å**	**Calculated lattice constants (a = b, c) in Å**	**Calculated results B(GPa)**	**Calculated results B'**
$RbCuF_3$	a= b = 5.901[x], c = 7.724[x]	a =b = 5.916, c =7.899	63.7868	4.8403
$RbAgF_3$	a = b = 6.0756[y] , c =8.5457[y]	a = b= 6.1023 , c =8.6607	54.396	5.4395

Experimental values,

[x] (Kaiser *et al*.,1990), [y](Lufaso et al., 2001)

5.2 Density of State (DOS) for Alkali and Transition Elements

In this section, the results of calculations of density of states (DOS), will be presented for the combination of systems of choice namely $RbBF_3$ (B = Cu, Ag) Calculations for this purpose has been done by using the approximations for the exchange-correlation potentials such as GGA and mBJ under FP-LAPW method on the base of density functional theory (DFT). The details of these methods have already been given in Chapter-2. In this method, the space is divided into non-overlapping muffin-tin (MT) spheres separated by an interstitial region. The basis functions are expanded into spherical harmonic functions inside the muffin-tin sphere ad the Fourier series in the interstitial region. The convergence of basis set was controlled by a cutoff parameter R_{MT} x K_{max} = 7 where R_{MT} is the smallest of the MT sphere radii and K_{max} is the largest reciprocal lattice vector used in the plane wave expansion. The cutoff energy which defines the separation of valence and core states was chosen as -8.0 Ry. For k point sampling, a 1000 k-point mesh in the first Brillouin zone was used. The self-consistent calculations were considered to be converged until the integrated charge difference between the last two iterations was less than 10^{-4} eV. Even though the ground state is well described by GGA, the values of the band gaps are sometimes underestimated. For this reason we have the modified Becke Johnson potential (mBJ) to calculate for improved values of the band gaps (Perdew *et al*., 1996) for all the systems. The theoretically obtained lattice parameters calculated in Chapter-3 have been used here for DOS and energy bands calculations. We present in this section the results of total DOS and partial DOS in the case of $RbBF_3$ (B = Cu, Ag). The DOS for these systems had been calculated using the same method but for the exchange correlation potential calculated by GGA and mBJ approximations.

5.2.1 Calculation of DOS by using GGA method for Alkali and Transition Elements

(a) $RbCuF_3$

In this section the calculated results of total density of states (TDOS) and partial density of states (PDOS) for $RbCuF_3$ compound are given. The plot of TDOS of $RbCuF_3$ and individual atoms Rb, Cu and F are given in Fig.5.5. In the valence region below the Fermi level, we have found the maximum peak in TDOS for $RbCuF_3$ at – 1.22 eV. The occurrence of this maximum in peak in TDOS of $RbCuF_3$ at -1.22 eV appears to be the contribution due to Cu atom. The reason is that the TDOS of Cu atom is also maximum at -1.22 eV. Also in valence band region, we have found other two peaks in TDOS for $RbCuF_3$ at -3.15 eV and at -8.76 eV. The occurrence of these peaks in TDOS of $RbCuF_3$ at -3.15 eV, appear due to contribution by F atom only. Rb atom is in the core state and hence do not contribute to DOS. Similarly, in the conduction band above the Fermi level in Fig. 5.5, the maximum peak in TDOS for $RbCuF_3$ is observed at 10.36 eV. The occurrence of this maximum in peak in TDOS of $RbCuF_3$ at 10.36 eV is due to the contribution by Rb atom. The reason for this beeing is that the TDOS of atoms Cu and F are very low.

In Fig. 5.6, the plots of TDOS and partial density of states (PDOS) of Rb atom in $RbCuF_3$ compound are shown. In the valence band below the Fermi level, we have found a maximum peak in TDOS of Rb atom at -8.76 eV which is in the core state. Hence there is no contribution to DOS by Rb atom. However in the conduction band region, we find from the plots that the maximum peak in TDOS occurs at 10.36 eV. This is due to the main contribution by the Rb-*d* electrons of Rb atom. The reason is that the maximum of PDOS of Rb-*d* is also found at 10.36 eV.

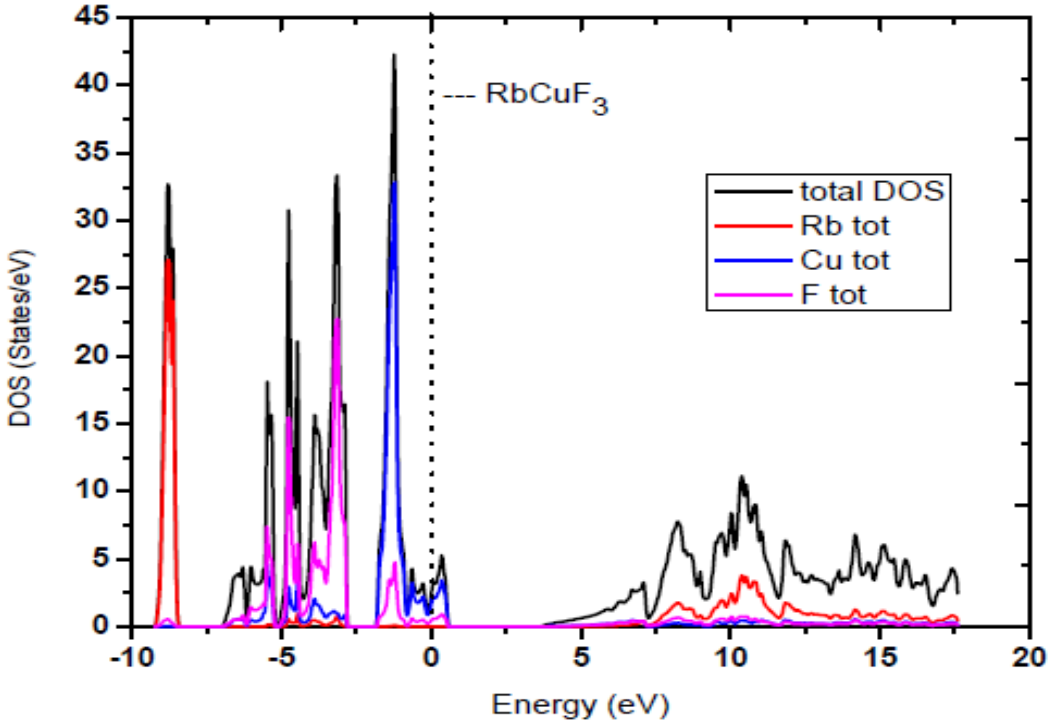

Fig. 5.5: Plots of total DOS for $RbCuF_3$ and atoms Rb, Cu, F

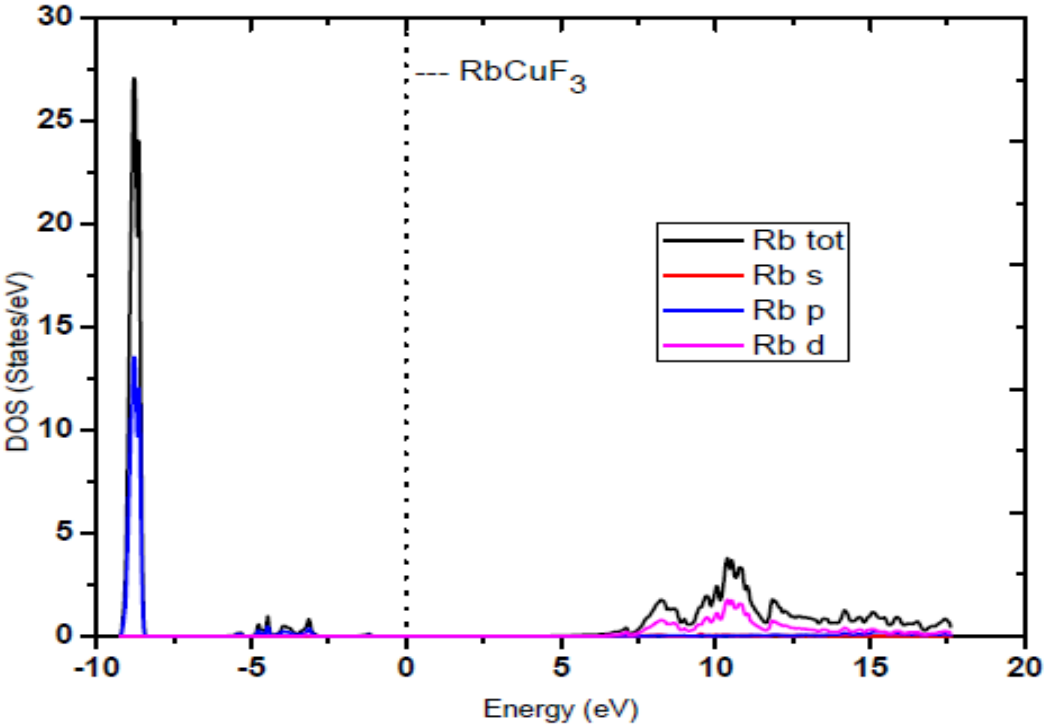

Fig. 5.6: Total and partial DOS plots of atom Rb

Fig.5.7 shows the plot of TDOS and PDOS of Cu atom of $RbCuF_3$ compound. In the valence band below the Fermi level, we have found a maximum peak in TDOS of Cu atom at -1.22 eV. The occurrence of this maximum in peak in TDOS of Cu atom at -1.22 eV appears to be the contribution due to Cu-*d* electrons of Cu atom. However in the conduction band above the Fermi level, negligible contribution is found to TDOS and PDOS in Cu atom as shown in Fig. 5.7.

The plot of TDOS and PDOS of F atom in $RbCuF_3$ compound is shown in Fig. 5.8. The maximum peak in TDOS is found at – 3.15 eV in the valence region below the Fermi level. From the plot we find that the contribution to the occurrence of this peak at -3.15 eV is due to the contribution by F-*p* state electrons. There is negligible contribution to TDOS and PDOS in conduction band in F atom as shown in Fig. 5.8.

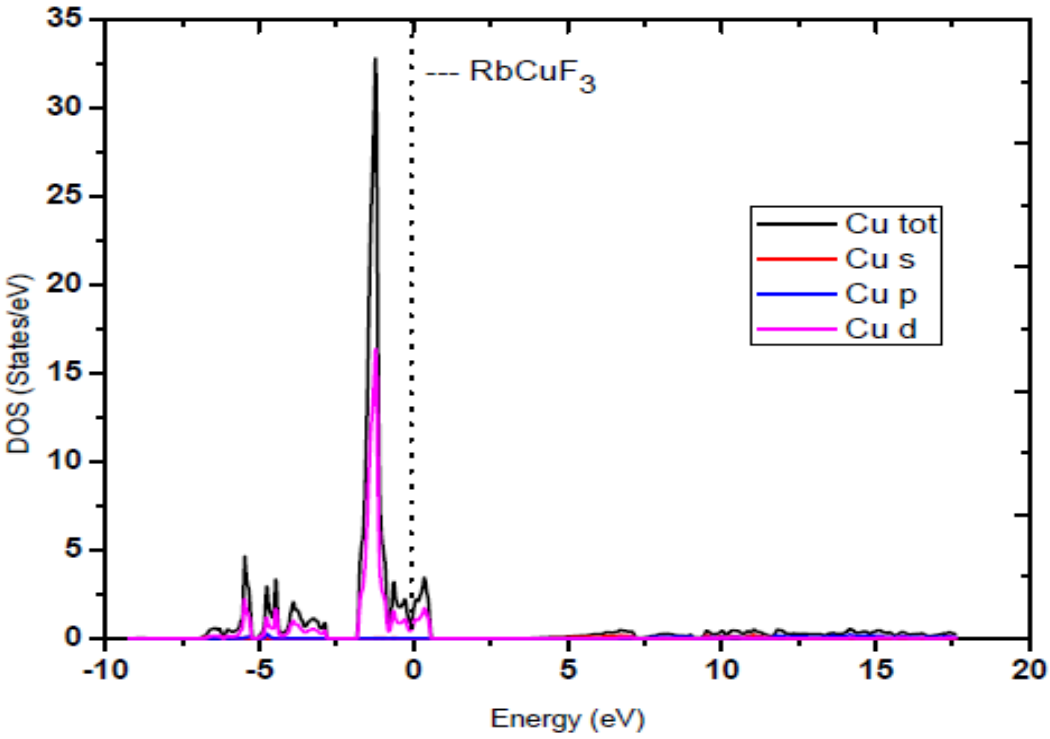

Fig. 5.7: Total and partial DOS plots of atom Cu

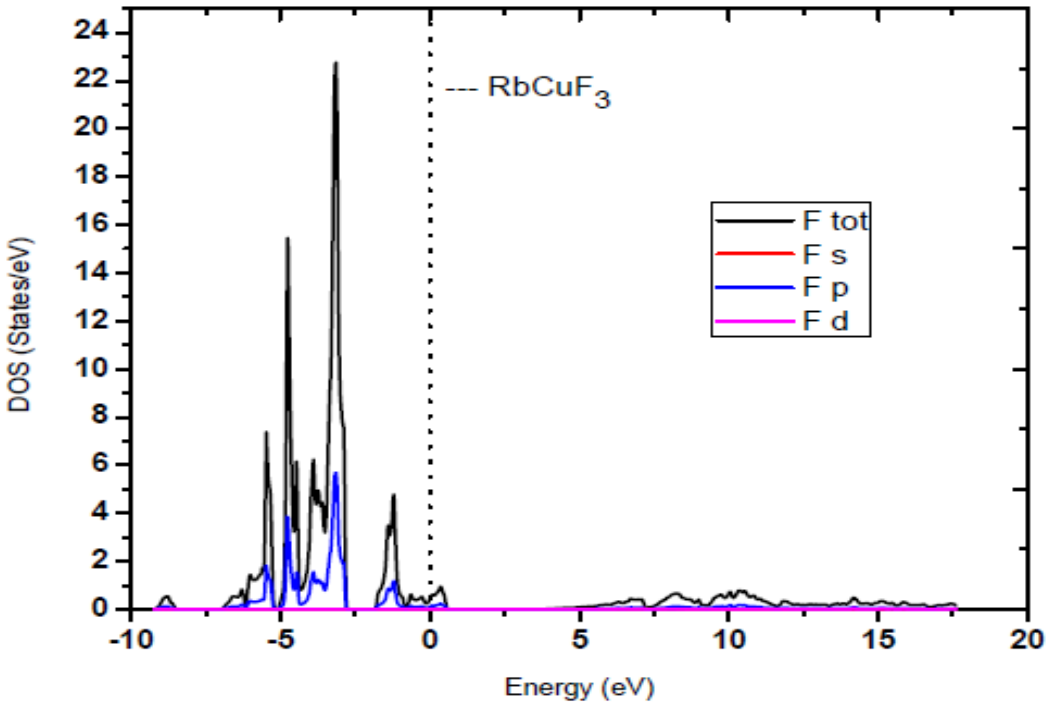

Fig. 5.8: Total and partial DOS plots of atom F

(b) $RbAgF_3$

The calculated results of total density of states (TDOS) and partial density of states (PDOS) for $RbAgF_3$ compound are given in this section. Fig.5.9 shows the plot of total density of states (TDOS) for $RbAgF_3$ and individual atoms Rb, Ag, and F. In the valence region below the Fermi level, we have found the maximum peak in TDOS for $RbAgF_3$ at – 1.61 eV. The occurrence of this maximum in peak in TDOS of $RbCuF_3$ at -1.61eV appears to be the contribution due to Ag atom. The reason is that the TDOS of Ag atom is also maximum at -1.61 eV. Also in valence band region, we have found another peak in TDOS for $RbAgF_3$ at -2.73 eV. The occurrence of this peak in TDOS of $RbAgF_3$ at -2.73 eV appears to be the contribution due to F atom. Similarly, in the conduction band above the Fermi level in Fig. 5.9, the maximum peak in TDOS for $RbAgF_3$ is observed at 10.11 eV. The occurrence of this maximum in peak in TDOS of $RbAgF_3$ at 10.11eV is due to the main contribution by Rb atom. The reason is that the TDOS of Rb atom is also maximum at 10.11 eV. We find from the plots in Fig. 5.9, TDOS of $RbAgF_3$ by other atoms Ag and F are very low.

In Fig. 5.10, the plots of TDOS and partial density of states (PDOS) of Rb atom in $RbAgF_3$ compound are shown. In the valence band below the Fermi level, we have found that there is negligible contribution to TDOS and PDOS by electrons of Rb atom. However in the conduction band region, we find from the plots that the maximum peak in TDOS occurs at 10.11 eV. This is due to the main contribution by the Rb-*d* electrons of Rb atom. The reason is that the maximum of PDOS of Rb-*d* is also found at 10.11 eV which is seen in Fig. 5.10.

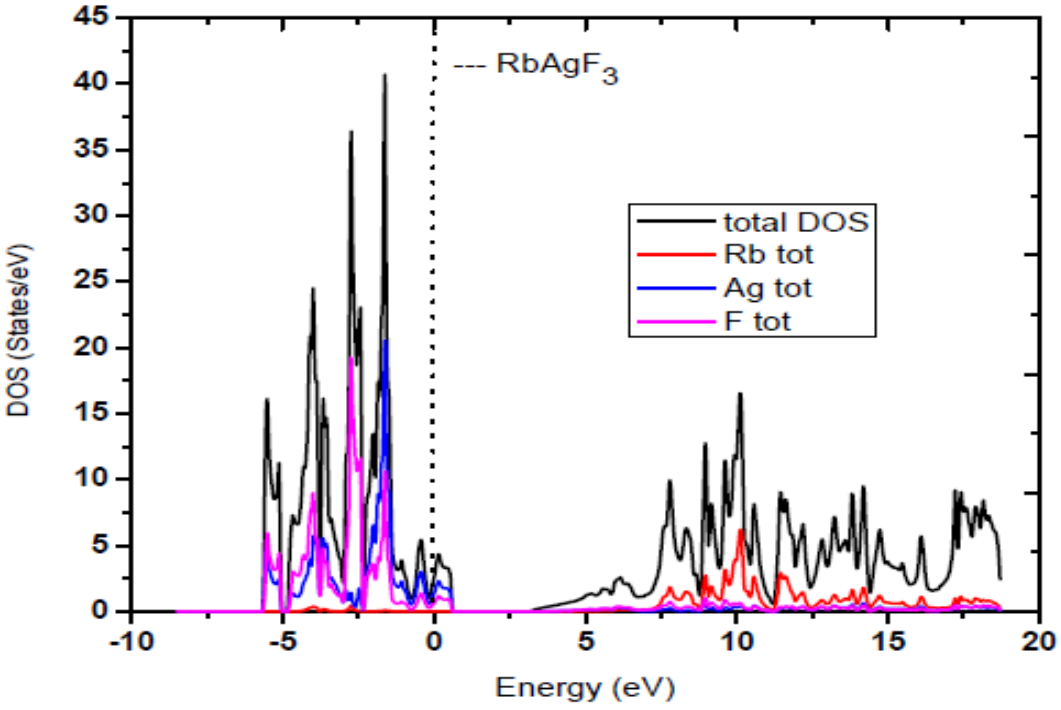

Fig. 5.9: Total DOS plots for $RbAgF_3$ and atoms Rb, Ag, F

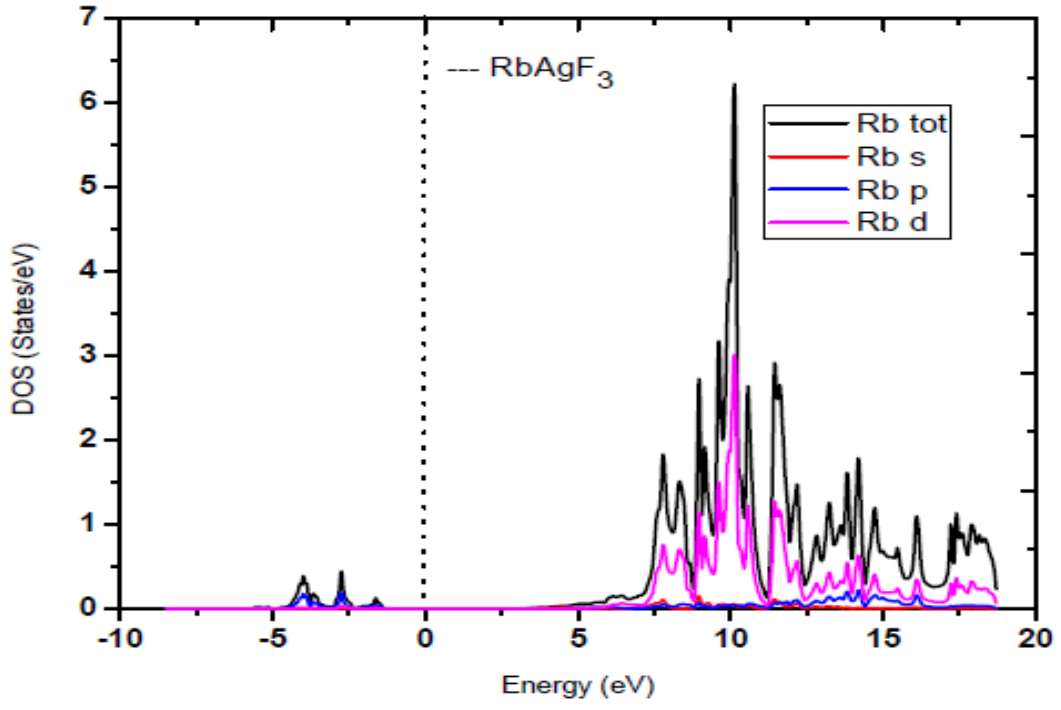

Fig. 5.10: Total and partial DOS plots for Rb atom

Fig.5.11 shows the plot of TDOS and PDOS of Ag atom of $RbAgF_3$ compound. In the valence band below the Fermi level, we have found a maximum peak in TDOS of Ag atom at -1.61 eV. The occurrence of this maximum in peak in TDOS of Ag atom at -1.61 eV appears to be the contribution due to Ag-*d* electrons of Ag atom. However in the conduction band above the Fermi level, negligible contribution is found to TDOS and PDOS in Ag atom as shown in Fig. 5.11.

The plot of TDOS and PDOS of F atom in $RbAgF_3$ compound is shown in Fig. 5.12. The maximum peak in TDOS is found at – 2.73 eV in the valence region below the Fermi level. From the plot we find that the contribution to the occurrence of this peak at -2.73 eV is due to the contribution by F-*p* state electrons. We have found that there is negligible contribution to TDOS and PDOS in conduction band in F atom as shown in Fig. 5.12.

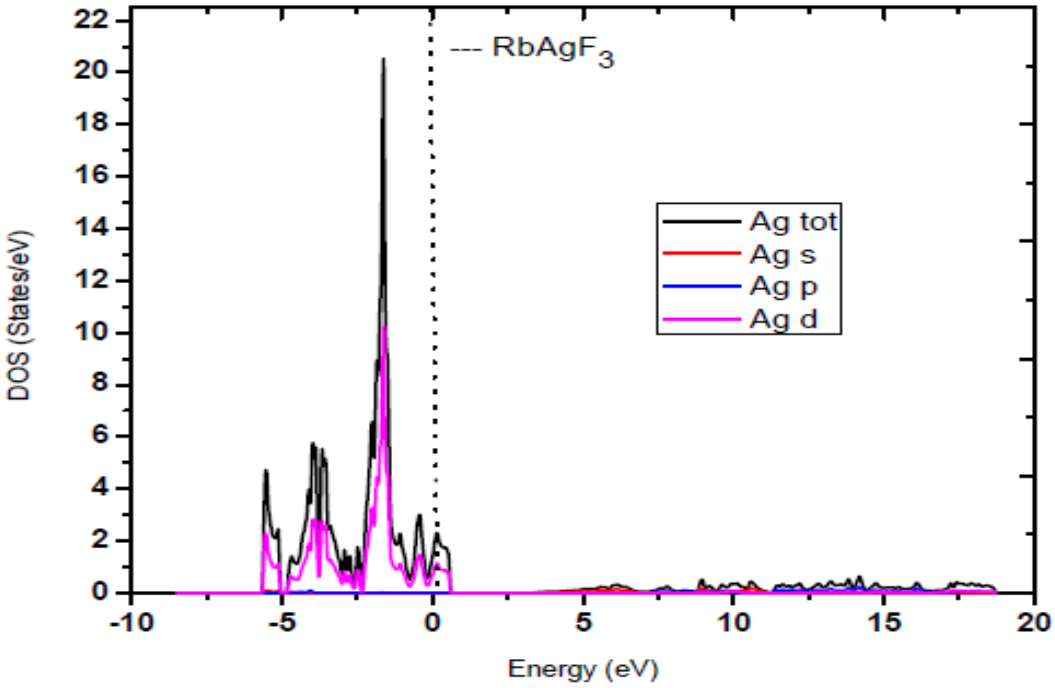

Fig. 5.11: Total and partial DOS plots for Ag atom

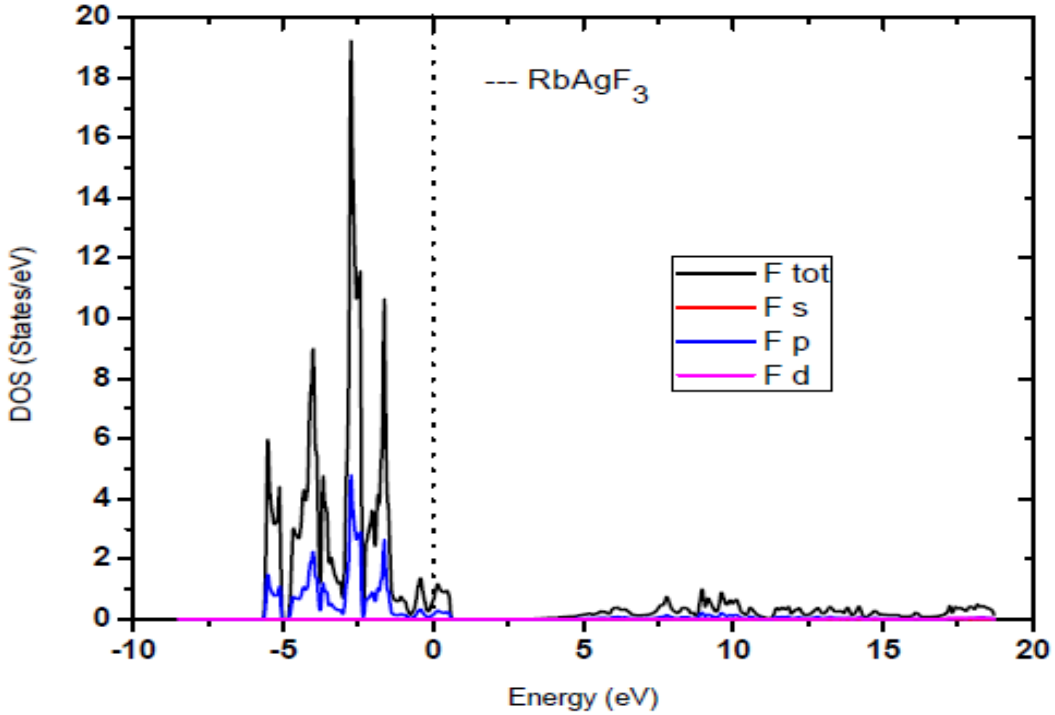

Fig. 5.12: Total and partial DOS plots for F atom

5.2.2 Calculation of DOS by using mBJ method for Alkali and Transition Elements

(a) $RbCuF_3$

In this section the calculated results of total density of states (TDOS) and partial density of states (PDOS) for $RbCuF_3$ compound are given. The plot of TDOS of $RbCuF_3$ and individual atoms Rb, Cu and F are given in Fig.5.13. In the valence region below the Fermi level, we have found the maximum peak in TDOS for $RbCuF_3$ at – 1.94 eV. The occurrence of this maximum in peak in TDOS of $RbCuF_3$ at -1.94 eV appears to be the contribution due to Cu atom. The reason is that the TDOS of Cu atom is also maximum at -1.94 eV. Also in valence band region, we have found other two peaks in TDOS for $RbCuF_3$ at -4.61 eV and at -10.54 eV. The occurrence of these peaks in TDOS of $RbCuF_3$ at -4.61 eV, -10.54 eV appear to be the contribution due to F and Rb atoms respectively. Similarly, in the conduction band above the Fermi level in Fig. 5.13, the maximum peak in TDOS for $RbCuF_3$ is observed at 10.43 eV. The occurrence of this maximum in peak in TDOS of $RbCuF_3$ at 10.43 eV is due to the main contribution by Rb atom. The reason is that the TDOS of Rb atom is also maximum at 10.43 eV. We find from the plots in Fig. 5.13, TDOS of $RbCuF_3$ by other atoms Cu and F are very low.

In Fig. 5.14, the plots of TDOS and partial density of states (PDOS) of Rb atom in $RbCuF_3$ compound are shown. In the valence band below the Fermi level, we have found a maximum peak in TDOS of Rb atom at -10.54 eV. The occurrence of this maximum in peak in TDOS of Rb atom at -10.54 eV appears to be the contribution due to Rb-*p* electrons of Rb atom. However in the conduction band region, we find from the plots that the maximum peak in TDOS occurs at 10.43 eV. This is due to the main contribution by the Rb-*d* electrons of Rb atom. The reason is that the maximum of PDOS of Rb-*d* is also found at 10.43 eV.

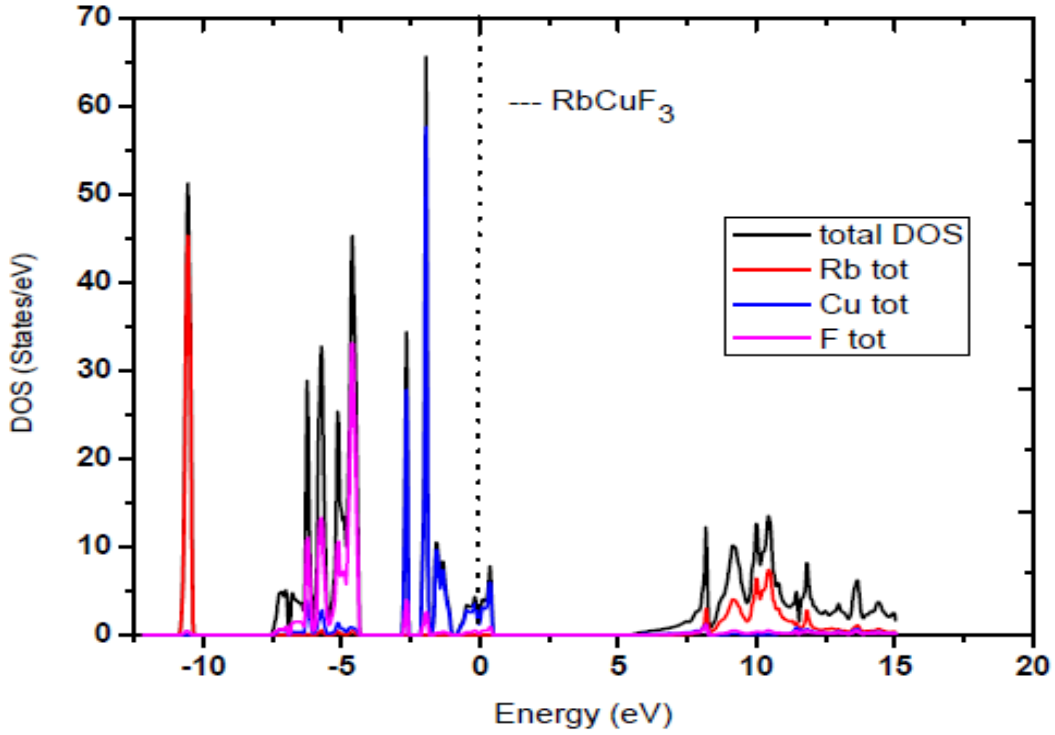

Fig. 5.13: Total DOS plots for $RbCuF_3$ and atoms Rb, Cu, F

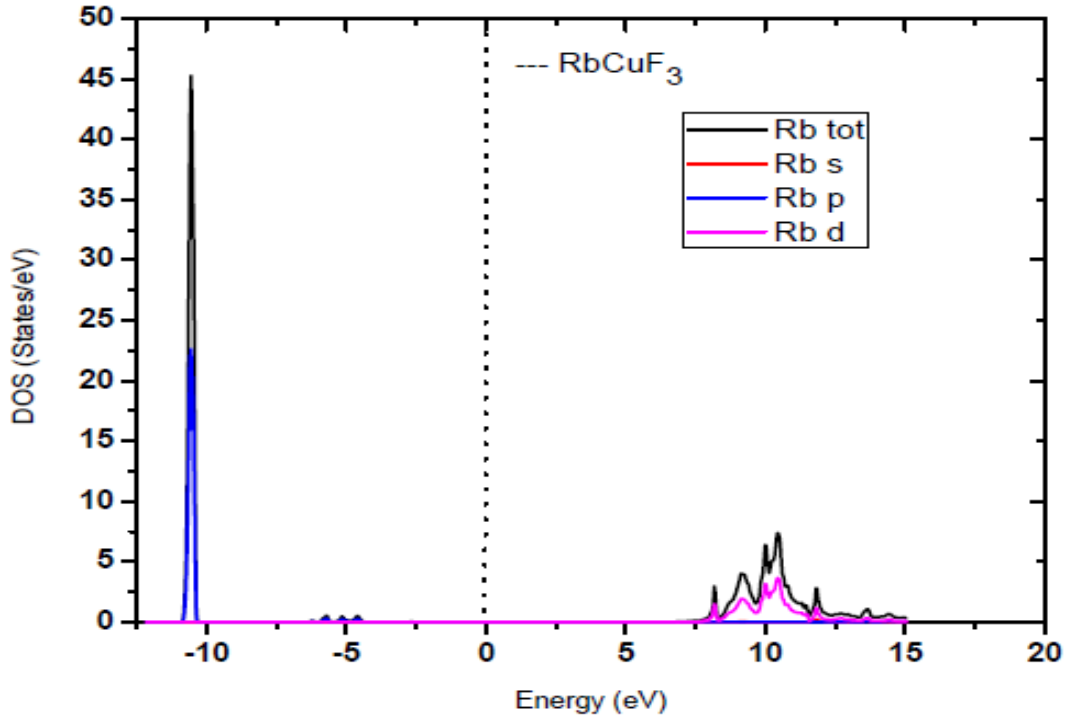

Fig. 5.14: Total and partial DOS plots for atom Rb

Fig.5.15 shows the plot of TDOS and PDOS of Cu atom of $RbCuF_3$ compound. In the valence band below the Fermi level, we have found a maximum peak in TDOS of Cu atom at -1.94 eV. The occurrence of this maximum in peak in TDOS of Cu atom at -1.94 eV appears to be the contribution due to Cu-*d* electrons of Cu atom. However in the conduction band above the Fermi level, negligible contribution is found to TDOS and PDOS in Cu atom as shown in Fig. 5.15.

The plot of TDOS and PDOS of F atom in $RbCuF_3$compound is shown in Fig. 5.16. The maximum peak in TDOS is found at – 4.61 eV in the valence region below the Fermi level. From the plot we find that the contribution to the occurrence of this peak at -4.61 eV is due to the contribution by F-*p* state electrons. There is negligible contribution to TDOS and PDOS in conduction band in F atom which is shown in Fig. 5.16.

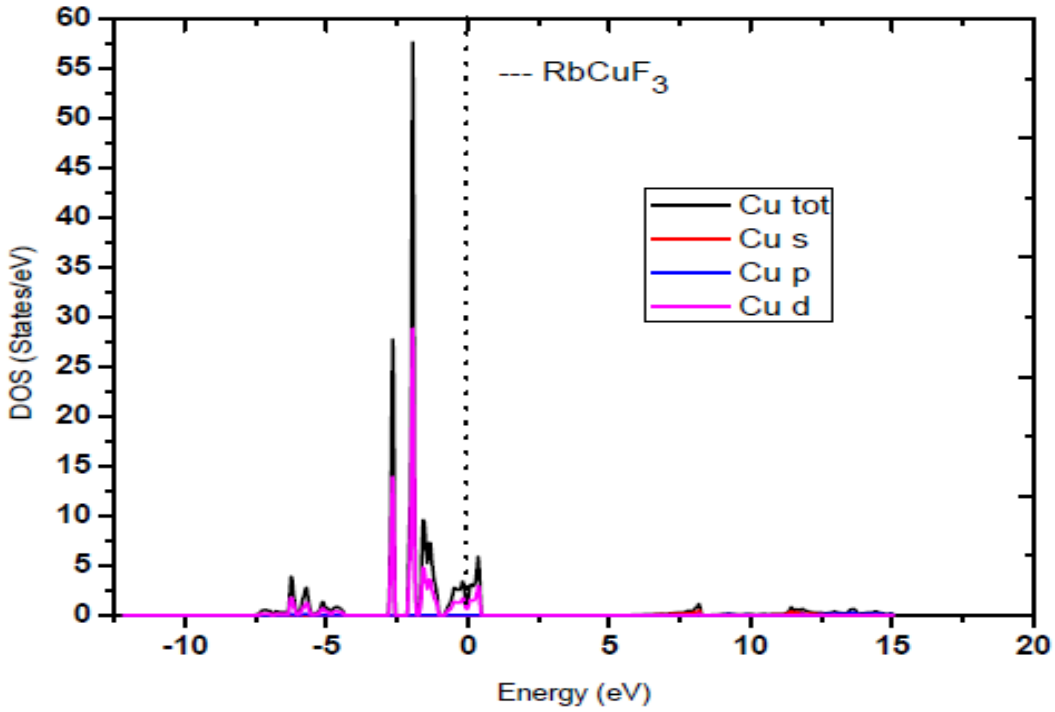

Fig. 5.15: Total and partial DOS plots for atom Cu

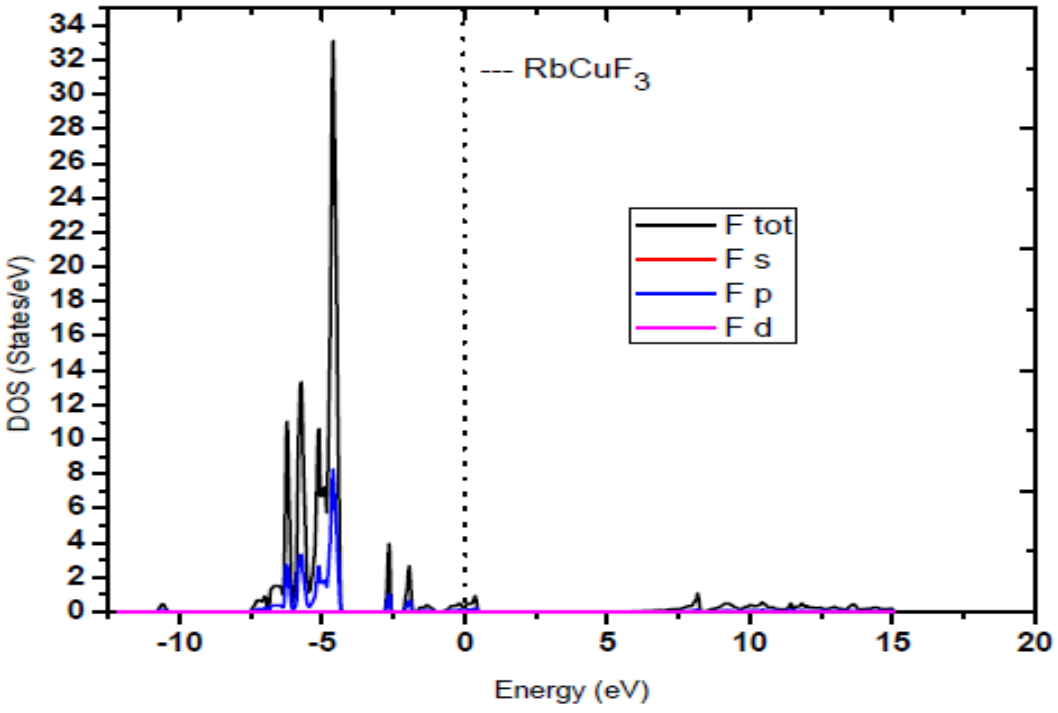

Fig. 5.16: Total and partial DOS plots for atom F

(b) $RbAgF_3$

The calculated results of total density of states (TDOS) and partial density of states (PDOS) for $RbAgF_3$ compound are given in this section. Fig.5.17 shows the plot of total density of states (TDOS) for $RbAgF_3$ and individual atoms Rb, Ag, and F. In the valence region below the Fermi level, we have found the maximum peak in TDOS for $RbAgF_3$ at – 4.25 eV. The occurrence of this maximum in peak in TDOS of $RbCuF_3$ at -4.25 appears to be the contribution due to F atom. The reason is that the TDOS of F atom is also maximum at -4.25 eV. Also in valence band region, we have found another peak in TDOS for $RbAgF_3$ at -2.67 eV. The occurrence of this peak in TDOS of $RbAgF_3$ at -2.67 eV appears to be the contribution due to Ag atom. Similarly, in the conduction band above the Fermi level in Fig. 5.17, the maximum peak in TDOS for $RbAgF_3$ is observed at 10.38 eV. The occurrence of this maximum in peak in TDOS of $RbAgF_3$ at 10.38eV is due to the main contribution by Rb atom. The reason is that the TDOS of Rb atom is also maximum at 10.38 eV. We find from the plots in Fig. 5.17, TDOS of $RbAgF_3$ by other atoms Ag and F are very low.

In Fig. 5.18, the plots of TDOS and partial density of states (PDOS) of Rb atom in $RbAgF_3$ compound are shown. In the valence band below the Fermi level, we have found that there is negligible contribution to TDOS and PDOS by electrons of Rb atom. However in the conduction band region, we find from the plots that the maximum peak in TDOS occurs at 10.38 eV. This is due to the main contribution by the Rb-*d* electrons of Rb atom. The reason is that the maximum of PDOS of Rb-*d* is also found at 10.38 eV which is seen in Fig. 5.18.

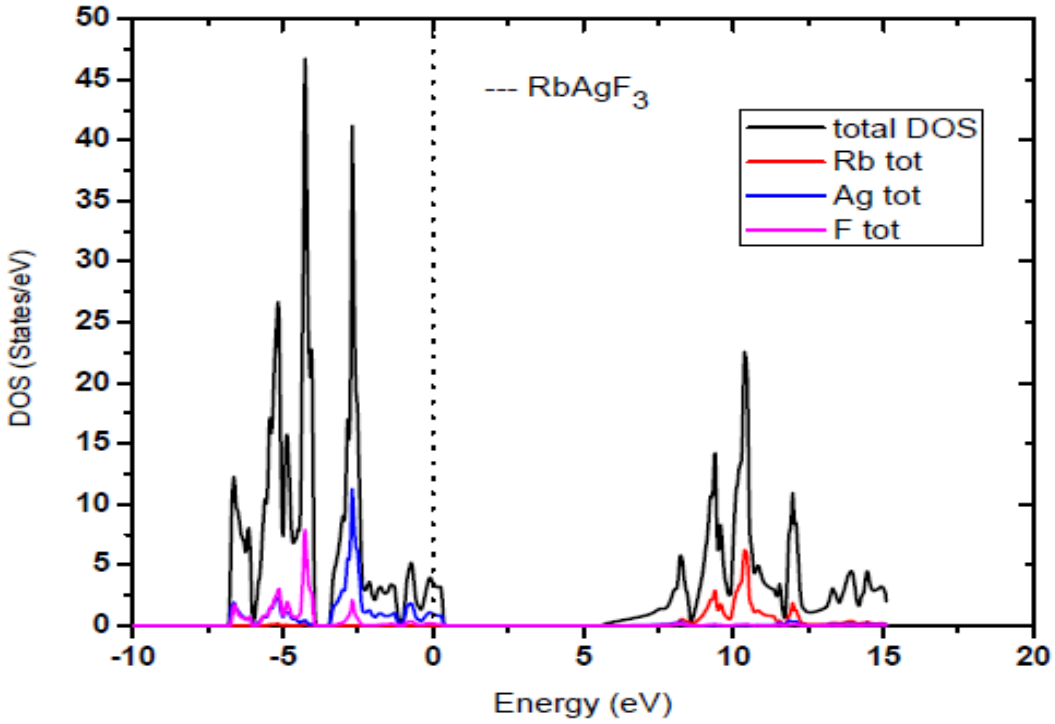

Fig. 5.17: Total DOS plots for $RbAgF_3$ and atoms Rb, Ag, F

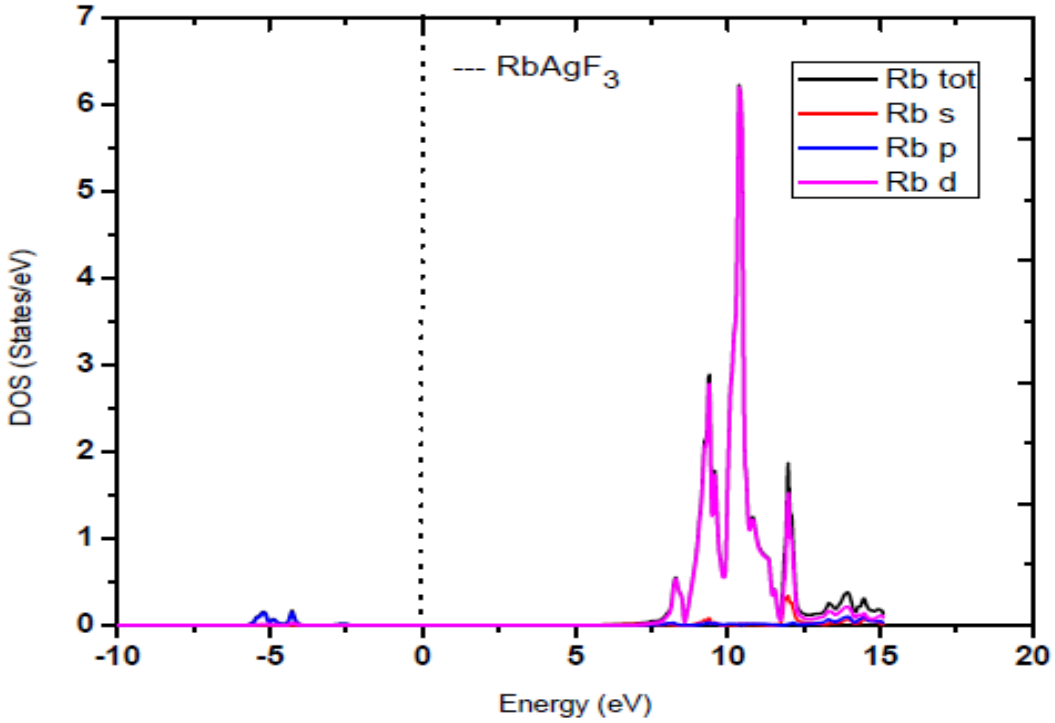

Fig.5.18: Total and partial DOS plots for atom Rb

Fig.5.19 shows the plot of TDOS and PDOS of Ag atom of $RbAgF_3$ compound. In the valence band below the Fermi level, we have found a maximum peak in TDOS of Ag atom at -2.67 eV. The occurrence of this maximum in peak in TDOS of Ag atom at -2.67 eV appears to be the contribution due to Ag-*d* electrons of Ag atom. However in the conduction band above the Fermi level, negligible contribution is found to TDOS and PDOS in Ag atom as shown in Fig. 5.19.

The plot of TDOS and PDOS of F atom in $RbAgF_3$ compound is shown in Fig. 5.20. The maximum peak in TDOS is found at – 4.25 eV in the valence region below the Fermi level. From the plot we find that the contribution to the occurrence of this peak at -4.25 eV is due to the contribution by F-*p* state electrons. We have found that there is negligible contribution to TDOS and PDOS in conduction band in F atom as shown in Fig. 5.20.

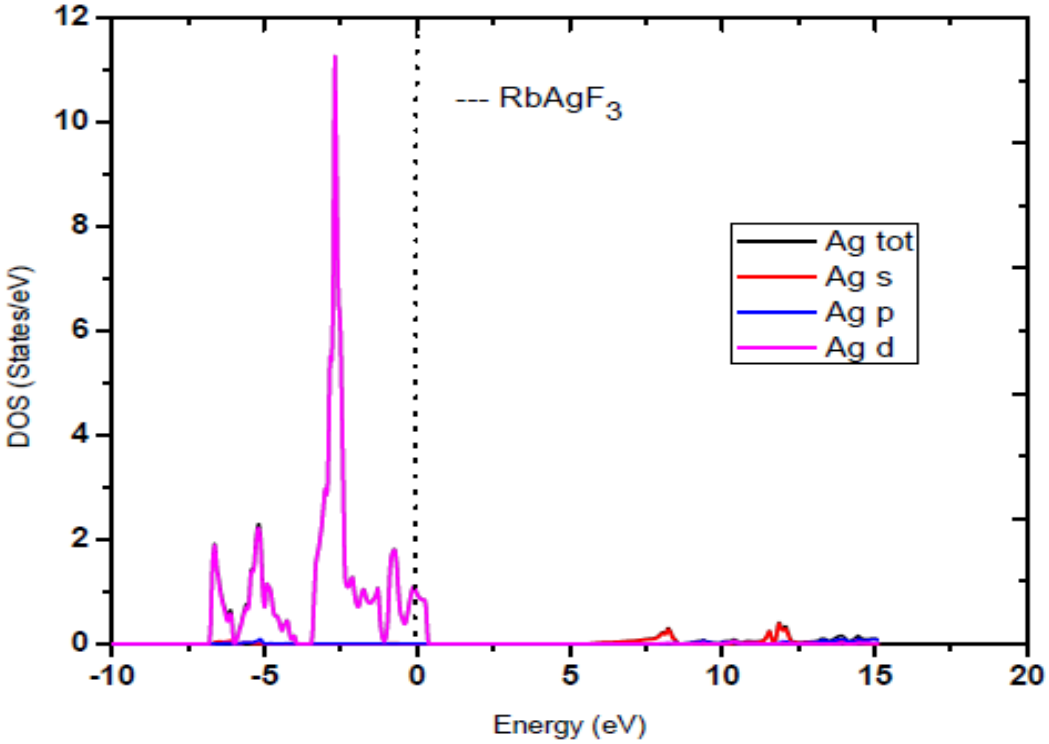

Fig. 5.19: Total and partial DOS plots for atom Ag

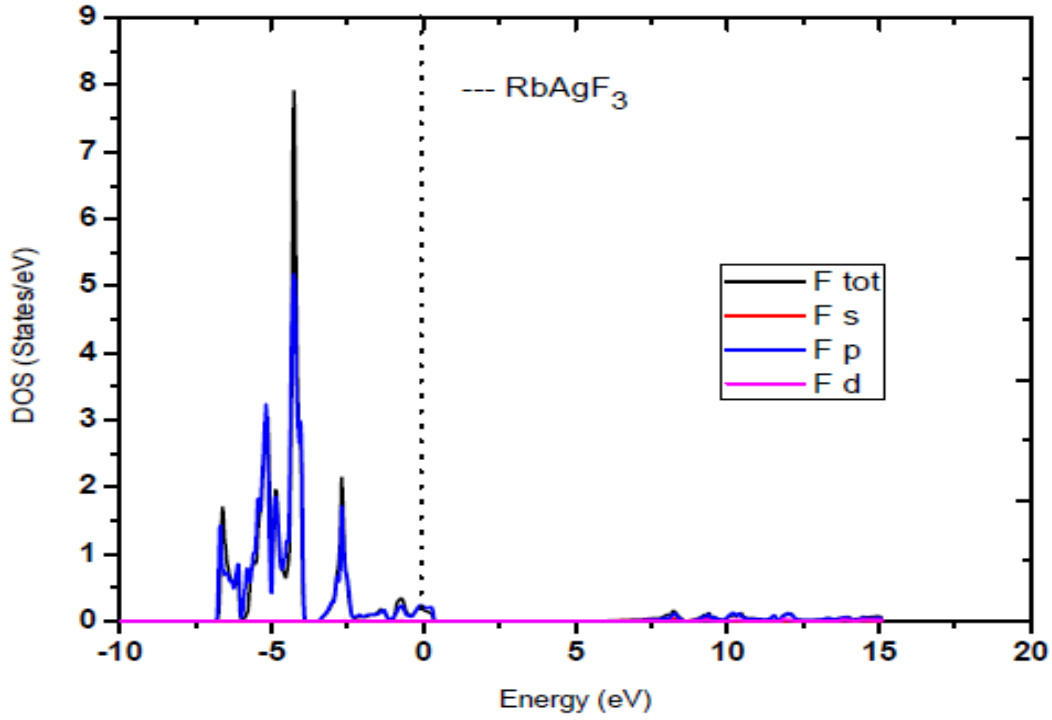

Fig. 5.20: Total and partial DOS plots of atom F

5.3 Electronic Band Structures for Alkali and Transition Elements

We present here the result for each compound calculated by using GGA method which is followed by results of calculation done by suing mBJ potential. In this section, the results of calculation of band structures in the case of a combination of $RbBF_3$ (B = Cu, Ag) is presented. Calculations have been done by using FP-LAPW method as discussed in Chapter-2. For this purpose, the approximations for exchange-correlation potential used is Generalized Gradient approximation (GGA).The calculated band gaps obtained by using the GGA approximations is underestimated i.e. usually smaller than experimentally obtained values in most of the insulating materials. Hence in order to reproduce a comparable value of band gaps, modified Becke-Johnson (mBJ) potential approach will also be used to calculate the energy gaps in the system. The mBJ potential is used in conjunction with the WIEN2k code to calculate band gaps (E_{BG}) as in the case of GGA approaches.

5.3.1 Study of Energy Bands for Alkali and Transition Elements

(a) Energy Bands of $RbBF_3$ (B = Cu, Ag) using GGA method

The electronic properties of $RbBF_3$ (B = Cu, Ag) are calculated with first principles FP-LAPW method using GGA and mBJ exchange potential. To calculate DOS and band structure of $RbBF_3$, the optimized lattice parameters are used. The calculated electronic band structures for fluoroperovskites $RbBF_3$ (B = Cu, Ag) along the high-symmetry directions of the Brillouin zone are shown in Figs. 5.21-5.22. We have found that the maximum of the valence band are found to be at a symmetry point Γ whereas the minimum conduction bands are located at the Γ point of the Brillouin zone in $RbBF_3$ compounds, resulting into direct band gaps in all the compounds. The calculated indirect band gaps $(\Gamma-\Gamma)$ are found as 3.0 eV and 2.5 eV $RbCuF_3$ and $RbAgF_3$ respectively by using the GGA approach.

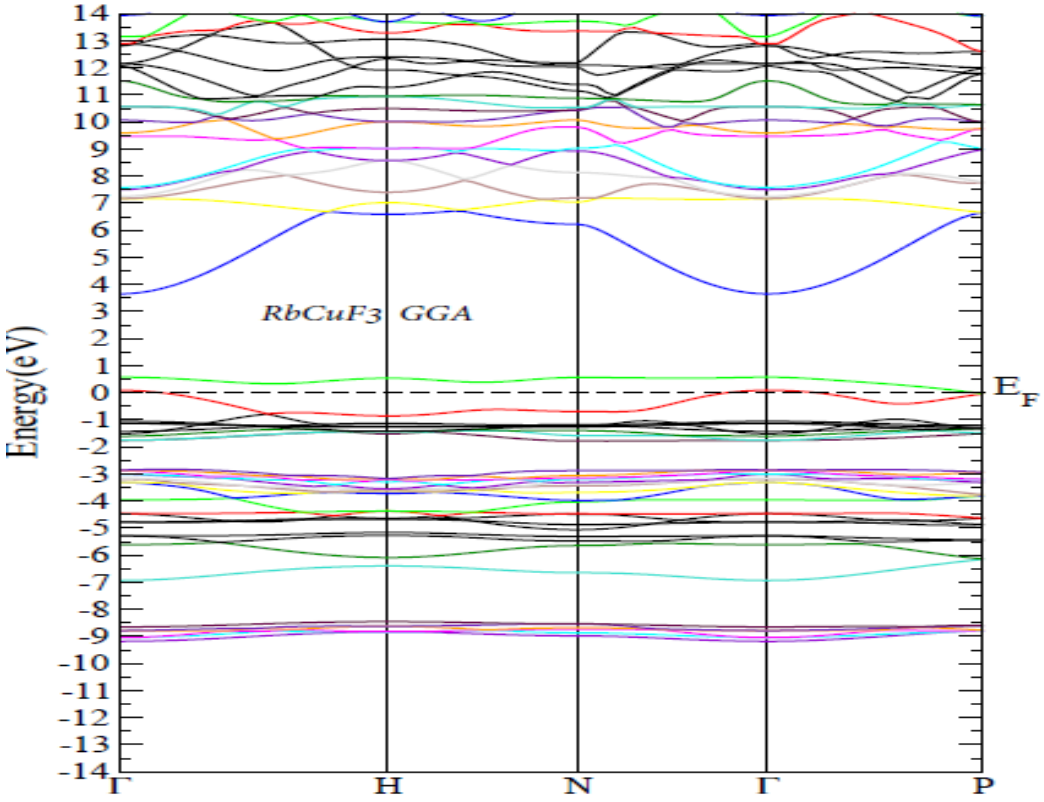

Fig. 5.21: Band structures for $RbCuF_3$ in GGA

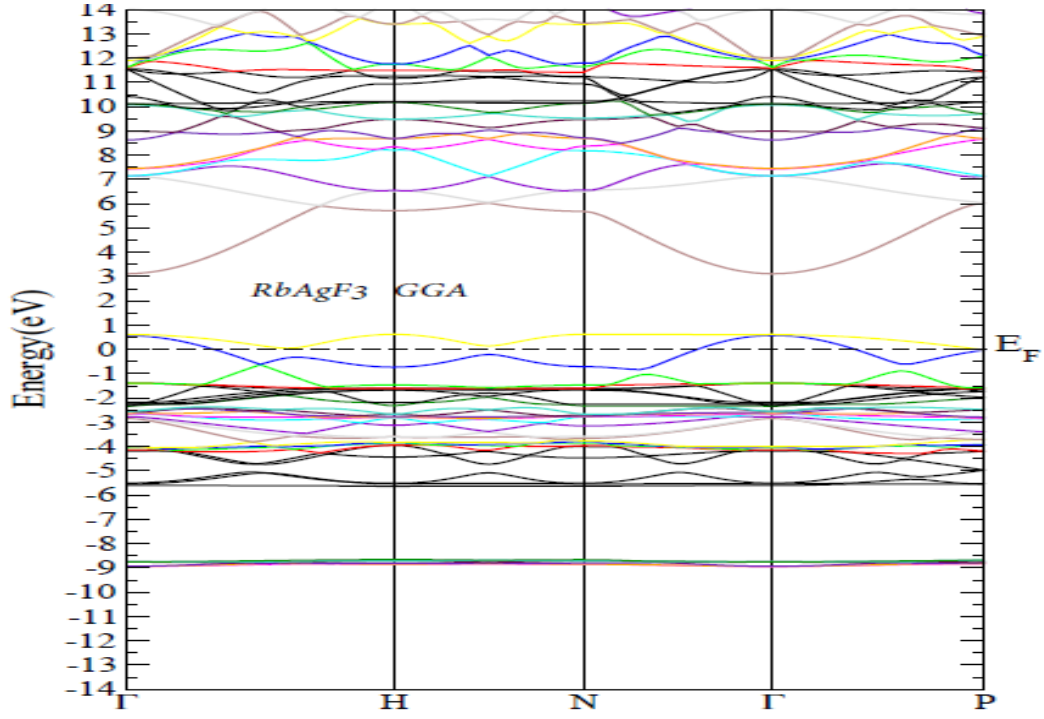

Fig. 5.22: Band structures for $RbAgF_3$ in GGA

(b) Energy Bands of $RbBF_3$ (B = Cu, Ag) using mBJ method

In this section, the calculated results of energy bands by using mBJ method is presented. Gaps arise due to direct type of transition of electrons in the symmetry direction $(\Gamma - \Gamma)$ as shown in Figs.5.23-5.24. We have found that the maximum of the valence band are found to be at a symmetry point Γ whereas the minimum conduction bands are located at the Γ point of the Brillouin zone in $RbBF_3$ compounds, resulting into direct band gaps in all the compounds. The calculated values of energy band gaps for the systems are 5.0 eV and 5.3 eV for $RbCuF_3$ and $RbAgF_3$ respectively.

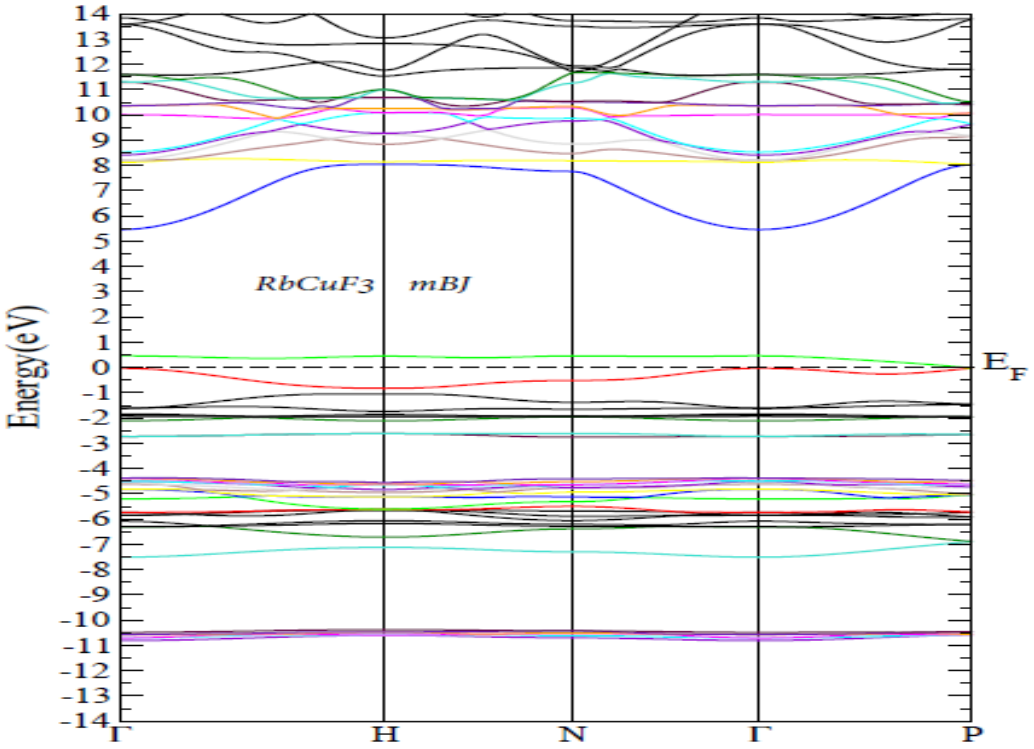

Fig. 5.23: Band structures for $RbCuF_3$ in mBJ

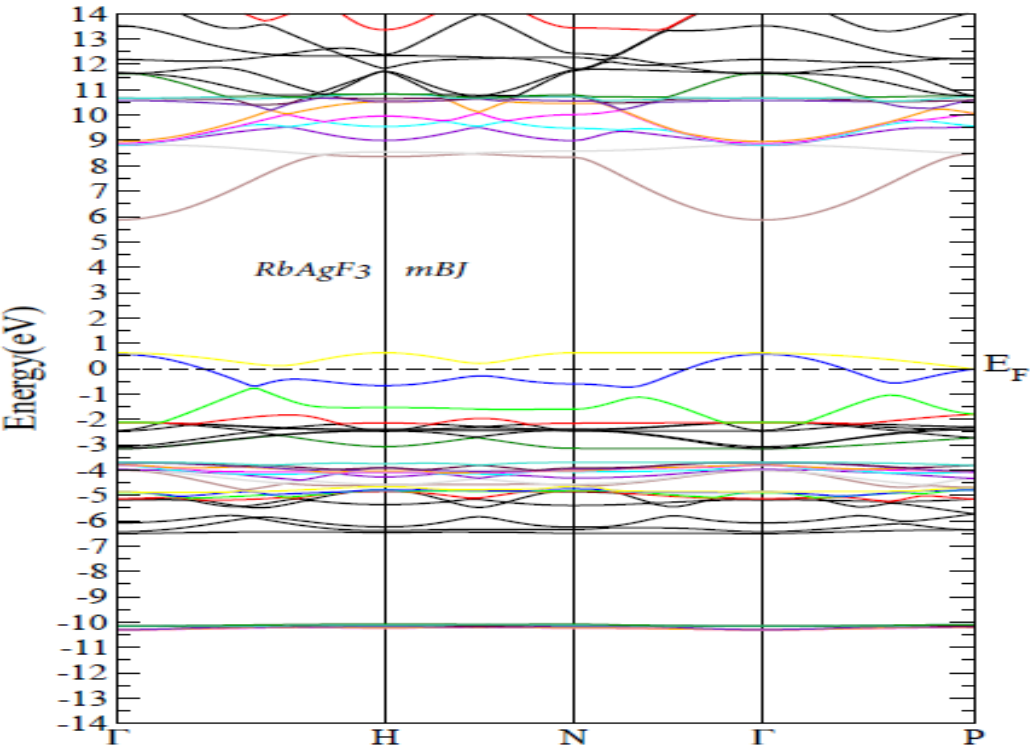

Fig. 5.24: Band structures for $RbAgF_3$ in mBJ

Chapter-6

Study of Optical Properties of Fluoride Perovskite ABF_3 with Alkali or Alkaline Earth and Transition Elements

The study of the optical properties of a compound in the spectral range of infrared to ultraviolet and above the band gap plays an important role to understand the nature of the material and also to understand about its applications in optoelectronics devices (Mutou and Saso, 2009). We have studied the optical properties by calculating the dielectric constants and other optical parameters like the refractive index, the reflectivity, the extinction coefficient, the absorption coefficient, the energy loss function and the optical conductivity of the compounds as a function of incident photon energy. In our calculations, FP-LAPW method is used to calculate the real and imaginary dielectric constant as a function of incident photon energy. The calculated dielectric constants are fitted into Eqns. (2.51–2.56) in Chapter-2 for calculating various optical parameters to study optical properties as a function of photon energy. This is then incorporated into wien 2k code for calculating several optical parameters via respective programmes.

We have calculated the various optical parameters of the fluoride perovskite of ABF_3 type combinations of alkali metals A and alkaline or transition metals B respectively. For this, the combination of A and B taken are as follows:

A = K, Rb, Cs, Ba and B = Li, K, Rb, Ca, Cu, Ag

For calculational purpose, here also we have used two approximations for the exchange correlation functionals namely; GGA and mBJ. In this context, we have considered only the

GGA method. The reason for this being that, with the inclusion of mBJ potential in our calculations of optical parameters, the qualitative features in the plots of parameters like, refractive indices, reflectivity, absorption coefficients, electron energy loss etc. have similar features as obtained by using GGA method. The detail discussions of the formulae used for calculations are given in chapter-2.

6.1 Calculation of Optical parameters by using GGA method for various combinations of Alkali or Alkaline and Transition Elements

6.1.1 Combination for Alkali and Alkaline Earth Elements

(a) Real and Imaginary parts of dielectric function

The optical spectra as a function of photon energy for cubical fluoroperovskite $ACaF_3$ (A = K, Rb, Cs) are shown in Figs. 6.1-6.8. We have studied the optical spectra in the photon energy range of 0 – 40 eV. The nearly same band structure plots of the compounds under study give similar profile in the optical spectra of these materials. Each peak in ε_1 and ε_2 in the optical response plots can be determined by the electric-dipole transitions between the occupied and unoccupied states of the band structure plots. Fig. 6.1 represents real part $\varepsilon_1(\omega)$ of dielectric function of $ACaF_3$ in the approach of GGA. From our calculation, we have found maximum value of $\varepsilon_1(\omega)$ at 9.45 eV, 9.34 eV, 8.83 eV for $KCaF_3$, $RbCaF_3$ and $CsCaF_3$ respectively. We note that the peak heights are increased as we move from K to Cs that is seen in table 6.1. Real part starts to decrease below zero in the negative scale for the range of 22.326-22.925 eV, 26.28-26.68 eV and 28.939-29.565 eV for $KCaF_3$, 19.469-20.204 eV, 20.39-21.40 eV, 26.27- 26.82 eV and 28.91-29.429 eV for $RbCaF_3$ and 13.64-14.04 eV, 15.82-17.37 eV, 17.61-18.27 eV, 18.43-18.78 eV and 28.74-29.15 eV for $CsCaF_3$.

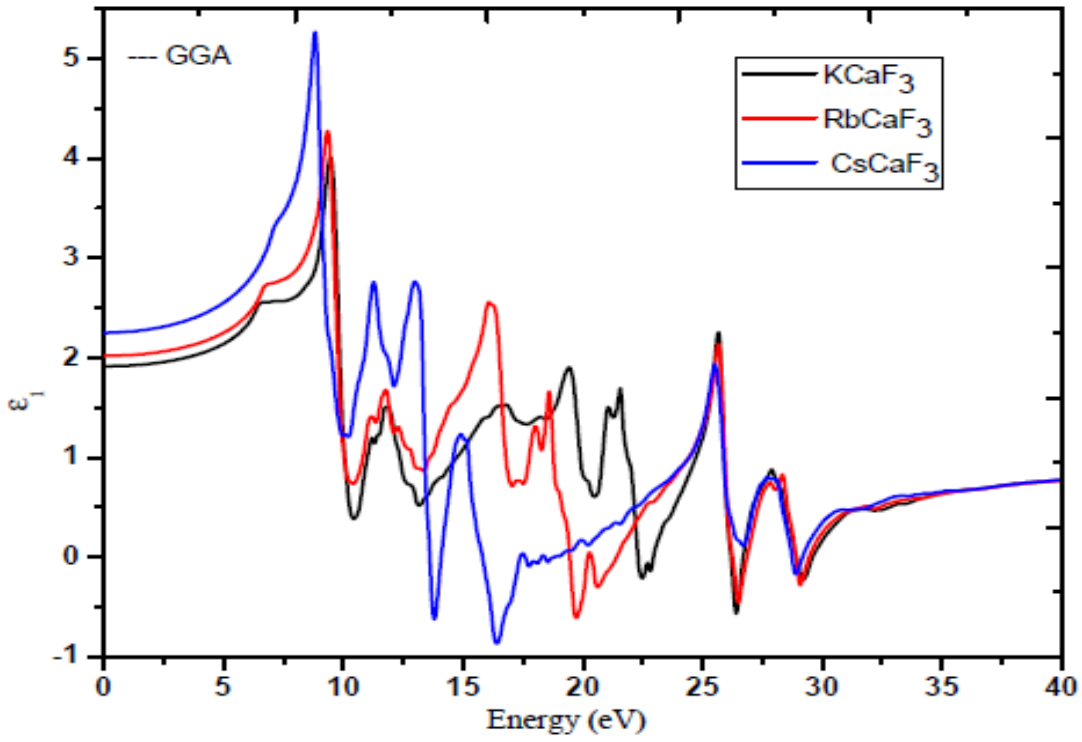

Fig. 6.1: Real $\varepsilon_1(\omega)$ part of dielectric function for $ACaF_3$ (A = K, Rb, Cs)

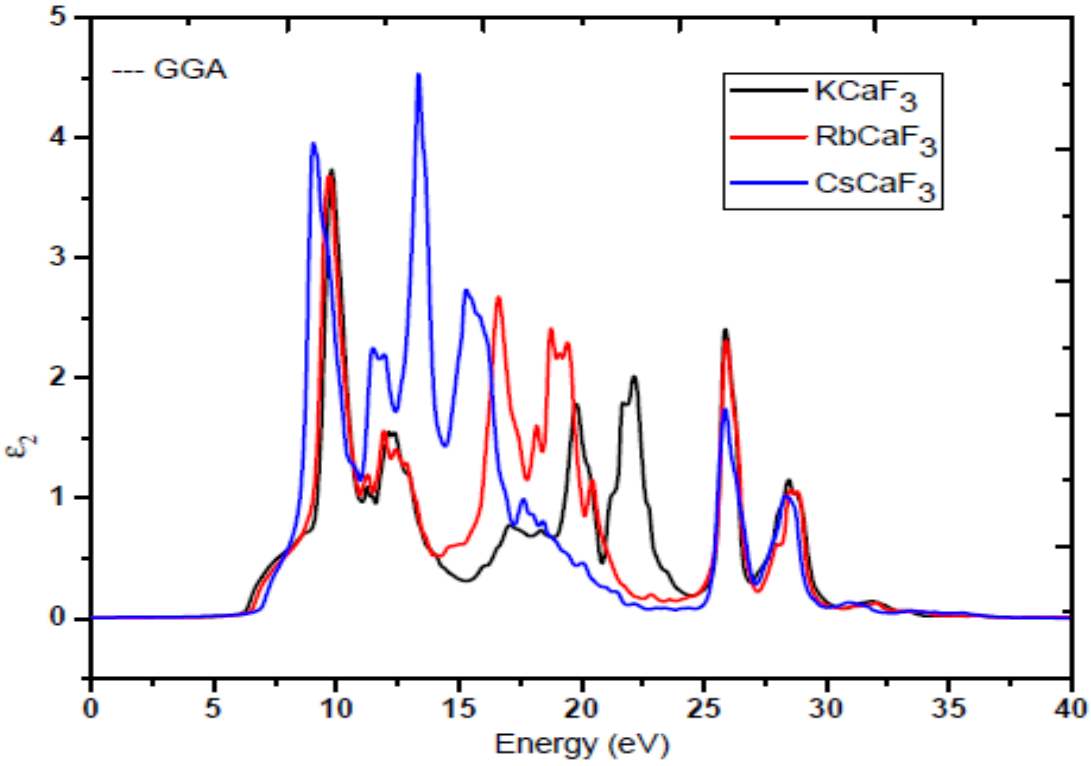

Fig. 6.2: Imaginary $\varepsilon_2(\omega)$ part of dielectric function for $ACaF_3$ (A = K, Rb, Cs)

Fig. 6.2 represents the imaginary part $\varepsilon_2(\omega)$ in the approach of GGA and we have found the threshold energy of dielectric function occurs at E_0 = 6.1 eV, 6.3 eV and 6.9 eV for $KCaF_3$, $RbCaF_3$ and $CsCaF_3$ respectively which correspond to the fundamental gaps at the equilibrium.

(b) Refractive index and Reflectivity

Fig. 6.3 represents the refractive index $n(\omega)$ of dielectric function of $ACaF_3$ compound. The refractive index is one of important characteristic for optical design and applications. High refractive materials are used in ophthalmic lenses, filters and optical adhesives, antireflection coating and advanced optoelectronic devises compound. The calculated static refractive index $n(0)$ and maximum value of refractive index $n(\omega)_{max}$ are mentioned in Table 6.2. The refractive index greater than one means photons which travelling in the material are slowed down due to the interaction with electrons of the medium. The refractive index less than unity shows that the phase velocity greater than light velocity, which is in disagreement to relativity. This suggests that in a dispersive medium signal transmitted as wave packet propagating at the group velocity. At zero frequency limits, the static refractive indices are given in Table 6.2.

Fig. 6.4 represents the reflectivity $R(\omega)$ of $ACaF_3$ compound. The static reflectivity $R(0)$ and maximum reflectivity $R(\omega)_{max}$ are mentioned in Table 6.2. From our calculation, we have found the static reflectivity increases from K to Cs in a compound $ACaF_3$ (A = K, Rb, Cs).

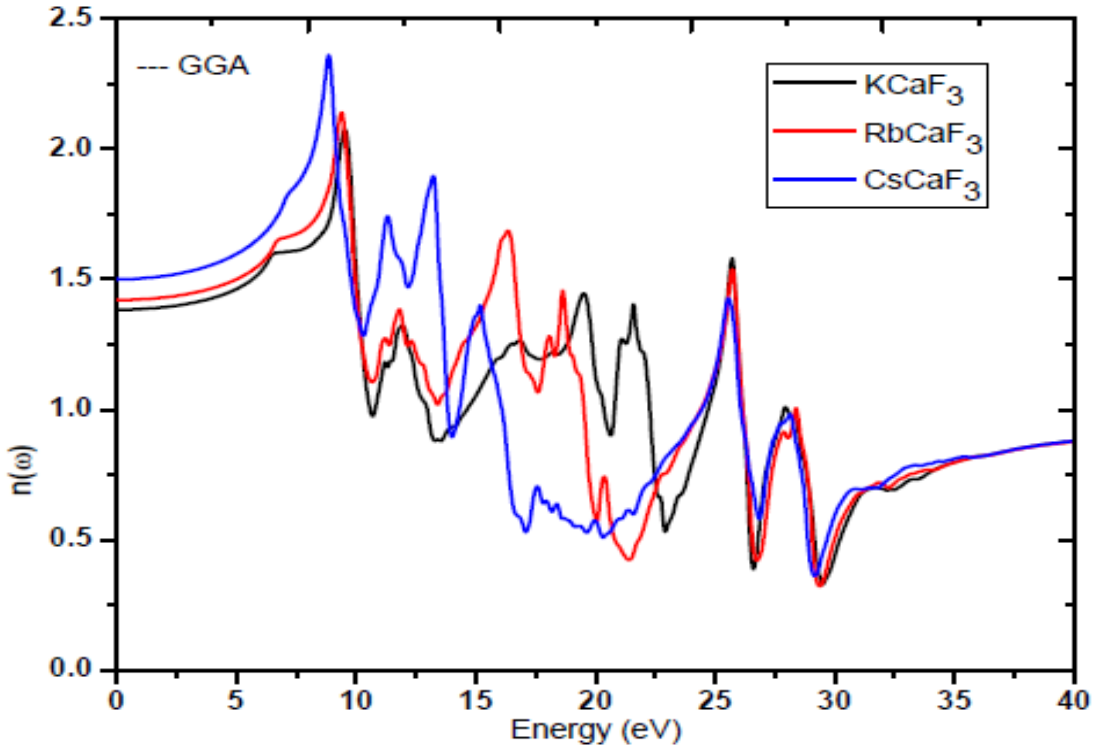

Fig. 6.3: The refractive index $n(\omega)$ for $ACaF_3$ (A = K, Rb, Cs)

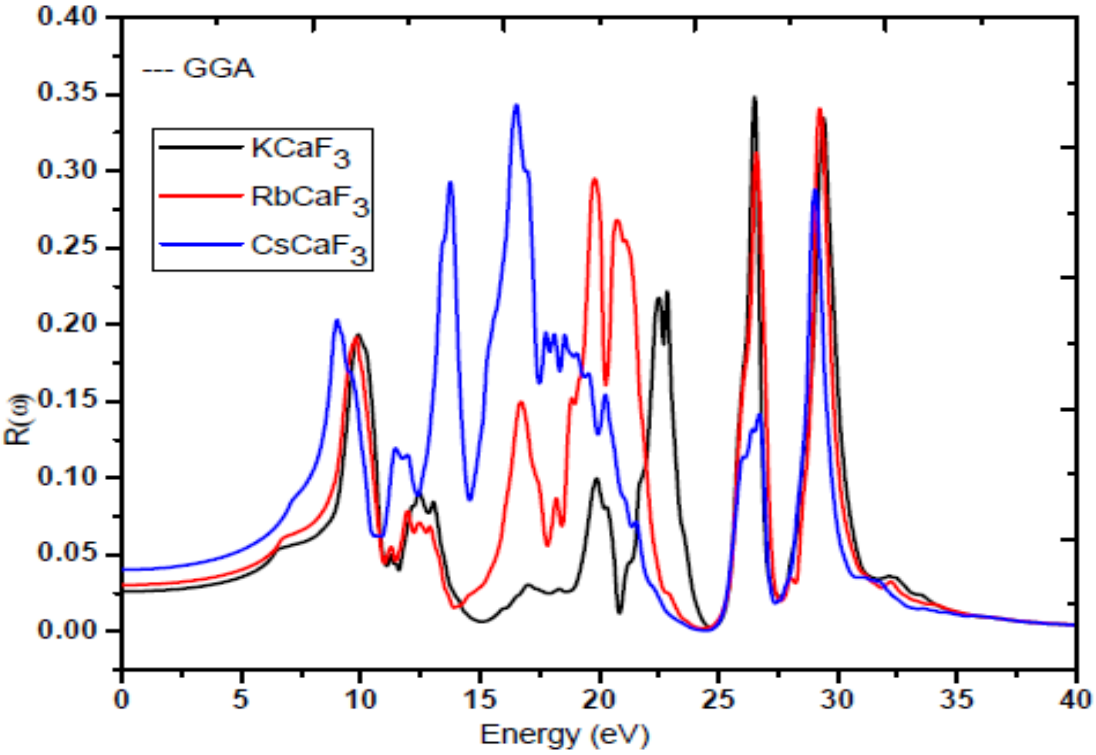

Fig. 6.4: The Reflectivity $R(\omega)$ for $ACaF_3$ (A = K, Rb, Cs)

Table 6.1: Calculated energy band gap (E_g), static dielectric constant and its maximum values for $ACaF_3$ (A = K, Rb, Cs) compound.

Compound	E_g in eV	$\varepsilon_1(0)$	$\varepsilon_1(\omega)_{max}$
$KCaF_3$	6.1	1.92	4.01
$RbCaF_3$	6.3	2.02	4.28
$CsCaF_3$	6.9	2.25	5.27

Table 6.2: Calculated static refractive index $n(0)$, reflectivity $R(0)$ and their maximum values for $ACaF_3$ (A = K, Rb, Cs) compound.

Compound	$n(0)$	$n(\omega)_{max}$	$R(0)\%$	$R(\omega)_{max}\%$
$KCaF_3$	1.38	2.08	2.6	34.9
$RbCaF_3$	1.42	2.14	3.02	34.1
$CsCaF_3$	1.50	2.36	4.01	34.3

(c) Absorption coefficient and Electron energy loss function

Fig. 6.5 shows the absorption coefficient $\alpha(\omega)$ of photon energy of $ACaF_3$ compound. The absorption characters are observed in the range up to 40 eV. The maximum absorption coefficient is 255 m^{-1} at 26.32 eV for $KCaF_3$, 250 m^{-1} at 26.42 eV for $RbCaF_3$ and 202 m^{-1} at 16.25 eV for $CsCaF_3$ in GGA that is seen in Fig.6.5.

Electron energy loss spectroscopy is a precious tool for the investigation of the different physical aspects of a material (Lougin *et al*., 1996). It provides information about elastically scattered and non-scattered electrons and the number and type of atom being struck by the beam. The electron energy loss spectra for $ACaF_3$ (A = K, Rb, Cs) systems under study are given in Figs. 6.6. Fig. 6.6 shows the electron energy loss (EEL) spectra of $ACaF_3$ compound for the energy range 0-40 eV in which it represents characteristic plasmon oscillations. From the Fig. 6.6 in GGA, it is found that the most resonant peak occurs at 29.72 eV, 29.53 eV and 29.29 eV for $KCaF_3$, $RbCaF_3$ and $CsCaF_3$ respectively.

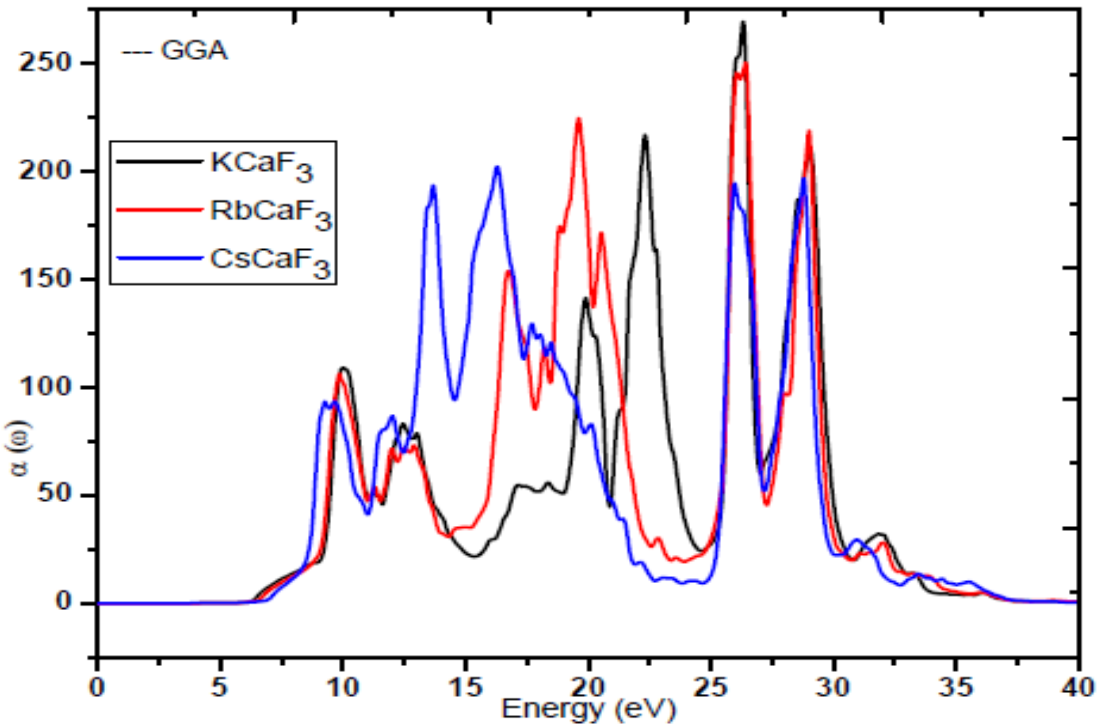

Fig. 6.5: The absorption coefficient $\alpha(\omega)$ for $ACaF_3$ (A = K, Rb, Cs)

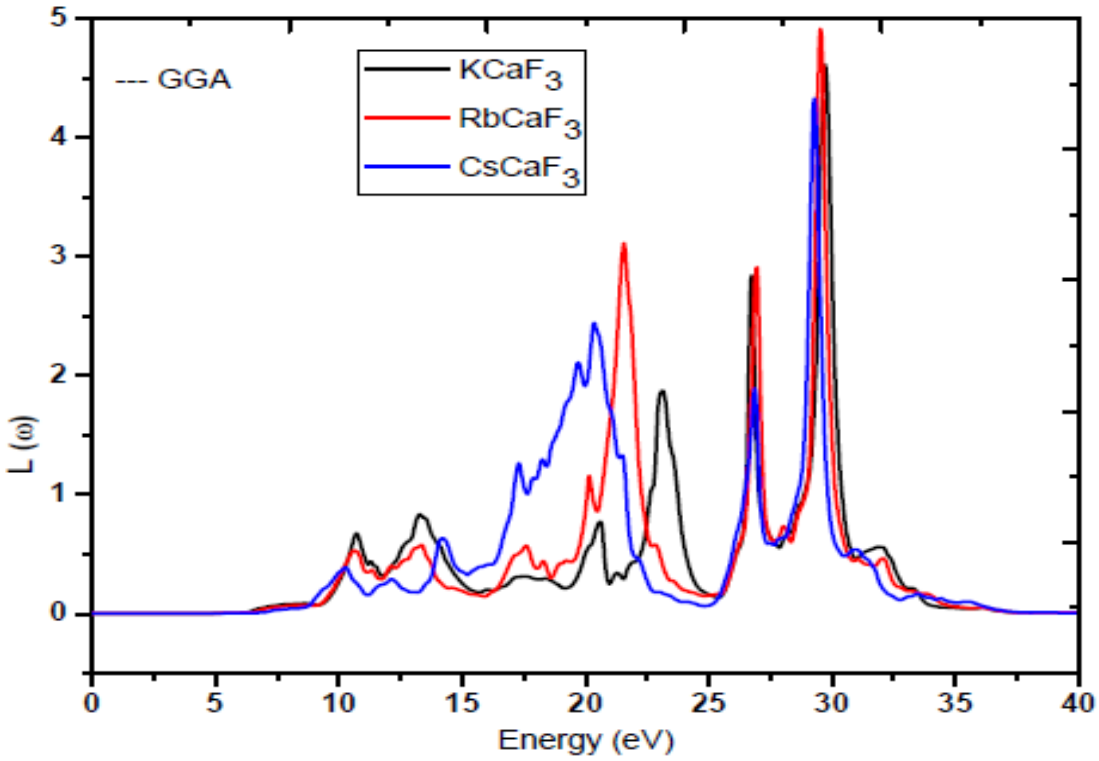

Fig. 6.6: Energy loss function $L(\omega)$ for $ACaF_3$ (A = K, Rb, Cs)

(d) Optical conductivity and Extinction coefficient

Fig. 6.7 shows the optical conductivity of $ACaF_3$ compound in the energy range 0-40 eV. The conduction of electrons due to an applied electromagnetic field is characterized by optical conductivity $\sigma(\omega)$. From the Fig. 6.7 in the approach of GGA, optical conduction starts form 5.80 eV, 6.65 eV and 7.0 eV for $KCaF_3$ $KCaF_3$, $RbCaF_3$ and $CsCaF_3$ respectively in GGA. The conductivity in the range 10.97- 16.36 eV is higher for $CsCaF_3$ as compared two other isoelectric compounds, while for range 16.42-19.63 eV, $RbCaF_3$ has higher conductivity. $KCaF_3$ dominates beyond 19.63 eV in conductivity, while the maximum conductivity is around 26 eV for all three compounds. The peak values of the conductivity are $8370\,\Omega^{-1}cm^{-1}$, 8050 $\Omega^{-1}cm^{-1}$ and 6070 $\Omega^{-1}cm^{-1}$ for $KCaF_3$, $RbCaF_3$ and $CsCaF_3$ respectively.

Fig. 6.8 shows the extinction coefficient for $ACaF_3$ (A = K, Rb, Cs) compound in the energy range 0-40 eV. When we look the behavior of imaginary part $\varepsilon_2(\omega)$ of dielectric function and extinction coefficient $K(\omega)$, a similar trend is observed from Fig.6.2 and 6.8. The extinction coefficient $K(\omega)$ reaches the maximum absorption at 13.5 eV for $CsCaF_3$ and 10.5 eV for both $KCaF_3$ and $RbCaF_3$.

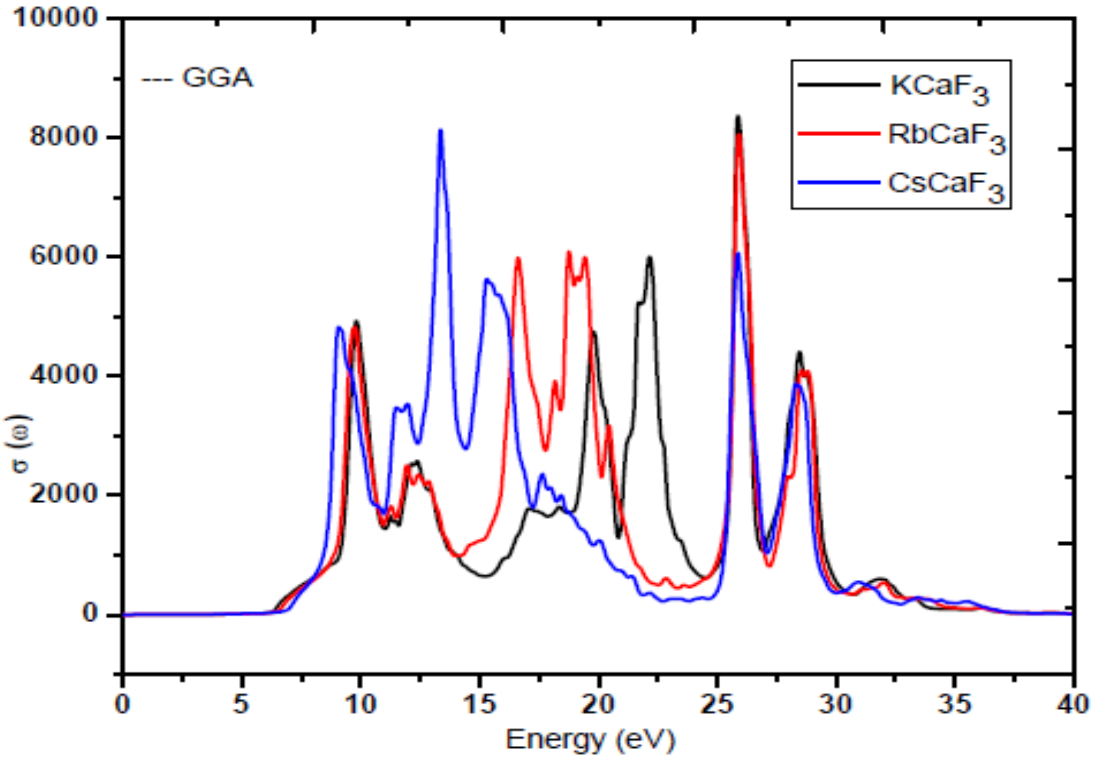

Fig. 6.7: The optical conductivity $\sigma(\omega)$ for $ACaF_3$ (A = K, Rb, Cs)

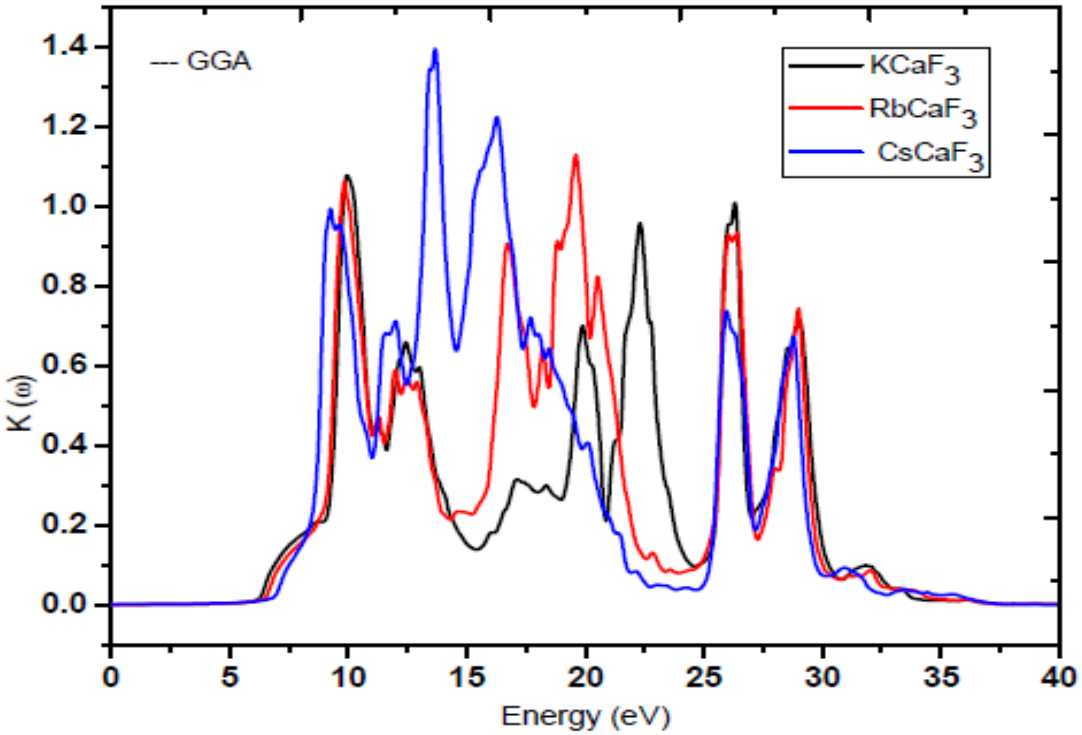

Fig.6.8: The extinction coefficient for $ACaF_3$ (A = K, Rb, Cs)

6.1.2 Combination for Alkaline Earth and Alkali Elements

(a) Real and Imaginary parts of dielectric function

The optical spectra as a function of photon energy for cubical fluoroperovskite $BaBF_3$ (B = Li, K, Rb), are shown in Figs. 6.9-6.16. The optical spectra are studied in the energy range of 0 – 40 eV. The Fig.6.9 represents real part $\varepsilon_1(\omega)$ of dielectric function $\varepsilon(\omega)$ of photon energy for cubic $BaBF_3$. The function $\varepsilon_1(\omega)$ provides the information about electronic polarization and dispersion of incident radiation on the material. The static dielectric constant at energy zero $\varepsilon_1(0)$ and maximum value of $\varepsilon_1(\omega)$ of $BaBF_3$ are noticed in Table 6.3. As the atomic radius of Rb is greater than Li and K atoms, so the value of $\varepsilon_1(\omega)$ increases from Li to Rb. From our calculation, we have found maximum value of $\varepsilon_1(\omega)$ at 9.78 eV, 18.7 eV, 18.84 eV for $BaLiF_3$, $BaKF_3$ and $BaRbF_3$ respectively. Real part starts to decrease below zero in the negative scale for the range of 18.55-23.27 eV for $BaLiF_3$, 19.54-20.93 eV, 23.00-23.52 eV, 24.17-24.36 eV and 25.42- 26.08 eV for $BaKF_3$ and 19.27-21.94 eV and 22.43-24.15 eV for $BaRbF_3$. This negative value of real dielectric function indicates that these materials be metal otherwise dielectric.

Fig. 6.10 represents imaginary part of dielectric function of $BaBF_3$ compound. The imaginary part $\varepsilon_2(\omega)$ provides information about absorption behavior of $BaBF_3$ compound. Fig. 6.10 represents the imaginary part $\varepsilon_2(\omega)$ in the approach of GGA.

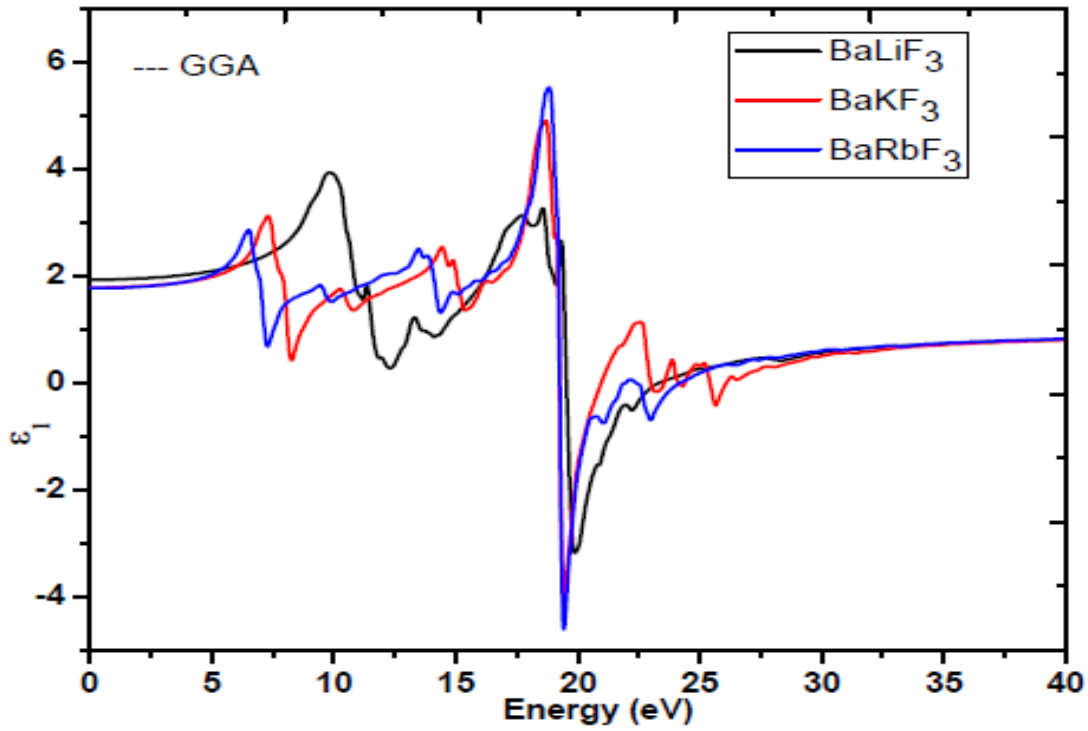

Fig. 6.9: Real part of dielectric function for $BaBF_3$ (B = Li, K, Rb),

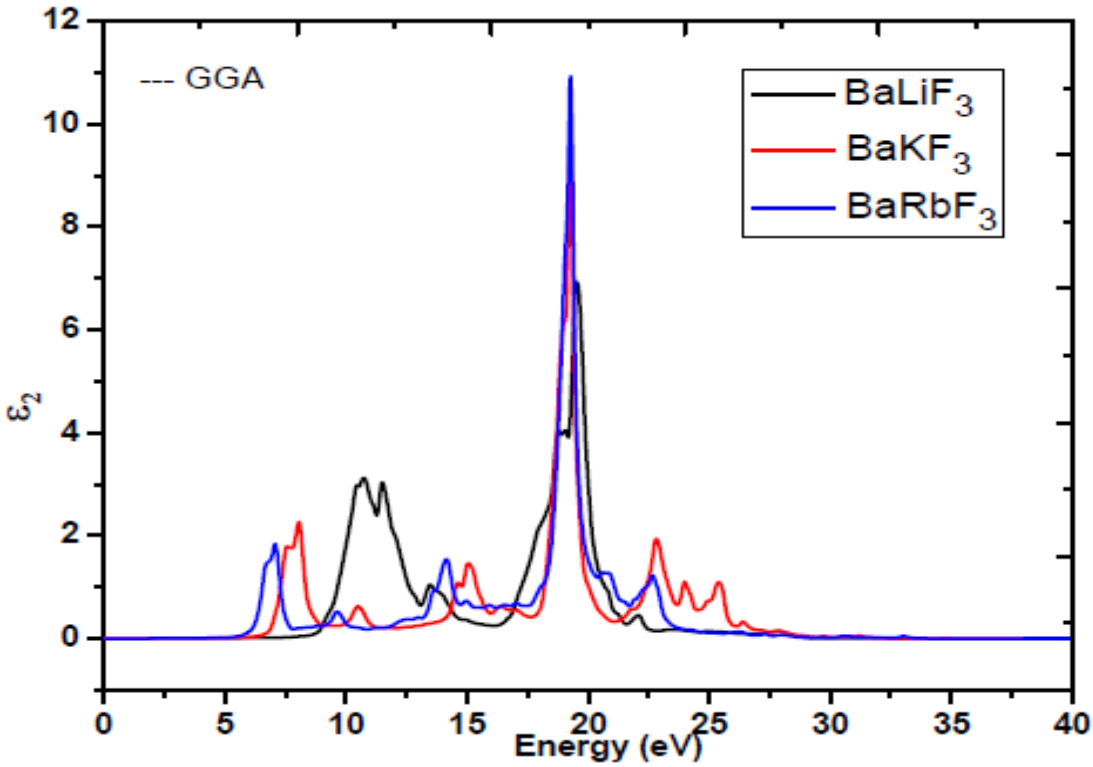

Fig.6.10. Imaginary part of dielectric function for $BaBF_3$ (B = Li, K, Rb)

(b) Refractive index and Reflectivity

Fig. 6.11 represents the refractive index $n(\omega)$ of dielectric function of $BaBF_3$ compound. The refractive index is one of important characteristic for optical design and applications. High refractive materials are used in ophthalmic lenses, filters and optical adhesives, antireflection coating and advanced optoelectronic devises compound. The calculated static refractive index $n(0)$ and maximum value of refractive index $n(\omega)_{max}$ are mentioned and compared with the available literatures in Table 6.4. The refractive index greater than one means photons which travelling in the material are slowed down due to the interaction with electrons of the medium. The refractive index less than unity shows that the phase velocity greater than light velocity, which is in disagreement to relativity. This suggests that in a dispersive medium signal transmitted as wave packet propagating at the group velocity.

Fig. 6.12 represents the reflectivity $R(\omega)$ of $BaBF_3$ compound. The static reflectivity $R(0)$ and maximum reflectivity $R(\omega)_{max}$ are mentioned in Table 6.4. From our study, the maxima of reflectivity are found as 66.8% at 21.04 eV for $BaLiF_3$, 61.6% at 19.71 eV for $BaKF_3$ and 57.7% at 19.57 eV for $BaRbF_3$. It is noted that the reflectivity spectra are prominent where the real part $\varepsilon_1(\omega)$ is below zero in the energy ranges which are seen in Fig. 6.9 and 6.12.

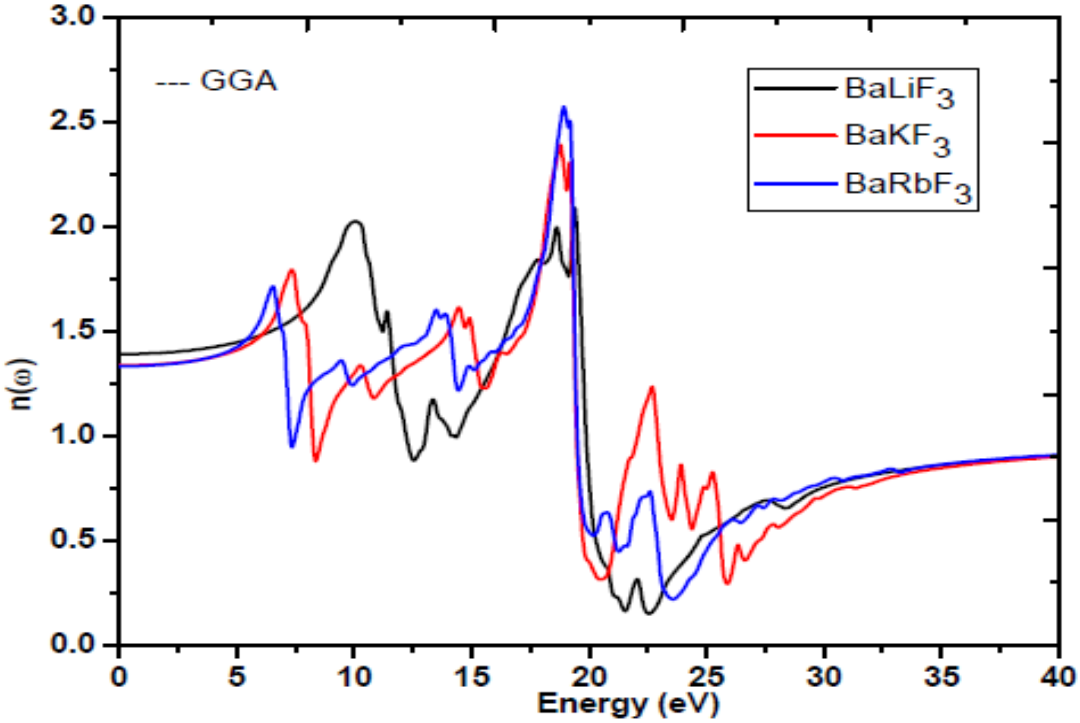

Fig.6.11: The refractive index for $BaBF_3$ (B = Li, K, Rb)

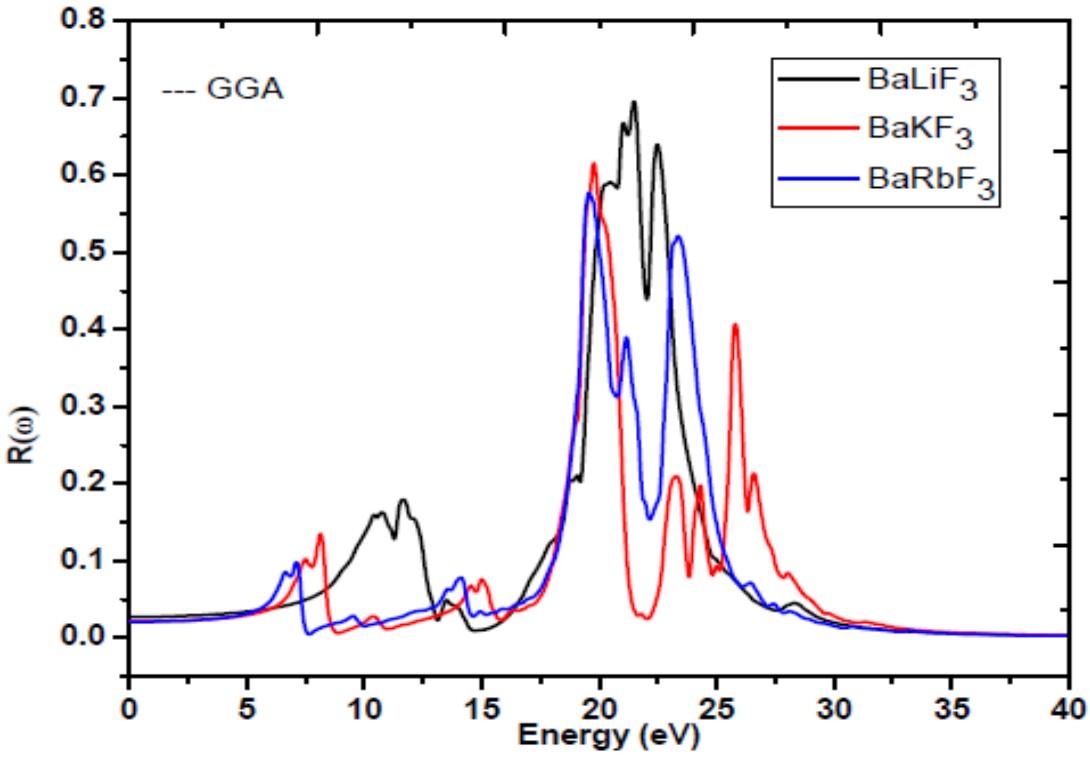

Fig.6.12: The reflectivity for $BaBF_3$ (B = Li, K, Rb),

Table 6.3: Calculated energy band gap (E_g), static dielectric constant and its maximum values for $BaBF_3$ (B = Li, K, Rb) compound.

Compound	E_g in eV	$\varepsilon_1(0)$	$\varepsilon_1(\omega)_{max}$
$BaLiF_3$	6.9	1.94	3.94
$BaKF_3$	4.8	1.79	4.91
$BaRbF_3$	3.9	1.78	5.54

Table 6.4 Calculated static refractive index $n(0)$, reflectivity $R(0)$, and their maximum values for $BaBF_3$ (B = Li, K, Rb) compound.

Compound	$n(0)$	$n(\omega)_{max}$	$R(0)\%$	$R(\omega)_{max}\%$
$BaLiF_3$	1.39	2.02	2.69	66.8
$BaKF_3$	1.34	2.39	2.09	61.6
$BaRbF_3$	1.33	2.57	2.05	57.7

(c) Absorption coefficient and Electron energy loss function

Fig. 6.13 shows the electron energy loss (EEL) spectra of $BaBF_3$ compound for the energy range 0-40 eV in which it represents characteristic plasmon oscillations. From the Fig. 6.13, it is found that the most resonant peak occurs at 23.19 eV, 26.10 eV and 24.17 eV for $BaLiF_3$, $BaKF_3$ and $BaRbF_3$ respectively. Fig. 6.14 shows the absorption coefficient $\alpha(\omega)$ of photon energy of $BaBF_3$ compound. The absorption characters are observed in the range up to 40 eV. The maximum absorption coefficient is 423 m^{-1} at 19.76 eV for $BaLiF_3$, 478 m^{-1} at 19.36 eV for $BaKF_3$ and 513 m^{-1} at 19.36 eV for $BaRbF_3$ that is seen in Fig.6.14.

(d) Optical conductivity and Extinction coefficient

Fig. 6.15 shows the optical conductivity of $BaBF_3$ compound in the energy range 0-40 eV. The conduction of electrons due to an applied electromagnetic field is characterized by optical conductivity $\sigma(\omega)$. From the Fig. 6.15, optical conduction starts form 8.66 eV, 6.73 eV and 5.94 eV for $BaLiF_3$, $BaKF_3$ and $BaRbF_3$ respectively. The conductivity in the range 18.65- 19.41 eV is higher for $BaRbF_3$ as compared two other isoelectric compounds and the maximum conductivity is around 19 eV for all three compounds. The peak values of the conductivity are $18200\,\Omega^{-1}cm^{-1}$, 24100 $\Omega^{-1}cm^{-1}$ and 28400 $\Omega^{-1}cm^{-1}$ for $BaLiF_3$, $BaKF_3$ and $BaRbF_3$ respectively. The peak values of the conductivity increases from Li to Rb.

Fig. 6.16 shows the extinction coefficient for $BaBF_3$ compound in the energy range 0-40 eV. When we look the behavior of imaginary part $\varepsilon_2(\omega)$ of dielectric function and extinction coefficient $K(\omega)$, a similar trend is observed from Fig.6.10 and 6.16. The extinction coefficient $K(\omega)$ reaches the maximum absorption at 19.74 eV for $BaLiF_3$ and 19.36 eV for both $BaKF_3$ and $BaRbF_3$. Hence $BaBF_3$ is wide band gap compound with high absorption power in ultraviolet energy range and it can be used in the optoelectronic devices like UV detectors.

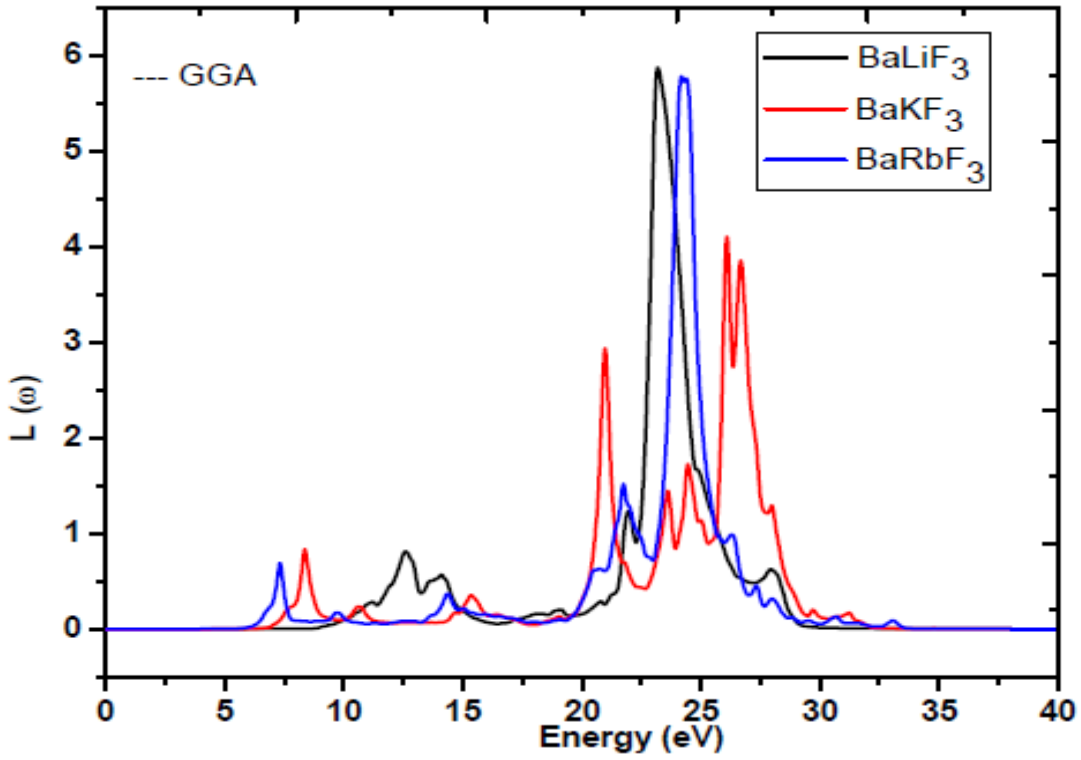

Fig. 6.13: The energy loss function for $BaBF_3$ (B = Li, K, Rb)

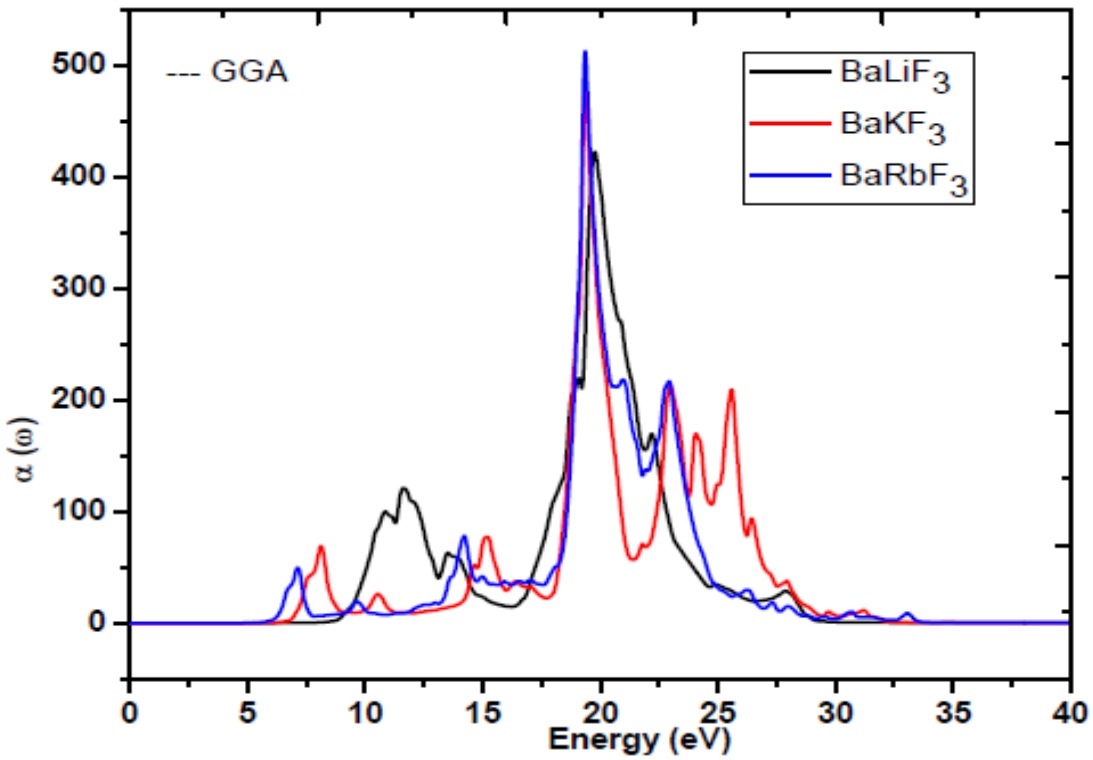

Fig. 6.14: The absorption coefficient for $BaBF_3$ (B = Li, K, Rb)

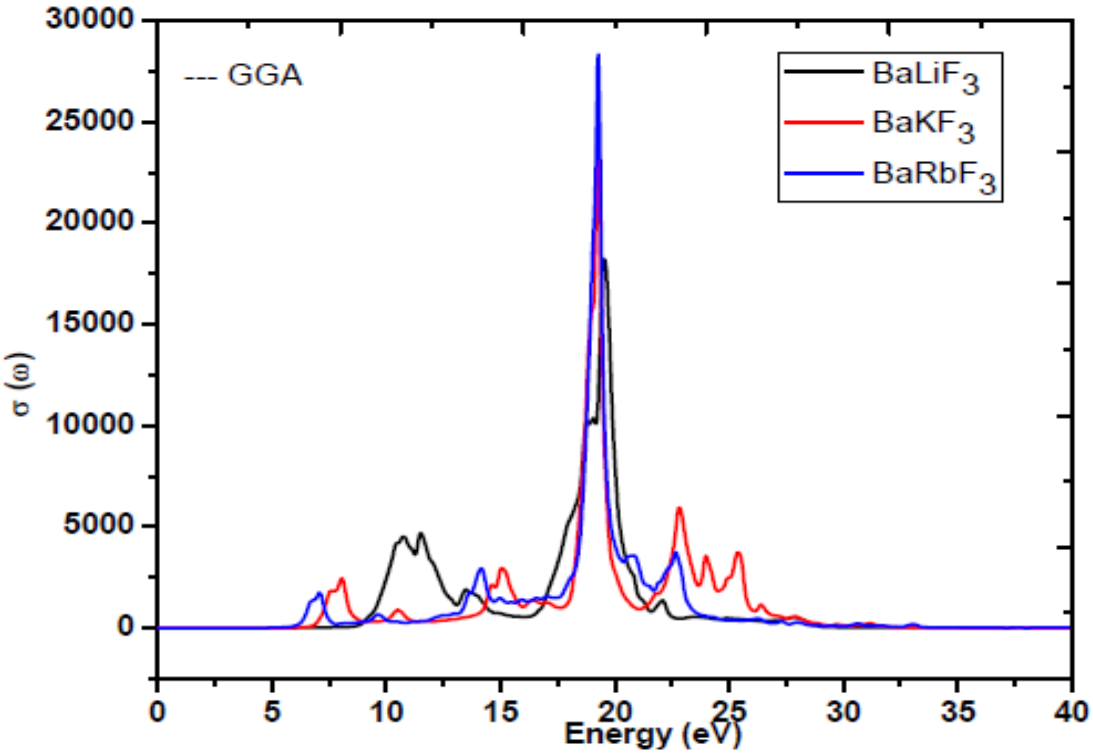

Fig.6.15: The optical conductivity for $BaBF_3$ (B = Li, K, Rb)

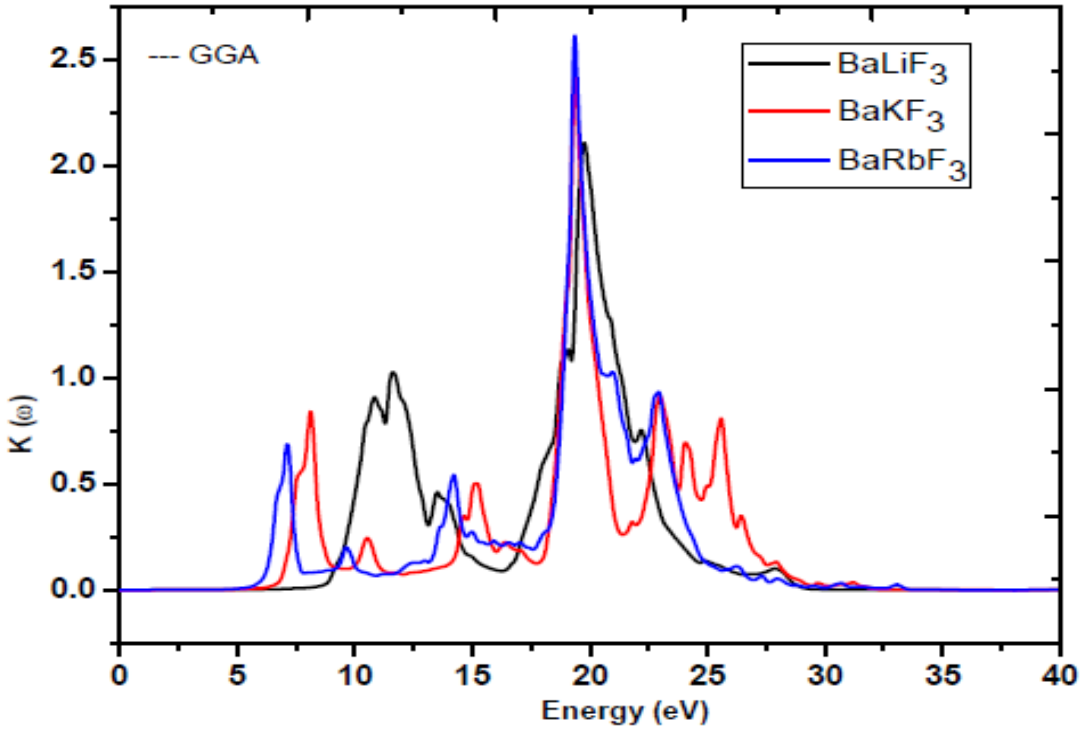

Fig.6.16: The extinction coefficient for $BaBF_3$ (B = Li, K, Rb)

6.1.3 Combination for Alkali and Transition Elements

(i) $RbCuF_3$

(a) Real and Imaginary parts of dielectric function

Fig. 6.17 represents real part $\varepsilon_1(\omega)$ of dielectric function of $RbCuF_3$ compound. From our calculation, we have found maximum value of $\varepsilon_1(\omega)$ at 15.41 eV then it starts to decrease up to 16.21 eV. From the plot in real part of dielectric function with photon energy, we have found the minimum value of $\varepsilon_1(\omega)$ at 21.53 eV. Fig. 6.18 represents the imaginary part $\varepsilon_2(\omega)$ of dielectric function of $RbCuF_3$ in the approach of GGA. From this calculation, we have found the maximum value of $\varepsilon_2(\omega)$ at 20.0 eV.

(b) Refractive index and Reflectivity

Fig. 6.19 represents the refractive index $n(\omega)$ of dielectric function of $RbCuF_3$ compound. High refractive materials are used in ophthalmic lenses, filters and optical adhesives, antireflection coating and advanced optoelectronic devises compound. The calculated static refractive index $n(0)$ is noted in Table 6.5. The refractive index greater than one means photons which travelling in the material are slowed down due to the interaction with electrons of the medium. The refractive index less than unity shows that the phase velocity greater than light velocity, which is in disagreement to relativity. This suggests that in a dispersive medium signal transmitted as wave packet propagating at the group velocity. At zero frequency limits, the static refractive indices are given in Table 6.5. At higher frequency range the refractive index tends to decrease showing the material absorbs high energy photons. Fig. 6.20 represents the reflectivity $R(\omega)$ of $RbCuF_3$ compound. From the calculation, we have found the static reflectivity $R(0)$ that is given in Table 6.5. From our calculation, we have found the static reflectivity is nearly equal to zero.

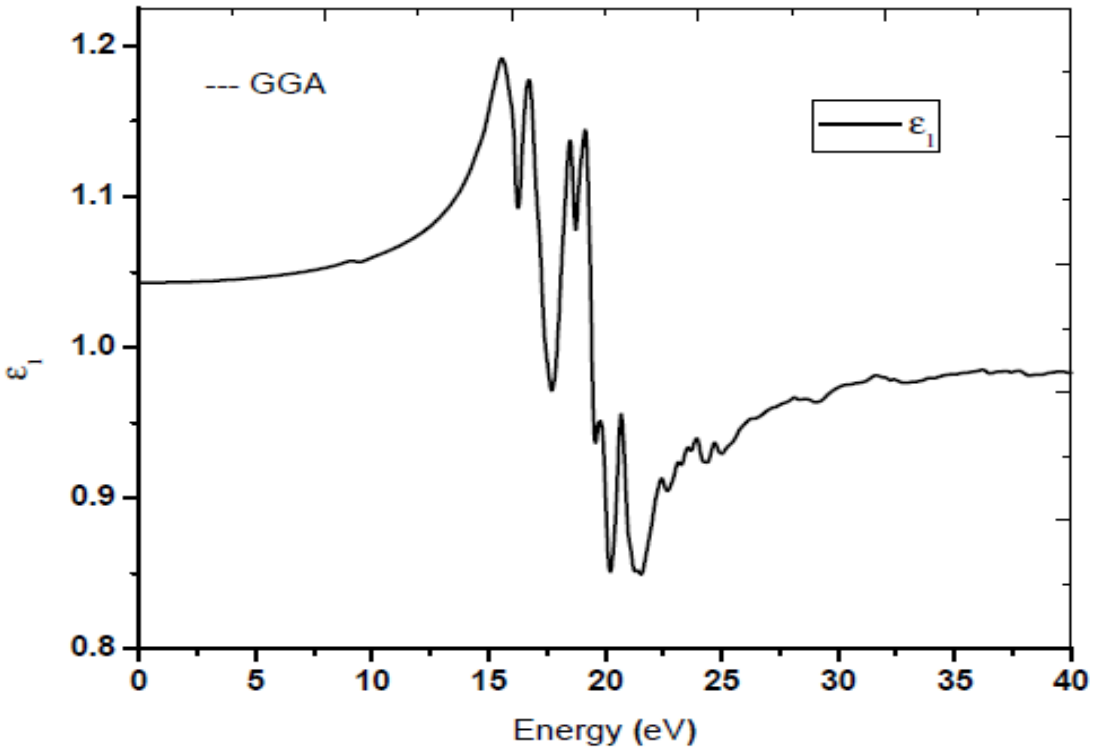

Fig. 6.17: Real $\varepsilon_1(\omega)$ part of dielectric function for $RbCuF_3$

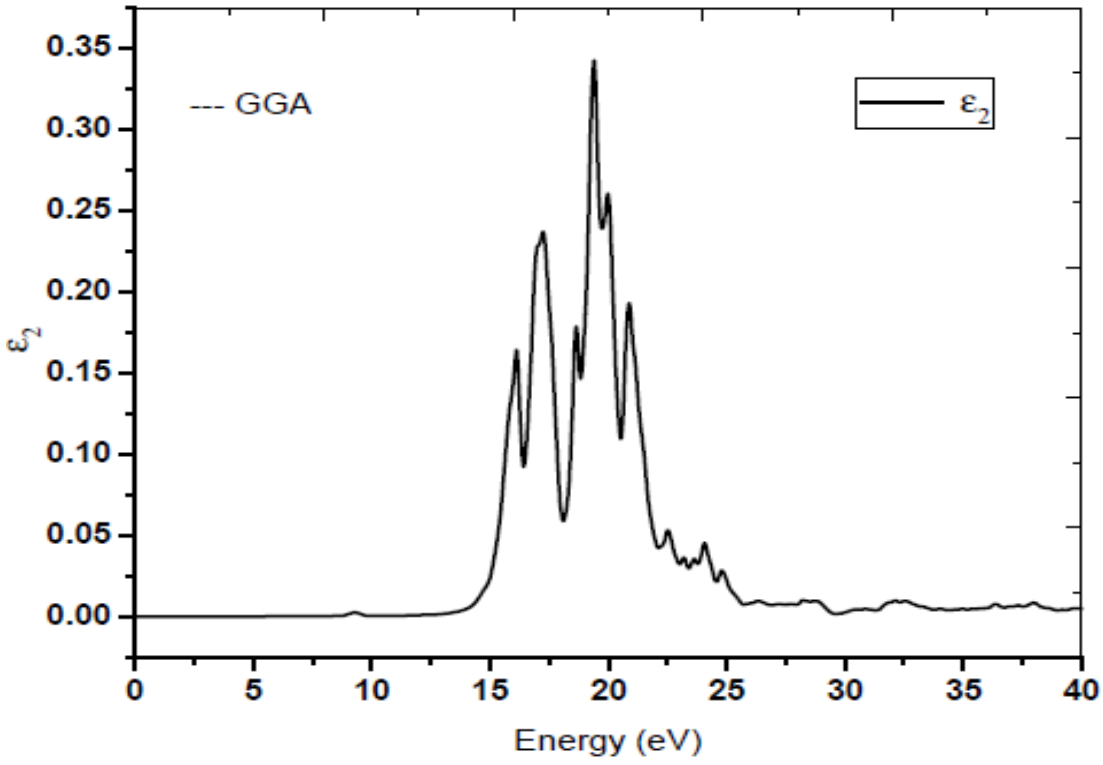

Fig. 6.18: Imaginary $\varepsilon_2(\omega)$ part of dielectric function for $RbCuF_3$

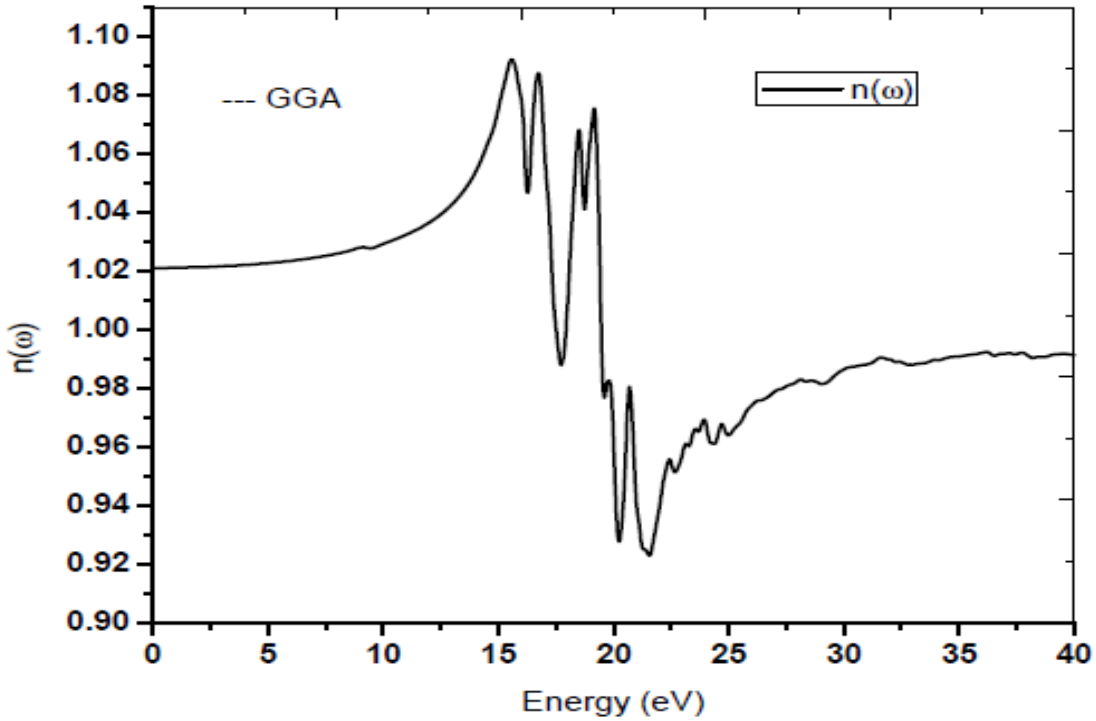

Fig. 6.19: The refractive index $n(\omega)$ for $RbCuF_3$

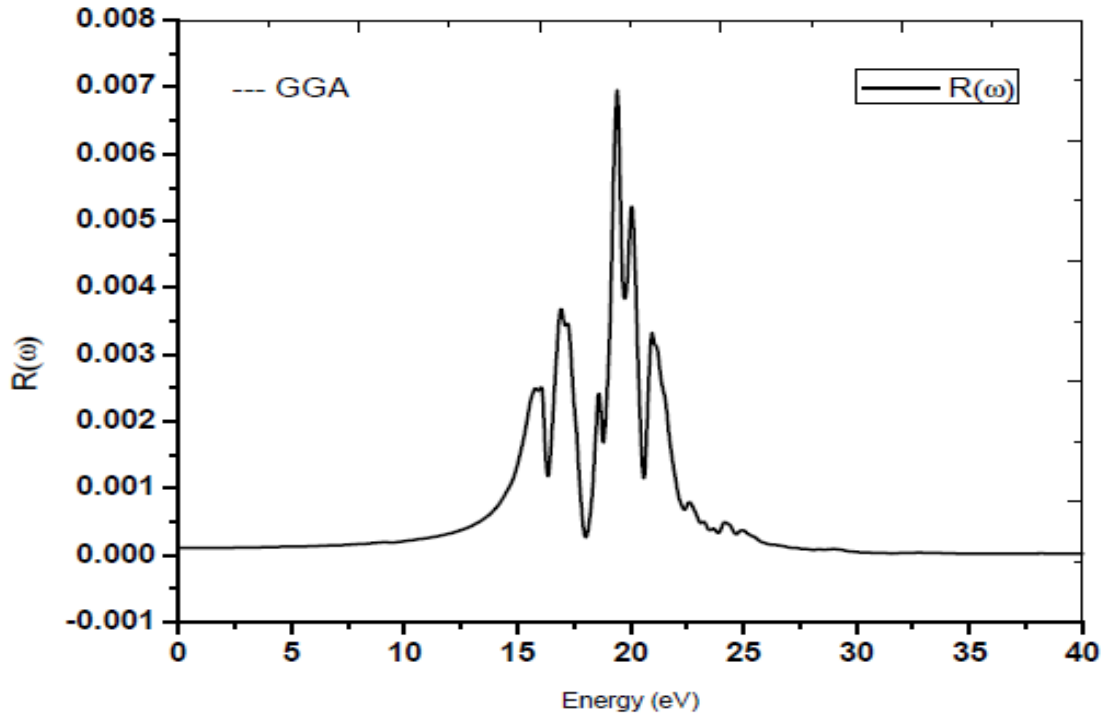

Fig. 6.20: The Reflectivity $R(\omega)$ for $RbCuF_3$

(c) Absorption coefficient and Electron energy loss function

Fig. 6.21 shows the absorption coefficient $\alpha(\omega)$ of photon energy for $RbCuF_3$ compound. The absorption characters are observed in the range up to 40 eV. The maximum absorption coefficient is 33.0 m^{-1} at 19.41 eV.

Electron energy loss spectroscopy provides information about elastically scattered and non-scattered electrons and the number and type of atom being struck by the beam. The electron energy loss spectra for $RbCuF_3$ systems under study are given in Figs. 6.22. Fig. 6.22 shows the electron energy loss (EEL) spectra of $RbCuF_3$ compound for the energy range 0-40 eV in which it represents characteristic plasmon oscillations. From the Fig. 6.22 in GGA, it is found that the most resonant peak occurs at 20.93 eV.

(d) Optical conductivity and Extinction coefficient

Fig. 6.23 shows the optical conductivity of $RbCuF_3$ compound in the energy range 0-40 eV. The conduction of electrons due to an applied electromagnetic field is characterized by optical conductivity $\sigma(\omega)$. From the Fig. 6.23 in the approach of GGA, optical conduction starts form 10.65 eV. From our calculation, we have found the maximum value of conductivity is at 19.41 eV. The peak value of the conductivity is $895\,\Omega^{-1}cm^{-1}$. Fig. 6.24 shows the extinction coefficient for $RbCuF_3$ compound in the energy range 0-40 eV. When we look the behavior of imaginary part $\varepsilon_2(\omega)$ of dielectric function and extinction coefficient $K(\omega)$, a similar trend is observed from Fig.6.18 and 6.24. The extinction coefficient $K(\omega)$ reaches the maximum absorption at 20.0 eV.

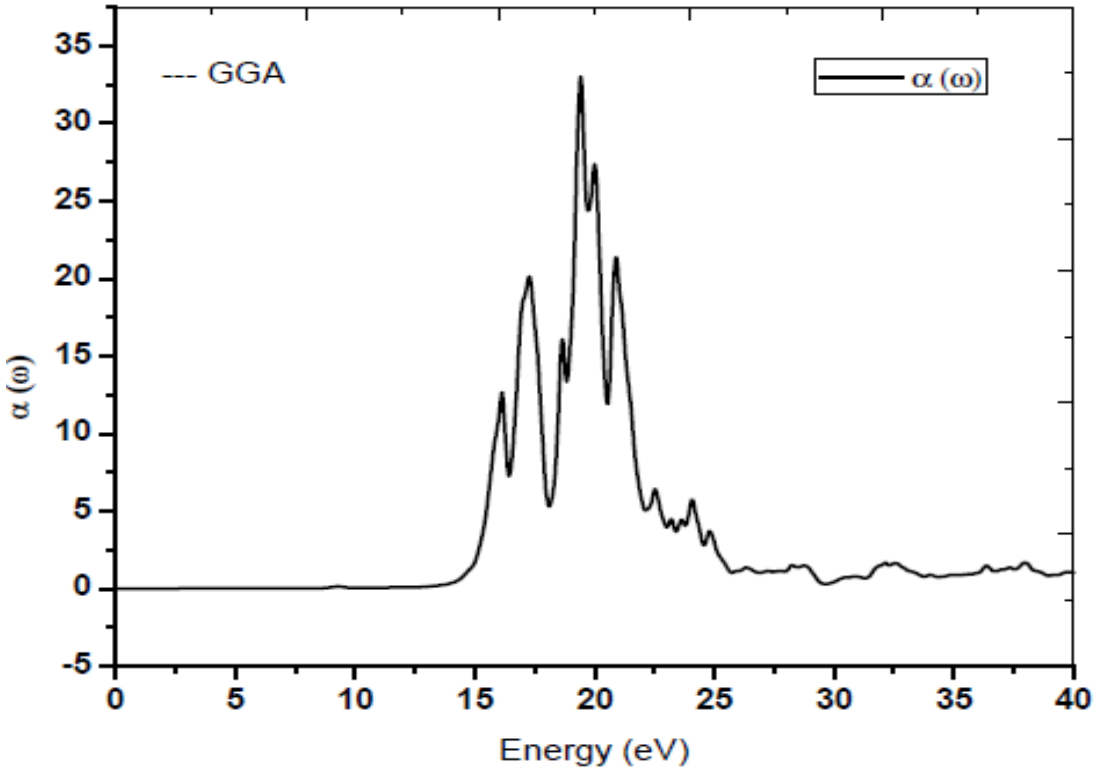

Fig. 6.21: The absorption coefficient $\alpha(\omega)$ for $RbCuF_3$

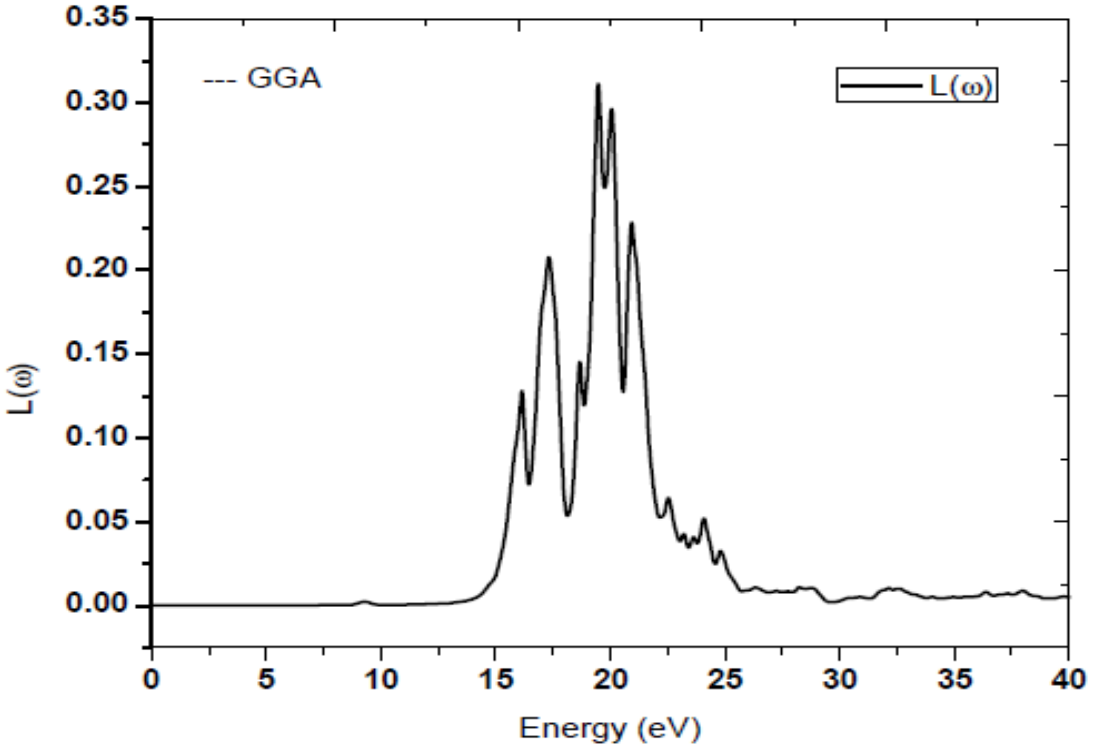

Fig. 6.22: Energy loss function $L(\omega)$ for $RbCuF_3$

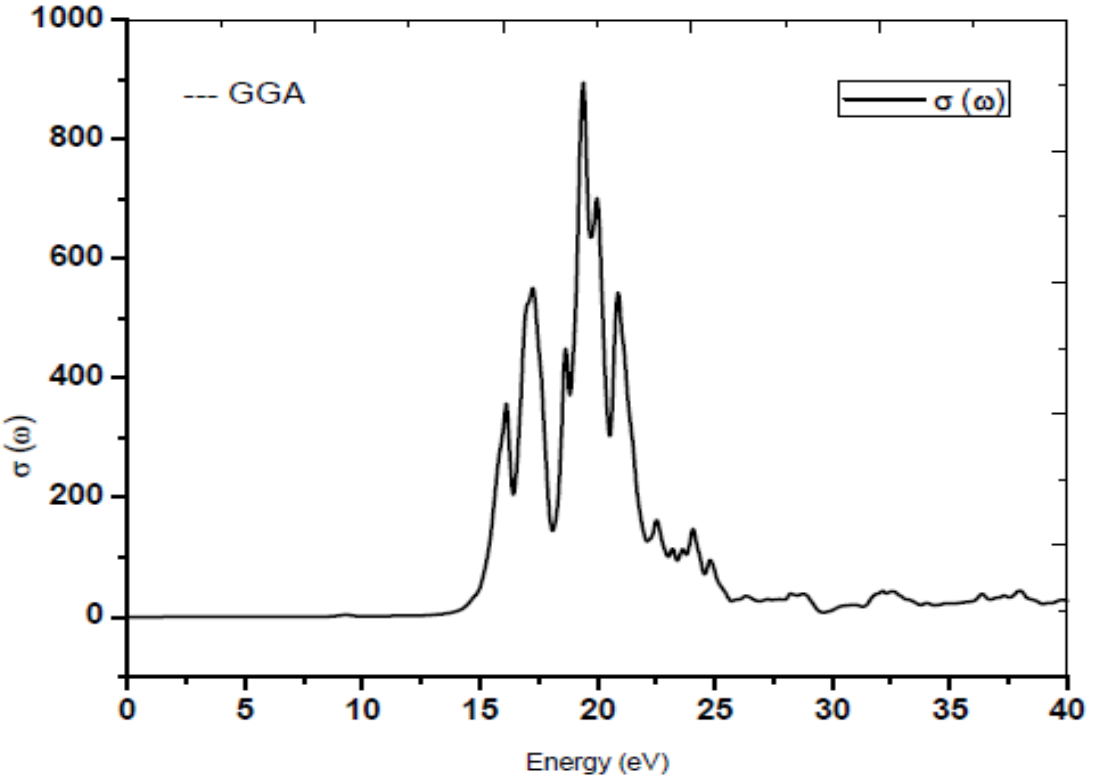

Fig. 6.23: The optical conductivity $\sigma(\omega)$ for $RbCuF_3$

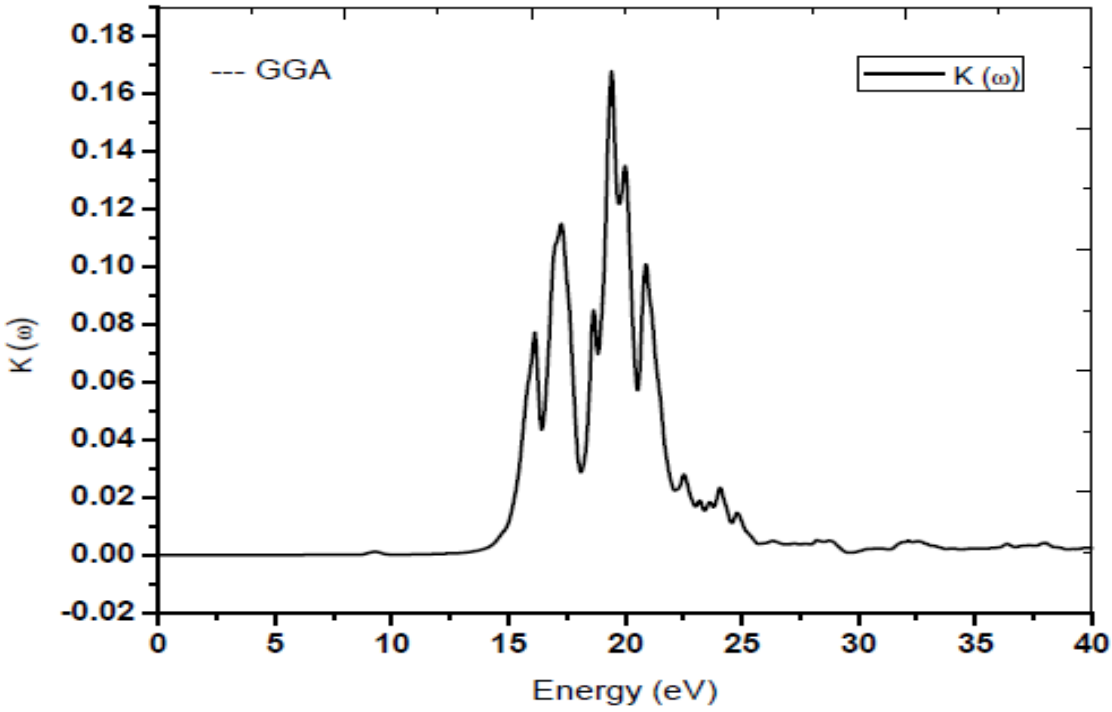

Fig.6.24: The extinction coefficient for $RbCuF_3$

(ii) $RbAgF_3$

(a) Real and Imaginary parts of dielectric function

Fig. 6.25 represents real part $\varepsilon_1(\omega)$ of dielectric function of $RbAgF_3$ in the approach of GGA. From our calculation, we have found maximum value of $\varepsilon_1(\omega)$ at 20.83 eV then it starts to decrease up to 23.71 eV. From the plot in real part of dielectric function with photon energy, we have found the minimum value of $\varepsilon_1(\omega)$ at 23.71 eV. Fig. 6.26 represents the imaginary part $\varepsilon_2(\omega)$ of dielectric function of $RbAgF_3$. From this calculation, we have found the maximum value of $\varepsilon_2(\omega)$ at 21.80 eV which is seen in Fig. 6.26.

(b) Refractive index and Reflectivity

Fig. 6.27 represents the refractive index $n(\omega)$ of dielectric function of $RbAgF_3$ compound. High refractive materials are used in ophthalmic lenses, filters and optical adhesives, antireflection coating and advanced optoelectronic devises compound. The calculated static refractive index $n(0)$ is mentioned in Table 6.5. The refractive index greater than one means photons which travelling in the material are slowed down due to the interaction with electrons of the medium. The refractive index less than unity shows that the phase velocity greater than light velocity, which is in disagreement to relativity. This suggests that in a dispersive medium signal transmitted as wave packet propagating at the group velocity. At zero frequency limits, the static refractive indices are given in Table 6.5. At higher frequency range the refractive index tends to decrease showing the material absorbs high energy photons. Fig. 6.28 represents the reflectivity $R(\omega)$ of $RbAgF_3$ compound. The static reflectivity $R(0)$ is mentioned in Table 6.5. From our calculation, we have found the static reflectivity is nearly equal to zero.

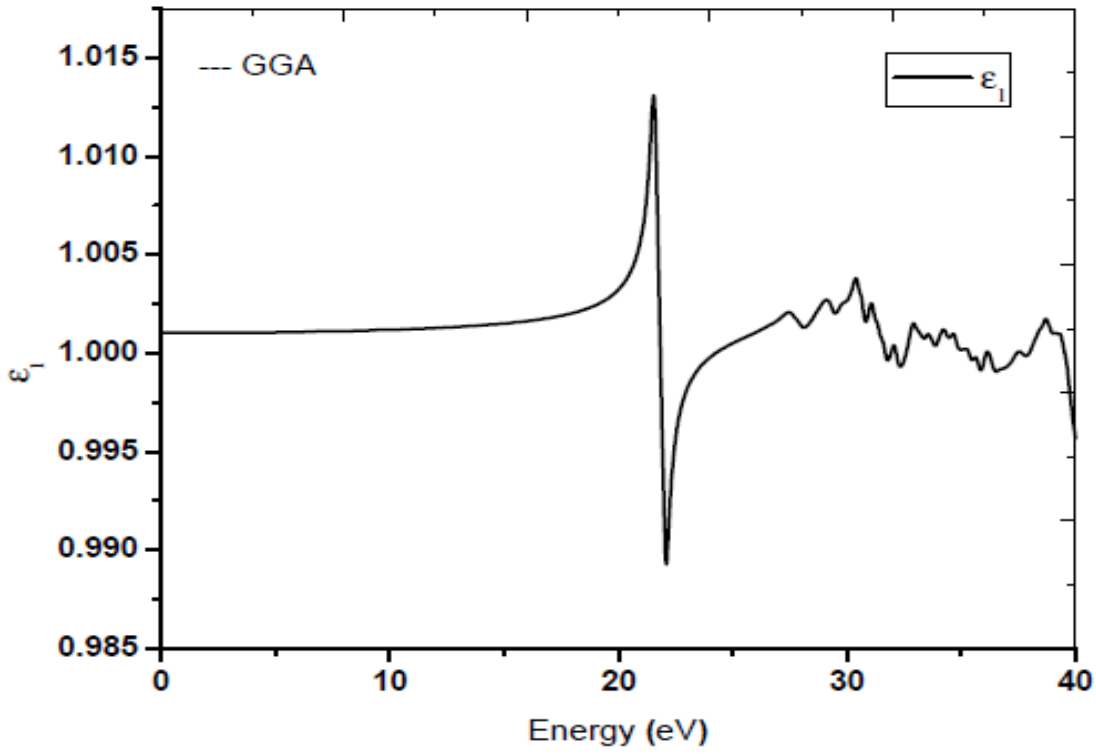

Fig. 6.25: Real $\varepsilon_1(\omega)$ part of dielectric function for $RbAgF_3$

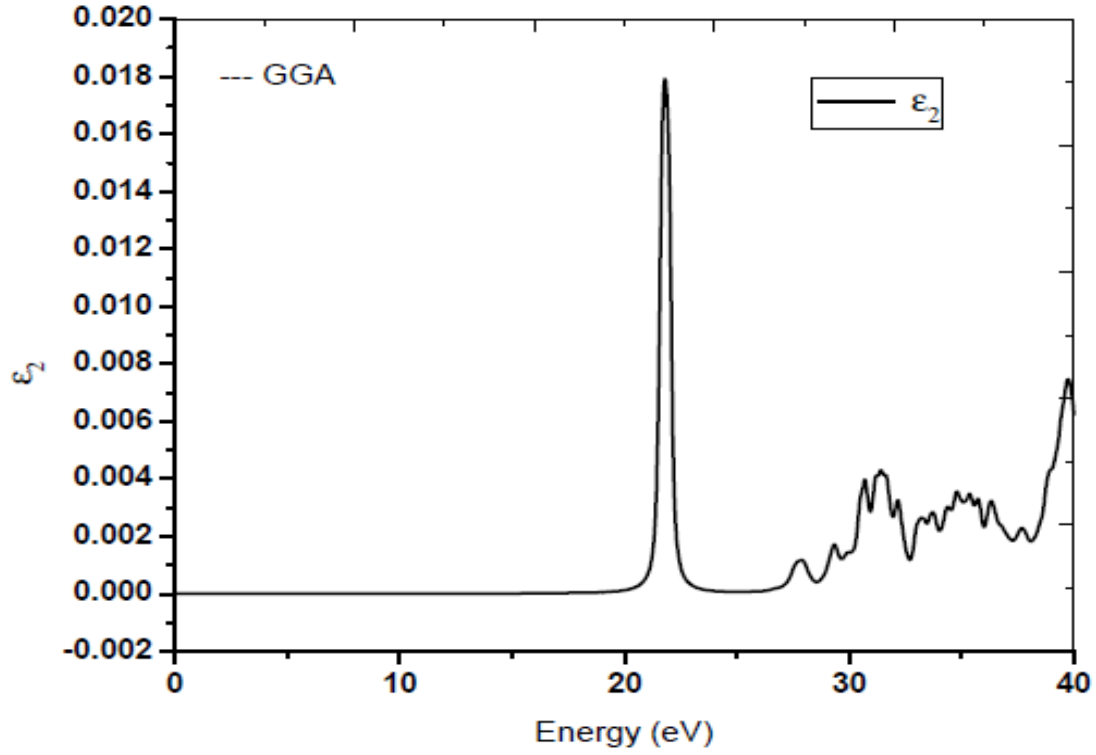

Fig. 6.26: Imaginary $\varepsilon_2(\omega)$ part of dielectric function for $RbAgF_3$

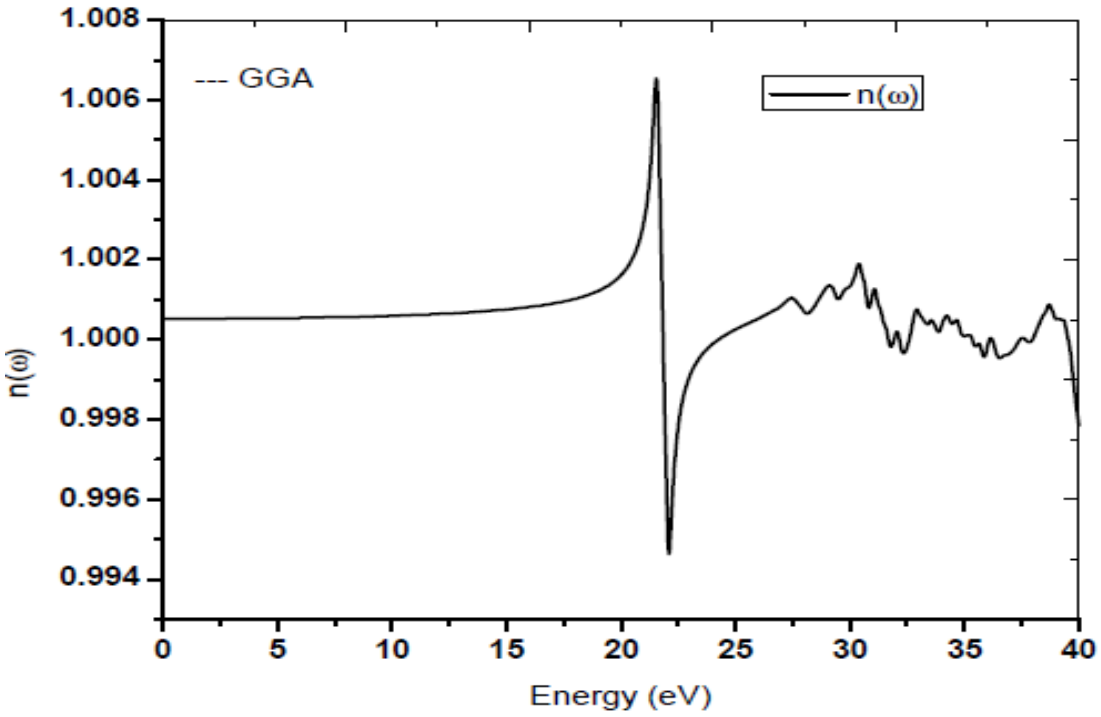

Fig. 6.27: The refractive index $n(\omega)$ for $RbAgF_3$

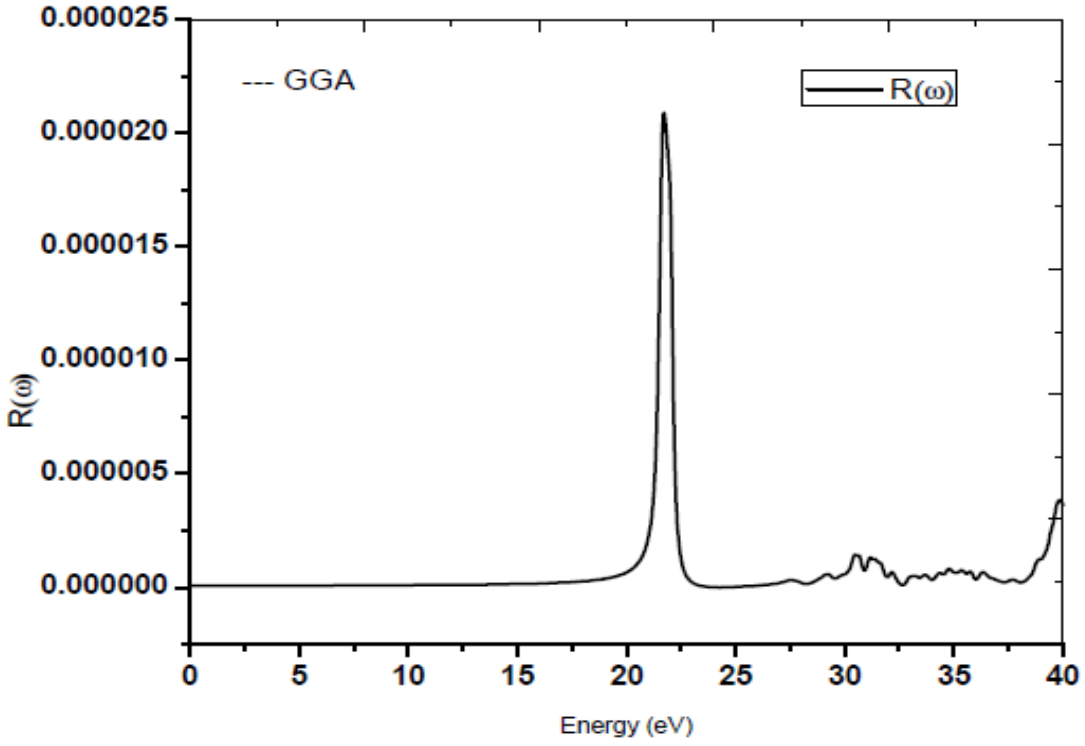

Fig. 6.28: The Reflectivity $R(\omega)$ for $RbAgF_3$

(c) Absorption coefficient and Electron energy loss function

Fig. 6.29 shows the absorption coefficient $\alpha(\omega)$ of photon energy for $RbCuF_3$ compound. The absorption characters are observed in the range up to 40 eV. The maximum absorption coefficient is $2.02m^{-1}$ at 22.10 eV.

Electron energy loss spectroscopy provides information about elastically scattered and non-scattered electrons and the number and type of atom being struck by the beam. The electron energy loss spectra for $RbAgF_3$ systems under study are given in Figs. 6.30. Fig. 6.30 shows the electron energy loss (EEL) spectra of $RbAgF_3$ compound for the energy range 0-40 eV in which it represents characteristic plasmon oscillations. From the Fig. 6.30 in GGA, it is found that the most resonant peak occurs at 22.10 eV.

(d) Optical conductivity and Extinction coefficient

Fig. 6.31 shows the optical conductivity of $RbAgF_3$ compound in the energy range 0-40 eV. The conduction of electrons due to an applied electromagnetic field is characterized by optical conductivity $\sigma(\omega)$. From the Fig. 6.31, optical conduction starts form 20.65 eV. From our calculation, we have found the maximum value of conductivity is at 22.10 eV. The peak value of the conductivity is $54.5\,\Omega^{-1}cm^{-1}$. Fig. 6.32 shows the extinction coefficient for $RbAgF_3$ compound in the energy range 0-40 eV. When we look the behavior of imaginary part $\varepsilon_2(\omega)$ of dielectric function and extinction coefficient $K(\omega)$, a similar trend is observed from Fig.6.26 and 6.32. The extinction coefficient $K(\omega)$ reaches the maximum absorption at 22.10 eV.

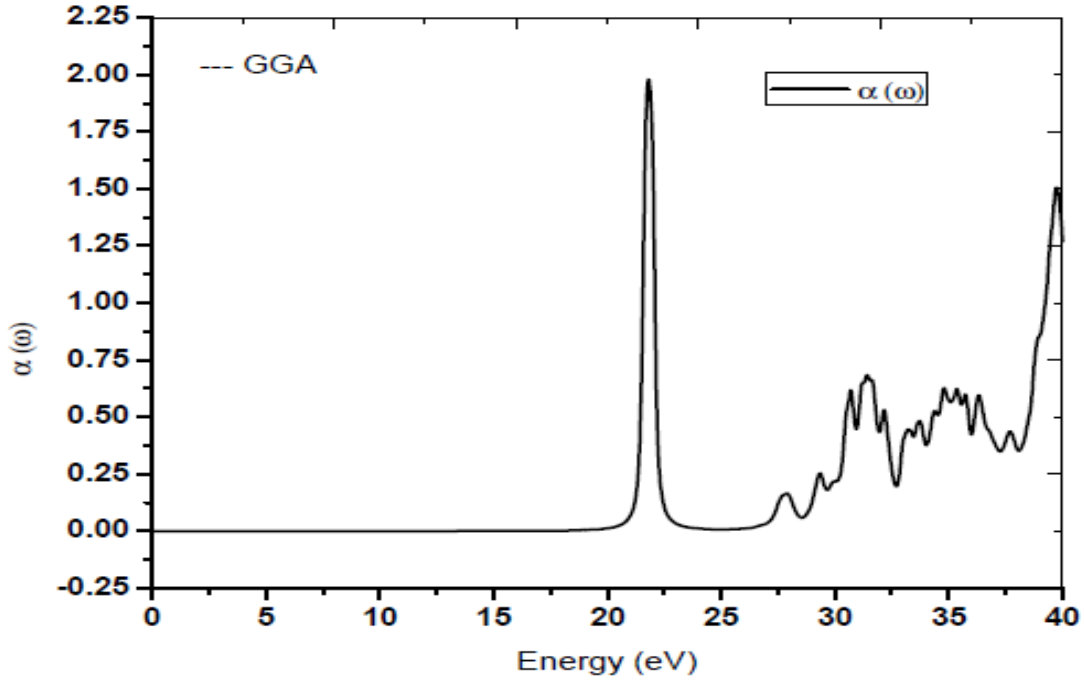

Fig. 6.29: The absorption coefficient $\alpha(\omega)$ for $RbAgF_3$

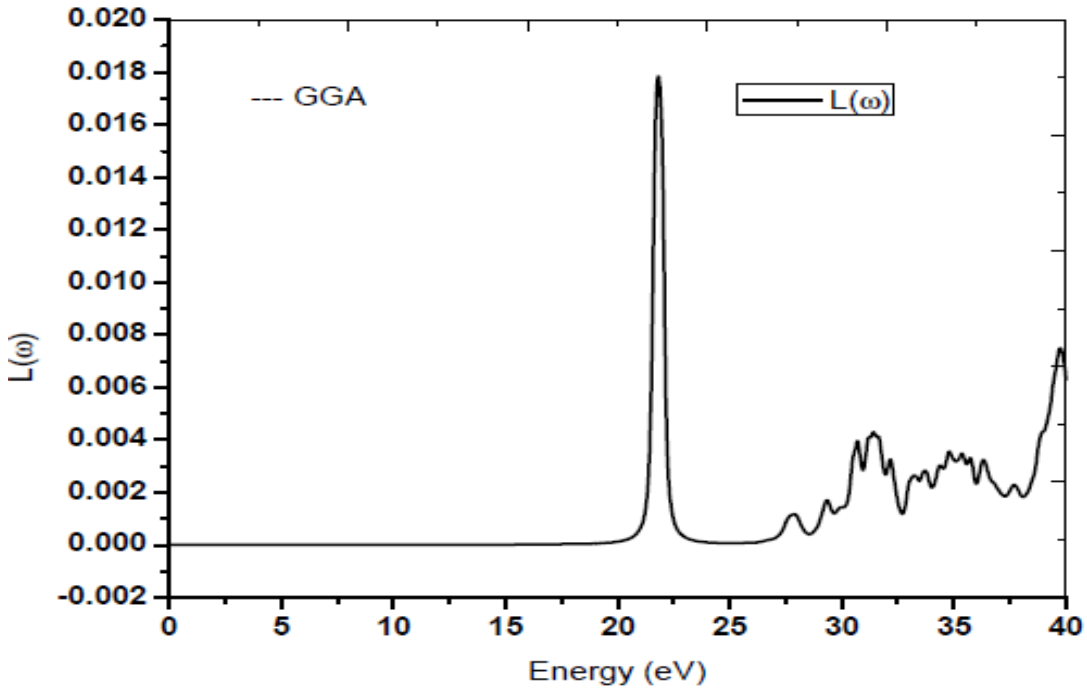

Fig. 6.30: Plot of energy loss function $L(\omega)$ for $RbAgF_3$

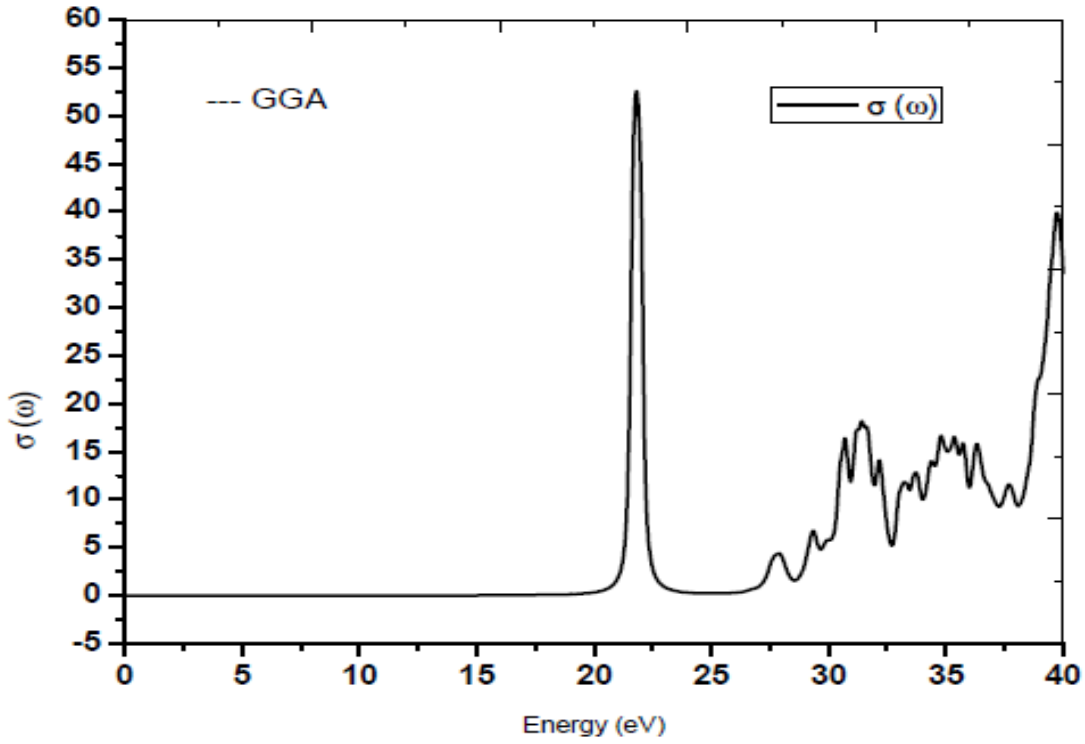

Fig. 6.31: The optical conductivity $\sigma(\omega)$ for $RbAgF_3$

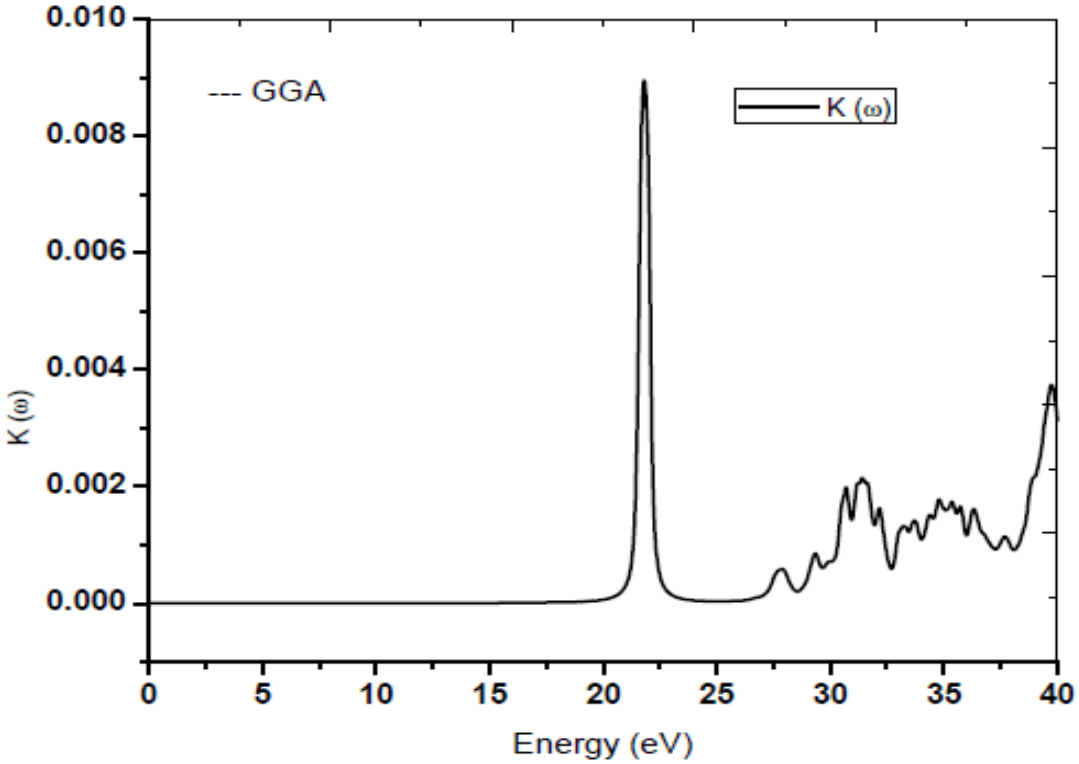

Fig.6.32: The extinction coefficient for $RbAgF_3$

Table 6.5: Calculated static refractive index, dielectric constant and reflectivity values for $RbBF_3$ (B = Cu, Ag) compound.

Compound	$n(0)$	$\varepsilon_1(0)$	R (0)%
$RbCuF_3$	1.02	1.04	0.0148
$RbAgF_3$	1.00	1.00	6.78×10^{-6}

Summary and Conclusion

In this thesis we reported the study of structural, electronic and optical properties of ABF_3 type fluro perovskite using self-consistent full-potential linearized augmented plane wave (FP-LAPW) method on the base of density functional theory (DFT). The combinations of the alkali metals or alkaline earth metals A and the transition metals B are as A = K, Rb, Cs, Ba; B = Li, K, Rb, Ca, and Cu and Ag. The methodology followed had been discussed in detail in chapter-2. The electronic properties studied in this thesis are concerned with calculation of density of states (DOS) and energy band structures as well as the optical properties. The optical property is studied by calculating the frequency dependent isotropic complex dielectric function, refractive index, reflectivity and energy loss spectra followed by the optical conductivity of the crystal as a function of incidentphoton.

In Chapter 3, we discuss the structural and electronic properties of properties of $KCaF_3$, $RbCaF_3$ and $CsCaF_3$ respectively by using GGA and mBJ potentials. We have found that calculated values of lattice parameters, bulk moduli and pressure derivatives for these systems were more or less similar to experimental values and previously calculated results as referred in the Table 3.1. From the plots of DOS it is found that Ca atom of $KCaF_3$ compound has negligible contribution to TDOS and PDOS in the valence band below the Fermi level. However in the conduction band, a maximum peak in TDOS is observed at 9.68 eV in the conduction band. This can be attributed to Ca-dt_{2g} state electrons. It is also found that the contribution to the occurrence of this peak at -0.27 eV is due to the contribution by F_{px+py} state electrons. There is negligible contribution to TDOS and PDOS in conduction band by F atom.

There is similar trend in the values of TDOS and PDOS in the systems $KCaF_3$, $RbCaF_3$ and $CsCaF_3$ as calculated by using the mBJ potential. Also there is not much differences found in the calculated energy bands in several symmetry direction by using GGA and mBJ methods. However the point of difference is that mBJ over estimates the energy gaps for all the systems $KCaF_3$, $RbCaF_3$ and $CsCaF_3$. The energy band gaps calculated is wide and the values are 10.6 eV, 10.4 eV and 9.8 eV for $KCaF_3$, $RbCaF_3$ and $CsCaF_3$respectively.

Chapter 4, we have the results of structural and electronic properties of ABF_3 type perovskite with alkaline earth metal A as Ba, and alkali metals as Li, K and Rb. The combinations of the systems are namely $BaLiF_3$, $BaKF_3$ and $BaRbF_3$ respectively. In these cases also, it is found that calculated values of lattice parameters, bulk moduli and pressure derivatives for these systems were more or less similar to experimental values and previously calculated results as referred in the Table 4.1. From the results it is found that in the valence bands, it is the F-*p* state electrons which contributes maximum to DOS. In the conduction band, it is seen that Ba atom contributes maximum to DOS. There is similar trends in the values of TDOS and PDOS in the systems $BaLiF_3$, $BaKF_3$ and $BaRbF_3$ as calculated by using the mBJ potential. Also there is not much differences found in the calculated energy bands in several symmetry directions by using GGA and mBJ methods. However the point of difference is that mBJ over estimates the energy gaps for all the systems $BaLiF_3$, $BaKF_3$ and $BaRbF_3$. The energy band gaps calculated is wide and values are 8.3 eV, 6.3 ev and 5.3 eV for $BaLiF_3$, $BaKF_3$ and $BaRbF_3$ respectively.

In Chapter 5, we have described results obtained for structural and electronic properties of ABF_3 type perovskite with alkali metals A as Rb; and transition metal B as Cu and Ag. The combinations of the systems studied are namely, $RbCuF_3$ and $RbAgF_3$.

In this case we have done the calculations of DOS by using GGA and mBJ method. We have observed that there is not much difference in DOS results by using the mBJ method with GGA method. There was similar behaviors of DOS and bands. We found here that contributions in the valence bands were due to mainly *d*-state electrons of transition metals Cu and Ag, and in the conduction bands, again the F electron states were mostly contributing. There was band gaps in both the systems studied and the values are 3.0 eV and 2.5 eV for $RbCuF_3$ and $RbAgF_3$ respectively in GGA method. Similarly, we have found the band gaps as 5.0 eV and 5.3 eV for $RbCuF_3$ and $RbAgF_3$ respectively in mBJ method.

In chapter-6, the results of various optical parameters are discussed in respect of the fluoride perovskite of ABF_3 type combinations of alkali metals A and alkaline or transition metals B respectively. For this, the combination of A and B taken are as namely like A = K, Rb, Cs, Ba and B = Li, K, Rb, Ca, Cu, Ag. For calculational purpose, here also we have used two approximations for the exchange correlation functionals namely; GGA and mBJ. In this context, we have considered only the GGA method. The reason for this being that, with the inclusion of mBJ potential in our calculations of optical parameters, the qualitative features in the plots of parameters like, refractive indices, reflectivity, absorption coefficients, electron energy loss etc. have similar features as obtained by using GGA method. The detail discussions of the formulae used for calculations are given in chapter-2.

In case of $ACaF_3$ (A = K, Rb, Cs) combination of elements in chapter-6, we found that real and imaginary parts of dielectric constants showed a typical behavior. There were many structures shown when plotted as a function of photon energy. Due to this type of variations, metallic type behavior cannot be attributed. However a very wide band gap was calculated which may be interest in wide band gap devices in electronics

or opto-electronics. However, in the case of $BaBF_3$ (B = Li, K, Rb) combinations of elements, we have observed that we found that real and imaginary parts of dielectric constants showed similar behavior as shown by solids like silver or copper (Figs. 6.9 and 6.10). For example, with the increase of photon energy, there is increase in dielectric constant (real) and reaches maximum and decreases with the further increase in the photon energy. However, the value where real dielectric constant ε_1 is zero at around 18 eV, the imaginary dielectric ε_2 constant becomes maximum for both $BaKF_3$ and $BaRbF_3$ except for $BaLiF_3$ (Fig. 6.10). This is interesting phenomena as all other optical parameters are related to these two dielectric constants as discussed in chapter-2. For example, real dielectric constant $\varepsilon_1 = n^2 - K^2$ and imaginary by $\varepsilon_2 = 2nK$. Hence as shown in Fig. 6.11, the occurrence of maxima in refractive index n takes place also at 10 eV photon energy where ε_2 is maximum and ε_1 is minimum or zero. However this trends is not found in the case of $BaLiF_3$. Related behaviors of other optical parameters like reflectance, absorption, conductivity, EEL spectra etc. are also seen to have co-relative behaviors with real and imaginary dielectric constants. The optical results in the case of $RbCuF_3$ and $RbAgF_3$ are also discussed but the combination did not show metallic type behavior.

In this thesis, we have worked on the structural, electronic and optical properties of alkali and or alkaline earth or transition metals combinations of A and B with flourine making making fluro perovskites. We have calculated several optical parameters for these systems due to which they may be useful in the technical applications. For example, these flouro-perovskite systems are foud to have wide band gaps due to which may have tremendous applications in optoelectronic devices and color televisions. They have been found to have wide band gaps ranging from 2 eV to 7 eV and the trnsitions which takes place across the gap are both direct and indirect types. For example, direct

transitions occurs in the case of alkali and transition metals combinations of A and B with flourine as well as in the alkaline earth and alkali metals combinations of A and B with flourine. For these combinations, the transition takes place only at symmetry point Γ. For combinations of alkaline earth metals for both A and B with flourine, the transition across the band gap is indirect and occurs along R to Γ symmetry direction. In conclusion, flouro-perovskites are wide band insulators possesing both direct and indirect band gaps which had been inferred both from GGA and mBJ study.

Reference

Anisimov V. I., Zaanen J. and Andersen O. K. (1991), Band theory and Mott insulators: Hubbard U instead of Stoner I, *Phys. Rev. B*, **44:** 943-954.

Anisimov V. I., Aryasetiawan F. and Lichtenstein A. I. (1997), First-principles calculations of the electronic structure and spectra of strongly correlated systems: the LDA+U method, *J. Phys.: Condens. Matter.*, **9:** 767-808.

Babu, E. K.,Veeraiah, A., Swamy, T. D. and Veeraiah, V. (2012), First-Principles Study of Electronic Structure and Optical Properties of Cubic Perovskite $CsCaF_3$, *Chin.Phys.Lett.* **29:**117102-117105.

Babu, K.E., Murali, N., Babu, V., Babu, B. K. and Veeraiah, V. (2014), Structural, Elastic, Electronic, and Optical Properties of Cubic Perovskite CsCaCl3 Compound: An ab initio Study, *Acta Phys.Polonica A*, 125: 1179-1186.

Babu, K.E., Murali, N., Babu, V., Babu, B. K. and Veeraiah, V. (2015), Structural, electronic and elastic properties of KCaF3 and RbCaF3 for vacuum ultraviolet- transparent lens materials. *AIP Conference Proceedings* **1661:** 100002-100005.

Bagayoko, D., Zhao, G. L., Fan, J. D. and Wang, J. T. (1998), Ab initio calculation of the electronic structur and optical properties of ferroelectric tetragonal BaTiO3, *J. Phys. Condensed Matter* **10:**5645-5655.

Ball J. M., Lee M. M., Hey A. and Snaith H. J. (2013), Low- temperature processed meso-superstructured to thin-film perovskite solar cells, *Energy Environ.Sci.,* **6:** 1739-1743.

Bechstedt F., Fuchs F., and Kresse G. (2009). Ab-initio theory of semiconductor band structures: New developments and progress. *Phys. Status Solidi,* **246**(8), 1877-1892.

Becke A. D., and Johnson E. R. (2006). A simple effective potential for exchange. *J. Chem. Phys.* ***124****, 221101-221104.*

Becke A. D., and Roussel M. R. (1989). Exchange holes in inhomogeneous systems: A coordinate-space model. *Phys. Rev. A*, **39**(8), 3761-3767.

Blaha P., Schwarz K., Madsen G. K. H., Kvasnicka D., Luitz J., Schwarz K. (2012), *An Augmented Plane Wave plus Local Orbitals Program for Calculating Crystal Properties,* Wien2K User's Guide, Techn. Universitat Wien, Wien.

Blaha P., Schwarz K., Madsen G. K. H., Kvasnicka D., and Luitz J. (2001). wien2k. *An augmented plane wave+ local orbitals program for calculating crystal properties*.

Bloch P. E., Jepson O. and Anderson O. K. (1994), Improved tetrahedron method for Brillouin-zone integrations, *Phys. Rev. B*, **49**: 16223-16233.

Bulou, A., Ridou, C., Rousseau, M., Nouet, J. and Hewat, A. (1980), The temperature dependence of the structure of $RbCaF_3$ and the determination of the low temperature phases, *J. Phys*. **41**: 87-96.

Callaway J. (1974a), *Quantum Theory of Solids*, Academic Press: New York.

Callaway J. (1974b), *Energy Bands in Solids*, Academic Press: New York.

Chornodolskyy, Y., Syrotyuk, S., Stryganyuk, G., Voloshinovskii, A. and Rodnyi P. (2007), "Electronic Energy Structure and Core-Valence Luminescence of ABX_3" (A = K, Rb, Cs; B = Ca; X = F), *Journal of Physical Studies*, **4:** 421–426.

Cottenier S. (2002), *Density Functional Theory and the family of (L) APW-methods: a step-by-step introduction*, Belgium: Instituut voor Kern-en Stralingsfysica, K. U. Leuven.

Daniel, P. H., Rousseau, M., and Toulouse, J. (1997), "Raman Scattering Study of Potassium Calcium Fluoride $KCaF_3$", *Phys. Status. Solidi. (b)*, **203:** 327–335.

Delin, A., Eriksson, O., Ahuja, R., Johansson, B., Brooks, M. S. S., Gasche, T., Auluck, S. and Wills, J. M., (1996), Optical properties of the group-IVB refractory metal compounds, *Phys. Rev.* B 54: 1673-1682.

Demetriou, D. Z., Catlow, C. R. A., Chadwick,A. V., Mclntyre, G. J. and Abrahams, I., (2005). "The Anion Disorder in the Perovskite Fluoride KCaF3", *Solid State Ionics*, **176:** 1571-1575.

Dressel M. and Gurner G., (2001*), Electrodynamics of solids: Optical properties of electrons in matter*, Cambridge University Press, Uk.

Ederer C. and Spaldin N. A. (2006), Electric-field-switchable magnets: The case of $BaNiF_4$, *Phys. Rev***. B 74:** 020401-3.

Engel E. (2009). Relevance of core-valence interaction for electronic structure calculations with exact exchange. *Phys. Rev. B,* **80**(16), 161205-16209.

Erdinc, B. (2011), Density Functional Calculations of the Electronic Band Structure and Optical Properties of KCaF3, *GUJ Sci*, **24(4):** 671-677

Ernst A., Henk J. and Thapa R. K. (2005), Ultrathin antiferromagnetic films on a ferromagnetic substrate: A first principle study of Mn on Fe (001), *J. Phys. Condens. Matter,* **17:** 3269-3283.Fetter A. L. and Walecka J. D. (1971), *Quantum theory of many particle systems*, McGraw-Hill, New York.

Filippi C., Umrigar C. J. and Taut M. (1994), Comparison of exact and approximate density functionals for an exactly soluble model, *J. Chem. Phys.*, **100**:1295-7.

Flocken J. W., Guenther R. A., Hardy J. R., and Boyer, L. L. (1986), "A Priori Predictions of Phase Transitions in $KCaF3_3$ and $RbCaF_3$: Existence of a New Ground State**",** *Phys. Review Lett*, **56:** 1738–1741

Fox M., (2002*). Optical Properties of Solids*, Oxford University Press, New York.

Garcia-Castro, A. C., Spaldin, N. A., Romero, A. H. and Bousquet, E. (2013), Geometric Ferroelectricity in Fluoro-Perovskites, *cond-mat. mtrl-sci, 1-6.*

Gardana, M. (1965), Optical Properties and Band Structure of $SrTiO_3$ and $BaTiO_3$, *Phys. Rev.* **140:** A651.

Georges A., Kotliar G., Krauth W., and Rozenberg M. J. (1996). Dynamical meanfield theory of strongly correlated fermion systems and the limit of infinite dimensions. *Rev. Mod. Phys.*, **68**(1), 13-125.

Gross E. K. U. and Dreizler R. M. (1981), Gradient expansion of the Coulomb energy, *Z. Phys A-Atoms and Nuclei,* **302:** 103-106.

Hao A., Yang X., Wang X., Zhu Y. and Liu X. J. (2010), First-principles investigations on electronic, elastic and optical properties of XC (X = Si, Ge, and Sn) under high pressure, *J. Appl. Phys.*, **108**: 063531-063537.

Heyd J., Peralta J. E., Scuseria G. E., and Martin R. L. (2005). Energy band gaps and Lattice parameters evaluated with the Heyd-Scuseria-Ernzerhof screened hybrid functional. *J. Chem. Phys.*, **123**(17), 174101-174110.

Hohenberg P. and Kohn W. (1964), Inhomogeneous Electron Gas, *Phys. Rev. B*, **136:** 864-871

Jiang, L. Q., Guo, J. K., Liu, H. B., Zhu, M., Zhou, X., Wu, P. and Li, C. H. (2006), Prediction of Lattice Constant in Cubic Perovskites, **67:**1531-1536.

Kaiser V.,Otto M., Binder F.and Babel D. (1990), Jahn-Teller effect and crystal structure-verzerrung copper Fluoroperovskites $NaCuF_3$ and $RbCuF_3$, *Z. anorg. Chem*. **585**:93-104.

Kohn W. and Sham L. J. (1965), Self-Consistent Equations Including Exchange and Correlation Effects, *Phys. Rev. A*, **140**:1133-1138.

Kresse G. and Furthmüller J. (1996), Efficient iterative schemes for ab initio total-energy calculations using a plane-wave basis set, *Phys. Rev. B*, **54**:11169-11186.

Lee M. M., Teuscher J., Miyasaka T., Murakami T. N. and Snaith H. J. (2012), Efficient hybrid solar cells based on meso-superstructured organametal halide perovskites, *Science* **338:** 643-647.

Lovinger A. J. (1983), Ferroelectric polymers, *Science*, **220:** 1115-1121.

Lufaso M.W. and woodward P. M. (2001), Prediction of the Crystal Structures of Perovskites using the software program SPuDs, *Acta Cryst.,* **B57**: 725-738.

Mara, R. T., Sutherland, G. B. B. and H. V. Tyrell, H. V. (1954), Infrared Spectrum Barium Titanate, *Phys. Rev*., **96:** 801-809.

Ma S.K. and Brueckner K. A. (1968), Correlation Energy of an Electron Gas with a Slowly Varying High Density, *Phys. Rev.,***165**: 18-31.

Meziani A. and Belkhir H., (2012), First-principles calculations of structural, elastic and electronic properties of CsCaF3 compound, *Computational Material Science,* **61:** 67-70

Moller C. K. (1958), Crystal Structure and Photoconductivity of Caesium Plumbohalides, *Nature,* **182:** 1436-1436.

Mubark, A. A. and Mousa, A. A. (2012). *The electronic and optical properties of the fluoroperovskite $BaXF_3$ (X= Li, Na, K and Rb),* Computational Materials Science. **59:** 6-13.

Murat, A. and Bahattin, E. (2016), DFT Study of $CsCaF_3$: Eu, *GUJ Sci*. **29(2):**273-278

Murnaghan, F. D. (1944), The Compressibility of Media under Extreme Pressures, *Proc. Natl. Acad. Sci., USA,* **30**: 244-247.

Murtaza, G., Ahmad, I. and Afaq, A. (2013). Shift of indirect to direct band gap in going from K to Cs in $MCaF_3$ (M = K, Rb, Cs*), Solid State Science,* **16:**152-157.

Mutou T. and Saso T. (2004), Optical conductivity of Ce-based filled skutterudites, *J.*

Phys. Soc. Jpn., **73:** 2900-2905

Park N.G. (2013), Organometal Perovskite Light Absorbers Towards a 20% Efficiency Low-Cost Solid-State Mesoscopic Solar Cell, *The Journal of Physical Chemistry Letters* **4:** 2423-2429.

Perdew J. P. (1985), Accurate Density Functional for the Energy: Real-Space Cut off of the Gradient Expansion for the Exchange Hole, *Phys. Rev. Lett.*, **55**:1665–16.

Perdew J.P.(1986). Density-functional approximation for the correlation energy of the inhomogeneous electron gas. *Phys. Rev. B,* **33**(12), 8823-8826.

Perdew J. P., and Zunger A. (1981). Self-interaction correction to density-functional approximations for many-electron systems. *Phys. Rev. B,* **23**(10), 5048-5079.

Perdew J. P., Burke K. and Ernzerhof M. (1996), Generalized Gradient Approximation Made Simple, *Phy. Rev. Lett.*, **77:** 3865–3868.

Perdew J. P., and Wang Y. (1992). Accurate and simple analytic representation of the electron-gas correlation energy. *Phys. Rev. B,* **45**(23), 13244-13249.

Pilania, G. and Sharma, V. (2013), First principles investigations of structural, electronic, elastic, and dielectric properties of $KMgF_3$, J Mater Sci **48:**7635–7641.

Pines D. (1963), *Elemantary Excitations in Solids*. W. A. Benjamin, Inc, New York

Piskunov S., Heifets E., Eglitis R. I. and Borstel G. (2004), Bulk properties and electronic structure of $SrTiO_3$, $BaTiO_3$, $PbTiO_3$ perovskites : an ab initio HF/DFT study, *Computational Materials Science,* **29:**165-178.

Reshak A. H. (2007). *Linear and Nonlinear Optical Properties.* Habilitation Thesis, Institute of Physical Biology, South Bohemia, Nove Hrady.

Rousseauy, M., Daniely, Ph. and Hennion, B. (1997), "The dynamic signature of highly

anisotropic correlation near the phase transition in KCaF3", *J. Phys. Condens. Matter*, **9:** 8963–8971.

Salhei H. Hosseini S. M. and Shahtahamasebi N. (2004), First Principles Study of Electronic Structure of $BaTiO_3$, *Chinese Journal of Physics*, **42:**115-120.

Schwarz K. and Blaha P. (2003), Solid state calculations using WIEN2k, *Computational Materials Science*, **28**: 259-273.

Scott J. F. (2012), Applications of magnetoelectrics, *J Mater Che* **22:** 4567-4574.

Singh D. J. (1994), *Plane waves pseudopotential and the LAPW method*, Kluwer Academic Publishers, 02061.

Soleimanpour, S.and Kanjouri, F. (2015). Elastic, electronic and optical properties of the cubic fluoro-perovskite, Indian J. Phys. **89(7):** 687–697.

Syrotyuk S. V. and Shaved V. M. (2015), The GW electronic structure of cubic $RbMF_3$ perovskites (M= Be, Mg, Ca, Sr, Ba), *Eur. Phys. J.B*, **88:** 229-237

Tran F., and Blaha P. (2009). Accurate band gaps of semiconductors and insulators with A semilocal exchange-correlation potential. *Phys. Rev. Lett.* **102**(22), 226401-226404.

Tran F., Blaha, P., and Schwarz, K. (2007). Band gap calculations with Becke–Johnson exchange potential. *J. Phys.: Condens. Matter*, **19**(19), 196208-196207.

Watson, G. W., Parker, S. C. and Wall, A., J. (1992), "Molecular Dynamics Simulation in Fluoride Perovskites", *J. Phys. Condens. Matter*, **42:**2097–2108.

Wooten F. (1972), *Optical Properties of Solids*, Academic Press: New York.

Yu, P. Y. and Cardona, M. (1996), *Fundamentals of Semiconductors* , Springer-Verlag, Berlin, p.233.

BIODATA

Name	**:**	Khimananda Neupane
Father's name	**:**	Ghana Shyam Neupane
Date of birth	**:**	28 - 04 - 1967
Address	**:**	Panini 3, Dist. Arghakhanchi, Nepal.
Subject of Specialization	**:**	Advanced Solid State Physics

Educational Qualifications :

• Madhyamik Pariksha	1985	Second Division.
• Higher Secondary	1988	Second Division.
• B. Sc. (Physics)	1991	First Division..
• M. Sc. (Physics)	1993	First Division.
• Pre-Ph. D. Course	2015	Grade 'A'

Employment **:** Associate Professor of Physics at
T.U, Butwal Multiple Campus, Butwal, Nepal.

Research Experience:

- Started research works in Condensed Matter Theory Research group under the supervision of Prof. R. K. Thapa, Department of Physics, Mizoram University, Aizawl, Mizoram since August 2015 till date.
- Calculations of Structural, Electronic Band Structures and Optical properties. By using WIEN2k code (Ver. 14.2)
- Working knowledge of operating systems DOS/WINDOS XP and LINUX: CENTOS

Life member:

- The Nepal Physical Society, Kathmandu.

Research Publications

(A) Journals

1. Neupane, K. and Thapa, R. K. (2016).Study of DOS and band structures of fluoride perovskites ($RbCaF_3$) : ab initio study, *IJEART*, **5**,31-33.(ISSN: 2454-9290)

2. Neupane, K. and Thapa, R. K., Study of structural and electronic properties of fluoride perovskite $KCaF_3$ using FP-LAPW method, *The Himalayan Physics*,**6&7,** 100-103 (2017). (ISSN: 2542-2545)

3. Neupane, K. and Thapa, R. K., Study of structural and electronic properties of fluoride perovskite $RbMgF_3$ using FP-LAPW method, *JNPS* **4 (1)**, 101-104 (2017). (ISSN: 2392-473X)

4. Neupane, K. and Thapa, R. K., Study of Electronic Properties of Fluoride Perovskite $BaLiF_3$ Using FP-LAPW Method, *Journal of Material Science and Engineerig* **A 7** (11-12) 2017.(ISSN: 2161-6213)

5. Neupane, K. and Thapa, R. K., Study of Structural, Electronic and Optical Properties of Fluoride Perovskite $CsCaF_3$ Using FP-LAPW Method, *IJCER*, **07 (12)** 2017, 07-12. (ISSN (e): 2250-3005).

6. Neupane, K. and Thapa, R. K., Study of Structural, Electronic and Optical Properties of Fluoride Provskite $XCaF_3$ (X = K and Rb) using Generalized Gradient Approximation (GGA) Exchange Potential, *International Journal of Recent Scientific Research*, **9** (2018), 24295-24300.(ISSN: 0976-3031)

7. Neupane, K., Joshi, H., Hnamte, L. and Thapa, R. K., Study of structural and electronic properties of $KCaF_3$ type fluoro-perovskite, International Research Journal

of Advanced Engineering and Science (IRJAES),ISSN (online): 2455-9024, (Accepted).

8. Neupane, K. and Thapa, R. K., *Investigation of Electronic and Optical Properties Fluoride Perovskite $XCaF_3$ (X = K, Rb, Cs) Using Generalized Gradient Approximation and modifiedBecke- Johnson Exchange Potential, Physica* B (Communicated)

(B) Conference Procedings

1. Devi, L. N., Neupane, K., Ghimire,M. P. and Thapa, R. K.(2016*). A Theoretical study of photofield emission in Gallium Arsenide*, International conference on Electrical, Electronics, and Optimization Techniques, *ICEEOT*
2. Neupane, K. and Thapa, R. K., Study of structural and electronic properties of fluoride perovskite $KMgF_3$ using FP-LAPW method , *Journal of Physics C: Conference Series* **765** (2016).(ISSN: 1742-6596)

Conferences Attended

1. Annual Convention of Nepal Physical Society, Study of structural and electronic properties of fluoride perovskite $RbMgF_3$ using FP-LAPW method, **K Neupane** and R K Thapa, Pokhara, Nepal, 2-3 July (2016).
2. Condensed Matter Days (CMDAYS), Study of structural and electronic properties of fluoride perovskite $KMgF_3$ using FP-LAPW method, **K Neupane** and R K Thapa, Mizoram University, Aizwal, Mizoram (India), 29-31 August (2016).
3. Condensed Matter Days (CMDAYS), Study of Structural, Electronic and Optical

Properties of Fluoride Perovskite $CsCaF_3$ Using FP-LAPW Method, **K Neupane** and R K Thapa,Tezpur University, Tezpur, Assam (India), 29-31 August (2017).

4. National Conference on nanomaterials and its applications (NCNA17), Study of Structural, Electronic and Optical Properties of Fluoride Provskite $XCaF_3$ (X = K and Rb) using FP-LAPW method, **K Neupane** and R K Thapa, D.R.College, Golaghat, Assam (India), 20-21 September (2017).

5. 2^{nd} International Conference on Condensed Matter and Applied Physics (2017), Calculation of Energy Bands in $RbCaF_3$ using modified Becke-Johnson Potential, **K Neupane** and R K Thapa, Govt. Engineering College, Bikaner, Rajasthan (India), 24-25 November 2017.

Workshop Attended

1. Error Propagation in Nuclear Reaction Data Measurement-2017 (A Two Days National WORKSHOP), Mizoram University, Aizwal, Mizoram (India), 13-14 March 2017.

Journal of Materials Science and Engineering A 7 (11-12) (2017) 311-314
doi: 10.17265/2161-6213/2017.11-12.005

Study of Electronic Properties of Fluoride Perovskite $BaLiF_3$ Using FP-LAPW Method

K. Neupane and R. K. Thapa

Department of Physics, Condensed Matter Theory Research Group, Mizoram University, Aizawl 796004, Mizoram

Abstract: We have studied the electronic properties of cubical perovskite $BaLiF_3$, by using the first principles method within the full potential linearized augmented plane wave (FP-LAPW). Here the exchange correlation effects are included through the generalized gradient approximation (GGA) exchange potential on the basis of density functional theory (DFT). The calculated structural properties such as equilibrium lattice constant, the bulk modulus and its pressure derivative are in agreement with the published results of other authors. We have found that the band gap of $BaLiF_3$ is 6.8 eV which indicates that the insulating behavior perovskite $BaLiF_3$.

Key words: DFT, GGA, FP-LAPW, DOS (density of state), band structure.

1. Introduction

The ternary fluoro-perovskite like $BaLiF_3$ has great potential for a variety of device applications in optical, ferroelectric, antiferromagnetic systems due to their wide band gaps [1]. It is always an advantage to know the physical and electronic properties of such order to understand their possible applications. Perovskites are well known for their applications in different fields of science and technology because of their wide range of electro-optic, mechanical, semiconducting and insulating behavior. $BaLiF_3$ is used as a vacuum-ultraviolet-transparent material for lenses in optical lithography steppers in electro-optical applications [2-3]. This shows photo-luminescence properties when it is doped with lanthanide ions . It is therefore desirable for scintillators and radiation dosimeters when it is doped approximately [4].

In this paper, we will do the theoretical investigations of the structural and electronic properties of fluoride type perovskite $BaLiF_3$. In this work, for exchange correlation potentials, the GGA (generalized gradient approximation) is employed which is implemented in WIEN2k code [5].

Corresponding author: Ram Kumar Thapa, professor, research field: Condensed Matter Physics.

2. Computational Details

The unit cell of fluoro-perovskite $BaLiF_3$ with space group (P m-3 m) contains three atoms that form the cubical structure. The atoms of $BaLiF_3$ are located at the Wyckoff positions Ba (0, 0, 0), Li (0.5, 0.5, 0.5), F (0, 0.5, 0.5) [6] to form the crystal structure. For volume optimization of $BaLiF_3$, we have used at first the calculated lattice constant a = 4.04Å [7] followed by the theoretically obtained optimized lattice constant to study the DOS (density of state) and band energy of $BaLiF_3$. Non spherical contributions to the charge density and potential within the MT (muffin tin) spheres are considered andthe cut-off parameter is $R_{MT} \times K_{max} = 7$ where K_{max} is the maximum value of the reciprocal lattice vector in the plane wave expansion and R_{MT} is the smallest atomic sphere radii of all atomic spheres. In the interstitial region, the charge density and potential are expanded as a Fourier series with wave vectors up to G_{max} =12 $a{\cdot}u^{-1}$. The number of k-points used in the irreducible part of the Brillouin zone is 1,000. The criterion for the convergence of the self-consistent density functional theory (DFT) calculation is 0.0001 Ry in total energy.

However the core states are treated relativistically, the semi-core states are treated semi-relativistically by ignoring the SO (spin-orbit) coupling.

3. Results and Discussions

3.1 DOS and Band Structures

Fig. 1 shows the plot of total DOS in the case of $BaLiF_3$ and individual atoms Ba, Li and F respectively. We have found a maximum peak at -1.11 eV below the Fermi level due to the main contribution by F atom and very less contribution of Ba atom. Similarly we have observed other narrow peaks from -2.5 eV to 0 eV below the Fermi level. In the conduction region above the Fermi level, we have found a maximum peak at 13.36 eV due to the main contribution by Ba atom.

From the partial DOS plots of Ba atom as shown in Fig. 2, we have found a very small peak in the valence band due to the contributions of only *p* and *d* state electrons of Ba atom. However, in the conduction band, *d* state electron contributes mainly up to 11.25 eV and *f* state electron contributes above 11.25 eV. In the conduction band in the Fig. 2, we have observed a maximum peak at 13.36 eV due to the main contribution ofBa-*f*state electrons.

We have observed very small peaks in the range of -2.5 eV to 0 eV below Fermi level for the partial DOS plots of Li atom as shown in Fig. 3. In the valence band, the main contributions are by *s*, *p* and *d* state electrons. However, in the conduction band, we have observed a sharp narrow peak at 17.06 due to the hybridization of *s* and *d* state electrons and other small peaks are observed due to the contribution by *s*, *p* and *d* state electrons of Li atom.

Fig. 4 shows the plot of total and partial DOS of F atom. In the valence band, there is a sharp peak occurring at -1.11 eV and other small peaks are observed from -2.5 ev to 0 eV below the Fermi level due to the contribution of *p* state electrons and virtually with no contribution by *s* and *d* state electrons. However, in the conduction band small peaks occur due to the *p* and *d* state electrons.

The calculated electronic band structure for fluoro-perovskites $BaLiF_3$ along the high-symmetry directions of the Brillouin zone is shown in Fig. 5. In the valence band (Fig. 5), the lowest lying band has been found to occur at 9.0 eV below Fermi level due to the core state electrons of Ba, Li and F atoms. We also observe from Fig. 5 that the maximum band energy occurs at the Fermi level at the symmetry point R.In the conduction band, minimum in energy occurs at 6.8 eV above the Fermi level at the point symmetry Γ and from this plot in Fig. 5, we find that it is an indirect type of transition which takes place along R-Γ symmetry directions.

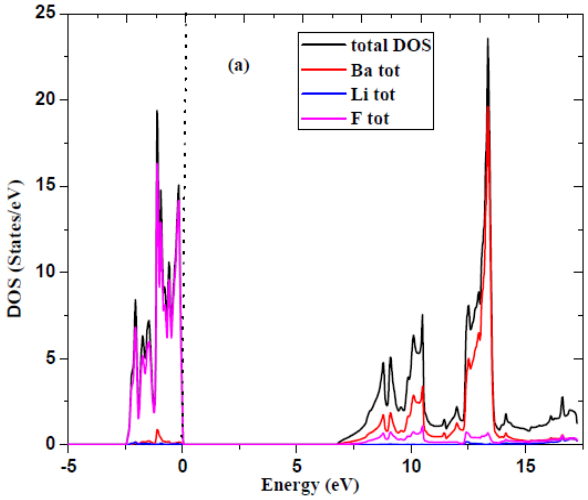

Fig. 1 Total DOS of $BaLiF_3$, Ba, Li and F.

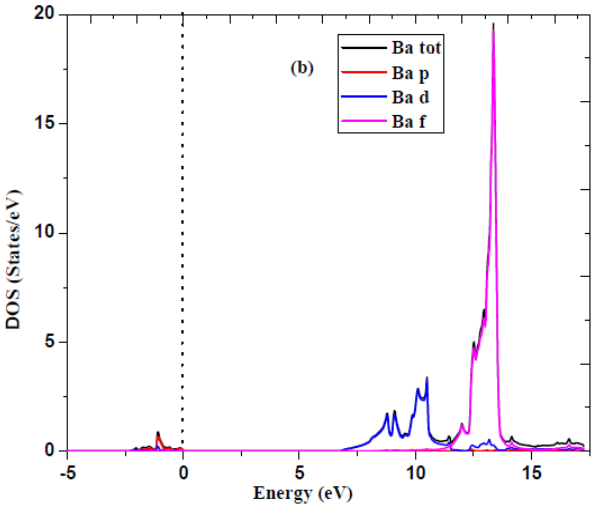

Fig. 2 Total and partial DOS of Ba.

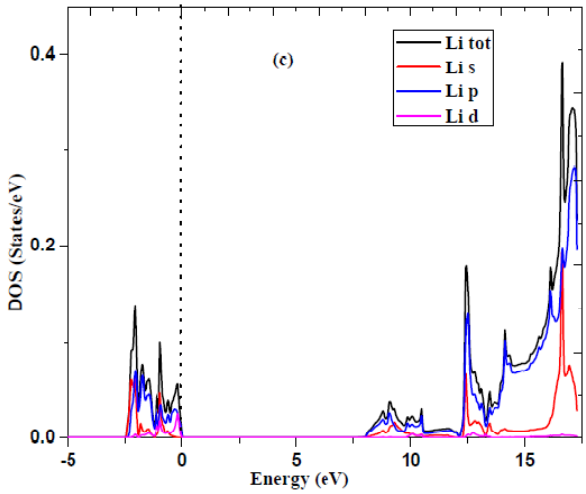

Fig. 3 Total and partial DOS of Li.

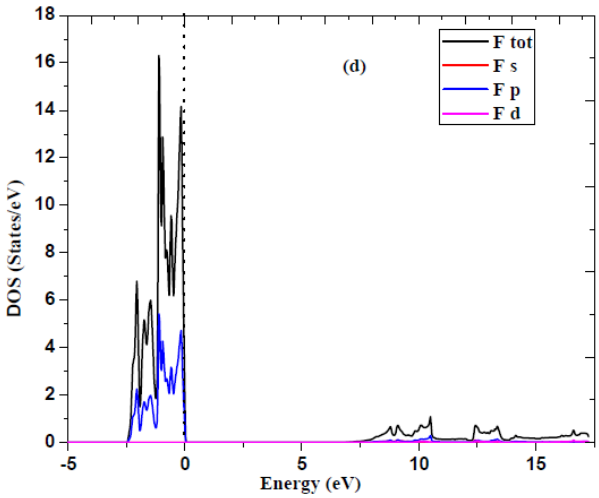

Fig. 4 Total and partial DOS of F.

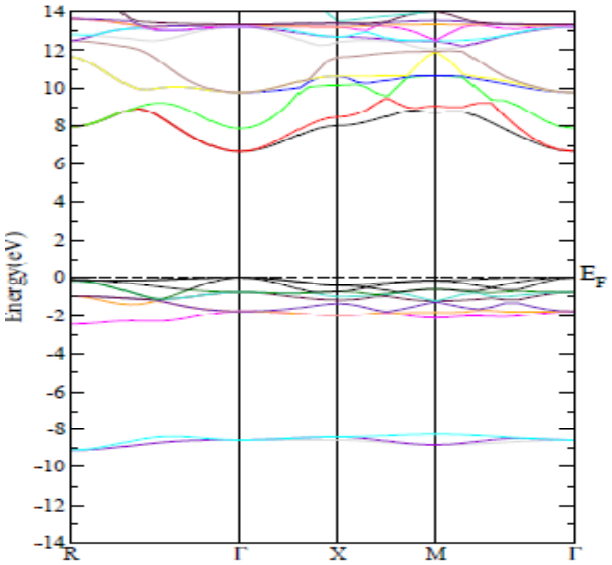

Fig. 5 Electronic band structure of $BaLiF_3$.

4. Conclusions

From the total DOS plots of $BaLiF_3$ as given in Fig. 1, we find that maxima in peaks in the valence region are due to only F atom. This is also evident from the partial DOS plots of Ba, Li and F atoms as given in Figs. 2-4 respectively. From Fig. 4, we find that the maxima in peaks are due to *p* state electrons of F atom in the valence region. We have found a maximum peak at 13.36 eV due to the main contribution of Ba atom in the conduction region that is shown in Fig. 1. From the plot of partial DOS of Ba, Li and F in Figs. 2-4 respectively, we have found that the maxima peaks are observed due to the main contribution of *p* and *f* state electrons of Ba atom. In Fig. 5, we have found from our study that the band gap of $BaLiF_3$ is 6.8 eV which is large and hence $BaLiF_3$ is an insulator.

Acknowledgments

KN thanks Mizoram University for a fellowship and RKT thanks SERB (India) for a research grant vide. No. EMR/2015/001407, Dt. 10-08-16.

References

[1] Ouenzerfi, R. E., Ono, S., Quema, A., Goto, M., Sakai, M., and Sarukura, N. 2004. "Design of Wide-Gap Fluoride Hetrostructure for Deep Ultraviolet Optical Devices" *J. Appl. Phys.* 96: 7655-59.

[2] Horsch, G., and Paus, H. J. 1986. "A New Color Center Laser on the Basis of Lead-Doped $KMgF_3$." *Opt. Commun* 60: 69-73.

[3] Fukuda, T., Shimamura, K., Yoshikawa, A., and Villora, E. G. 2001. "Crystal Growth of New Functional Materials for Electro-Optical Applications". *Opto. Electron Rev.* 9 (2): 109-16.

[4] Furetta, C., Santopietro, F., Sanipoli, C., and Kitis, G. 2001. "Effect of Pre-irradiation Heat Treatment and Rate on the Thermoluminscence Glow Peaks of Natural CaF_2". *Appl. RadiatIsot* 55: 533-42.

[5] Blaha, P., Schwarz, K., Madsen, G. K. H., Kvasnicka, D., Luitz J., and Schwarz, K. 2012." An Augmented Plane Waveplus Local Orbitals Program for Calculating Crystal Properties." In *Wien2K User's Guide*. Techn. Universitat Wien, Wien.

[6] Gregory, S. R. 2004. *Structure and Bonding in*

Crystalline Materials. United Kingdom: Cambridge University Press.

[7] Mubark, A. A., and Mousa, A. A. 2012. "The Electronic and Optical Properties of the Fluroperovskite $BaXF_3$ (X= Li, Na, K, and Rb) Compounds". *Computational Materials Science* 59: 6-13.

Study of structural and electronic properties of fluoride perovskite KMgF3 using FP-LAPW method

2016 J. Phys.: Conf. Ser. 765 012016

(http://iopscience.iop.org/1742-6596/765/1/012016)

Study of structural and electronic properties of fluoride perovskite $KMgF_3$ using FP-LAPW method

K Neupane [1*] and R K Thapa[1]

[1]Department of Physics, Condensed Matter Theory Research Group, Mizoram University, Aizawl 796 004-Mizoram

Corresponding Author:kneupane22@gmail.com

Abstract. In this paper, we present the electronic properties of fluoride perovskite $KMgF_3$ by using the full potential linearized augmented plane wave (FP-LAPW) method. The densities of states and energy band structures have been calculated by using the generalized gradient approximation (GGA) as exchange-correlation potential. The results obtained are in agreement with the previous experimental and theoretical results. The obtained value of energy band gap of 7.2 eV indicates the insulating behaviour of the sample material.

1. Introduction

The ternary fluoro-perovskite like $KMgF_3$ has great potential for a variety of device applications in optical, ferroelectric, antiferromagnetic systems due to their wide band gaps [1-2]. It is always an advantage to know the physical and electronic properties of such order to understand their possible applications. Perovskites are well known for their applications in different fields of science and technology because of their wide range of electro- optic, mechanical, semiconducting and insulating properties. $KMgF_3$ is a technologically important fluoro-perovskite which finds applications as a vacuum- ultraviolet-transparent material for lenses in optical lithography steppers in electro- optical applications [3-5]. It is desirable for scintillators and radiation dosimeters when it is doped approximately [6]. Neupane *et al.* [7] have reported an energy band gap of 6.8 eV for $RbCaF_3$ from the FP-LAPW method based calculation, which also suggests an insulating behaviour of this material.

In this paper, we will do the theoretical investigations of perovskite-type fluoride $KMgF_3$. For this purpose for exchange correlation, generalized gradient approximation (GGA) is employed which is implemented in wien2k code [8].

2. CRYSTAL STRUCTURE AND COMPUTATIONAL DETAILS

The unit cell of fluoro-perovskite $KMgF_3$ with space group (Pm-3m) contains three independent atoms that form the cubical structure. The atoms of $KMgF_3$ are located at the Wyckoff positions K(0.0,0.0,0.0), Mg(0.5,0.5,0.5), F1(0.0,0.5,0.5), F2(0.5,0.0,0.5) and F3(0.5,0.5,0.0) [10] to form the crystal structure as shown in figure1.

The generalized gradient approximation (GGA) as proposed by Perdew *et al*. [9] has been used to correct the exchange-correlation effect. For volume optimization of $KMgF_3$, we have used the experimental lattice constant a=3.979 Å [10] and the optimized volume versus energy curve is shown in Fig.1. This optimized lattice constant is used to study the density of state (DOS) and band energy of $KMgF_3$ by using the full potential linearized augmented plane wave (FP-LAPW) method of KS-DFT [11].We used here GGA to describe the electron exchange and correlation potential. Non spherical contributions to the charge density and potential within the muffin tin (MT) spheres are considered and the cut-off parameter is $R_{MT} \times K_{max} = 7$ where K_{max} is the maximum value of the reciprocal lattice vector in the plane wave expansion and RMT is the smallest atomic sphere radii of all atomic spheres. In the interstitial region, the charge density and potential are expanded as a Fourier series with wave vectors up to G_{max}=12 $a.u^{-1}$. The number of k-points used in the irreducible part of the Brillouin zone is 1000. The criterion for the convergence of the self-consistent DFT calculation is 0.0001 Ry in total energy. However the core states are treated relativistically, the semi-core states are treated semi-relativistically by ignoring the spin-orbit (SO) coupling.

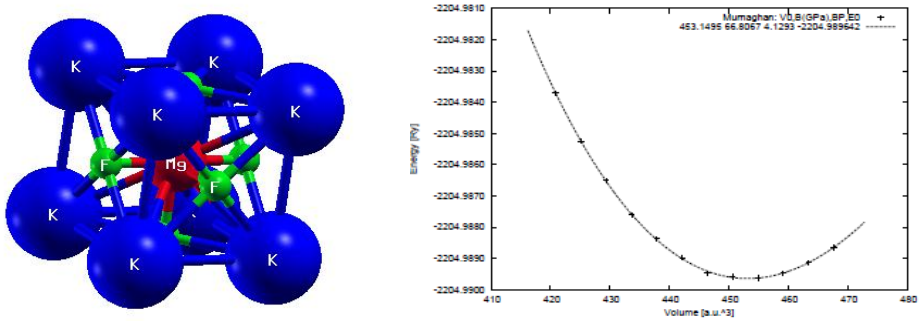

Figure 1. (Left) Crystal structure of $KMgF_3$, (right) volume optimization curve.

3. RESULT AND DISCUSSIONS

3.1. *Crystal structure*

The variation in the total energy as a function of volume is shown in figure1.The calculated value of the equilibrium lattice constant (a) is found as 4.0646 Å. The energy versus volume data was fitted to a Murnaghan equation of state [12] to obtain the bulk modulus (B) and its first pressure derivative (B'). Our calculated values of lattice constant, B, and B' are compared with previous experimental and theoretical results which are shown in table 1. We note that the result of the lattice constant obtained is slightly higher than the experimental values [10, 15].

Table 1.

	Lattice Constant a (in Å)	Bulk Modulus B (in GPa)	Pressure Derivative B'
This study	4.0646	66.8067	4.1293
Other, GGA	4.081 [13]	72.01 [13]	4.65[13]
	4.040 [14]	72.15 [14]	4.68 [14]
Experimental	3.989 [15]	70.40 [15]	
	3.979 [10]		

3.2 *Density of states (DOS)*

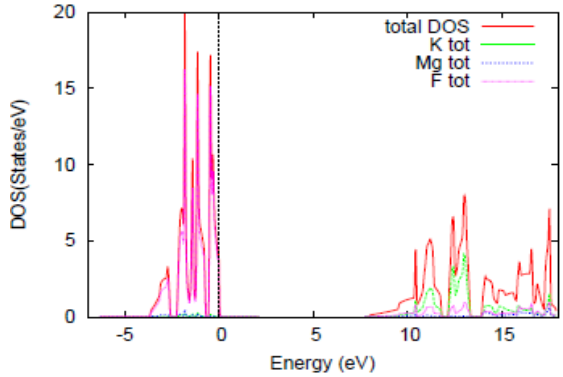

Figure 2. Plot of total DOS for $KMgF_3$, K, Mg and F (Fermi energy is at zero)

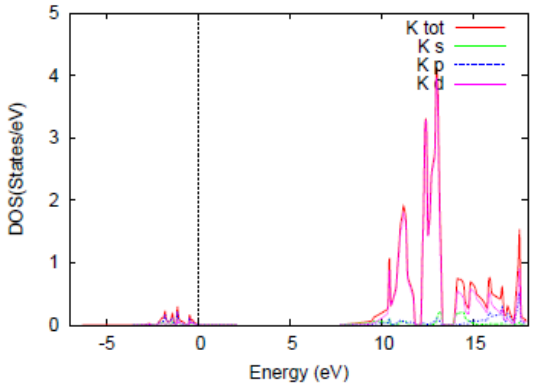

Figure 3. Plot of total and partial DOS for K Fermi energy is at zero)

Figure 2 shows the plot of total density of states (DOS) of $KMgF_3$ and individual atoms K, Mg and F respectively. The maximum peak and other two narrow peaks are occurred at 1.82 eV, 1.14 eV and 0.45 eV respectively in valence region below the Fermi level. In the case of total DOS, contribution of the individual atoms in the valence region, we find only the contribution due to F atom which is accountable in the valence region. The total contribution by K and Mg atoms are more or less negligible in the valence region which is evident from the small hump in DOS. In the conduction region above the Fermi level in figure 2, we find the value of DOS is maximum at 13.07 eV due to the main contribution of K atom and small peaks in DOS occur from 10.45 eV to17.50 eV due to the contribution of K, Mg and F atoms.

From the total and partial DOS plots of K atom as shown in figure 3, we find no sharp peaks in valence band but only *p* and *d* state electrons are contributing to the DOS in negligible height. However, in the conduction band, the highest peak in DOS is contributed by *d* state electron of K atom at 13.0 eV and other smaller peaks are observed from 10.33 eV to 17.55 eV due to the main contribution of *d* state electrons of K atom.

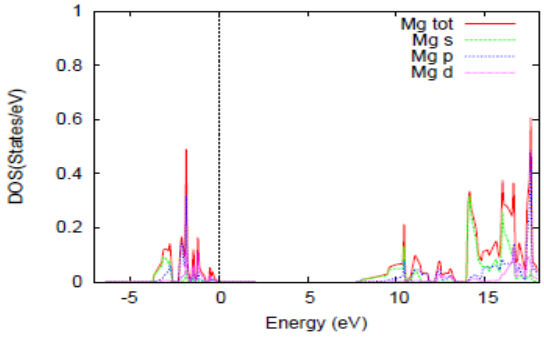

Figure 4. Plot of total and partial DOS for Mg (Fermi energy is at zero)

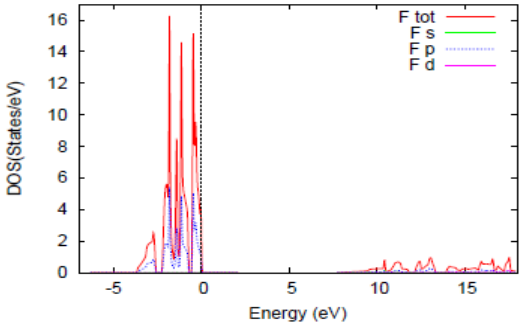

Figure 5. Plot of total and partial DOS for Mg (Fermi energy is at zero)

From the total and partial DOS of plots of Mg atom as shown in figure 4, we find a narrow peak at 1.85 eV in the valence band due to the *p* and *d* state electrons and small peaks are observed from 0.43 eV to 2.93 eV due to the contribution of *s*, *p* and *d* state electrons below the Fermi level. However, in the conduction band, *p* state electron of Mg atom contributes to the occurrence of peak at 17.55 eV and small peaks are observed from 10.33eV to 17.55eV due to the contribution of *s*, *p* and *d* state electrons of Mg atom.

Figure 5 shows the total and partial DOS of plots of F. In the valence band, there is a sharp peak occurring at 1.82 eV and other two small peaks are observed at 1.14 eV and 0.45 eV respectively below the Fermi level due to the *p* state electrons and virtually with no contribution by *s* and *d* state electrons. However, in the conduction band, there are very small peaks occur due to the *s*, *p* and *d* state electrons of F atom.

3.2. Band structures

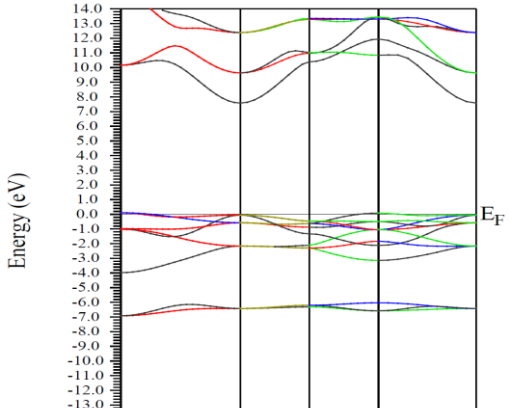

Figure 6. Electronic band structure of $KMgF_3$ along the high-symmetry directions of the first Brillouin zone.

The calculated electronic band structure for fluoro-perovskite $KMgF_3$ along the high-symmetry directions of the Brillouin zone is shown in figure 6. In the valence band (figure 6), the lowest lying band has been found to occur at 9.5 eV below Fermi level due to the core state electrons of K, Mg and F atoms. We also observe from figure 6 that the maximum band energy occurs at the Fermi level at the symmetry point R. In the conduction band, minimum in energy occurs at 7.2 eV above the Fermi level at the point symmetry and from this plot in figure 6, we find that it is an indirect type of transition which takes place along R - symmetry directions. The calculated value of indirect band gap is 7.2 eV, which is much smaller than the experimental value 12.4 eV [16] for $KMgF_3$.

4. CONCLUSIONS

From the volume optimization in figure1, we have found the optimized lattice constant, pressure, pressure derivative and total energy are as 4.0646 Å, 66.8067 GPa, 4.1293 and -2204. 9896 Ry respectively. From the total DOS plots of $KMgF_3$ as given in figure 2, we find that maxima in peaks in the valence region are due to only F atom. This is also evident from the partial DOS plots of K, Mg and F atoms as given in figure 3, figure 4 and figure 5 respectively. We find the maxima in peak is due to *p*-state electrons of Mg and F atoms in the valence region of partial DOS of Mg and F atoms. The peak heights in partial DOS due to electrons from K atom in the valence region is negligible. Similarly in the conduction region, it is only *d*-state electrons of K (figure 3) which is a main contribution to the maxima in the total DOS of $KMgF_3$.We have found from our study (figure 6) that the band gap of $KMgF_3$ is 7.2 eV which is large and hence $KMgF_3$ is an insulator.

References

[1] Ouenzerfi R E, Ono S, Quema A, Goto M, sakai M 2004 *J. Appl. Phys.***96** 7655
[2] Zhang F, Mao Y, part T J, Wong S S 2008 *Adv. Funct. Mater.* **18** 103
[3] Nishimatsu T N, Terakubo N, Mizuseki H, Kawazoe Y, Pawlak D A,Shimamura K, Ichinose N, Fukuda T 2003 *Jpn. J. Appl. Phys.* **42** 5082
[4] Ho¨rsch G, Paus H J 1986 *Opt. Commun.***60** 69
[5] Fukuda T, Shimamura K, Yoshikawa A, Villora E G 2001 *Opt. Elect. Rev.* **9** 109
[6] Furetta C, Santopietro F, Sanipoli C, Kitis G 2001 *Appl Radiat Isot* **55** 533
[7] Neupane K Thapa R K 2016 *IJEART* 2454-9290 **2** 31-33
[8] Blaha P, Schwarz K, Madsen G K H, Kvasnicka D, Luitz J, Schwarz K 2012 *An Augmented Plane Wave plus Local Orbitals Program for Calculating Crystal Properties* Wien2K User's Guide Techn. Universitat Wien,Wien
[9] Perdew J P, Burke F S I, Borodi G 1996 *J. Cryst. Growth.* **169** 89
[10] Darabont A, Neamtu C, Ouenzerfi R E, Ono S, Quema A, Goto M, sakai M 2004 *J. Appl. Phys.* **96** 7655.

[11] Kohn W, Sham L J 1965 *Physical Review* **A140** 1133
[12] Murnaghan F D 1944 *Proc Natl Acad Sci* **30** 244
[13] Vaitheeswaran G, Kanchana V, Kumar R S, Cornelius A L, Nicol M F, Svane A, Delin A, Johansson B 2007 *Phys. Rev.* **B 76** 014107
[14] Pilania G, Sharma V 2013 *J. Mater. Sci.* **48** 7635-7641
[15] Rosenberg H M, Wigmore J K 1967 *Phys. Lett.* **A 24** 317
[16] Heaton R A, Lin C C 1982 *Phys. Rev.* **B 25** 3538

A Theoretical Study of Structural, Electronic and Optical Properties of ABF_3 (A, B = Alkali or Alkaline Earth and Transition Elements) Type Perovskite by Using FP-LAPW Method

(Synopsis of the proposed research for the Ph.D. degree under Mizoram University)

Name of the Scholar : **Mr. Khimananda Neupane**

Name of the Supervisor : **Prof. R. K. Thapa**

Date of Admission : **August 12 2015**

Date of Completion of Ph.D. Course Work with Grade : **February 17, 2016, 'A' Grade**

Date of Approval by BOS : **07- 04- 2016**

Date of Approval by School Board : **21- 04- 2016**

Department of Physics

School of Physical Sciences

Mizoram University

Tanhril, Aizawl

APRIL 2016

A Theoretical Study of Structural, Electronic and Optical Properties of ABF_3 (A, B = Alkali or Alkaline Earth and Transition Elements) Type Perovskite by Using FP-LAPW Method

INTRODUCTION

Since its discovery in BaTiO3, ferroelectricity in perovskite-structure oxides has attracted tremendous interest, ranging from fundamental studies to technological applications. Indeed, the transition-metal/oxygen bond, with its large polarizability, is particularly favourable for promoting the transition-metal offcentering that can result in a ferroelectric ground state. Ferroelectrics also exist, of course, in many material chemistries that do not contain oxygen, with a particularly extensive range of fluorine-based examples, including both polymers (Lovinger, 1983) and ceramics in many crystal classes (Scott et al., 2011). Perhaps not surprisingly given the low polarizability of bonds with fluorine, the mechanisms for ferroelectricity in fluorine-based ferroelectrics are distinct from those in oxides, ranging from molecular in ceramics (Ederer et al., 2006). These alternative mechanisms are of particular interest because, again unlike the oxides, they are not contra-indicated by transition metal d electrons, and so allow simultaneous ferroelectricity and magnetic ordering (multiferroism). Interestingly, however, none of the known perovskite-structure fluorides is reported to be ferroelectric.

Since late 2012, organic and inorganic halides with the perovskite structure have strongly attracted the attention of the photovoltaic community when efficiencies close to 10% were first achieved in solid state cells (Lee et al., 2012). The excellent properties and the innovative device possibilities in perovskite-structured organometal and metallic halides has resulted in a frenzied increase of publications reporting high efficiencies (Ball et al., 2013). Recently, 15% efficient solar cells were reported with $CH_3\ NH_3PbI_3$ target efficiencies of 20% identified as a feasible goal (Park, 2013). It is therefore pertinent to evaluate the potential and analyze the prospects of this exciting technology that have galvanized the photovoltaic research community.. Organic/inorganic metal halides as light absorbers although these class of materials have been

widely studied for decades (Moller, 1957, 1958), only recently have they been introduced in solar cells.

Halide perovskites have recently emerged as promising materials for low-cost, high-efficiency solar cells. The efficiency of perovskite-based solar cells has increased rapidly from 3.8% in 2009 to 19.3% in 2014, by using the all-solid-state thin-film architecture and engineering cell structures with mixed-halide perovskites. The emergence of perovskite solar cells revolutionized the field not only because of their rapidly increased efficiency, but also flexibility in material growth and architecture. The superior performance of the perovskite solar cells suggested that perovskite materials possess intrinsically unique properties.

In this proposal, we will use the first-principles density functional calculations to investigate the tendency towards ferroelectricity in perovskite-structure fluorides like ABF_3. This will be possible only when we study in detail the structural, physical, electronic energy bands, magnetic and optical properties of this type of perovskite materials. Our goals are two-fold: First, by comparing to the behavior of ferroelectric perovskite-structure oxides, we further understanding of the driving forces for, and competition between, polar and non-polar structural distortions in both systems. Second, we aim to identify conditions, for example of strain or chemistry, under which ferroelectricity, and perhaps multiferroism, could be stabilized in the fluoride perovskites. We will calculate the band gaps and also see if this value for these systems is within the range of absorption of solar energy so that this can be made viable in solar cells applications. Computation will be done by using the WIEN2k code (Blaha et al. 2012).

SCOPE OF STUDY

Semiconductors with a band gap of 1.1 eV are considered most suitable for harvesting the solar spectrum from visible to near infrared (NIR). Strength of the potential developed is dependent on this band gap, with low potential leading to drawing of extra current at the expense of reduced voltage. The balancing of these two parameters dictates the optimal band gap in the range of 1.4eV for cells made of single material. Perovskite structure incorporating mixed halide has continuously tuneable band gap allowing for light harvesting over the complete solar spectrum. This investigation on the proposed type of perovskite will see that there is tuneable

type of band gaps in and around Fermi level so as to make it easily viable to required bandwith of solar spectrum.

The proposed study will also study the Born effective charges of ABF_3 cubic perovskites, and compare them with the values of $BaTiO_3$ to understand the differences that might arise between oxide and fluoride perovskites. The phonon dispersion study will be also done to see if the instability in polarisability is similar to the behavior of typical perovskite oxide ferroelectrics.

REVIEW OF LITERATURE

The electronic structure, energy band structure and density of states of $BaTiO_3$ have studied by using the full potential linearized augmented plane wave (FP-LAPW) method on the density functional theory (DFT) (Salhei *et al*., 2004). They found these are in good agreement with both the theoretical and experimental results. The structural, electronic and optical properties of $KMgF_3$ have studied by using the FP-LAPW method and local density approximation (LDA). They have studied the contribution of different bands from the total and partial density of states curves.

Meziani *et al.* (2012) have studied the structural, elastic and electronic properties of fluoro-perovskite $CsCaF_3$ by using the FP-LAPW to the DFT. They have found the elastic properties such as elastic constants, anisotropy factor, Shear modulus, Young's modulus, Poisson's ratio and Debye temperature in the first time. They have obtained electronic band structure and the density of states but $CsCaF_3$ is found as a direct band gap material with the LDA and an indirect band gap material with the GGA.

The electronic, magnetic and optical properties of neodymium chalcogenides have studied by performing Local spin density approximation with Coulomb interaction (LSDA + U) and FP-LAPW method (Shankar *et al*., 2012). The electronic structure calculation shows that the electronic states in Nd-chalcogenides were mainly contributed by Nd-4f electrons near the fermi energy and 3p, 4p, and 5p state electrons of X (S, Se and Te), respectively. They have also studied the absorption of light via imaginary parts of the dielectric function of Nd-chalcogenides.

The existence and origin of the ferroelectric instability in the ABF_3 fluoro-perovskites have studied and found that many fluoro-perovskites have a ferroelectric instability in their high symmetric cubic structure same as in oxide perovskites (Garcia-Castro *et al*., 2013). They found no sensitive to pressure and strain in ABF_3 which are constrast to the oxide perovskites.

The structural, elastic, electronic and optical properties of cubic perovskite $CsCaCl_3$ have studied by using the FP-LAPW method in the density functional theory. The exchange-correlation potential has evaluated using the LDA and Generalized Gradient Approximation (GGA). The calculated structural properties such as equilibrium lattice constant, the bulk modulus and pressure derivative are found in good agreement with the available data. The elastic properties such as elastic constants, anisotropic factor, Shear modulus, Young's modulus and Poisson's ratio are calculated. Again, they have calculated electric band structure, density of states and charge density which shows that this compound has an indirect energy band gap with a mixed ionic and covalent bonding. Optical spectra such as the real and imaginary parts of dielectric function, optical reflectivity, refractive index and electron energy loss are performed for the energy range of 0-30 eV.

Babu *et al.* (2015) have studied the structural, electronic and elastic properties of cubic perovskite type compound $KCaF_3$ and $RbCaF_3$ by using the FP-LAPW method. They have observed the exchange- correlation effects through the LDA and GGA exchange potentials. The calculated structural properties such as equilibrium lattice constant, the bulk modulus and it's pressure derivative are in good agreement with the available data. They have found the wide and indirect band gaps of these compounds, which are agree with experimental values. These compounds are found as elastically anisotropic and ductile from the observations of elastic properties.

Syrotyuk *et al.* (2015) have studied the electronic band spectra of cubic $RbMF_3$ perovskites (M= Be, Mg, Ca, Sr, Ba) by using the projector augmented wave (PAW) and obtained good result with the published result of other authors in the LDA. The electronic, elastic and optical properties of the cubic perovskite $KCdF_3$ have studied by solving the Kohn-Sham equations by using the FP-LAPW method (Babu *et al.*, 2015). They observed the exchange correlation effects through LDA and GGA. The calculation of the electronic band structure, density of states and charge density show that this compound has an indirect energy band gap with a mixed ionic and covalent bonding. All the optical properties are responsible for energy

range of 0-40 eV. They have calculated the elastic properties of this compound and it can be used for high-frequency optical and optoelectronic devices.

OBJECTIVES

The objectives of the proposed research investigation:

- To study electronic, magnetic and optical properties of ABF_3 type poerovskites to see the tendency towards ferroelectricity in perovskite-structure fluorides.
- To study the effect of the exchange and correlations potentials on the origin of energy band gaps and ferroelectric behavior.
- By comparing the behavior of ferroelectric perovskite-structure oxides, we further understanding of the driving forces for, and competition between, polar and non-polar structural distortions in both systems.
- We will also try to identify conditions, for example, of strain or chemistry, under which ferroelectricity, and perhaps multiferroism, could be stabilized in the fluoride perovskites.

THEORY

A solid is a collection of a heavy positively charged nuclei and lighter negatively charged electrons. If we have N nuclei, we are dealing with N+ZN electromagnetically interacting quantum particles. This is a quantum many body problem and the exact many particle hamiltonian for such a system is,

$$\hat{H} = -\frac{\hbar^2}{2}\sum_i \frac{\nabla^2_{\boldsymbol{R}_i}}{M_i} - \frac{\hbar^2}{2}\sum_i \frac{\nabla^2_{\boldsymbol{r}_i}}{m_e} - \frac{1}{4\pi\varepsilon_\circ}\sum_{i,j}\frac{e^2 Z_i}{\left|\boldsymbol{R}_i - \boldsymbol{R}_j\right|} + \frac{1}{8\pi\varepsilon_\circ}\sum_{i\neq j}\frac{e^2}{\left|\boldsymbol{r}_i - \boldsymbol{r}_j\right|} + \frac{1}{8\pi\varepsilon_\circ}\sum_{i\neq j}\frac{e^2 Z_i Z_j}{\left|\boldsymbol{R}_i - \boldsymbol{R}_j\right|} \quad (1)$$

Where M_i is the mass of the nucleus at $\boldsymbol{R}_i$, m_e is the mass of the electron at $\boldsymbol{r}_i$. The first term is the kinetic energy operator for the nuclei, the second term represents kinetic energy operator for the electrons. The last three terms describe the coulomb interaction between electrons and

nuclei, between electrons and other electrons and between nuclei and other nuclei. It is impossible to solve Eq. (1) exactly, as such in order to obtain acceptable appropriate eigen states, approximations are made. Using the Born-Oppenheimer approximation, Eq. (1) gives the total kinetic energy of the electron gas, the potential energy due to electron-electron interactions and the potential energy of the electrons in the (now external) potential of the nuclei, hence the Hamiltonian can be written now as,

$$\hat{H} = \hat{T} + \hat{V} + \hat{V}_{ext} \tag{2}$$

One of the well- known methods used to reduce Eq. (2) to an approximate but tractable form is the density functional theory. It is based on the two theorems of Hohenberg and Kohn. With the help of these two equations, the exact ground-state density $\rho(\boldsymbol{r})$ of an N-electron system is

$$\rho(\boldsymbol{r}) = \sum_{i=1}^{N} \phi_i(\boldsymbol{r})^* \phi_i(\boldsymbol{r}) \tag{3}$$

where the single-particle basis functions $\boldsymbol{\phi_i(r)}$ are the N lowest-energy solutions of the Kohn-Sham equation

$$\hat{H}_{KS}\phi_i = \varepsilon_i \phi_i \tag{4}$$

where, the Kohn-Sham Hamiltonian is

$$\hat{H}_{KS} = \hat{T}_o + \hat{V}_H + \hat{V}_{xc} + \hat{V}_{ext}$$

$$= -\frac{\hbar^2}{2m_e}\nabla_i^2 + \frac{e^2}{4\pi\varepsilon_o}\int \frac{\rho(\boldsymbol{r}')}{|\boldsymbol{r}-\boldsymbol{r}'|} d\boldsymbol{r}' + V_{xc}\{\rho(\boldsymbol{r})\} + V_{ext}(\boldsymbol{r}) \tag{5}$$

where, V_{xc} is the exchange correlation potential and V_{ext} is the external potential from the nucleus. It must be noted that the single-particle wave function $\boldsymbol{\phi_i(r)}$ are not the wave functions of electrons but they describe mathematical quasi-particles without a direct physical meaning. Only the overall density of these quasi-particles is guaranteed to be equal to the true electron density. Also the single-particle energies ε_i are not single electron energies.

Both the Hartree operator V_H and the exchange-correlation operator V_{xc} depend on the density $\rho(\boldsymbol{r})$, which in turn depends on the basis functions $\phi_i(\boldsymbol{r})$ which are being searched. This means we are dealing with a self-consistency problem.

Full Potential-Linearized Augmented Plane Wave method

The linearized augmented plane wave (FP-LAPW) method is one of the most accurate methods for solving the Kohn-Sham equation. It is based on the density functional theory for the treatment of exchange and correlation and uses the local spin density approximation (LSDA). Like most energy-band methods, the FP-PW method is a procedure for solving the Kohn-Sham equations for the ground state density, total energy and (Kohn-Sham) eigenvalues (energy bands) of a many electron system (crystal) by introducing a basis set which is especially adapted to the problem. This adaptation is achieved by dividing the unit cell into (**I**) non-overlapping atomic spheres (centered at the atomic sites) and (**II**) an interstitial region (Fig. 1). In the two types of regions different types of basis sets are used:

(a) Inside the atomic sphere **I** of radius R_t, a linear combination of radial functions times spherical harmonics $Y_{lm}(r)$ is used as given below

$$\phi_{\boldsymbol{k}_n} = \sum_{lm} \left[A_{lm,\boldsymbol{k}_n} u_l(\boldsymbol{r}, E_l) + B_{lm,\boldsymbol{k}_n} \dot{u}_l(\boldsymbol{r}, E_l) \right] Y_{lm}(\boldsymbol{r}) \qquad (6)$$

where $u_l(\boldsymbol{r}, E_l)$ is the (at the origin) regular solution of the radial Schroedinger equation for energy E_l (chosen normally at the center of the corresponding band with *l*-like character) and spherical part of the potential inside the sphere **I**; $\dot{u}_l(r, E_l)$ is the energy derivative of u_l evaluated at the same energy E_l. A linear combination

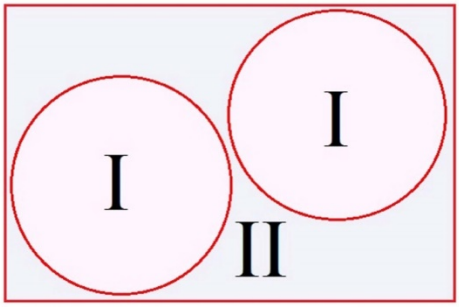

Fig. 1

of these two functions constitutes the linearization of the radial function. The coefficients A_{lm} and B_{lm} are functions of $\boldsymbol{k}_n$ determined by requiring that this basis function matches each plane wave (PW), the corresponding basis function of the interstitial region. u_l and $\dot{u}_l$ are obtained by numerical integration of the radial Schroedinger equation on a radial mesh inside the sphere.

(b) In the interstitial region **II**, a plane wave expansion is used

$$\phi_{k_n} = \frac{1}{\sqrt{\omega}} e^{i\,\boldsymbol{k}_n \cdot \boldsymbol{r}} \tag{7}$$

where $\boldsymbol{k}_n = \boldsymbol{k} + \boldsymbol{K}_n$; $\boldsymbol{K}_n$ are the reciprocal lattice vectors and $\boldsymbol{k}$ is the wave vector inside the first Brillouin zone. Each plane wave is augmented by an atomic-like function in every atomic sphere.

Basis functions given by Eq. (6) & (7) are used to derive the energy as a functional of density with appropriate approximations to calculate potentials. The approximations that will be used are GGA, LDA, LSDA, GGA+U, LDA+U etc.

Optical Properties

For the calculation of the optical properties, a dense mesh of uniformly distributed k-points is required. Hence, the Brillouin zone integration was performed using the tetrahedron method with many more k-points in the irreducible part of the Brillouin zone without broadening. The dielectric function

$$\varepsilon(\omega) = \varepsilon_1(\omega) + i\varepsilon_2(\omega) \tag{8}$$

is known to describe the optical response of the medium at all photon energies E = $\hbar\omega$. In this study, the imaginary part of the dielectric function is given as (Draxl et al. 1998).

$$\varepsilon_2(\omega) = (\frac{4\pi^2 e^2}{m^2\omega^2}) \sum_{i,j} \int \langle i | M | j \rangle^2 \; f_i(1 - f_j) \times \delta(E_f - E_i - \omega) d^3k \qquad (9)$$

where M is the dipole matrix, i and j are the initial and final states respectively, f_i is the the Fermi distribution function for the ith state, and E_i is the energy of electron in the ith state. The real part (ε_1 (ω)) of the dielectric function can be extracted from the imaginary part using the Kramers-Kronig relation in the form (Cardona et al., 1999).

$$\varepsilon_1(\omega) = 1 + \frac{2}{\pi} P \int_0^\infty \frac{\omega' \varepsilon_2(\omega') d\omega'}{(\omega'^2 - \omega^2)} \qquad (10)$$

where P implies the principal value of the integral. The optical reflectivity spectra are derived from the Fresnel's formula for normal incidence assuming an orientation of the crystal surface parallel to the optical axis using the relation

$$R(\omega) = \left| \frac{\sqrt{\varepsilon(\omega)} - 1}{\sqrt{\varepsilon(\omega)} + 1} \right|^2 \qquad (11)$$

while the electronic energy-loss function $-I_m(\frac{1}{\varepsilon})$ is given by (Cardona et al.,1999, Fox 2001,Dressel et al., 2002).

$$-\mathrm{I}_m(\frac{1}{\varepsilon}) = \frac{\varepsilon_2(\omega)}{\varepsilon_1^2(\omega) + \varepsilon_2^2(\omega)} \qquad (12)$$

We calculate the absorption coefficient I(ω) and the real part of optical conductivity Re [$\sigma(\omega)$] using the following expressions

$$I_{\omega} = 2\omega\left\{\frac{\sqrt{\varepsilon_1^2(\omega)+\varepsilon_2^2(\omega)}-\varepsilon_1(\omega)}{2}\right\}^{1/2} \quad (13)$$

$$\mathrm{Re}\left[\sigma(\omega)\right] = \frac{\omega\varepsilon_2}{4\pi} \quad (14)$$

We calculate the absorption coefficient I(ω) and the real part of optical conductivity Re[σ(ω)] using the following

$$n(\omega) = \left\{\frac{\varepsilon_1(\omega)}{2} + \frac{\sqrt{\varepsilon_1^2(\omega)+\varepsilon_2^2(\omega)}}{2}\right\}^{1/2} \quad (15)$$

$$k(\omega) = \left\{\frac{\sqrt{\varepsilon_1^2(\omega)+\varepsilon_2^2(\omega)}}{2} - \frac{\varepsilon_1(\omega)}{2}\right\}^{1/2} \quad (16)$$

TENTATIVE ORGANISATION OF THE THESIS

The tentative arrangement of the thesis in the form of chapters will be as follows:

Chapter 1: This chapter will contain the introduction of the present studies.

Chapter 2: In this chapter, the theory and the methodology involved in the calculations will be discussed in detail.

Chapter 3: In this chapter, the thorough discussions of the results obtained in respect of various types of perovskite will be presented. This will be concerned with the results of the physical properties, density of states and energy bands.

Chapter 4: This chapter will consist of discussions on the magnetic and the optical properties of systems studied.

Chapter 5: It will include the conclusion that could be drawn out of the proposed research work. This will be followed by References and Appendices.

REFERENCES

Adroja, D. T., Mcewen, K. A., Park,J. G., Hillier, A.D., Takeda, N., Riseborough, P.S. and Takabatake, T., (2008). Inelastic neutron scattering study of spin gap formation in heavy fermion compounds, *Jour. Optoelectronics and Adv. Mat*. **10:** 1719-1737.

Akinlami J.O., Ashamu A.O., (2013). Optical properties of GaAs. *Jour. of Semiconductors* **34:** 032002-5.

Ashcroft N. W. and Mermin ,N.D., (1976). *Solid State Physics*, Saunders College, U.S.A.

Babu, K. E., Murali, N., Babu, K. V., Babu, B. K. and Veeraiah, V., (2015). Elastic and optoelectronic properties of $KCdF_3$: *Chin. Phys. Lett*., **32**, 016201-5.

Ball J. M., Lee M. M., Hey A. and Snaith H. J., (2013). Low- temperature processed meso-superstructured to thin-film perovskite solar cells, *Energy Environ.Sci.*, **6**, 1739-1743.

Blaha, P., Schwarz K., Madsen G. K. H., Kvasnicka D., Luitz J., Schwarz K. (2012), *An Augmented Plane Wave plus Local Orbitals Program for Calculating Crystal Properties,*Wien2K User's Guide, Techn. Universitat Wien, Wien.

Callaway, J., (1974). *Energy Bands in Solids,* Academic Press: New York.

Cardona M. and Yu Y. P., (1999). *Fundamental of semiconductors: Physics and materials properties,* Springer-Verlag, Berlin.

Danebrock, M. E., Evers, C. B. H. and Jeitschko W., (1996). *Jour. Phys. Chem. Solids*, **57**: 381-387.

Dressel M. and Gurner G., (2002). *Electrodynamics of solids: Optical properties of electrons in matter*, Cambridge University Press, Uk.

Ederer C. and Spaldin N. A. (2006). *Phys. Rev***. B 74**, 020401-3.

Fox M., (2001*). Optical Properties of Solids*, Oxford University Press, New York.

Galasso, Francis, S., (2013). Structure, Properties and Preparation of Perovskite Type Compounds, *International Series of Monographs in Solid State Physics,* Academic Press.

Garcia-Castro, A. C., Spaldin, N. A., Romero, A. H. and Bousquet, E., (2013). Geometric Ferroelectricity in Fluoro-Perovskites*, cond-mat. mtrl-sci, 1-6.*

Jasprit Singh., (2003). Electronic and Optoelectronic properties of Semiconductor structures*;* Univ. of Michigan, Ann Arbor, Cambridge Univ. Press.

Kohn W and Rostoker N., (1954). Solution of the Schrodinger Equation in Periodic Lattices with an Application to Metallic Lithium; *Phys. Rev.* **94** : 1111-1120.

Kohn W., (1975). Green's function method for crystal films and surfaces, *Phys. Rev*. **87**: 3756-3760.

Lee M. M., Teuscher J., Miyasaka T., Murakami T. N. and Snaith H. J., (2012). Efficient hybrid solar cells based on meso-superstructured organametal halide perovskites, *Science* **338**, 643-647.

Lovinger A. J., (1983).*Science* **220**, 1115-1121.

Moller C. K., (1958).*Nature* **182**, 1436-1436.

Meziani A. and Belkhir H., (2012). *Computational Material Science*, **61**: 67-70.

Park N.G., (2013). *The Journal of Physical Chemistry Letters* **4**, 2423-2429.

Pines D., (1963). *Elemantary Excitations in Solids,* W. A. Benjamin Inc, New York.

Shankar, A., Sandeep, Ghimire, M. P. and Thapa, R. K., (2012). Electronic and magnetic properties of X_2YZ (X = Co, Y = Cr, Z=Al, Ga) Heusler compounds: A First Principles method. *Int. Jour. Mord. Phys.* ,**B28:** 1250071-12.

Reshak A. H., (2007). *Linear and Nonlinear Optical Properties*, Habilitation Thesis, Institute of Physical Biology, South Bohemia, Nove Hrady.

Salhei H. Hosseini S. M. and Shahtahamasebi N.(2004). First Principles Study of Electronic Structure of $BaTiO_3$, *Chinese Journal of Physics*, **42**,115-120.

Scott J. F. and Bline R.,(2011).Jour. *Phys. Condens. Matter* **23**, 113202-19.

Singh J., (2006). *Optical Properties of Condensed Matter and Applications*, John Wiley.

Singleton J., (2010). *Band Theory and Electronic Properties of Solid*, University of Oxford, New York, Oxford Univ. Press.

Syrotyuk, Stepan V and Shaved Viram., (2015). *Eur. Phys.* J. B., 016201-5.

Tejuca, L. G., Fierro L. G., (2000). *Properties and Applications of Perovskite-Type Oxides*, CRS Press.

Thapa, R .K., Khating D. T., Patra P. K., Hashemifar J.,Jamol M., Lalmunpuia., Ghimire, M. P., Sandeep., Rosangliana., and Rai D. P.,(2010). Study of Co2MnAl Heusler alloy as half - metallic ferromagnet, *Indian Jour. Phys.* **84**, 717-721.

Wooten F., (1972). *Optical Properties of Solids*, Academic Press, London .

ISSN: 0976-3031

Available Online at http://www.recentscientific.com

CODEN: IJRSFP (USA)

International Journal of Recent Scientific Research
Vol. 9, Issue, 2(H), pp. 24295-24300, February, 2018

International Journal of Recent Scientific Research

DOI: 10.24327/IJRSR

Research Article

STUDY OF STRUCTURAL, ELECTRONIC AND OPTICAL PROPERTIES OF FLUORIDE PEROVSKITE $XCaF_3$ (X= K AND RB) USING GENERALIZED GRADIENT APPROXIMATION (GGA) EXCHANGE POTENTIAL

Neupane K and Thapa R K

Department of Physics, Condensed Matter Theory Research Group Mizoram University, Aizawl 796 004, Mizoram

DOI: http://dx.doi.org/10.24327/ijrsr.2018.0902.1636

ARTICLE INFO

Article History:

Received 17th November, 2017
Received in revised form 21st December, 2017
Accepted 05th January, 2018
Published online 28th February, 2018

Key Words:

DFT; GGA; FP-LAPW; DOS; band structure; dielectric function; refractive index; absorption coefficient

ABSTRACT

The first principles calculation within the full potential linearized augmented plane wave (FP-LAPW) method is applied to study the structural, electronic and optical properties of cubical perovskite$XCaF_3$on the base of density functional theory (DFT).The exchange correlation effects are included through the generalized gradient approximation (GGA) exchange potential. The calculated structural properties such as equilibrium lattice constant, the bulk modulus and its pressure derivative are in agreement with the published results of other authors. From our study we have found that the band gap of $KCaF_3$ and $RbCaF_3$ are 6.1 eV and 6.3 eV respectively that indicates insulating nature of $XCaF_3$ compound. Calculation of optical spectra such as real and imaginary parts of dielectric function, refractive index and absorption coefficient are performed on the range of energy 0 - 40 eV.

INTRODUCTION

The ternary compounds belonging, having the general formula ABF_3, where A and B stand for the alkali metals and alkaline earth or transition metals respectively. The ternary fluoroperovskite like $XCaF_3$ (X= K and Rb) has great potential for a variety of device applications in optical, ferroelectric, antiferromagnetic systems due to their wide band gaps (Ouenzerfi *et al.* 2004). It is always an advantage to know the physical and electronic properties of such order to understand their possible applications. Perovskites are well known for their applications in different fields of science and technology because of their wide range of electro- optic, mechanical, semiconducting and insulating behavior. $CsCaF_3$ and $KMgF_3$ are used as a vacuum- ultraviolet-transparent material for lenses in optical lithography steppers in electro- optical applications (Ho¨rsch *et al.* 1986; Fukuda *et al*. 2001).and they have many applications for a tunable laser due to their unique properties (Knierim *et al.*1986). Murat *et al.*(2016) have investigated structural, electronic and optical properties of $CsCaF_3$ when doped with Eu atoms and they found that the energy band gap decreases 6.9 eV to 0.13 eV when added dopant Eu atom in $CsCaF_3$ compound. Babu *et al.*(2015) have studied the structural, electronic and optical properties of cubic fluoride $CsCaF_3$ compound using FP-LAPW $+l_o$ method within the generalized gradient approximation (GGA) in the framework of density functional theory. Mubark *et al*. (2012) have studied structural, electronic and optical properties of fluoroperovskite BXF_3 (X= Li, Na, K and Rb) compounds, using FP-LAPW method with exchange- correlation functional GGA in which energy band gap decreases as traverses from Li to Rb. In this paper, we will do the theoretical investigations of the structural, electronic and optical properties of fluoride type perovskite$XCaF_3$ which will be benefit in electro-optical applications.

Crystal Structure and Computational Details

The unit cell of fluoro-perovskite $XCaF_3$ with space group (Pm-3m) contains three atoms that form the cubical structure. The atoms of $XCaF_3$ (X= K andRb)are located at the Wyckoff positions X(0, 0, 0), Ca(0.5,0.5,0.5), and F(0,0.5,0.5)(Gregory S. Rohrer, 2004)to form the crystal structures as shown in Fig.1. For volume optimization of $KCaF_3$ and $RbCaF_3$, we have used the experimental lattice constant a=4.41 Å (Tran*et al.,*

Corresponding author:* **Neupane K
Department of Physics, Condensed Matter Theory Research Group Mizoram University, Aizawl 796 004, Mizoram

2009) and a= 4.455Å(Bulou *et al*., 1980) respectively. The optimized volume versus energy curves are shown in Fig.2. The obtained optimized lattice constants are used to study the density of state (DOS) and band energy of $XCaF_3$ by using the full potential linearized augmented plane wave (FP-LAPW) method of KS-DFT (Kohn *et al.,* 1965) as implemented in the WIEN2K code (Blaha *et al.,* 2012). The generalized gradient approximation (GGA) as proposed by Perdew *et al*. (1996) is used to describe the electron exchange and correlation potential. Non spherical contributions to the charge density and potential within the muffin tin (MT) spheres are considered and the cut-off parameter is $R_{MT}\times K_{max}= 7$ where K_{max} is the maximum value of the reciprocal lattice vector in the plane wave expansion and R_{MT} is the smallest atomic sphere radii of all atomic spheres. In the interstitial region, the charge density and potential are expanded as a Fourier series with wave vectors up to $G_{max}=12$ a.u^{-1}. The number of k-points used in the irreducible part of the Brillouin zone is 1000. The criterion for the convergence of the self-consistent DFT calculation is 0.0001 Ry in total energy. However the core states are treated relativistically, the semi-core states are treated semi-relativistically by ignoring the spin-orbit (SO) coupling. The optical properties of a material can be described on the base of the dielectric function $\varepsilon(\omega)$, which is expressed as

$$\varepsilon(\omega) = \varepsilon_1(\omega) + i\varepsilon_2(\omega)$$

The imaginary part $\varepsilon_2(\omega)$ of the dielectric function $\varepsilon(\omega)$ was calculated from the electronic band structure of a solid.

$$\varepsilon_2(\omega)=\left(\frac{4\pi^2e^2}{m^2\omega^2}\right)\sum_{i,j}\int_k \langle i \mid M \mid j\rangle^2 f_i(1-f_i)\times\delta\left(E_{j,k}-E_{i,k}-\omega\right)d^3k$$

Where e is the charge of free electrons, m be the mass of free electrons, ω is the angular frequency of the incident photons, M is the dipole matrix, i and j be the initial and final states respectively, f_i be the Fermi distribution function for the i-th state and E_i be the energy of the electro in i-th state with crystal wave vector k. The real part $\varepsilon_1(\omega)$ of dielectric function can be extracted from the imaginary part using the Kramers-Kronig dispersion relation:

$$\varepsilon_1(\omega)=1+\frac{\pi}{2}p\int_0^\infty\frac{\omega'\varepsilon_2(\omega')}{(\omega'^2-\omega^2)}d\omega'$$

Here p represents the principal value of integral. The refractive index $n(\omega)$ and the absorption coefficient $\alpha(\omega)$ of the sample are given by the relations

$$n(\omega)=\frac{1}{\sqrt{2}}\left[\sqrt{\varepsilon_1^2(\omega)+\varepsilon_2^2(\omega)}+\varepsilon_1(\omega)\right]^{\frac{1}{2}}$$

$$\alpha(\omega)=\sqrt{2}\omega\left[\sqrt{\varepsilon_1^2(\omega)+\varepsilon_2^2(\omega)}-\varepsilon_1(\omega)\right]^{\frac{1}{2}}.$$

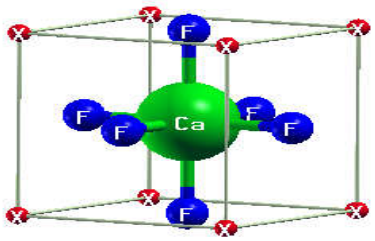

Figure 1 Crystal structure for $XCaF_3$ (X= K andRb)

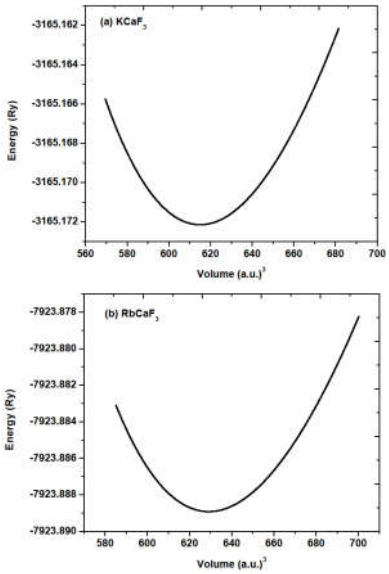

Figure 2 Volume optimization curve (a) $KCaF_3$and (b) $RbCaF_3$

RESULT AND DISCUSSIONS

Crystal structure

To study the crystal structure, we start with the total energy minimization of cubic $XCaF_3$ as a function of volume. The variation in the total energy as a function of volume is shown in Fig.2. The energy versus volume data was fitted to aMurnaghan equation of state (1944) to obtain the equilibrium lattice constant (a), the bulk modulus (B) and its first pressure derivative(B'). Our calculated values of a, B, and B' are compared with previous experimental and theoretical results which are mentioned in table 1.We note that the result of the lattice constants obtained within our GGA calculations are in increasing order from K to Rb.

Table 1 Calculated lattice constant a (in Å), bulk modulus B (in GPa) and its pressure derivative B' of $XCaF_3$ compared with other theoretical and experimental results.

Lattice Constant a(in Å)	Bulk Modulus B(GPa)	Pressure Derivative B'
For **$KCaF_3$**		
Our study 4.498		
Other, GGA 4.41[a]		
4.45[b]	49.334	5.199
4.5293[c]	49.583[a]	3.577[a]
Experimental	46.0[c]	3.95[c]
4.410[d]		
4.4584[e]		
For **$RbCaF_3$**		
Our study 4.5134	48.067	4.967
Other, GGA 4.452[f]	49.77[f]	5.00[f]
Experimental 4.455[h]		

[a]Ref. (Babu *et al.,* 2015), [b] Ref. (Soleimanpour *et al*., 2015), [c] Ref.(BahattinErdinc, 2011),
[d] Ref.(Tran *et al.,* 2009), [e] Ref. (Demetriou *et al*., 2005), [f] Ref(Murtaza *et al*., 2013),
[h] Ref. (Bulou *et al*., 1980)

Density of states (DOS) and band structuresof $XCaF_3$

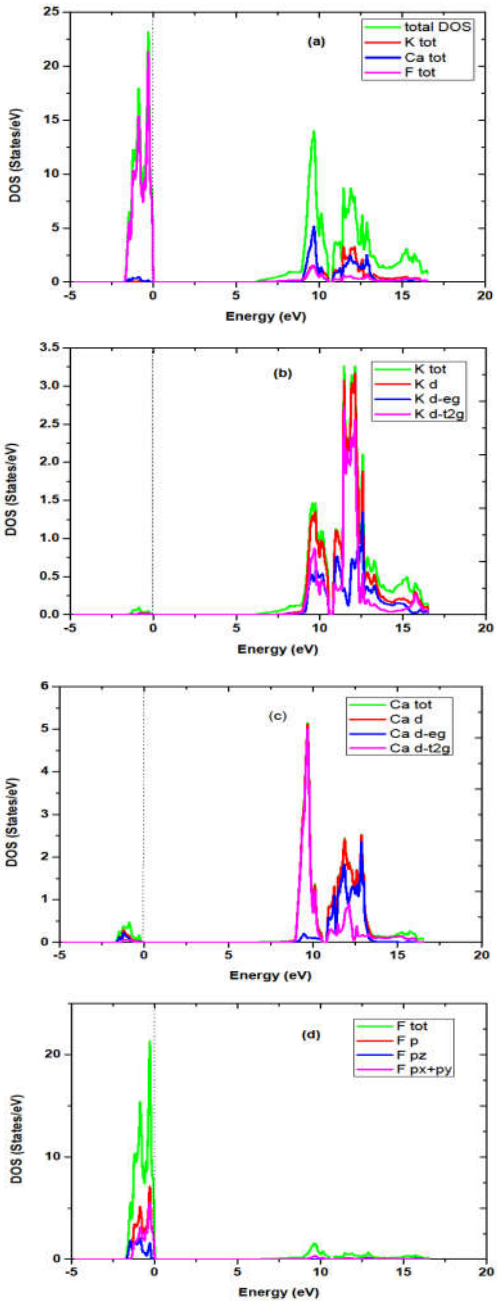

Figure 3 (a) TDOS of $KCaF_3$, K, Ca and F, (b) PDOS of K, (c) PDOS ofCa and (d) PDOS of F

Fig. 3 (a) shows the plot of total density of states (TDOS) of $KCaF_3$, K, Ca and F. In the valence region below the Fermi level, we have found the maximum peak at 0.27 eV due to the main contribution of F atomand negligible contribution of Rb and Ca atoms. In the conduction band above the Fermi level in Fig. 3 (a), the maximum peak is observed at 9.68 eV due to the main contribution of Ca atom, less contribution of K atom and negligible contribution of F atom. Fig. 3 (b) shows the partial density of states (PDOS) of K atom of $KCaF_3$ compound.

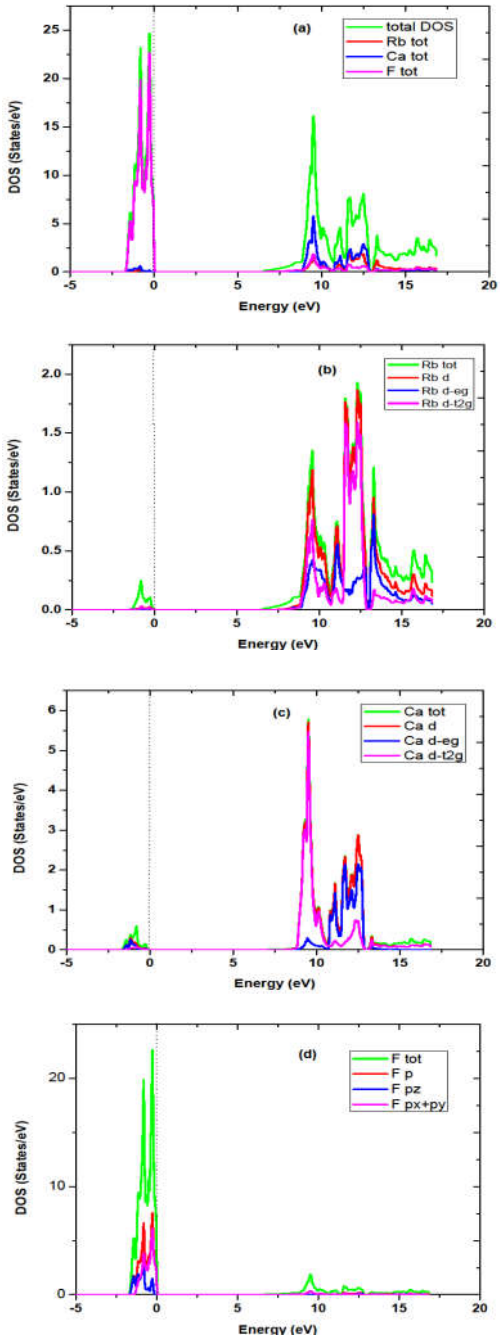

Figure 4 (a) TDOS of $RbCaF_3$, Rb, Ca and F, (b) PDOS of Rb, (c) PDOS of Ca and (d) PDOS of F

The contribution of K-*d* state is negligible in the valence band and the maximum peak is found at 11.92 eV in the conduction band due to the contribution of K *d-t2g* which is seen in Fig.3 (b). Fig.3 (c) shows the plot of partial DOS of Ca atom of $KCaF_3$ compound. The negligible contribution of Ca-d is found in the valence band below the Fermi level and a maximum peak is observed at 9.68 eV in the conduction band due to the main contribution of Ca*d-t2g* states which is evident of Fig. 3 (c). The plot of partial DOS of F atom of $KCaF_3$ compound is shown in Fig. 3 (d). The maximum peak is found at 0.27 eV in the valence region below the Fermi level due the main contribution of F *px+py* states of electrons. The negligible contribution is occurred in conduction band which is shown in Fig. 3 (d). Hence, the energy band gap of $KCaF_3$ is found due

to the contribution of F *px+py* states in the valence band and K *d-t2g* statesin the conduction band.

The plot of total density of states (TDOS) of $RbCaF_3$, Rb, Ca and F is shown in Fig. 4 (a). In the valence region below the Fermi level, a maximum peak is found at 0.25 eV due to the main contribution of F atom and negligible contribution of Rb and Ca atoms. In the conduction band above the Fermi level in Fig.4 (a), a maximum peak is found at 9.51 eV due to the main contribution of Ca atom, less contribution of Rb atom and negligible contribution of F atom. The plot of total and partial DOS of Rb atom of $RbCaF_3$ compound is shown in Fig.4 (b). The contribution of Rb-*d* state is negligible in the valence band and a maximum peak is found at 12.5 eV in conduction band due to the main contribution of Rb*d-t2g* state which is seen in Fig. 4 (b). The total and partial DOS of Ca atom of $RbCaF_3$ compound is plotted in Fig. 4 (c), in the valence band below the Fermi level, no contribution of Ca-*d* state is found. In the conduction band above the Fermi level, a maximum peak is observed at 9.51 eV due to the main contribution of Ca*d-t2g* state that is seen in Fig.4 (c). Fig. 4 (d) shows the total and partial DOS of F atom of $RbCaF_3$ compound. In the valence band, a maximum peak is found at 0.25 eV due to the main contribution of F *px+py* states of electrons and negligible contribution F-*p* state is observed in the conduction region which is seen in Fig. 4 (d). From the study of DOS, the energy band gap of $RbCaF_3$ is observed due to the contribution of F *px+py* states in the valence band and Ca*d-t2g* states in conduction band.

Hence, from the study of total and partial DOS of $XCaF_3$ compound, we have found that the energy band gap occurs due to the contribution of F *px+py* states in the valence band and Ca*d-t2g* states in the conduction band.

The electronic properties of $XCaF_3$ (X = K and Rb) are calculated with first principles FP-LAPW method using GGA exchange potential. To calculate DOS and band structure of $XCaF_3$, the optimized lattice parameters are used. The calculated electronic band structures for fluoroperovskites $XCaF_3$ (X = K and Rb) along the high-symmetry directions of the Brillouin zone are shown in Fig. 5 (a-b).

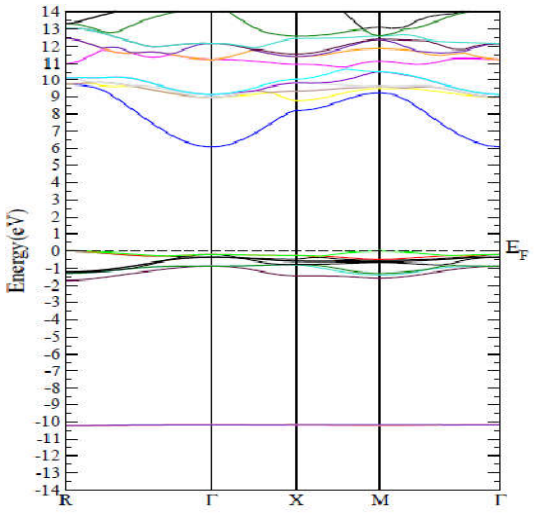

a

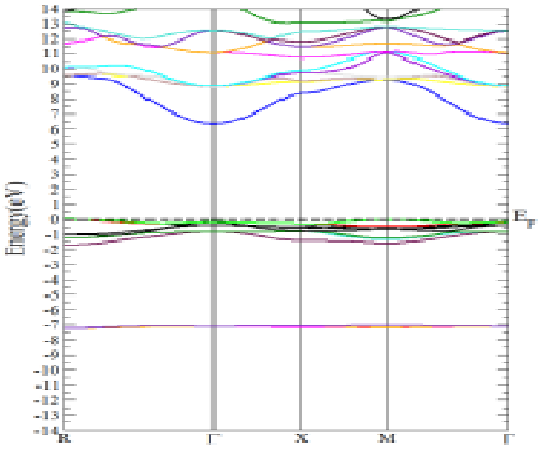

b

Figure 5 Band structure for (a) $KCaF_3$ and(b) $RbCaF_3$along the high-symmetry directions of the first Brillouin zone.

We have found that the maximum of the valence band are found to be at a symmetry point R whereas the minimum conduction bands are located at the Γ point of the Brillouin zone in $XCaF_3$ compounds, resulting into indirect band gaps in all the compounds. The calculated band gaps (R - Γ) are found as 6.1 eV and 6.3 eV for $KCaF_3$ and $RbCaF_3$respectively. From the study of DOS, the band gaps are found due to the contribution of F-p state electrons in the valence band below the Fermi level and most of Ca d-t2g state electrons in conduction band above the Fermi level. From our study, we have found the energy band gaps increase from K to Rb for $XCaF_3$ compound.

Optical properties

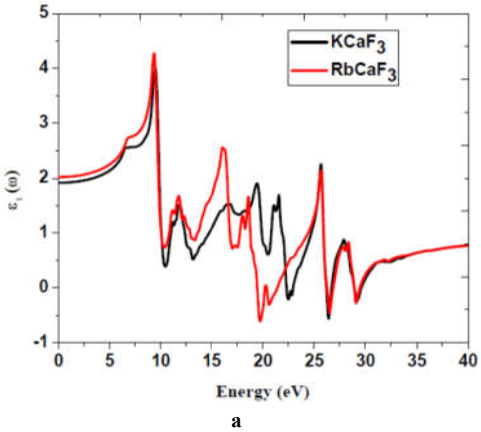

a

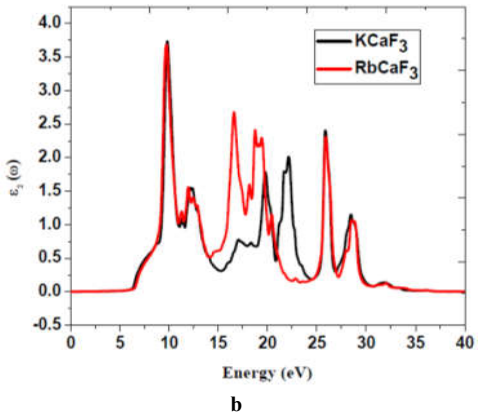

b

Fig 6 (a)Real $\varepsilon_1(\omega)$ part, (b) Imaginary $\varepsilon_2(\omega)$ part of dielectric function

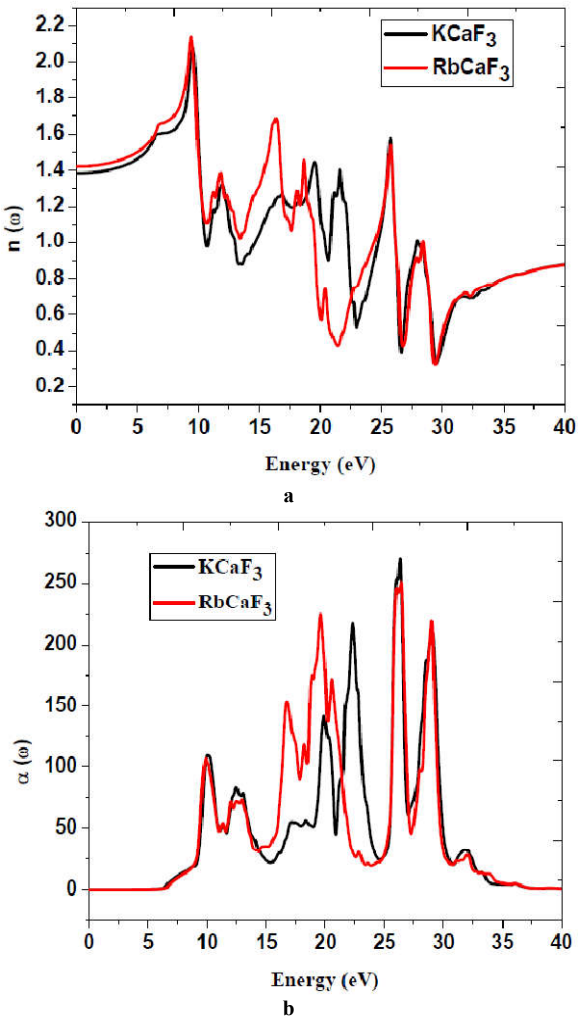

Fig 7 (a) Refractive index n(ω), (b) Absorption coefficient α (ω) of dielectric function

The optical spectra as a function of photon energy for cubical fluoroperovskite $XCaF_3$ (X=K and Rb) are shown in Fig. (6, 7).The optical properties are studied in the energy range of 0 – 40 eV. The Fig.6 (a) represents real part$\varepsilon_1(\omega)$ of dielectric function$\varepsilon(\omega)$ of photon energy for cubic $XCaF_3$. The functionε_1 (ω) provides the information about electronic polarizability of the material. The static dielectric constant at energy zero isε_1 $(0) = 1.92$ for $KCaF_3$ and $\varepsilon_1(0)= 2.02$ for $RbCaF_3$. From zero frequency limit, real part of $XCaF_3$ starts to increase and reaches the maximum value of 4.01 at 9.41eV for $KCaF_3$ and 4.28 at 9.347 eV for $RbCaF_3$. After reaching the 1.69 at 21.56 eV for $KCaF_3$, real part starts to decrease below zero in the negative scale for the range of22.326-22.925eV, 26.28-26.68eV and 28.939-29.565 eV. Similarly for $RbCaF_3$, the negative values are found as for the range of 19.469-20.204 eV, 20.39-21.40 eV, 26.27- 26.82 eV and 28.91-29.429 eV. These negative values of real dielectric function indicate that these materials be metal otherwise dielectric. Fig.6 (b) represents the imaginary partε_2 (ω) of dielectric function $\varepsilon(\omega)$ which provides information about absorption behavior of $XCaF_3$. In the imaginary partε_2 (ω), the threshold energy of dielectric function occurs at E_0 = 6.1 eV and 6.3 eV for $KCaF_3$and $RbCaF_3$ respectively which correspond to the fundamental gaps at the equilibrium. We have observed six peaks for $KCaF_3$ at 9.80 eV, 12.36 eV,19.76 eV, 22.10 eV, 25.86 eV and 28.45eVhaving imaginary part of dielectric function as 3.74, 1.55, 1.76,2.01, 2.41 and1.15 respectively. Similarly for $RbCaF_3$, we have observed six peaks at 9.67 eV, 11.93 eV, 16.61 eV, 18.72 eV, 25.89 eV and 28.50 eV having imaginary part of dielectric function as 3.68, 1.56, 2.68, 2.41, 2.31 and1.07 respectively. Fig.7 (a) represents the refractive index n (ω) of photon energy for cubic $XCaF_3$. The static refractive indexn(0)are found to have the values 1.38 and 1.42 for $KCaF_3$and $RbCaF_3$ respectively. The refractive index reaches the maximum value of 2.08 at 9.58eV for $KCaF_3$ and 2.14 at 9.42 eV for $RbCaF_3$. The refractive index greater than one means photons which travelling in the material are slowed down due to the interaction with electrons of the medium. Fig.7 (b) shows the absorption coefficient α(ω)of photon energy. The absorption characters are observed in the range up to 40 eV. The maximum absorption coefficient is 2.55% at 26.32eV for $KCaF_3$and 2.5% at 26.42 eV for $RbCaF_3$. $XCaF_3$ is wide band gap compound with high absorption power in ultraviolet energy range and it can be used in the optoelectronic devices like UV detectors.

CONCLUSIONS

The structural and electronic properties of $XCaF_3$ are studied using the FP-LAPW method based on density functional theory (DFT) with GGA exchange-correlation potential. From the volume optimization curve in Fig. 2 (a-b), we have found the optimized lattice constants, pressures and pressure derivatives of $XCaF_3$ (X = K and Rb) which are mentioned in table 1 in which experimental and theoretical values are noted. Our optimized lattice constants are slightly more than the experimental values and they increase from K to Rb (table 1). From the total and partial DOS plots of $KCaF_3$ in Fig. 3 (a-c) and in Fig. 4 (a-c) for $RbCaF_3$, we have found that F *px+py* state electrons are contributing in valence band and Ca*d-t2g*state electrons contribute in the conduction band which provides band gap energy. From the study of band structure of $XCaF_3$ in Fig. 6 (a-b), we have found the band gaps are as 6.1 eV and 6.3 eV for KCaF3 and $RbCaF_3$ and respectively which is the indication of insulating behavior. The optical properties such as real and imaginary parts of dielectric function, refractive index and absorption coefficient of $XCaF_3$ compound are studied as the energy range of 0 - 40 eV. This compound has a wide band gap and high absorption power, which suggests that it is useful for optoelectronic devices.

References

Babu, K.E., Murali, N., Babu, V., Babu, B. K. and Veeraiah, V. (2015). *Structural, electronic and elastic properties of KCaF3 and RbCaF3 for vacuum ultraviolet-transparent lens materials*. AIP Conference Proceedings 1661, 100002-100005

BahattinErdinc (2011). Density Functional Calculations of the Electronic Band Structure and Optical Properties of KCaF3 *GU J Sci,* 24(4):671-677

Blaha, P., Schwarz K., Madsen G. K. H., KvasnickaD., Luitz J., Schwarz K. (2012). *An Augmented Plane Wave plus Local Orbitals Program for Calculating Crystal Properties,*Wien2K User's Guide, Techn. Universitat Wien, Wien

Bulou, A., Ridou, C., Rousseau, M., Nouet, J. and Hewat, A. (1980). The temperature dependence of the structure of

$RbCaF_3$ and the determination of the low temperature phases, *J. Phys*. 41: 87-96.

Demetriou, D. Z., Catlow, C. R. A., Chadwick, A. V., Mclntyre, G. J. and Abrahams, I.,(2005).“The Anion Disorder in the Perovskite FluorideKCaF3”, *Solid State Ionics*, 176: 1571-1575

Fukuda, T., Shimamura, Yoshikawa, K. A. and Villora, E. G. (2001).Crystal Growth of New Functional Materials for Electro-Optical Applications, *Opto Electron Rev*;9 (2):109-116.

Gregory S. Rohrer (2004), *Structure and bonding in crystalline* materials, Cambridge university press, United Kingdom

Ho¨rsch, G. and Pau, H. J. (1986). A New Color Center Laser on the Basis of Lead-DopedKMgF$_3$,*Opt. Commun;*60:69-73

Knierim W, Honold A, Brauch U and Durr U (1986). Tunable Lasers with Transition Metal Doped Fluoride Crystals*, J. Opt.Soc. Am*. B 3(1):151-158.

Kohn W. and Sham L. J. (1965), Self-Consistent Equations Including Exchange and Correlation Effects, *Phys. Rev. A*, 140:1133-1138

Mubark, A. A. and Mousa, A. A. (2012). *The electronic and optical properties of the fluoroperovskite $BaXF_3$ (X= Li, Na, K and Rb)*, Computational Materials Science. 59: 6-13

Murat, A. and Bahattin, E. (2016). DFT Study of $CsCAF_3$:Eu, *GUJ Sci*. 29(2):273-278

Murnaghan, F. D.(1944). The Compresibility of Media under Extreme Pressure, *ProcNatlAcad Sci;* 30: 244-247.

Murtaza, G., Ahmad, I. and Afaq, A. (2013).*Shift of indirect to direct band gap in going from Kto Cs in $MCaF_3$ (M = K, Rb, Cs)*, *Solid State Science*, 16:152-157

Perdew, J. P., Burke, S. and Ernzerhof, M. (1996). Generalized Gradient Approximation Made Simple, *Phys. Rev. Lett*., 77: 3865-3869

Ouenzerfi, R. E., Ono, S., Quema, A., Goto, M., Sakai, M. and Sarukura, N. (2004). Design of Wide-gapFluoride Hetrostructure for Deep Ultraviolet Optical Devices, *J. Appl.Phys;* 96:7655-7659.

ShSoleimanpour and F Kanjouri (2015).Elastic, electronic and optical properties of the cubicfluoro-perovskite, *Indian J. Phys*. 89(7):687-697

Tran F. and Blaha P. (2009), Accurate Band Gaps of Semiconductors and Insulators with a Semilocal Exchange - Correlation Potential, *Phys. Rev. Lett*. 102: 226401-4.

How to cite this article:

Neupane K and Thapa R K.2018, Study of Structural, Electronic and Optical Properties of Fluoride Perovskite $XCaF_3$ (X= K ANDRB) Using Generalized Gradient Approximation (GGA) Exchange Potential. Int J Recent Sci Res. 9(2), pp. 24295-24300. DOI: http://dx.doi.org/10.24327/ijrsr.2018.0902.1636

****